The University Of Sheffield.

Mutli-Stage Granulation in a High Shear Mixer

Ali Zainalabb'deen Asker Al Hassn

A thesis submitted in partial fulfilment of the requirements for the degree of

Doctor of Philosophy

Department of Chemical and Biological Engineering

The University of Sheffield

November 2018

ABSTRACT

The wet granulation process is generally conducted by adding the formulation to the granulator and running the granulator under fixed operating conditions from the starting point until the end point. This type of granulation process is referred to as normal granulation (NG). In the current work, a novel granulation method was used termed as Multi-Stage Granulation (MSG), as the granulation process was performed over three stages of process variables rather than one stage as in the NG.

The MSG process, besides to the NG process, were carried out in a lab scale Eirich mixer using calcium carbonate (as a powder) and Polyetheylene Glycol (as a binder). The effect of varying the granulation time and the impeller speed on the granule properties was studied. In the NG process, the granule size was noticed to increase progressively with time, but with different tendencies depending on the impeller speed and liquid to solid ratio. The rate of increase was higher at 2000 RPM compared to 7000 RPM and was higher for a L/S=0.15 compared to L/S=0.14. While, the porosity, and the specific surface area of the granules decreased as the granulation time was increased. The size distribution of the granules also narrowed with time. This was inferred by examining the span of the size distribution with granulation time. For instance, at impeller speed 2000 RPM and L/S=0.14 the span was 1.47 at 400 sec while it was 1.26 at 600 sec. The amount of the binder was noticed to affect the span as well, where it was slightly higher at L/S=0.14 compared to the L/S=0.15.

In the MSG process, the speed of the impeller was adjusted from a moderate speed to a high speed then to moderate speed again, creating three stages of the process parameters. The granule median size changed clearly during the process due to occurrence of different granulation mechanisms (growth and breakage) during the different stages. However, the granule porosity did not change enormously during the process. Although the granule porosity did not increase satisfactorily, the granule size distribution interestingly became narrower at the beginning of the third stage of MSG compared with corresponding points in NG process. For example, the span decreased from 1.47 (NG) to 0.99 (MSG) at L/S=0.14 and 400 sec, while at 600 sec it decreased from 1.26 (NG) to 0.88 (MSG). This means the span was reduced to about 30% when using MSG process compared to the NG process. The surface area of the granules was also affected by the stages of the MSG process. The surface area of granules decreased with time in the first stage then increased

in the second stage, and it was high in the third stage, as well. This, consequently, affected the dissolution time of the granules.. The dissolution time for the granules at the third stage was reduced, by approximately 21%, compared with granules from the first stage, which could be attributed to the increase in the surface area.

Since the flow of the granular bed has an impact on the granule properties and there is lack of studies available in the literature about it, the velocity distribution of granular bed surface was studied using PIV . The flow in the Eirish mixer is different to the typical vertical high shear mixer. The area inside Eirich mixer was divided into different zones depending on the velocity of the granular bed monitored. The motion in the zone after the impact of the impeller to the granular bed (zone 2) was the most intensive one, which is believed to have caused granule breakage. While in the zone before the contact with the impeller (zone 1) was the lowest intensive motion condition, which could motivate the growth process. The highest and lowest intensive motion was happening during the second stage and the first stage of MSG, respectively. Power consumption during the different stages was also monitored and correlated with the granulation process of growth/breakage.

The flow of the particle bed was also examined by simulating the motion of the particle using Discrete Element Method (DEM),. The simulation work was validated by experimental work using PIV results. The velocity distribution obtained by DEM was similar to the PIV results. The particles had high velocity after been impacted by the impeller and low velocity before the impact. The mixing of the particles was also characterized using Lacey's Mixing Index (LMI). The results showed that the LMI was higher in the second stage of MSG compared to the first/third stage. This gives an indication that the mixture after the second stage was increasing in homogeneity, i.e. the binder distribution was better during the second stage of MSG process.

Finally, the outcomes from this research provide valuable insight into how granular properties from the high shear mixer can be adjusted by utilising a multi-stage approach. This is useful as it allows methods, which can be adopted to optimise granular properties for the end purpose and offers industries a novel route for tailoring products for consumers and for assuring product quality in the global market.

ACKNOWLEDGEMENTS

Firstly, I would like to express my deep thanks my supervisors Prof. Agba D. Salman and Prof. Michael J. Hounslow for their outstanding guidance, supervision, and continuous support throughout my PhD, particularly Prof. Salman who was, persistently, advising, motivating, and directing me.

I'm also very grateful to Dr. Washino and Dr. Chan, for their help in part of my work (simulation part), namely Dr. Washnio for his help, suggesting ideas related to the DEM, and imparting the knowledge of DEM.

My special gratitude is for the PPG group (past and present people) for their encouragement and general help. Special thanks for Dr. Chalak, Dr. Syed, Dr, Mohamed, Osama and Bilal for their support.

I am also grateful to the Ministry of Higher Education and Scientific Research/Iraq, Iraqi cultural attaché/London, and the University of Diyala for the financial support.

My exclusive gratitude goes to my parents, my wife and my kids, for their continuous, unconditional support and endless patience. They were always making my life happier.

The utmost thanks and gratitude is for my God for the help, great graces, and conciliation.

PUBLICATION AND CONFERENCES

- Al hassn, A.Z., Jeßberger, S., Hounslow, M.J., Salman, A.D., 2018. Multi-stage granulation: An approach to enhance final granule attributes. *Chemical Engineering Research and Design*, 134, pp.26–35.

- Al hassn, A.Z. Washino, K., Chan, E.L., Hounslow, M.J., Salman, A.D., Granular Flow in an Intensive Mixer. Poster presentation at the 7th International Granulation Workshop, Sheffield, UK. 1st – 3rd July 2015

- Al hassn, A.Z., Jeßberger, S., Hounslow, M.J., Salman, A.D., Multi-stage granulation: An approach to enhance final granule attributes. Conference oral presentation at the 8th International Granulation Workshop, Sheffield, UK. 28th – 30th June 2017.

TABLE OF CONTENT

LIST OF FIGURES

LIST OF TABLES

NOMENCLATURE

Δt	The time step
Δx	The displacement in the direction of x-axis (in PIV analysis)
Δy	The displacement in the direction of y-axis (in PIV analysis)
μ_f	The sliding friction respectively
μ_r	The rolling friction coefficient
C	The conductivity of the solution at any time
$C_{(m, n)}$	Correlation number (in PIV analysis)
C_0	The conductivity of the solution at time=0 sec
C_∞	The final conductivity of the solution
D	The dissolution in percentage
e	The restitution coefficient
E_p	Young's modulus of the particle
Fc_i	The total force (contact force) on the particle including particle-particle and particle-wall interaction forces
$Fc_{n,ij}$	The contact force (normal) between particle *i* and particle *j*
$Fc_{t,ij}$	The contact force (tangential) between particle *i* and particle *j*
g	The gravitational velocity
G_p	The particle's shear modulus
I_i	The moment of inertia
k_n	The stiffness in the normal direction
k_t	The stiffness in the tangential direction
Mc_i	Total torque applied on the particle
m_i	The mass of the particle (in DEM simulation)
m_p	The mass of the particle
n_{ij}	The unit vector directed from the centre of first particle *i* to the centre of the other one *j*
N_p	The number of all particles.
R	The average radius of the particles and it is equal to the r_p
r_p	The radius of the particle (in DEM simulation)
S_{max}	Maximum pore saturation

St_{def}	Stokes deformation number
t_{90}	The dissolution time for 90% of the material
t_{ij}	a unit vector towards the tangential motion (given in the Equation 7-8)
u	The velocity component in the direction of x-axis
U_0	collision velocity
v	The velocity component in the direction of y-axis
v_i	The translational velocity
w	Represents liquid to solid ratio (mass ratio)
X_i	The mean number fraction of the component *i*
X_j	The mean number fraction of the component *j*
Y	Dynamic yield strength
δ_{nij}	particle displacement (in normal direction) due to the normal force
δ_{tij}	The tangential displacement
ε	The average porosity of the granules
ε_{min}	The minimum granule porosity
η_n	The damping coefficient in the normal direction
η_t	The damping coefficient in the tangential direction
$v_{r,ij}$	The relative velocity of the particle *i* with respect to the particle *j*
$v_{rt,ij}$	The relative velocity in the tangential direction
ρ	The density of the particle
ρ_a	The apparent density
ρ_b	The binder density
ρ_l	The liquid density
ρ_s	The solid density
ρ_t	The true density
σ	The sample variance
σ_0	The variance of the fully segregation
σ_R	The variance of the fully random state
υ_p	Poisson's ratio for the particle
φ_b	The binder mass fraction
φ_s	The solid mass fraction
ωi	The rotational velocity
ω_i	The rotational velocity for the particle *i*

ω_j	The rotational velocity for the particle j

Acronyms

CCD	charge-coupled device
DCC	Direct Cross-Correlation
DEM	Discrete Element Method
EP	Early Pulse process
FFT	Fast Fourier Transform
FTT	Fast Fourier Transform
L/S	Liquid to Solid ratio
LDA	Laser Doppler Anemometry
LDV	Laser Doppler Velocimetry
LMI	Lacey's mixing index
LP	Late Pulse process
MCC	Microcrystalline cellulose
MQD	Minimum Quadratic Difference
MSG	Multi-Stage Granulation process
NG	Normal Granulation process
NIR	Near Infrared
PDF	The velocity probability distribution function
PEG	Polyethylene glycol
PEPT	Particle Emission Positron Tracking
PIV	Particle Image Velocimetry
RPM	Revolutions Per Minute
SSA	The specific surface area

CHAPTER 1 INTRODUCTION

This chapter will introduce the granulation process and highlights its importance in the industry. The scope of the project and the ideas of the current work will be explained as well. Followed by the thesis structure.

1.1 Definition and uses

Dealing with powder is usually associated with problems in many industrial applications and finding solutions for those problems is what many industries are looking for. Granulation is the solution for miscellaneous powder problems. It is known as to be the process of fine particles agglomeration. The particles of the powder are promoted to aggregates by creating attraction forces between them using different techniques. Granulating the particles of the powder improves the product properties such as flowability and compressibility or to decrease some undesirable inadvertent agglomeration of particles due to storage or handling (Ennis, 2005). Therefore, the granulation is an important process in many industries such as fertilizers, foods, detergents and pharmaceuticals. The following are further uses of the granulation process:

1. Maintaining the homogeneity of a powder mixture.
2. Limiting the segregation.
3. Enhancing particles characteristics such as flow properties, handling, low storage space and getting preferred particle geometry and shape.
4. Reducing the risks of toxic dusts.
5. Production of a desired size distribution of particles.

1.2 Granulators

Granulation is predominantly classified as wet and dry process depending on how the inter-particle bonds are form. In wet granulation, liquids are usually used as a binder to promote bonds formation (liquid bridges) between primary particles (Ennis, 2008) as it is the case in high shear mixer, twin screw granulator, fluidized bed granulator and tumbling drum granulator, in which they are considered to be wet process equipment. While in dry

granulation, high stress is used instead of liquid binder to produce granules by enhancing the attraction forces between primary particles as in the roller compactor. These equipment are classified further as batch process or continuous process . In the wet granulation process, the twin screw granulator is a continuous process. While the high shear mixer and the fluidized bed granulators are batch processes. On the other hand, the roller compactor represents a continuous dry granulation process.

Each of these granulators are, traditionally, used in a certain area in industry. The high shear mixers are usually used in pharmaceutical, detergents, ceramics, and chemical processes. The twin screw is similarly used commonly in the pharmaceutical sector as an intermediate process. Tumbling drums are usually used in fertilizers, agricultural, and iron ore industries. The fluidised bed granulators always could noticed in pharmaceutical, chemical, and the nuclear wastes industries. The roller compactor, currently, could be seen in the pharmaceutical industries as well as in the food production processes.

1.3 Granulation using high shear mixer

The properties of the granules produced by the aforementioned equipment are not the same due to the difference in conditions that the powder undergoes in the granulator. This is a consequence of the difference in process and formulation variables related with each equipment. The process and formulation variables of the granulation process should be chosen carefully in order to produce granules with certain properties. However, this is not an easy task especially with equipment that involves a wide variety of variables for example the high shear mixer which is used in the current work. Granulation via the high shear mixer offers several advantages compared with the other granulators such as short process time, less binder could be used, granulating cohesive materials and producing more uniform granule size distribution (Ennis, 2005). Hence, it is the equipment that could be noticed in miscellaneous industrial applications.

There are different types of high shear mixers which are used for the granulation purposes. Eirich is one of these mixers. It has a unique design. It is widely used in industrial applications e.g. ceramic, fertilizer, and chemical industries. Due to its unique design (different modes of mixing) and ability to mix intensively, it could affect the properties of the produced granule, crucially. Hence, this mixer was used in the current work.

1.4 Key properties of the granules

The granular product have different properties like median size, size distribution, porosity, surface area, dissolution sphericity and appereance. Some of these are related to the inner side of the granule such as porosity, and others are related to the outer side of the granules e.g. surface area, appearance and size. Among these, the granule size distribution, porosity and dissolution time are the most interesting properties of the granular material, namely, for pharmaceutical industry due to their relevance to tablets production and dissolution time. They are also important in manufacturing detergent products since fast dissolving product, which is highly desired in the market, is related with granule porosity and surface area. The size distribution is also an important property in most applications. This is due to a certain size class of granules is usually required by the consumers.

The properties of the granules, mentioned above, could be affected by the process and formulation variables of the granulation process. For this reason, many researches that could be found in the literature are dedicated to know how the process and formulation variables could influence the final granule properties and how to control the final granule attributes to get the best granule design (Reynolds et al., 2007). The studies which are related to the high shear mixer, generally, state that the porosity and surface area decreases with granulation time while the granule size and dissolution time increases with the granulation time (Hoornaert et al., 1998; Ramachandran et al., 2008; Seo and Schæfer, 2001; Shi et al., 2011a). The granulation processes in these studies were conducted by following the conventional process in which the process parameters are fixed over the whole granulation process. However, if the process parameters were changed during the granulation process, the properties of the granular products could be affected, accordingly. This type of granulation process could not be found in the literature. Therefore, there is a gap of knowledge in the literature about how the granule properties will be affected if the process parameters, e.g. impeller speed, were changed during the granulation process. This will be tackled in this work by conducting a new granulation method in Eirich mixer. This process will be explained in the next section in more details. In addition, the flow characteristics of the material in Eirich mixer could also affect the granule properties which is not reported sufficiently in the literature. This will be studied in this work, as well.

1.5 The scope of the project

Most of the granulation studies in high shear mixer were carried out by applying constant conditions throughout the whole granulation time. This means that the granules were exposed to fixed process parameters (e.g. impeller and chopper speed and temperature) from the starting point to the end point of the granulation process. This was represented by route 1 in Figure 1-1, in which it shows that the $(powder)_A$ is converted to granular product $(Granules)_A$ in a single stage process. This "traditional" single stage process was considered here as normal granulation process (NG). As mentioned in the previous section, extensive work could be found in the literature about this type of process in a high shear mixer and the effect of the process variables on granule properties has been extensively studied by many researchers (Reynolds et al., 2007). Granulation using the NG process usually leads to produce granules of low porosity which are difficult to dissolve in water.

In this work, a new and non-traditional method of granulation process was proposed which will follow the route 2 in Figure 1-1. This new process implies exposing granules to different stages of process variables during granulation process, stages A, B and C in Figure 1-1, route 2. In each stage, the process variables will be different particularly the impeller speed. When the granules will pass through these stages of process variables, which is named as multi-stage process (MSG), the final granule attributes will respond to the change in the applied conditions since they are vulnerable to the changes occurring within the mixer. Hence, this multi-stage process could be exploited to have a manipulation the final granule properties and could give a solution for one of the problems of granule properties which is, how to enhance the final granule attributes in terms of size uniformity, porosity and dissolution at the same time.

Nevertheless, before going through the investigating of this unique type of granulation (MSG), it is also important to investigate the wet granulation process using the conventional (NG) granulation process since it will be important to compare the results of the MSG process with the NG process.

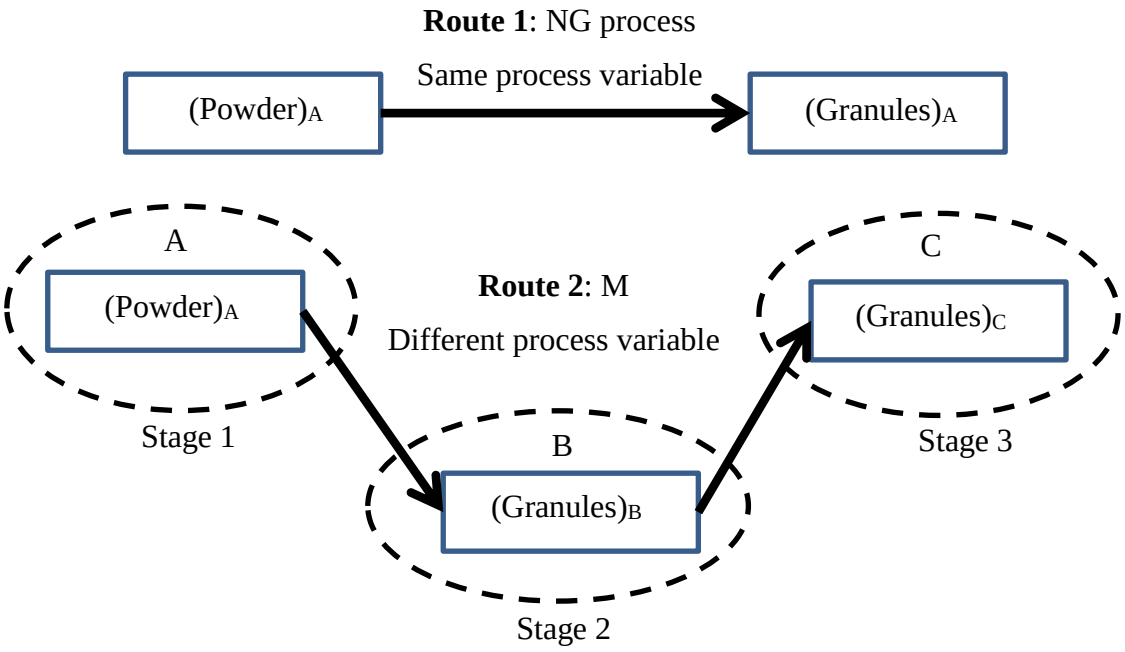

Figure 1-1: Granulation procedures: Route 1 is traditional method; Route 2 is a new (proposed) method.

On the other hand, investigating and understanding the granulation mechanism accompanied with the aforementioned granulation process (MSG) is an important step, too. This is because understanding the mechanisms will give greater insights about how the granulation process is taking place using the MSG. Since the mechanisms of the granulation (growth and breakage) are always related to the dynamics of the granules inside the granulator, the granules flow characteristics (e.g. velocity vector) will be taken in consideration and will be studied as well. The granule flow will be monitored practically using Particle Image Velocimetry (PIV) technique and the process of mixing will be simulated using Discrete Element Method (DEM) as well.

Thesis structure

The work in the current thesis is organized in the following order

In Chapter **Two**, the previous work available in the literature were identified in this chapter and the related researches to the topic area of the current work were presented.

In Chapter **Three**, the properties of the materials used in the current wok were exhibited and the lab scale Eirich mixer was described. Then the methods of the wet granulation were conducted in this work were illustrated. The method of the granule characterization and the method of granule visualization in the mixer were also described.

While in Chapter **Four**, the first experimental results were presented. The results of this chapter are related with the normal granulation process in Eirich mixer.

Followed by the Chapter **Five**, which is about the new method in wet granulation process which is Multi-Stage Granulation. The results were presented, discussed, and compared with the normal granulation process.

Then in Chapter **Six**, an attempt has been made to understand the kinetics of the wet granulation process in Eirich mixer using the method of particle image velocimetry (PIV). The chapter gives information about granule velocity in the mixer and where the granule breakage possible could happen.

Chapter **Seven** is the last chapter of results which is about the DEM. The mixing process in the Eirich mixer was simulated using the Discrete Element Method (DEM). This chapter gives more understanding about the particle flow in the mixer namely within the particle bed.

Finally, in Chapter **Eight**, the main conclusion about this work was given and ideas for the future work were also recommended.

There are also some **Appendices** which give further information (supplementary results).

CHAPTER 2 LITERATURE REVIEW

2.1 Wet Granulation

In the wet granulation process a liquid binder is added onto powder bed by direct pouring, melt-in or spraying. Then the binder will disperse in the powder bed by mixing them together within the granulator equipment. As a consequence, the powder particles will aggregate forming bigger size particulates which are granules. Depending on the severity of mixing and the applied mechanical forces on the granules, the wet process granulators are classified as following (Litster and Ennis, 2004):

Low shear granulators in which fluidized bed is an example of this type of granulator. The applied stress is usually low in these granulators. They could be run as batch or continuous mode. They are usually used in fertilizer, metallurgical, pharmaceutical and coating applications. The properties of the granules produced by these methods are generally porous and weak.

The other type of granulators are high shear granulators or high shear mixers. They are most commonly used since 1980s in pharmaceutical industry (Ennis, 2005) because of the possibility to granulate different types of powders (including cohesive) using viscous binders. However, they are required to be controlled carefully due to their dependency on process and formulation variables. Granules produced by this method, mostly have spherical shape and high density. In the next section, high shear mixer will be discussed briefly.

2.2 High Shear Mixer

High shear mixers are mainly consist of bowl, impeller and chopper or scraper, (see Figure 2-1. The impeller is primarily responsible to move the powder particles in the bowl. It consists of three or more blades and rotates with adjustable speed from low to high speed reaching sometimes to 7000 RPM for instance in Eirich mixer. The chopper which moves with high speed introduces more turbulence to the granular flow and increases the possibility of big granules breakage. In some types of high shear mixers, for

example Zanchetta Roto Jounior mixer, the bowl wall is provided with water jacket to control the temperature. This is useful particularly to control the viscosity of liquid binder.

High shear mixers are further categorized as vertical, horizontal and eccentric mixers according to the position of the impeller. Gral, Lodige and Eirich are examples of these mixers respectively. The interesting one among of them is Eirich mixer because it allows the control of more process variables. It has a unique design, in which the impeller is positioned eccentrically to the centre of the bowl and it can rotate in both directions, clockwise and counter-clockwise. The bowl can rotate at the same time but with lower speed. The stage of the mixer can be tilted as well with different angles. As a result, this type of mixer combines high shear granulator and tumbling granulator features. Granules produced by Eirich mixer are mostly spherical, narrow size distribution and dense granules (Litster and Ennis, 2004; Nold et al., 2008). It is used in many industries e.g. agricultural, ceramics and metallurgy.

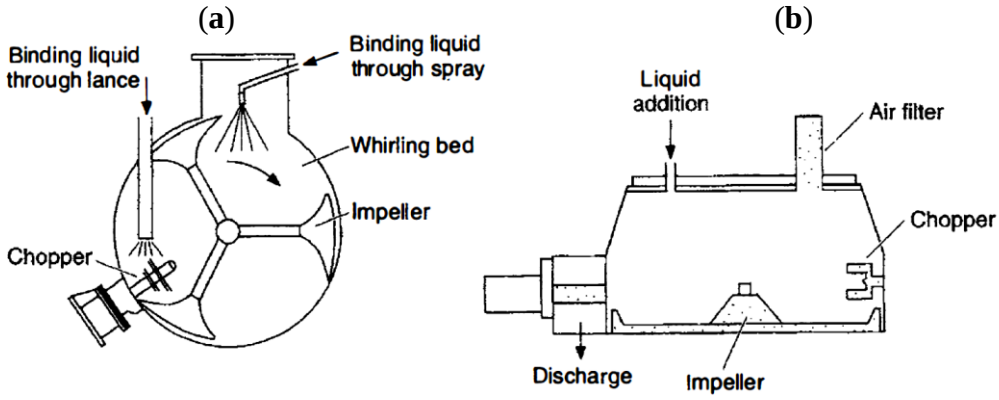

Figure 2-1: High shear mixers, (a) Horizontal type, (b) Vertical type (Litster and Ennis, 2004).

2.3 Mechanisms of Wet Granulation

To improve the granule properties in the granulator and produce granules with certain properties, the mechanisms of the granulation process have to be unambiguous. The wet granulation process is complex and it involves different physical phenomena in competition. However, there are traditionally three well known mechanisms in wet granulation process as depicted in Figure 2-2. It includes wetting and nucleation, consolidation and coalescence and breakage and attrition, where they implies binder distribution and nuclei generation, granule growth and increasing in size and granules

size reduction respectively (Simon M. Iveson et al., 2001; Kapur, 1978; Sastry and Fuerstenau, 1973).

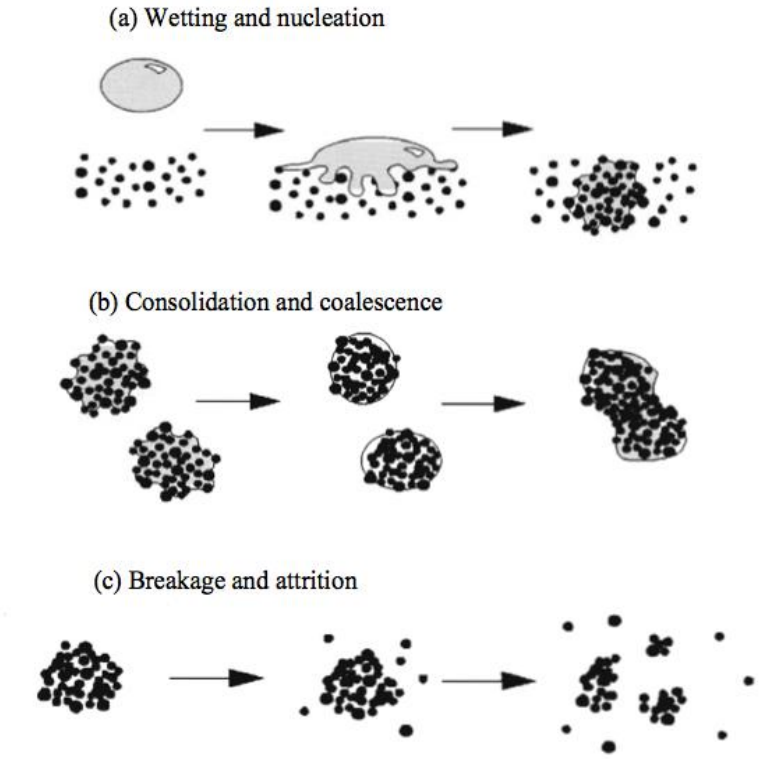

Figure 2-2: Mechanism of wet granulation (a) wetting and nucleation, (b) consolidation and coalescence, (c) breakage and attrition (Simon M. Iveson et al., 2001).

2.3.1 Wetting and nucleation

Granulation process commences with wetting the powder bed with the liquid binder. It is crucial stage since the rate and method of wetting could affect size distribution of the granules (Knight et al., 1998). As stated previously, the binder could be added to the powder by spray, melt-in and direct pouring. When the liquid sprayed on the powder, nuclei start forming as the liquid droplet interacts with particles and then disperse and penetrate into the moving powder bed, as shown in Figure 2-3 (Ennis, 2008). Depending on the relative size difference between droplets and powder particles, there are two uttermost cases of nuclei formation. First, when droplet size is small compared to the primary particle size, then the mechanism of distribution will occur, as illustrated in Figure 2-4. This mechanism increases the chances to yield narrow granule size distribution. The other case is when the droplet size is relatively big compared to the

particle size, the immersion mechanism will take place and more probably it will leads to produce granules with wide size distribution (Schæfer and Mathiesen, 1996). Affinity between the liquid binder and the powder particles and mechanical agitation besides to the spray flux which is wetted area of the powder in a unit time, affect the uniformity of the produced granules (Hapgood et al., 2004; Litster et al., 2001).

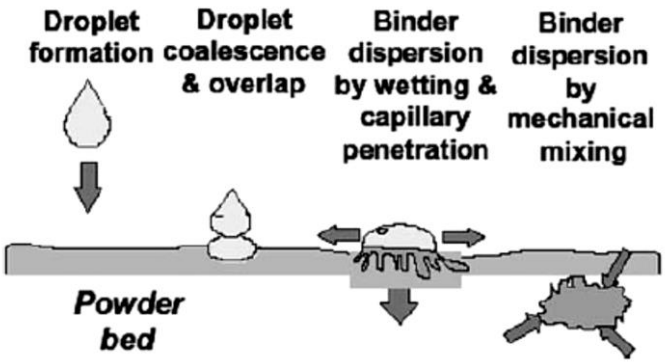

Figure 2-3 Stages and mechanism of fine powder wetting (Ennis, 2008).

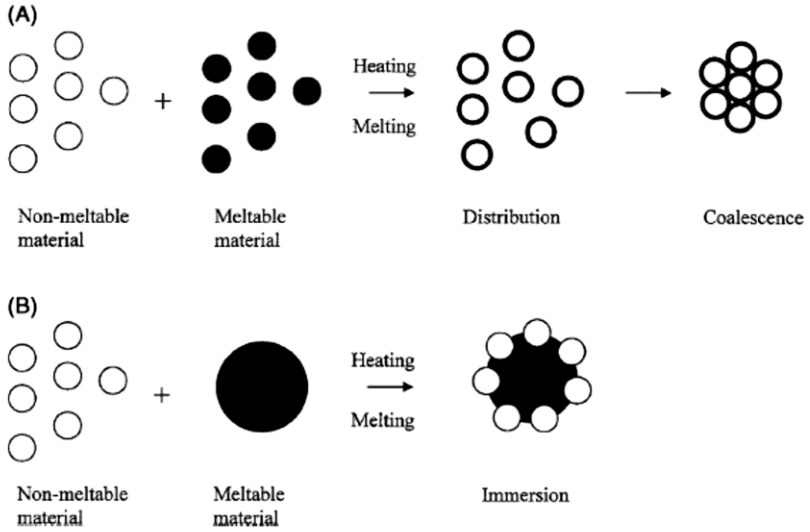

Figure 2-4 Nucleation mechanism modes: (A) distribution mode and (B) immersion mode (Ennis, 2008).

2.3.2 Growth and consolidation

By adding the binder on the moving powder bed, the nuclei will be formed. Then the nuclei and small granules will start to collide each other by virtue of the applied mechanical forces. If successful collision take place between them, it will lead to granule growth. This process is responsible for granule size enlargement in the granulators. The rate of the process depends on the successful collisions and the strength of bonds created. This in turn depends on granules deformability, velocity and the amount of binder that exists on the contact surface, see Figure 2-5.

Layering is another mechanism that could lead to the granule growth. When fine granules in the granulator stick to the surface of the big one, the big granule will be bigger with time and the number of the small ones will decrease with time (Ennis, 2005). In this mechanism, the number of big granules usually does not change but their size changes progressively and the increase in size usually described to be differential.

Consolidation is the process of primary particles packing in a single granule, by squeezing out the existed entrapped gas (air) and liquid (binder) from inside of the granules to its surface. It tends to decrease granules porosity but at the same time it increases granules strength along the process time. Consolidation process has been studied by many investigators (Holm et al., 1985; Iveson et al., 1996; Kapur, 1978; Sastry and Fuerstenau, 1973).

The relationship between consolidation and granule growth is competitive. Where the strength of granules increases by more consolidation in, however, increasing the strength will impede granules deformation. At the same time, since binder quantity increases at the surface of the granules due to increasing pore saturation of the granules by virtue of consolidation, it enhances successful coalescence. According to this competition, Simon M Iveson et al. (2001) proposed regime map for granule growth (Simon M Iveson et al., 2001; Iveson and Litster, 1998a). It is based on the relation between maximum pore saturation and granules deformation during collision. The pore saturation depends on porosity, liquid to solid ratio and materials densities. While the granule deformation is related to granules kinetic energy and surface asperity (Ennis et al., 1991).

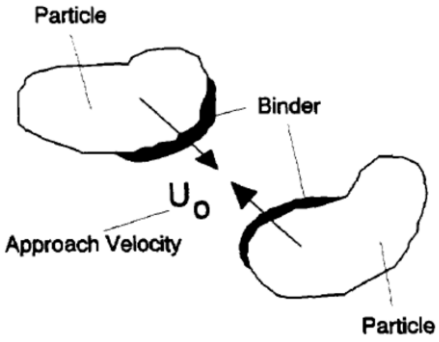

Figure 2-5 Coalescence of two particles covered by binder, (Tardos et al., 1997).

2.3.3 Attrition and Breakage

This is the third phenomena that can be observed in granulators particularly in high shear granulators, where the granules are intensively subjected to impact loads. It has an effect on the granule attributes such as size distribution and binder distribution. Breakage of the granules could result from collisions and impacts that may happen between granules itself or between granules and granulator wall and impeller. The collision forces cause deformation of the granules which may lead to coalescence but at the same time it could break the granules when the mechanical energies applied on the granules externally was enough (Tardos et al., 1997). Breakage may take place when the Stokes deformation number St_{def} was higher than the critical deformation number St^*_{def}. Otherwise, the granules either deform or coalesce. This means that:

$$St_{def} > St^*_{def} \qquad \text{Equation 2-1}$$

where, Stokes deformation number St_{def} and the St^*_{def} is the critical value of $St_{def.}$ The St_{def} represents the ratio of the kinetic energy applied externally on the granules to required energy for granule deformation, which is given by (Iveson and Litster, 1998a; Tardos et al., 1997; Van Den Dries and Vromans, 2002):

$$St_{def} = \frac{\rho_g \ U_0^2}{2 \ Y} \qquad \text{Equation 2-2}$$

where: ρ_g is granule density (kg/m^3), U_0 is collision velocity (m/s), Y is the dynamic yield strength of the granule (N/m^2).

Other workers, for example Kendall (1988) proposed that the breakage of the granules is because of subsequent propagation of a crack nucleation at some flaws in the granule.

This concept in combination with the effect of process parameters on the granules has been studied widely. Reynolds et al. (2005) pointed out that numerous parameters could affect the breakage of the granules in the granulator, for example intensity of agitation, binder properties, granulation time and size and shape of the particle size.

2.4 Saturation of liquid-bound granules

The static strength of granules depends on the amount of the binder present between primary particles. This is because the binder plays an important role in increasing the interparticle forces by forming solid bridges between the particles. In other words, the strength of granules depends on the saturation of pores in the granules by liquid binder (Ennis, 2005). Schubert, (1975) studied the relationship between the saturation of the wet granule (S) and the tensile strength (σ_t). The relationship between the tensile strength and the saturation would change, as he argued, and depends on the state of the granule saturation. Figure 2-6 shows this relationship. The S_c represents the begging of the capillary state and the S_p represents the end of the pendular state. When the ratio of liquid to solid (L/S) is low, a particle will connect with its neighboring particle via single liquid bridges. This state of saturation is called pendular state (granules are highly porous and low in strength). If all the voids within the granule are completely filled with the binder, there will be no air and this state is known as capillary (full saturation) state.

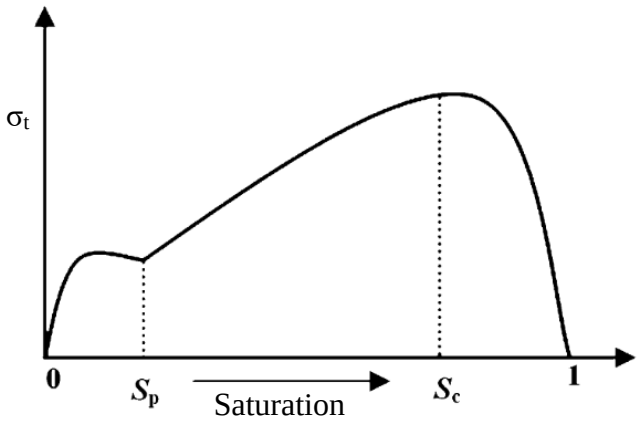

Figure 2-6 Saturation states of wet granule, adapted from (Ennis, 2005).

2.5 Regime Map for Granule Growth

The behaviour of granule growth in wet granulation process, as stated by Iveson et al. (2001a) and Iveson et al. (2001b), depends on two parameters. Firstly, the amount of binder occupying maximum number of pores in the granules which is called maximum pore saturation (S_{max}). It is given by the following equation:

$$S_{max} = \frac{w\,\rho_s\,(1-\varepsilon_{min})}{\rho_l\,\varepsilon_{min}} \qquad \text{Equation 2-3}$$

where, w represents liquid to solid ratio (mass ratio), ρ_s , ρ_l are densities of solid particles and liquid binder respectively and ε_{min} represents minimum granule porosity. Secondly, to what extent the granules are deformable, which is determined by Stokes number (St_{def}), see Equation 2-2 in previous sections. According to these parameters, Iveson & Litster (1998b) established a regime map for granule growth, as shown in Figure 2-7.

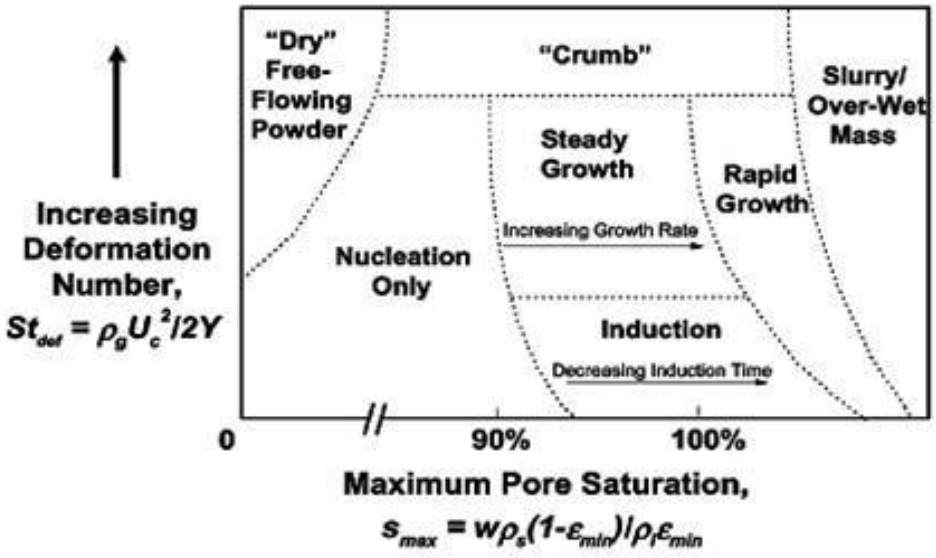

Figure 2-7: Regime map for granule growth (Iveson and Litster, 1998a).

As can be seen from Figure 2-7, that the granulation process will be in the stage of nucleation (i.e. nuclei formation), when the liquid content is not enough to promote granule growth by coalescence. When the granules do not deform easily, induction growth dominates. However, if the liquid binder is squeezed out to the granule surface, rapid growth may occur. Whereas granules could grow steadily, when they will be deformable and sufficient amount of liquid binder exists at the surface of the granules. These conditions lead to successful collision. The possibility of granule formation under

intensive conditions and weak binder will be low and causes crumb material formation. By adding excessive liquid to the system, slurry forms.

2.6 Effect of Process Variables on Granule properties

In the following sections, the effect of some important process parameters (impeller speed and granulation time) on important granule properties (size distribution, porosity and dissolution) will mainly be discussed.

2.6.1 Granule Size

There are many parameters that can affect the granule size in high shear mixer. One of these is the energy input into the granulator which is imparted on the granules by virtue of impeller and chopper. The effect of impeller speed on granule size were studied by many researchers (Knight 1993; Knight et al. 2000; Sanders et al. 2003; Tu et al. 2009; Benali et al. 2009).

The granulation time can also influence the granule size distribution. Generally, it is reported that the granule size increases with increasing the time of granulation in high shear mixer. This parameter has been studied by many researchers (Benali et al., 2009; Hoornaert et al., 1998; Knight, 1993; Knight et al., 2000; P. C. T. Knight et al., 1998; Ohno et al., 2007; Thies and Kleinebudde, 1999; Tu et al., 2009). Knight (1993) investigated the kinetics of wet granulation in high shear mixer. In this work, it is reported that the mean granule size increases linearly by prolonging the granulation time. This is clear in Figure 2-8, where median granule size increased linearly with time for various liquid to solid ratios. The reason behind this behaviour was the coalescence of granules during granulation process.

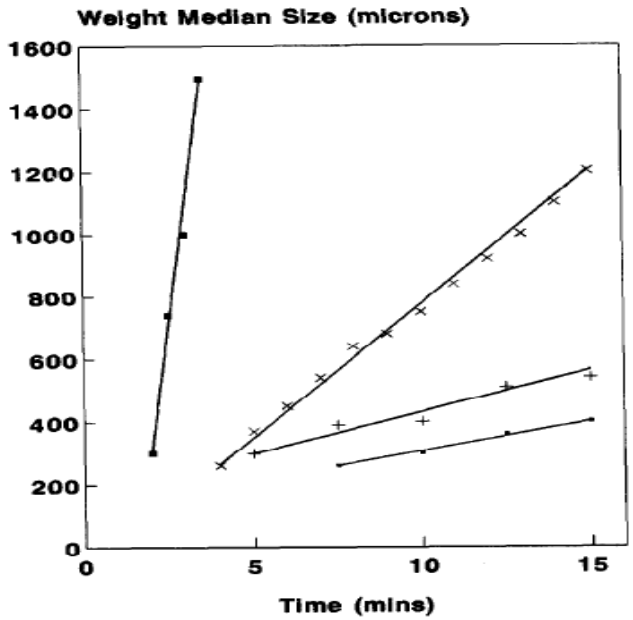

Figure 2-8 Granulation time verses mean granule size in mixer, at different liquid to solid ratio: ●, 0.2; +, 0.22; x, 0.24; ■, 0.26. The impeller and chopper speed were 100 and 3000 respectively (Knight, 1993).

The coalescence process could be promoted further if additional liquid is added to the powder which consequently leads to an increase in the granule size. This can be noticed in Figure 2-8. The figure shows that the mean granule size increases with time more rapidly at higher liquid to solid ratio (0.26) than lower liquid to solid ratio (0.22 or 0.2). Similar result was obtained by Tu et al. (2009) while they were investigating the regime map applicability that proposed by Iveson & Litster (1998a). They used high shear mixer to granulate MCC 102 (Microcrystalline cellulose, Avicel 102) and PEG 6000 (Polyethylene Glycol 6000). They observed that the granule mean size was increasing by increasing the time of granulation. In addition, they noticed that the granule growth was faster for the case of a higher liquid to solid to ratio. However, it is not always the same case that by increasing the time of the process will lead to an increase in the granule size. Hoornaert et al. (1998) noticed an initial period of time with no granule growth, but sometimes they observed rapid growth in granule size after the initial period. They argued that, during the initial period of granulation, the saturation level was not enough to cause granule growth which mainly depends on coalescence process. The effect of the granulation time on granule size were studied by further researchers (Realpe and Velázquez, 2008; Smirani-Khayati et al., 2009; Smrčka et al., 2015; Sochon et al., 2005). They generally stated that the granule size increases with prolonging the granulation time.

Knight (1993) investigated the effect of impeller speed on the granule size in high shear mixer using sodium phosphate and a binder of low molecular weight (polyethylene glycol). The investigator stated that the median size of granules increased with increasing the speed of impeller and granulation time. This is very clear in Figure 2-9. The change was non-linear, since the growth rate was 25 μm min^{-1} at low speed (100 RPM) and 110 μm min^{-1} at higher speed (300 RPM). In addition, Knight (1993) studied the effect of chopper on the median granule size and it is observed that chopper has no obvious influence on granule size. However, it was found that the effect of the chopper on the granule growth depends on the properties of powder and binder.

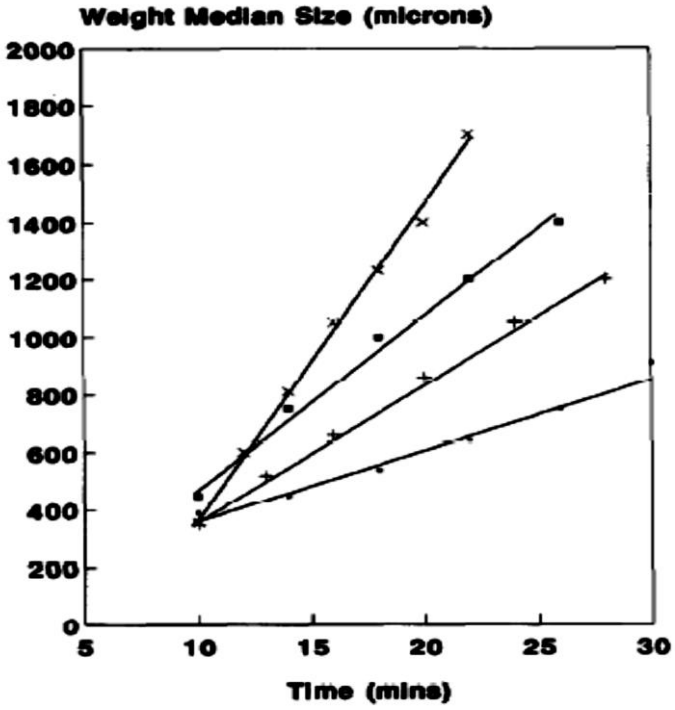

Figure 2-9 Granule median size as a function of time at different impeller speeds. Impeller speeds: ●, 100 RPM; +, 140 RPM; ■, 200 RPM; ×, 300 RPM. Chopper speed 3000 RPM, (Knight, 1993).

Afterward, Knight et al. (2000) studied further the effect of impeller speed on granule size using calcium carbonate powder with Polyethylene Glycol as a binder. They studied the effect of impeller speeds (450, 800, and 1500 RPM) on granule median size, and concluded that mean diameter of granules increased by increasing the impeller speed from 450 to 800 RPM. They noticed that by increasing the impeller speed further to 1500 RPM caused reduction in granule median size. The reason beyond that was the breakage process occurrence during granulation. Sanders et al. (2003) and Benali et al. (2009) found similar results. They reported that increasing the speed of impeller to a certain level

in high shear mixer will increase the mean size of granules, but after this value the size of granules started to decrease. They noticed that granules coalescence and breakage are influential processes in granulation mechanism. At low speeds, granule coalescence may take place and lead to increase in granule size, whereas breakage may occur at higher speed of impeller which in turn may lead to decrease in the mean granule size. Figure 2-10 depicts impeller speed effect on the mean granule diameter.

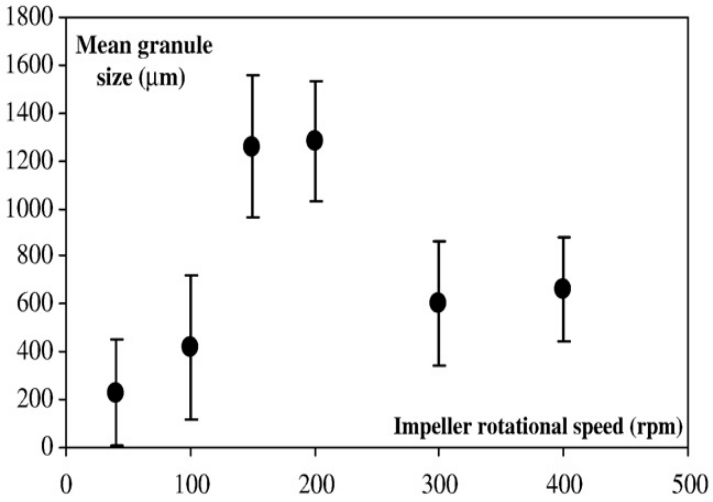

Figure 2-10 Effect of impeller speed on mean granule size in high shear mixer, (Benali et al., 2009).

Further studies on the influence of impeller speed on the granule size in high shear mixer were done by other researchers for example (Eliasen et al., 1999; Mangwandi et al., 2010).

On the other hand, the effect of liquid to solid ratio on the granule size distribution has been studied by many researchers due to its significant effect on granule growth mechanism. Since powders particles start to stick to each other by virtue of binder existence between them, it is logical to infer that by increasing the amount of liquid binder will lead to increase in granule growth (Reynolds et al., 2007). But the quantity of liquid binder should not be very high with respect to powder quantity (i.e. liquid to solid ratio) so that a phenomenon called overwetting will be avoided. If overwetting occurs, a paste will form. In fact, it is better to keep granules saturation with binder to a certain level because a high level of saturation leads to larger mean granule size (Reynolds et al., 2007). Alternatively, a very low saturation produces no granules.

2.6.2 Granule size distribution

It has been reported by some workers that longer granulation time leads to narrow size distribution (Knight, 1993; Knight et al., 1998). Ax et al. (2008) stated that the fraction of the fines will decrease if more binder was added and the agglomeration time increased. An example of their results was given in Figure 2-11 which shows that with longer agglomeration time, the size distribution will be narrower. They also observed that the pouring method of binder addition produces broader distribution of the granule size compared with the nozzle method even if the flow rate of the binder was the same, see Figure 2-11 B.

Sometimes, longer granulation time may not affect the size distribution especially for the big granules. Rahmanian et al. (2011), for instance, found that by increasing the granulation time from 6 min to 10 min the portion of the granules which has size bigger than 1 mm did not change, (see Figure 2-12 . They argued that the granulation process could reach to the equilibrium.

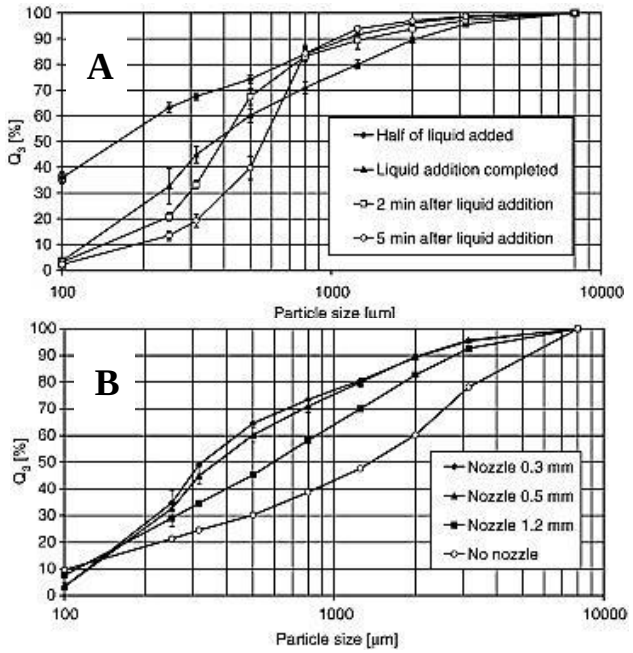

Figure 2-11: Cumulative distribution of the granule size with, A) agglomeration time, B) different binder addition method. No nozzle means pouring method, (Ax et al., 2008).

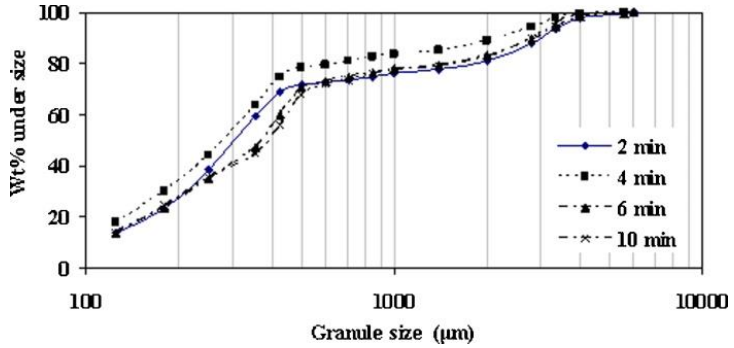

Figure 2-12: The granule size distribution at different granulation time, (Rahmanian et al., 2011).

Experimental results obtained by Knight et al., (1998) showed that the granule size distribution was bimodal during the initial period of the granulation time using pour-on methods of binder addition, regardless of the amount of the binder added, (see Figure 2-13. However, they reported that the granule size distribution was tending to be mono modal with granulation time. This is due to some of the course granules were disappearing with time because of the breakage process, which indicates that the size distribution was tending to be narrower. Similar result was also observed by Knight, (1993). Where he noticed that the size distribution of the granules was narrowing over the granulation time.

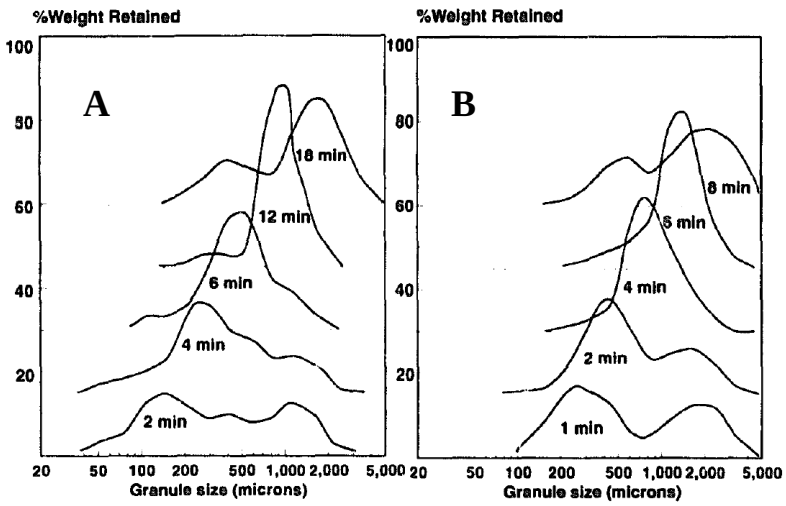

Figure 2-13: The size distribution of the granules versus granulation time, A) L/S = 0.14, B) L/S = 0.16, (Knight et al., 1998).

Rahmanian et al. (2011), in their investigation on the effect of the process parameters on the granule properties, found that the impeller speed has no significant effect on the size distribution of the granules produced from granulating calcium carbonate and PEG in a high shear mixer. However, they found that the size distribution was the most homogenous when the impeller tip speed was 4.13 m/s, see Figure 2-14.

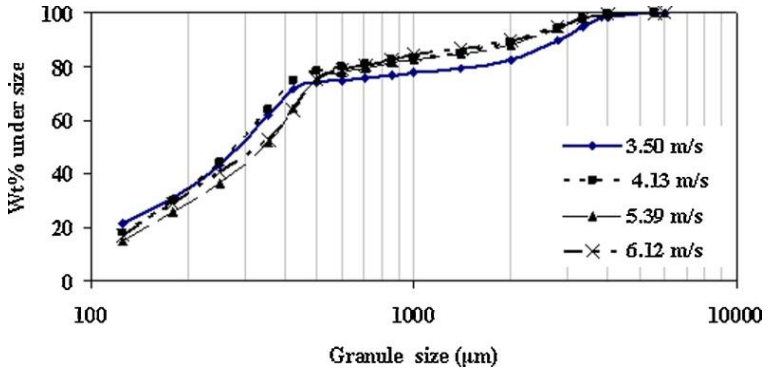

Figure 2-14: The granule size distribution at different impeller speed, (Rahmanian et al., 2011).

2.6.3 span

Sometimes, the distribution of the granule size is represented by the span. This parameter reflects the degree of homogeneity of the size distribution (Torrecillas et al., 2017). The span of granule size could be affected by the parameters of the granulation process. For example Rahmanian et al. (2011) noticed that the span of the granules will increase if binder was not distributing evenly and the possibility of a wider span increases if a more concentrated binder was used. In another study conducted by Rahmanian et al. (2013) while they were studying the scale-up in high shear granulator, they concluded that the span was decreasing when higher tip speed of the impeller was used. This was ascribed to the granule breakage that may take place at high impeller speed. The method of binder addition may also affect the span. This was approved by Tan et al. (2014). They found that the method of pour-in was resulting in wide granule size distribution compared to the pump-in method in the high shear granulation.

The span of a size distribution is given by:

$$Span = \frac{d_{90} - d_{10}}{d_{50}} \qquad \text{Equation 2-4}$$

2.6.4 Porosity

The porosity of granules is a significant end product specification in different granulation processes because of its effects on the properties of the granules namely dissolution, density and strength. Hence, many researchers investigated the influence of changing process variables and formulation variables on the final granule porosity especially in high shear granulators (Gabbott, 2007; Iveson and Litster, 1998b; Ohno et al., 2007; Ramachandran et al., 2008; Saleh et al., 2005; Schaefer, 1996; Schæfer, 2001; Schaefer and Mathiesen, 1996; Schaffer, 1996; Seo and Schæfer, 2001).

Ohno et al. (2007) investigated the influence of process variables on granule properties in high shear mixer during granulation of mefenamic acid, lactose monohydrate, hydroxypropylcellulose, low-substituted hydroxypropylcellulose, microcrystalline cellulose and magnesium stearate. They studied the effect of impeller speed, kneading time, and the amount of water on the pore diameter by means of mercury porosimetry. They observed that there was a reduction in 50% pore diameter of the generated granules with increasing the speed of the impeller, kneading time, and the amount of water added. The reason behind this result, as they proposed, was due to dissolution of the hydroxypropylcellulose and lactose in the present water and subsequently buried intensely into the granule and work as a binder to stick with the nuclei. Besides to this, the high shear in the mixer may tend to squeeze the air (pores) from the granules. Figure 2-15 shows the effect of selected process variables on the pore diameter.

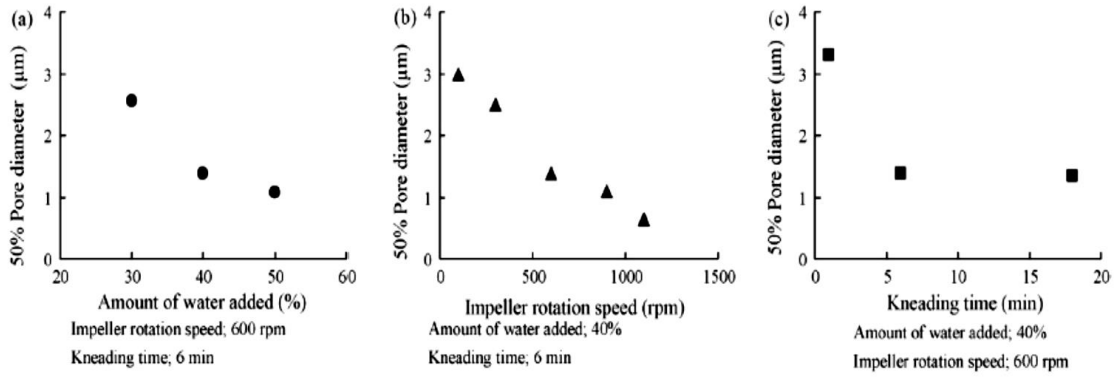

Figure 2-15 Effect of the process variables on the 50% pore diameter in high shear mixer, (Ohno et al., 2007).

Schæfer & Mathiesen (1996) studied melt pelletization in high shear mixer using lactose and different viscosity Poly ethylene Glycol (PEG) to examined the effect of viscosity of

PEG on pellets properties. They found that the granule porosity decreased with massing time within the first 6 minutes, however, after this time there was an increase in granule porosity. The reason behind this result was due to the creation of small pores in the granule structure when evaporation of water of crystallization happened.

Ramachandran et al. (2008) studied the effect of granulation operating conditions and formulation properties on the end-granule properties of the granules produced in a batch drum granulator. The powder they used was calcium carbonate and the liquid binder was Polyvinyl alcohol solution. As it could be noticed from Figure 2-16, the general trend in the granule porosity was reduction over time. This accentuates the influence of compaction and consolidation process of the granules over the granulation time. In addition, they studied the effect of binder to solid ratio and granule size class and on the porosity of the produced granules. They deduced that the porosity decreases with increasing granule size in which it may be caused by closely packing the granule structure that composed of small fine particle. While the granules porosity was found to reduce with adding more binder to the powder, and the reason behind that was an increase in the coalescence rate may happen leading to larger granules and more compacted.

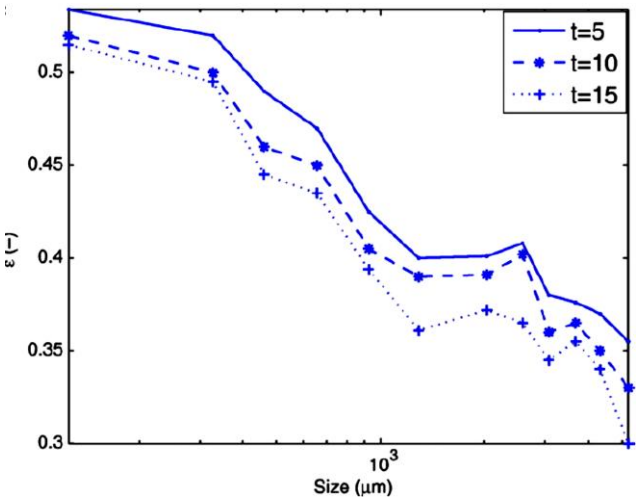

Figure 2-16 The distribution of porosity across the size, (Ramachandran et al., 2008).

Saleh et al. (2005) also found, during granulation in high shear mixer, that granule porosity decrease with increasing both L/S ratio and impeller speed. This might be because the consolidation process that occurred at higher impeller speed. Benali et al. (2009) also found that the porosity of granules, produced from MCC and water, decreased with increasing the impeller speed in high shear mixer due to the compaction process that occurred at high impeller speed. Similar results was found by Gabbott (2007), where the

researcher found that porosity decreases with increasing impeller speed because of the consolidation process.

Eliasen et al. (1999) examined the melt granulation of lactose monohydrate with stearic acid as a low viscosity binder in a high shear mixer. They reported that the porosity of produced granule increased with increasing the impeller speed. It was suggested that this result was due to the breakage process occurring at high impeller speed which prevent densification of granule and produced porous granules.

Oka et al. (2015) investigated the effect of process parameters namely impeller speed, massing time and liquid to solid ratio on granules critical quality attributes in high shear mixer. The material they used was microcrystalline cellulose (MCC) as an excipient and acetaminophen as active pharmaceutical ingredient (API). While the liquid binder was water. They characterized the porosity of 3 granules for each measurement using CT scan. They observed that the wet massing time and the liquid to solid ratio have significant effect on granule porosity as shown in Figure 2-17, where granule porosity revealed inverse proportion with time and liquid to solid ratio. The reason behind this relation, as they interpreted, is that the liquid binder (water) plays as lubricant and tends to decrease the inter-particle friction in the granules. As a consequence, this may lead to particles movement towards densifying the granules. This may also increase with increasing granulation time. On the other hand, they noticed that the relation between the granule porosity and impeller speed was not clear.

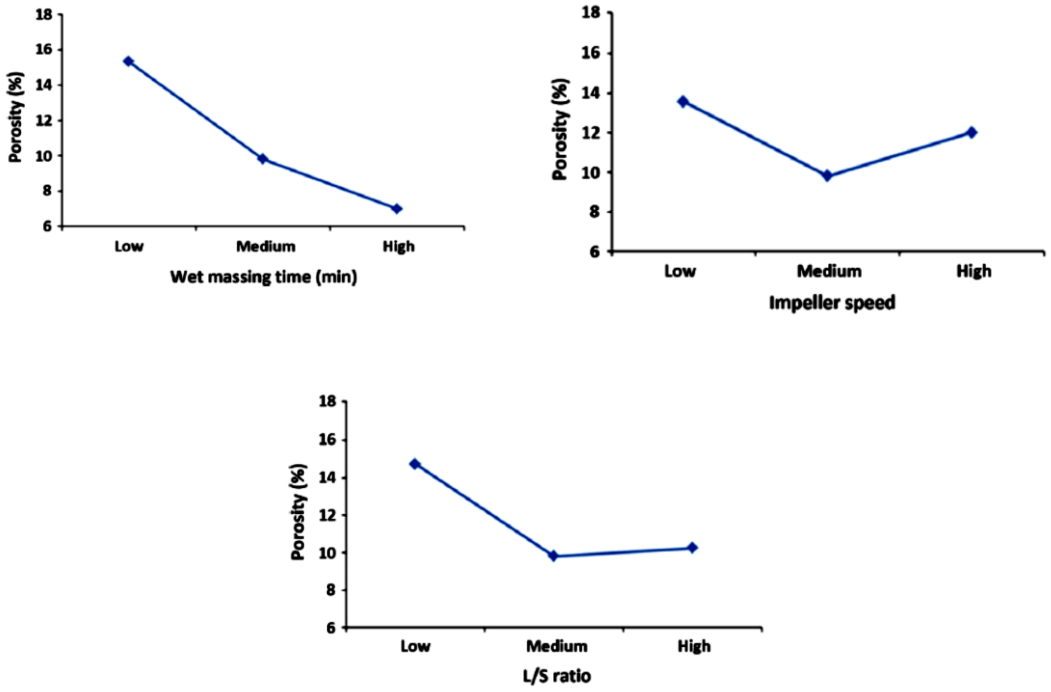

Figure 2-17 Effect of wet massing time, impeller speed and liquid to solid ratio on granule porosity (Oka et al., 2015).

To recap, many researches (Dries & Vromans 2002; Fu et al. 2005; Iveson & Litster 1998a; Saleh et al. 2005; Seo & Schæfer 2001; Shi et al. 2011; Thies & Kleinebudde 2000; Schaefer & Mathiesen 1996a) generally stated that the granule porosity decreases with longer processing time because of the consolidation process that may take place with extended process. However, this might not happen in some cases particularly when breakage process occurs. On the other hand, according to other investigators (Dévay et al., 2006; Gluba, 2005; Ohno et al., 2007; Oulahna et al., 2003) the granule porosity commonly decreases with increasing the impeller speed and liquid to solid ratio.

2.6.5 specific surface area

The specific surface area (SSA) of the granules could be affected by the granulation time and the amount of the binder. The SSA could reduce with increasing the granulation time and the amount of the binder. Shi et al. (2011a) studied the effect of massing time in high shear granulator on the characteristics of the granule products (MCC granule) including the specific surface area (SSA). They noticed significant effect of the massing time on the SSA. They found that the surface of the "well-plasticized" MCC granules was tending

to be smoother with longer massing time due to extensive shear and compacting inside the granulator. The surface area was decreasing during the first 10 min, then no significant change was noticed after that time, see Figure 2-18.

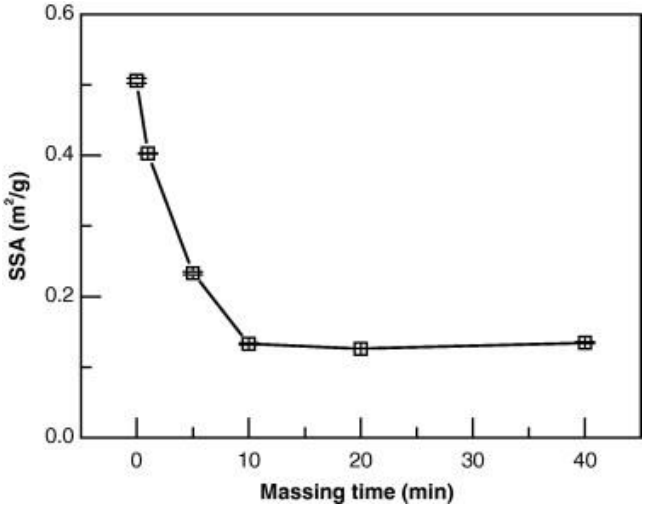

Figure 2-18: Effect of massing time on the granule specific surface area, (Shi et al., 2011a).

In another study carried out by (Shi et al., 2011b), they found that the specific surface area was decreasing with increasing the binder content and the level of change was depending on the amount of binder in the granules. A high decrease was noticed when the binder content increased from 25% to 45% while low decrease was noticed when the binder content changed form 5% to 25%. The reason behind this reduction, as they argued, was either due to the reduction of the fine features at the surface of the granules or the reduction in the intra-granule porosity.

2.6.6 Dissolution

The process of dissolution of a porous object by a liquid solvent is complex chemical process (McLeod et al., 1999). The dissolution process of granules is the measure of the granule ingredient released into a liquid solvent (Pitt and Sinka, 2007). The solvent usually tends to dissolve or break the binding material that exists between the primary particles of the granules. Hereby, the granule will disintegrate to its constituents and the dissolution process persists if the primary particles are dissolvable in the solvent. The dissolution process could highly be affected by the surface area and the porosity of the

granule, since the dissolution process takes place at the interface between the granule (solute) and the liquid (solvent). The hydrophilicity of the materials and the presence of disintegrants may also affect the dissolution process (Pitt and Sinka, 2007). However, the effect of the process and formulation variables on the granule dissolution were studied by many researchers.

Mangwandi et al. (2010) investigated the influence of impeller speed of the high shear mixer on the dissolution time. The powder they used was potato starch and lactose monohydrate, while they used two binders of different viscosities (HPC solution as high viscosity binder and water as low viscosity binder). They observed that the increase in the impeller speed causes a decrease in mean dissolution time of the granules produced with low viscosity binder. A reverse trend was observed for the granules produced with high viscosity binder, see Figure 2-19. This was due to, as they suggested, the change in the granule porosity that took place as a result of changing impeller speed.

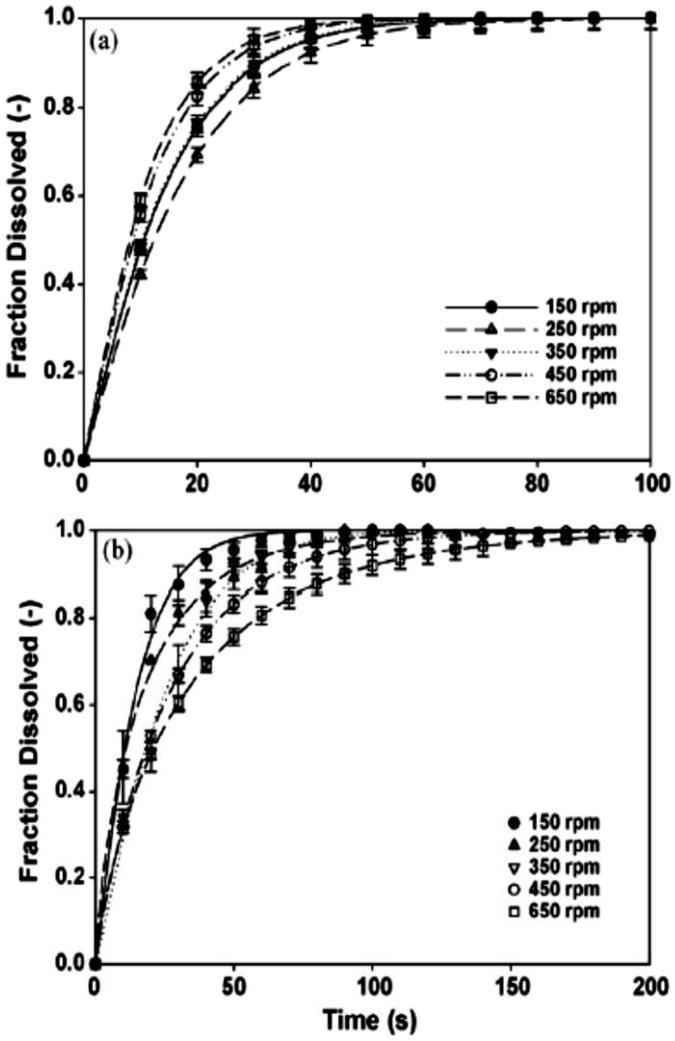

Figure 2-19 Granules dissolution profile, (a) low viscosity binder used, (b) high viscosity binder used, (Mangwandi et al., 2010).

Le et al. (2011) investigated the mechanisms of nucleation, growth and consolidation, and breakage on microscopic scale of single granule and their influence on granule characteristics e.g. porosity, binder content and dissolution. They used high shear mixer to granulate lactose and potato starch as a primary powder and Hydroxypropyl cellulose (HPC) solution as a binder. They added Sodium chloride (NaCl) to the powder to examine the dissolution rate. They concluded that the internal properties of the granules may also affect their dissolution besides to the granule properties which are, in consequence, could be affected by the process variables such as impeller speed and particle size. They noticed that some granules which are formed by virtue of coalescence and they named them as coalescence granule (COAG) dissolve faster than the consolidation granules (CONG) which are formed as a result of consolidation for different granule sizes, see Figure 2-20.

They argued that the consolidation granules (CONG) were containing more binder, low porosity and stronger than the coalescence granules (COAG).

Albertini et al. (2004) found that the granule surface morphology was important for the dissolution process while they were comparing two types of granules, smooth surface granules and rough surface granules. They noticed that the smooth granules were dissolving slower than the rough one. They ascribed this to the difference in the surface area besides to the difference in the porosity.

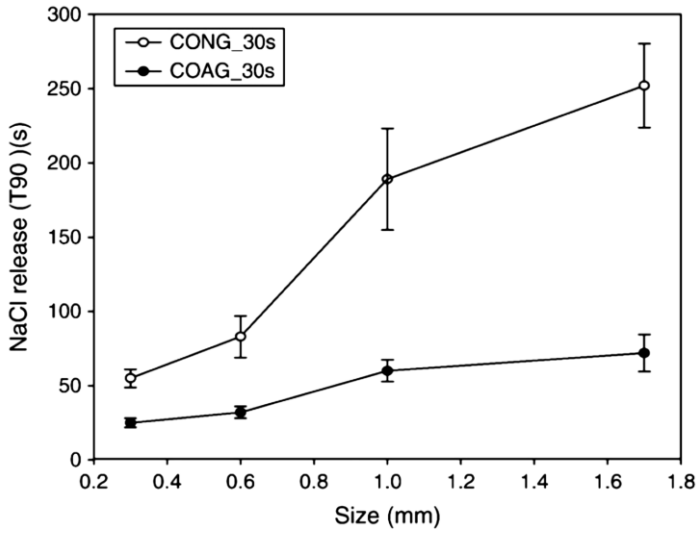

Figure 2-20 The dissolution rate of the coalescence (COAG) and consolidation (CONG) granules, (Le et al., 2011).

Flore et al. (2009) carried out comparative study on different granulation methods. They used water as binder to granulate dry polymeric powder in an intensive mixer (Eirich R02), fluidized bed. They also compared the granules produced by roller compactor and fluidized bed using spray granulation. They compared the rate of the granule dissolution of the products. They found that the granules of the high shear mixer and fluidized bed were dissolving in short time compared to the others. While the granules produced by the spray granulation of aqueous solution in fluidized bed needed longer time to dissolve.

2.7 Granular Flow in High Shear Mixer

In this section, the flow characteristics such as velocity vectors of the granules in high shear mixer will be explained along with the relevant measurement techniques.

Motivations: Since the particles and granules are moving continuously with different speeds in high shear mixer as a consequence of impeller and chopper movement, the flow characteristics of the granules, for instance, velocity vector, could elucidate what sort of forces are exerted on the particles or the granules. This in turn may lead to understand how the forces, for example impact forces and shear forces, affect the interaction between granules themselves or between the granules and mixer parts which influences essentially the rate of growth, coalescence and breakage.

2.7.1 Flow Measurement Techniques

Considering the importance of granular flow measurement for granulation study, a number of non-invasive techniques have been employed by many workers (Litster et al., 2002; McCarthy et al., 2000; Muguruma et al., 2000; Plank et al., 2003; Ramaker et al., 1998), for example, Positron Emission Particle Tracking PEPT, Laser Doppler Velocimetry LDV and Particle Image Velocimetry PIV. In these methods, granules are tracked either by optical methods (e.g. LDV and PIV) or by using radioactive materials (PEPT). On the other hand, numerical simulation can also be used for the same purpose (Michaels, 2003; Muguruma et al., 2000). Although numerical simulation could provide more information and details about the velocity profile, it has some drawbacks. Most of simulations are based on assumptions and they are not exactly compatible with real situation. In addition, it depends on computers ability. In the following sections, the mentioned measurement methods will be explained.

2.7.1.1 **Positron Emission Particle Tracking (PEPT)**

Since 1990s, many researchers have been working this technique for tracking particles and granules trajectory in dry and wet mixing processes (Broadbent et al., 1993; Forrest et al., 2003; Laurent et al., 2000; Ng et al., 2007; Parker et al., 2002). This method is alternative and modification of (PET) Positron Emission Tomography which is broadly used in medical field. It is based on tracking a single particular tracer particle path (in space and time) in the granulation equipment. The tracer particle is usually an isotope (proton-rich) of some materials, for instance, ^{22}Na, ^{18}F and ^{64}Cu. These materials produce some elementary particles and species such as a positron (e^+), a neutron (n) and a neutrino (ν) as a result of their decay. The positron (e^+) may collide inelastically with surrounding

electrons producing photons of gamma rays. These photons are then detected by a certain type of detectors and analysed by an electronic system. By this method, it is possible to have a 3D flow pattern of granular flow in high shear mixer. Despite of the advantages of this method e.g. non-invasive and 3D measurement of granules velocity and acceleration, it has some drawbacks and limitations (Bridgwater et al., 2004) that have to be taken in account, as in the following:

1. The geometry and the type of material of the equipment have a considerable effect on the measurement, as it may attenuate and scatters the signals.
2. The size and material type of the tracer particle necessarily needed to be the same as the feed material in order to avoid misrepresentation and inaccurate results due to incompatibility in physical properties.
3. By increasing the speed of the tracer particle, the spatial resolution reduces.

2.7.1.2 Laser Doppler Velocimetry (LDV)

Laser Doppler Velocimetry (LDV), or sometimes called as Laser Doppler Anemometry (LDA), is another non-intrusive technique used for estimating and measuring local particle size and velocity instantaneously. The method is based on using two beams of laser light intersecting at the same point (measurement point) constructing fringes. When the particles or granules pass through the constructed fringes, laser light will scatter with a shift occurrence in light phase (Doppler shift). The scattering phenomenon is based on Mie scattering theory (Hagemeier et al., 2015). The forward or the backward scattered light is then detected by optical detectors and the signals are analysed and displayed on a screen. Since this method is well-known in many text books (Albrecht et al., 2003; Durst et al., 1981), further details and general methodology explanation is not mentioned here. Apparently, this technique has limited applications because it needs optical access to the measuring point in the system. In addition, the occluded particles and granules will not be included in any determination of velocity vectors of the particles. Regardless of the mentioned limitations, Laser Doppler Velocimetry is widely used as measurement equipment in many studies namely in multiphase flow systems. The technique is confidently used by some investigators (Ibsen et al., 2002) for experimental researches in the fluidized bed of metal particles. It is also employed by Darelius et al., (2007) to measure the velocity of particles in high shear mixers.

2.7.1.3 Particle Image Velocimetry (PIV)

This technique is primarily used for studying the velocity gradient of fluid flow in different sections of ducts and channels. It is also used to monitor the granule movement in the granulators. High speed camera is usually used in this technique to take optical images for the moving granules (or powder). The frame rate, resolution and shutter speed of the camera besides to the intensity of the light should be chosen appropriately to ensure high quality images for the moving objects could be obtained. The images are then analysed with particular software that gives the velocity profile.

The technique is used by many researchers in different granulators. It is used for investigating particles flow in small size fluidized bed by Rix et al. (1996). They used Aron-ion laser as a light source and motor-driven camera for recording images. They presented the nature of the flow of the particles at two different levels above the surface of the glass ballotini particle bed.

The surface velocity of moving powder in a 25 L PMA Fielder mixer was measured by Litster et al. (2002) using PIV. The measurement was for the purpose of determining the area flux of particle bed passing through the spray zone, which is used in dimensionless spray flux calculations. They used a high speed camera (500 frames per second) and kept it inclined at an angle 45º centred on the sprayed area. The powder surface was illuminated with a large spotlight. A batch of 6-kg dry lactose powder was moved at impeller speed range from 100 to 500 RPM and the flow pattern was measured. The images taken by the camera were analysed by certain image processing software known as MetaMorph® (Universal Imaging, PA, USA). They observed two different flow regimes Bumping flow and Roping flow. In the Bumping flow the powder surface stays horizontal but the bed moves up and down when the impeller passes underneath. While in the Roping flow, the powder moves from the bottom to the top in the areas close to the vessel wall and then falls down towards the centre.

Chouk et al. (2009) used PIV system to study the behaviour of binder droplet (PEG 200) while it contacts a dynamic bed of calcium carbonate powder in a high shear mixer. They used a high speed camera of 2000 frames per second to take the images of droplet contacting the powder bed. These images were processed by using a PIV package in MATLAB called MPIV. They obtained velocity vectors for the droplet and the powder bed in x and y directions, as shown in Figure 2-21. They calculated the surface velocity

with a 0.5 ms temporal resolution. In addition, they obtained the vertical and horizontal relative velocities by subtracting the vectors from each other.

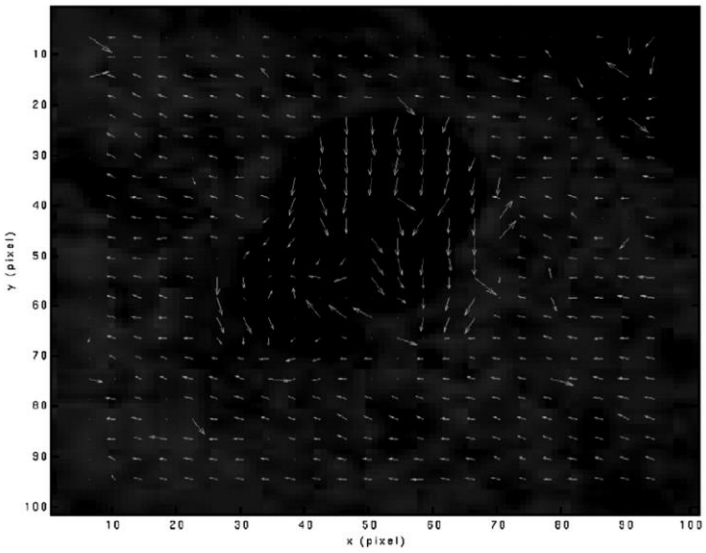

Figure 2-21 Velocity vectors (white arrows) of powder surface and droplet (Chouk et al., 2009).

Another set up was employed by Conway et al. (2005). They examined experimentally the flow and segregation of granules mixed by an impeller having four blades and inclined at 45º in a cylindrical container. They used a CCD camera with 0.15 mm/pixel of spatial resolution and 500 frames per second. Two cameras are directed to the mixer, one from top and the other from side, as shown in Figure 2-22. A dry sand near-monodispersed (355 to 425 µm) was used for characterizing the flow and polydispersed glass particles to study granule segregation in the mixer. They measured instantaneous and average velocity vectors as well as measuring fluctuation of flow fields at exposed surfaces (i.e. top surface and close the wall).

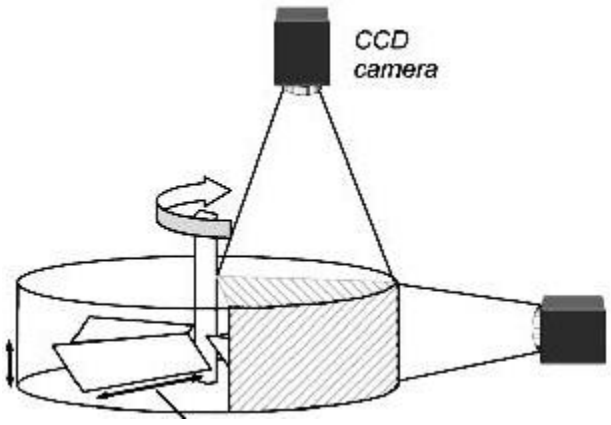

Figure 2-22 the schematic diagram of camera setup used by (Conway et al., 2005).

Nilpawar et al. (2006) used this method for measuring powder velocity in a high shear mixer. In this work, the influence of the viscosity of the liquid binder on the particle velocity has been studied. They used two liquid binders Polyethylene Glycol (PEG400) and Glycerol in which they are different in viscosity. The powder was calcium carbonate (Durcal-40). They noticed that the powder flow was affected by the viscosity of the binder. Where the powder motion was more sluggish when viscous liquid was used.

Many workers considered the granular flow during granulation process to be the same as the flow of powder in the granulator at steady state. However, this might not be acceptable in some cases especially when the granule properties change with granulation time, which leads to variation in flow pattern. Dorvlo (2010) investigated the velocity of powder in a high shear mixer using PIV. It was noticed that the surface velocity of powder bed decreased as the time of granulation elapsed.

There are some limitations in the PIV technique. It lacks the three dimensional information especially in the opaque systems, which is the strength point of PEPT technique. For this reason, the PIV technique is mainly used for surface velocity measurement (two dimensional). There is another point which is related with resolution of the camera. If the spatial resolution increased, the temporal resolution will be affected and vice versa. In addition to the above, some other problems can also contribute to the PIV limitations particularly when dealing with systems of powder, in which it can produce dust and obscure the powder surface.

2.7.2 Power consumed/torque of the impeller

The power consumed during mixing the granular materials as well as the torque of the impeller have been frequently used mutually as an indication about how the process parameters, for instance impeller speed, and the geometrical configuration of the mixer can affect the flow pattern inside the granulators (Cavinato et al., 2013). However, measuring the consumed power is usually preferred as it its measurement is straightforward (Hansuld and Briens, 2014).

It is known that by adding the liquid binder to the dry powder leads to an increase in the torque. This increase could be result from the presence of a free liquid on the surface of the particles, which tends to dissipating the applied energy to overcome the surface tension (capillary forces) and the viscous forces (Knight et al., 1998). This was

investigated by Knight et al. (1998). They found that by adding an excess binder to the powder, the torque increases. They also noticed a sharp increase in the torque during initial time of binder addition, and they attributed that to the compaction of the granules.

The power consumption is usually plotted versus granulation time or binder content. A typical profile power consumption for power consumption during wet granulation process is given in Figure 2-23 (Hansuld and Briens, 2014; Pepin et al., 2001). The x-axis in the figure is the percentage of the liquid and sometimes it is replaced by granulation time (Hansuld and Briens, 2014). There are four phases in the power curve. Phase I in which the power is constant at W_0 where no powder agglomeration takes place. By adding the binder the powder particles starts agglomerating with each other and more power will be consumed, as in phase II. Then followed phase III in which a plateau in the power profile observed indicating to achieve a useful granule. In the last phase IV, when over-wetting takes place there will fluctuation in the power curve, then the power curve will diminish when the when the powder suspends in the binder.

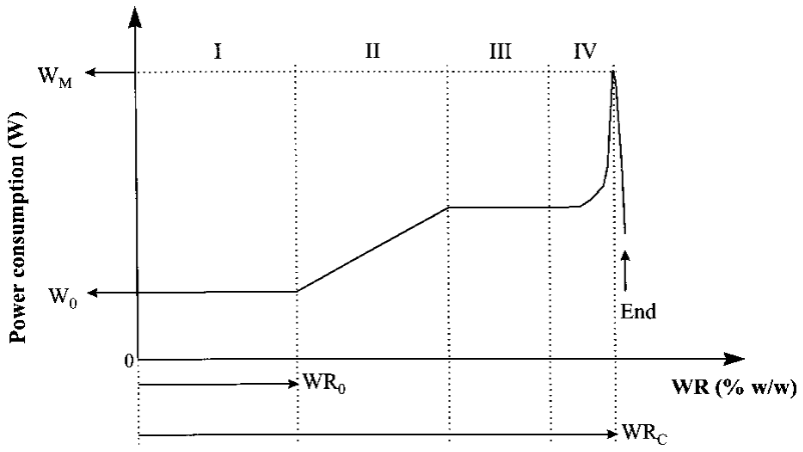

Figure 2-23: A sample of power consumption profile. W_M is the maximum power consumption, W_0 is the dry mixing power consumption, WR_0 represents the liquid required to increase the power from W_0, and the WRc is the liquid needed to for overwetting the powder, (Pepin et al., 2001).

2.8 Conclusion

The granulation process is usually conducted via the "normal granulation method" to produce granular products with most suited to the users' requirements. For this reason, numerous work can be found in literature tackling the influence of the granulation process parameters, namely in the wet granulation process, on the granular product characteristics such as size distribution porosity and dissolution, in which they are an important issue in many industrial applications. Generally, it could be noticed from the literature that the granule size is usually increases with the granulation time and the size distribution at the beginning of the granulation process is wider compared to the end of the process. Besides, the granules get denser with time which makes the dissolution time of the granules longer due to a decrease in the number of pores in the granule. Such available information in the literature is usually utilized to choose the best condition to get certain granule property in the industry. The aforementioned studies were conducted by following the granulation process normally, i.e. all the process parameters were fixed during the granulation process. This process is named in this work as Normal Granulation (NG). Although this method is studied well and utilized by the end users, there is still need to develop a new granulation process (not available in the literature) to obtain better granular product characteristics, e.g. size distribution and dissolution time, at the end of the process.

A new granulation process was conducted in the current work. This process is called as Multi-Stage Granulation (MSG) as the process parameters, namely the impeller speed, will be changed during the granulation process (three stages of process parameter). This granulation method could potentially affect the granule properties, hence, its effect on the granule properties will be investigated in the current work. To date, the author is not aware of any research which has been conducted utilising Multi-Stage Granulation.

To investigate the process of MSG in more details, the flow of the granular bed inside the mixer will be studied by the PIV technique. The importance of this study increases by knowing that the granule velocity has crucial effect on the granule properties. Meanwhile, there is limited work available in the literature about the flow of the granule in the Eirich mixer that is used in the current study. Besides to the PIV study, the system will be simulated using DEM simulation, which can give more insights to understand the process of MSG.

CHAPTER 3 MATERIALS AND METHODS

3.1 Materials

The granulation materials that were used in the current work were calcium carbonate powder ($CaCO_3$) and Polyethylene Glycol (PEG). Calcium carbonate was chosen in the current work as the reduction in the primary particle size during the granulation processes was expected to be less as it known to be hard material. The reduction could be due to the high speed impact of the mixer's impeller. While Polyethylene Glycol was chosen to reduce the change in the binder content during the granulation process as its boiling point is high compared to other binders (namely water solution binders). The following are some properties of these materials.

3.1.1 Calcium carbonate ($CaCO_3$)

Calcium carbonate in its nature is a tasteless and odourless white powder. It is used as pharmaceutical excipient particularly used as diluent in solid-dosage forms. It is also used as food additive. The calcium carbonate used in the current research is supplied by Longcliffe Quarries Ltd., UK. The particle size distribution was measured by using the Camsizer (XT0164, Retsch Technology, Germany), and is given in Figure 3-1 with median size. The powder was examined for the shape using SEM as shown in Figure 3-2.

Calcium carbonate has the following specifications (Armstrong, 2009):

- Specific gravity (true density): 2.9 g/cm^3.
- Melting point: It Decomposes at 825 ºC.
- Flowability: Cohesive.
- Solubility: Practically, it is insoluble in ethanol (95%) and water. Ammonium salts and carbon dioxide may increase its solubility in water.

The powder has the some impurities and the ingredients are given in Table 3-1 which is provided by the supplier.

Table 3-1: Ingredient of the $CaCO_3$ powder used.

$CaCO_3$	**99 %**
$MgCO_3$	0.3%
Al_2O_3	0.2%
SiO_2	0.3%
Others	0.2%

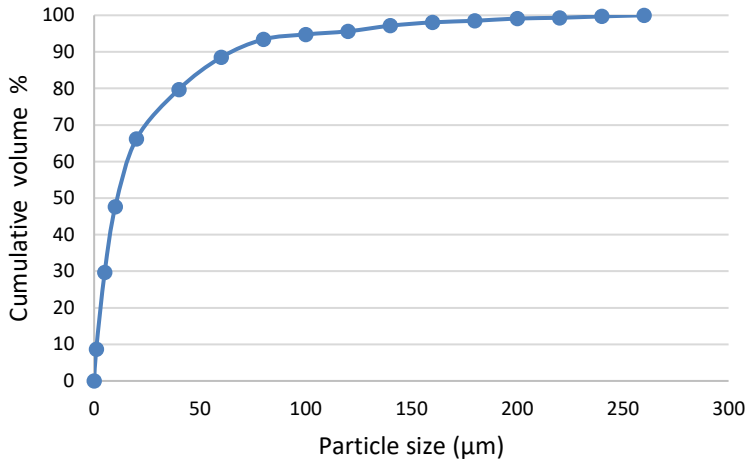

Figure 3-1: Size distribution of calcium carbonate, based on volume. d_{10}=5 µm, d_{50}=14 µm, d_{90}=74 µm.

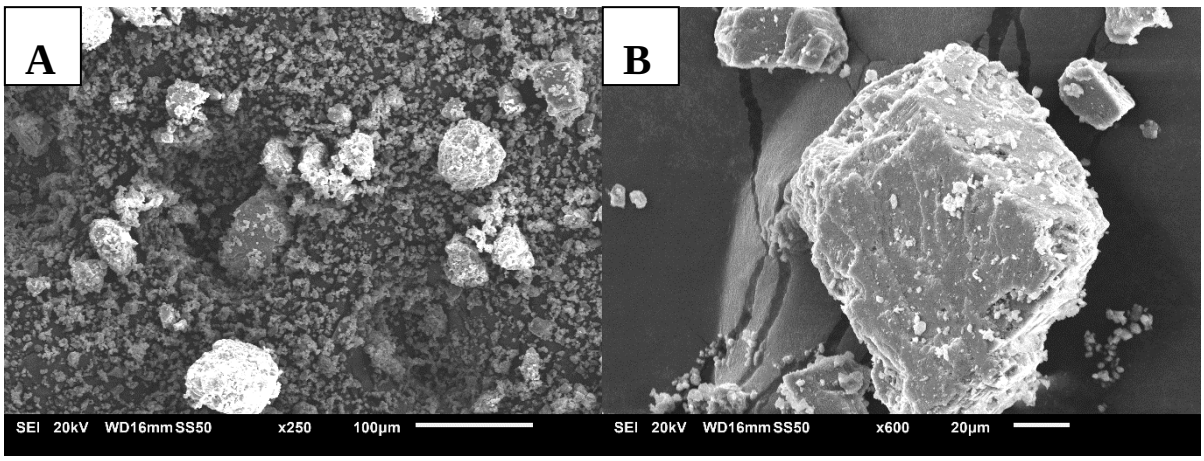

Figure 3-2: SEM image for the CaCO3 powder particles, A) Magnification = x250, B) Magnification = x600.

3.1.2 Polyethylene Glycol (PEG)

Polyethylene Glycol (also known as polyoxyethylene glycol or Carbowax) is a polymer that has a chemical formula $HOCH_2(CH_2OCH_2)_mCH_2OH$. Its chemical structure is given in Figure 3-3, where *m* represents the number of groups of oxyethylene that exists in the molecule.

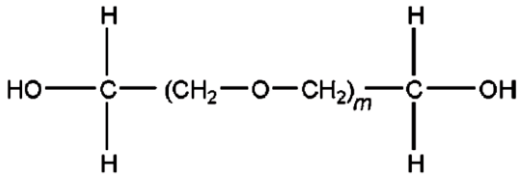

Figure 3-3: Structural formula of Polyethylene Glycol (PEG), (Armstrong, 2009).

PEG is the abbreviation used for Polyethylene Glycol. It is always followed by a number representing the average molecular weight. For PEG 1000 which is used in the current work, has m=22.3 and its average molecular weight = 950 - 1050 (Armstrong, 2009). The physical properties of PGE depend on its grade. For grades more than 1000 (PEG>1000), they occur mostly as white colour, solid or waxy form and they almost have sweet odour. Table 3-1 below, shows some specifications of PEG1000 (Armstrong, 2009):

Table 3-2: Specification data of Polyetheylene Glycol (PEG1000), (Armstrong, 2009).

Property	Quantity
Melting point	37–40 ºC
Boiling Point (760 mmHg)	> 200 °C Decomposes
Kinematic Viscosity	16.0 - 19.0 mm^2/s
Molecular Weight	950 - 1050 g/mol
Appearance	Waxy solid
Density	1.15–1.21 g/cm^3 at 25 ºC

Although the low grades of PEG (average molecular weight less than 2000) are hygroscopic, most of them are stable chemically in solution and in air and they do not assist microbial growth. Polyetheylene Glycols are widely used in different pharmaceutical formulations, including cosmetics and medicine.

3.1.3 Eirich mixer

The granulator that is used in this work was an intensive mixer from Maschinenfabrik Gustav Eirich GmbH (type: EL1). It has a unique design. The impeller is situated eccentrically to the centre of the vessel and there is a scrapper fixed at the top lid which tends to scrape any powder or granules that may stick to the wall of the vessel. Figure 3-4 shows a simple diagram of the mixer and Figure 3-5 shows the top and side view of the impeller, vessel and scrapper of the mixer. The motor of the impeller is positioned on the lid as well. It rotates the impeller from the speed of 300 to 7200 RPM. The impeller has a disk shape of 8 cm diameter with six small blades distributed around the disk and there are six small pins fixed on the disk perpendicularly. The wall of the vessel is made of stainless steel and its dimension is given in Figure 3-5. It rotates clockwise at two different speeds (85 RPM and 170 RPM). To measure the temperature of the material inside the vessel, the machine is provided with a thermocouple which could be inserted into the vessel from an opening at the top lid. The thermocouple is connected to the same machine via a cable and the data can be taken directly from the machine. This mixer was employed in the currect work because it can work in low shear and highe shear conditions distinctively in a single granulation process which is required to conduct the granulation process in the current work. In addition, the movment of the impeller and the vessel simultaneously could helps to distribute the material inside the mixer more evenly.

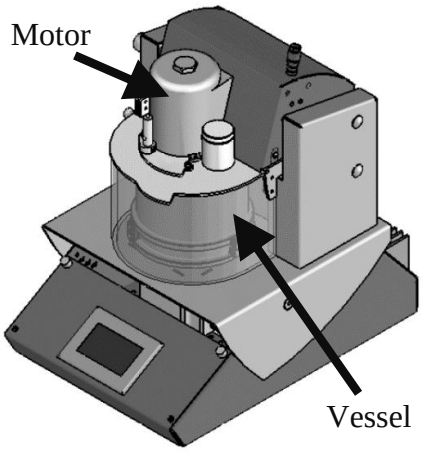

Figure 3-4: Eirich mixer, type: EL1 (Eirich GmbH & Co KG, n.d.).

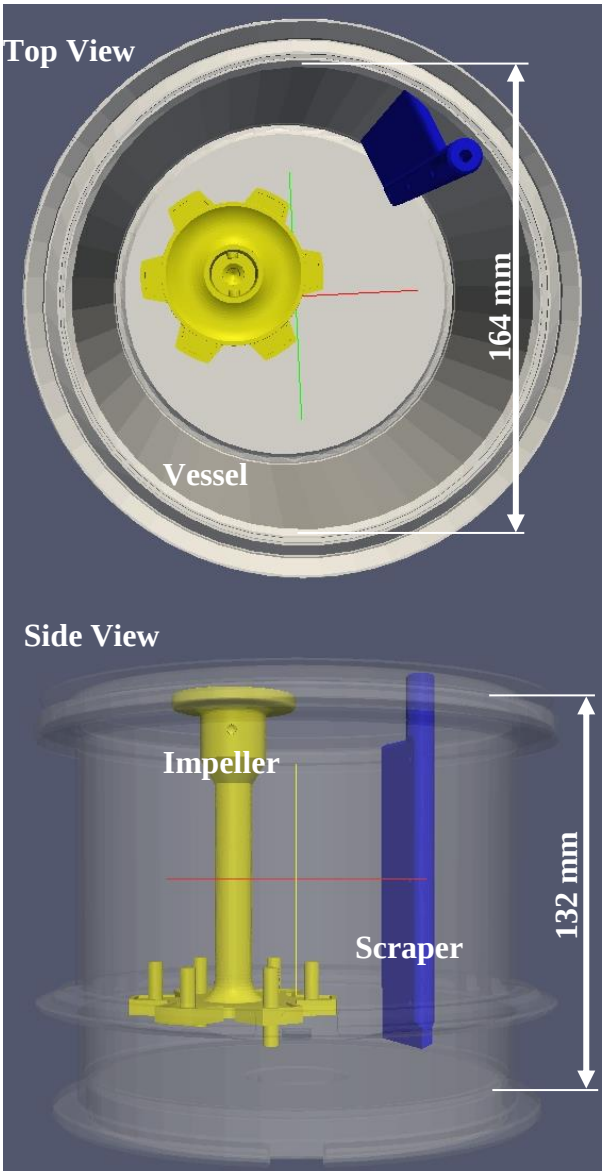

Figure 3-5: Top view and side view for the vessel, impeller, and scrapper of Eirich mixer.

3.1.4 Modified mixer

Some parts of Eirich mixer was modified for this study. The window on the lid of the mixer which is used for viewing was enlarged for better viewing. In addition, a hot air jacket was added around the vessel's wall (from outside) in order to control the temperature of the mixture inside the vessel, (see Figure 3-6. A hot air blower was used at about 50 °C and temperature was fairly fixed at that temperature. This is important since the binder viscosity may change with temperature, but the hot air jacket will tend to hinder this changes.

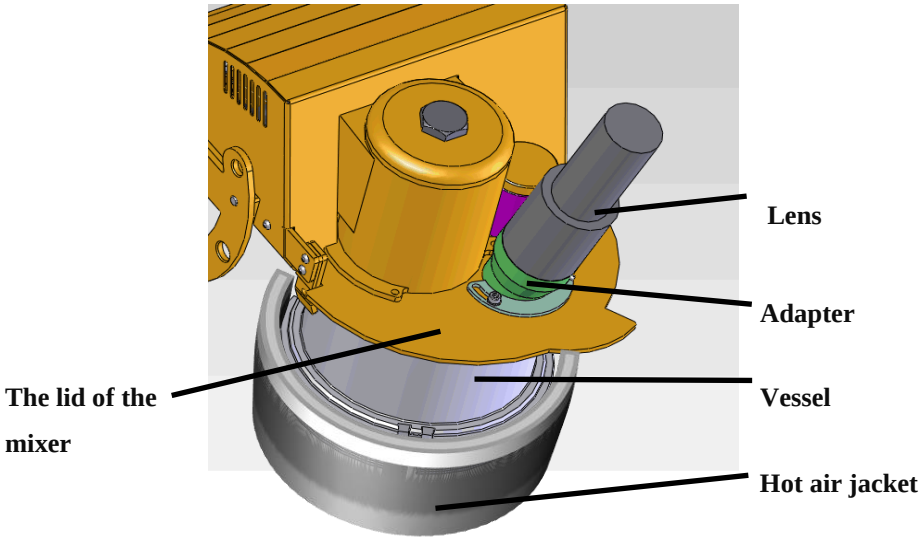

Figure 3-6: The diagram of the modified mixer, adapted from (Eirich GmbH & Co KG, n.d.).

3.2 Granulation procedures

3.2.1 Preparations

Beforehand starting the granulation process, the materials used in the process were prepared, firstly. This includes preparing the powder and the binder. Batches of calcium carbonate powder (500 g) were pre-heated in an oven at 50 °C alongside with the binder (PEG1000) which is solid at room temperatures (Knight et al., 1998). The materials were left in the oven overnight to maintain both of them at the same temperature. It is important to do this step, to avoid any problematic issue that may arise when adding the liquid binder on top of the powder bed. Where, if the powder bed was cold and the liquid binder was hot, the binder viscosity may change when they will meet. This temperature (50 °C) was

chosen to ensure that the binder (PEG) will be in liquid phase during the granulation process. Different powder loads were examined in the experiments (ranging from 250 g to 1250 g). The one which was chosen eventually was 500 g as this amount of powder was sufficient and allowed a better view to visualize how the impeller impacts the powder bed and how the granules impact each other in some areas inside the vessel namely in area around the scrapper.

On the other hand, the temperature of the vessel was preserve as close as possible to the temperature of the materials, i.e. (50 ± 3 °C), using the heating system (hot air jacket). The temperature of the used hot air was 50 - 55 °C and the velocity was 12 -12.5 m/s. The temperature inside the air jacket was controlled automatically using a temperature sensor which give feedback to the hot air blower. This procedure ensures having granulation process at constant temperature. Notice Figure 3-7 which shows the temperature profile for the material inside the mixer during the whole granulation time.

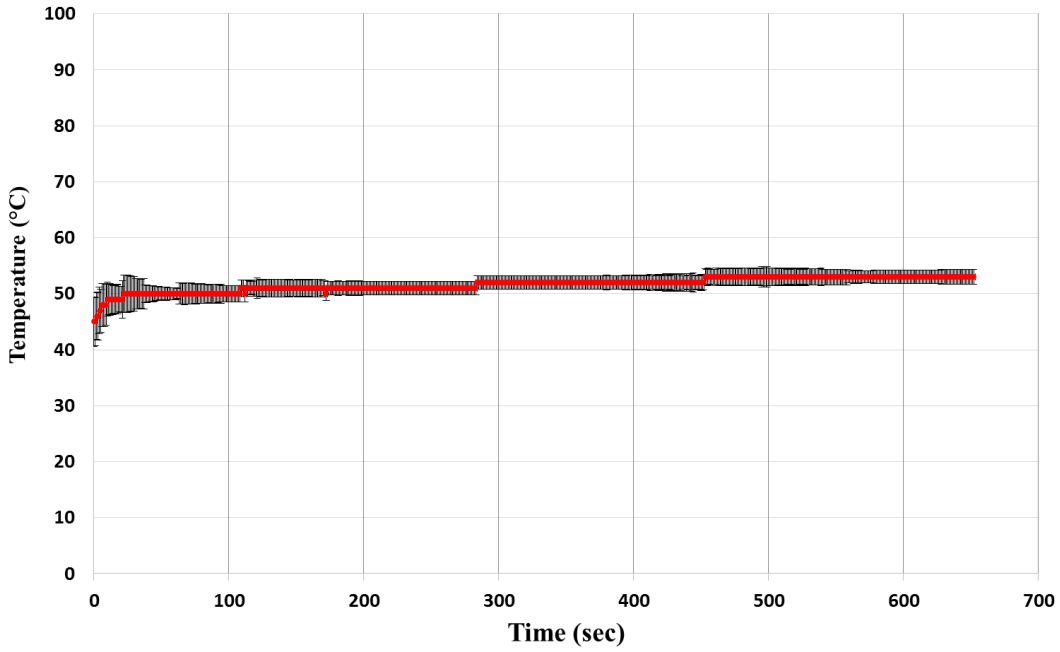

Figure 3-7: Temperature inside the mixer during a whole typical granulation process.

3.2.2 Granulation process (protocol)

The heated powder was added into the vessel of the mixer after the temperature of the vessel had reached approximately 50 °C (± 3 °C). The dry powder was premixed firstly

for about 100 sec. This period of time was enough to obtain a uniform temperature for the powder bed, see Figure 3-7. Then, the binder was added on top of the powder bed by pour-in method using an appropriate size syringe. The rate of addition was about 1 g/sec. The level and the position of the binder addition point were kept at the same position in all cases. Binder addition time was about 70-75 sec. The binder was falling on the powder bed continuously

After the step of binder addition, two method of granulation were conducted during this study based on how the process parameters were set, Normal granulation (NG) and Multi-stage granulation (MSG).

In normal granulation (NG), all the process parameters were fixed from the start point of the granulation process till the end of the process. The process parameters in the Table 3-3 were used in this work. It includes granulating with at two different liquid to solid ratios (0.14 and 0.15) and two impeller speeds (2000 RPM and 7000 RPM). If the impeller speed was 2000 RPM the vessel speed was 85 RPM, while it was 170 RPM if the impeller speed was 7000 RPM. The purpose of conducting these granulation processes were to examine how the granules properties will be under normal granulation process (NG).

Table 3-3: The process variables of the normal granulation process.

L/S	Impeller speed (RPM)	Vessel speed (RPM)	Granulation time (sec)
0.14	2000	85	200, 300, 400, 500, 600, 650
	7000	170	
0.15	2000	85	200, 300, 400, 500, 600, 650
	7000	170	

In the new process (MSG), the process parameter was changed throughout the granulation process for a certain duration of time making three different stages of the process parameter for a single granulation process. The main parameter which was changed here was the impeller speed. The granulation stages were as follows, see Figure 3-8:

- ✓ First stage: The impeller speed was fixed at 2000 RPM while the vessel speed was 85 RPM. This stage was considered as NG process as the speed of the impeller and the vessel are the same as NG process.
- ✓ Second stage: The impeller speed during this stage was changed abruptly to a higher speed at each different experiment. It was increased to 7000 RPM. The vessel speed was also changed during this stage from 85 RPM to 170 RPM. This is because a lot of granule were caking on the scrapper when the impeller speed was high and the vessel speed was low. However, by increasing the vessel speed the amount of caking reduced. This stage was considered to be intense shear granulation.
- ✓ Third stage: This stage was the same as the first stage, normal shear granulation stage but the granulation time was short (50 sec), see Table 3-4.

The change in the profile of the impeller speed and vessel speed was looking like a pulse change. If the first stage was relatively short (300 sec including the pre-mixing and binder addition time) then the pulse change is the speed was called Early Pulse (EP). While, if the first stage was relatively long (500 sec including the pre-mixing and binder addition time) then the process was called Late Pulse (LP). Table 3-4 and Figure 3-8 illustrate the process parameters.

Table 3-4: Process parameters in multi-stage granulation (MSG)

Process	First stage (including the time for the binder addition + pre-mixing)		Second stage		Third stage	
	Time (sec)	Speed (RPM)	Time (sec)	Speed (RPM)	Time (sec)	Speed (RPM)
EP	300	2000 (Impeller) 85 (Vessel)	100	7000 (Impeller) 170 (Vessel)	50	2000 (Impeller) 85 (Vessel)
LP	500	2000 (Impeller) 85 (Vessel)	100	7000 (Impeller) 170 (Vessel)	50	2000 (Impeller) 85 (Vessel)

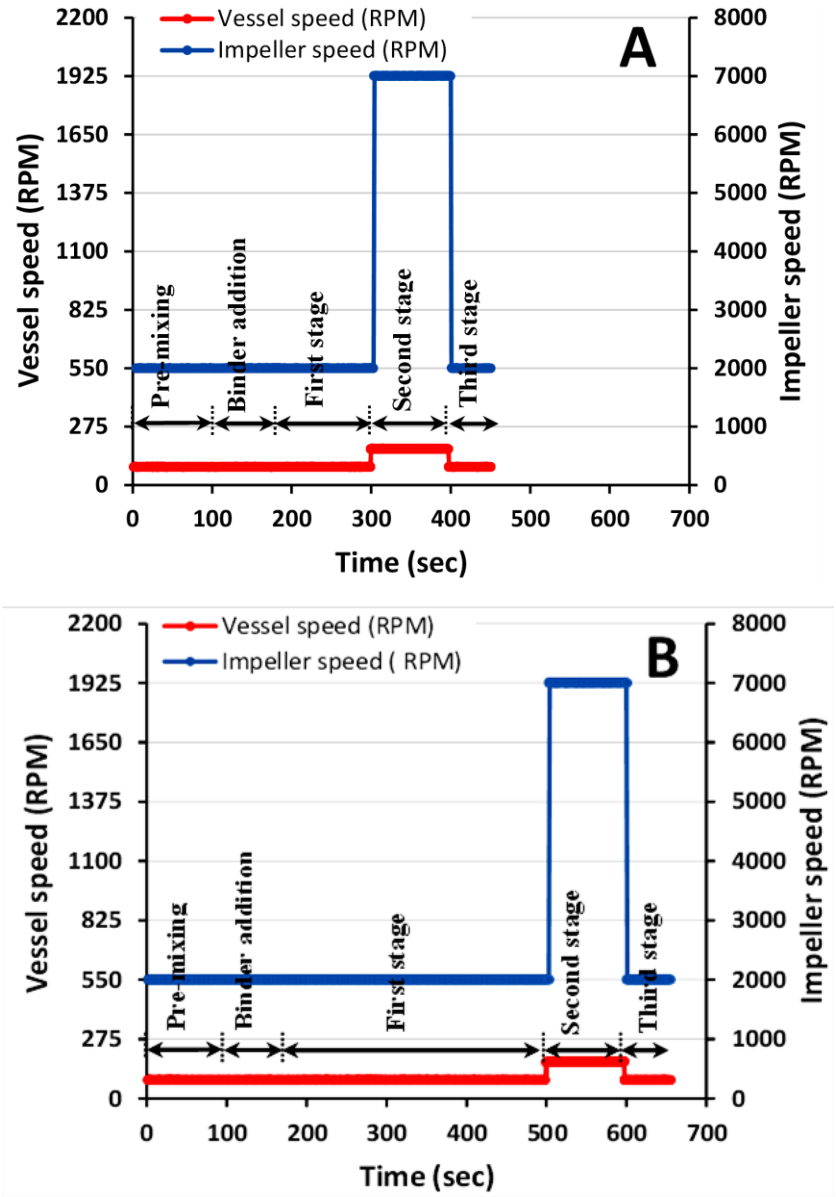

Figure 3-8 : The profile of the impeller speed and the vessel speed during MSG. A) EP process, B) LP process.

3.3 Granule size characterization

The size of the granule is one of the essential end product characteristics that needs to be determined after each granulation process. The size of the produced granules and the primary particles of the $CaCO_3$ powder was characterized by using two different size analysers Retsch Camsizer 0650 and Retsch Camsizer XT0164 (Retsch Technology GmbH & Co. KG, Germany), respectively. The first equipment can measure particle sizes within the range of 30 µm to 30000 µm, while the second one can measure particles of size range from 1µm to 3000 µm.The principle of measurement is based on analysing the images of granules and particles captured by two CCD cameras while the objects move between an illuminated plane (light source) and the two cameras. The cameras give the advantage of focusing on big and small particles at the same time. These equipment provides several characteristics e.g. size distribution, median size (d_{50}), aspect ratio, span, and sphericity.

The granule size presented in this work is the median size (d_{50}). It is the point in the size distribution that splits the population of the granules to 50% below and 50% above the median size. Since there are different types of the equivalent diameter for the particle size e.g. Chordal diameter, Feret diameter, sieve diameter …ect, the chordal mean (xcmin) was considered here, as it gives closest diameter to the sieving (Merkus, 2009).

In addition to sizing, sieving was used to separate samples of the granules to certain size classes to be prepared for further measurements e.g. the dissolution. Separation of the granules to size classes was, also, helpful to study the process of the breakage. Different sieve sizes (from 500 µm to 3000 µm) and a sieve shaker from (Retsch Technology, Germany) was used for this purpose.

In all cases of size characterization, a sample splitter was used to divide the big samples of the granules to a proper quantity (140 g) to be analysed. The measurement was repeated 3 times for each sample.

3.4 Shape and surface

The produced granules were viewed by an optical microscope to get more morphological information. A digital microscope (KEYENCE VHX-5000) was used to examine the

shape of the granules. It gives distinct visual outline of different shape of granules under test. In each test, more than 20 granules were examined via microscope (Tan et al., 2014).

In addition to the digital microscope, SEM (scanning electron microscope, Jeol, USA) microscope was also used for the purpose of examining the surface of the granules in more details. The samples (usually 2 or 3 granules) were first of all fixed on a stub using carbon tape, then it was coated with a thin film of gold and finally examined under SEM microscope. The voltage of the SEM was 10KV.

The SEM image usually illustrates more detailed information about the surfaces than the microscope namely at high magnification. On the other hand the digital microscope has the advantage of 3D viewing and numerical data e.g. surface profile and granule dimensions could also be obtained, unlike to the SEM.

3.5 Internal structure (*X-ray)*

The x-ray tomography is a non-destructive technique and gives the advantage of possibility of viewing the interior structure of the granules. In addition, it is helpful in calculating the total porosity, and visualizing the distribution and geometry of the pores within a single granule. Hence, it is has been utilized by many researchers in granule characterization (Barrera-Medrano et al., 2006). In fact, this technique is most frequently used in medical area, prior to be used in the granulation studies. The x-ray tomography was performed in the current work using microCT 35 (Scanco Medical AG, Switzerland). This technique was also used to evaluate the intra-granule porosity.

3.6 Porosity measurement of granules

3.6.1 Porosity definition

The porosity of the granules is an important parameter of the granular products, since it has a significant effect on some attributes of the final products. The porosity is the fraction of the pores volume to the granule volume. It is related to the density as they both depend on the volume of the granule. Different types of densities, for any granule assembly, could be defined based on which type of pores considered. The following are the foremost types of densities:

1. True density: sometimes called skeletal density, it is the mass of the material which composes a single granule divided by the volume of the granule excluding any closed pores within the granule and open pores at the surface of the granule.
2. Apparent density: This type of density takes in account the volume of the closed and open pores. So, it is the mass of the single granule divided by the volume of an imaginary envelope surrounding the single granule including its open and closed pores, see Figure 3-9.
3. Bulk density: is the mass of a number particles (or granules) divided by the totale volume of interparticle space, open pores, and closed pores.

In the current work, the apparent density is considered. This is because it is related to some important granule property, e.g. dissolution rate, in which it is highly dependent on the outer surface area of the granule. This density is important for the some physicochemical properties of the granule, e.g. solubility.

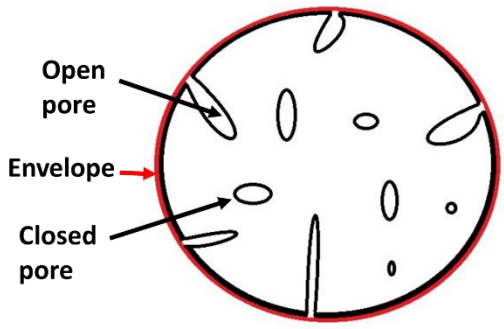

Figure 3-9: An imaginary envelope around a granule having open and closed pores.

3.6.2 Porosity measurement

Two methods are used to quantify the porosity of the granules, Liquid displacement method and x-ray. The porosity values presented in this work is based on the liquid displacement. However, the x-ray method was also used as an assistive tool to improve the scrutiny of the results:

3.6.2.1 Liquid displacement method

In this method, the volume fraction of pores or the average porosity was determined by measuring the apparent density of the granules and their true density (Gabbott, 2007; Iveson et al., 1996). The average porosity of the granules (ε) then given by:

$$\varepsilon = 1 - \left(\frac{\rho_a}{\rho_t}\right)$$ Equation 3-1

where ρ_a is apparent density and ρ_t is true density. The true density of the granules composed of two components ($CaCO_3$ and PEG1000) is given by:

$$\rho_t = \frac{\rho_s\, \rho_b}{\varphi_s\, \rho_b + \varphi_b\, \rho_s}$$ Equation 3-2

where ρ_s, φ_s, ρ_b, and φ_b are solid density, solid mass fraction, binder density and binder mass fraction, respectively. The mass fractions could be determined by separating the binder from the powder particles by heat, as it is followed by Gabbott (2007) and Knight et al. (1998). The granules under test are exposed to high temperature (around 500-600 ºC) in a furnace for approximately 2 hours, so that to remove the solidified liquid binder PEG1000 from granules and leaving calcium carbonate particles in the crucible container with no change in their mass. Then, by measuring the weight of the granules before and after the furnace, the quantity of each material could be determined. A precise balance of four digits is used for this purpose.

The apparent density is determined by measuring the mass of a group of granules (approximately 5 g of size calss 0.85-1.4 mm of granules were considered in this study) and the total envelope volume of the granules. The envelope volume of the granules was determined by measuring the volume of a liquid displaced by the granules in a 10 ml Pycnometer. The type of liquid should be chosen carefully, in order to get accurate results. Kerosene was used in this work since it does not dissolve the granule ingredient (i.e. PEG1000 and calcium carbonate). In addition, it can wet the surface of the granules, which is important to avoid retention of any air bubbles between the liquid and the granule surface (Gabbott, 2007; Knight et al., 1998). However, the liquid Kerosene can enter some of the open pores at the surface of the granule which increases the inaccuracy of the measurement method. This was checked by adding some dye in Kerosene and a granule was immersed in the dyed-kerosene which was examined under microscope. It was noticed that the areas which could be considered as open pores, were covered with dye, see Figure 3-10. This could cause a decrease in the measured porosity of the granules as some of the open pores will not be considered during measurement. This measurement is repeated for the samples three times and the average was considered.

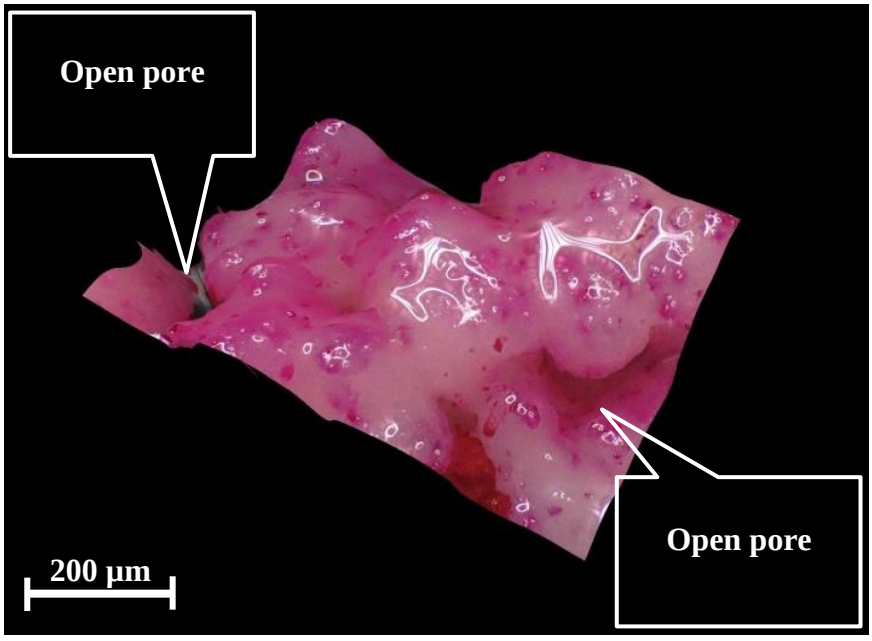

Figure 3-10: A section of a granule surface is coloured with red dye, after been immersed in kerosene contain red dye pigment. The figure shows how the dye reached into the open pores at the granule surface.

3.6.2.2 X-ray method:

Although the accuracy of a careful measurement of the liquid displacement method could be about ∓2%, the measurement may fail for very porous granules (Litster and Ennis, 2004). For this reason the porosity measurement is supported by x-ray tomography method. The X-ray tomography is the other method that used to quantify the porosity of the granules.

This method gives the advantage of possibility of viewing the interior structure of the granules (the geometry of pores and their distribution in a single granule), besides it is a non-destructive technique. However, it has some disadvantages; for instance, it relatively consumes long time to get the results compared to the other methods e.g. liquid displacement method. The method implies scanning a single granule (or more than one depending on the sample holder used) with the x-ray generating 2-D image which is a cross section image through a certain level in the granule. By taking a series of images through the granule, 3-D information could be collected. 240 images are taken during each measurement in this work. The obtained images then was analysed using certain software for example ImageJ. The x-ray tomography performed in the current work using micro CT 35 (Scanco Medical AG, Switzerland) which is setted to (70 kV, 114 µA) and

the software for the image analysis was ImageJ 1.50i, which is developed by "National Institutes of Health-USA".

In ImageJ, the despeckle tool (a function within the software) was used to improve the images . This tool takes the average of 3x3 pixel and replaces the center one with median value. This method removes some white pixles from air region that should be totally black, i.e. it reduces the noice in the image of the CT-scan. Then, the threshold of air (pores) is determined from the part of the image which is only air and considered as gray value for the pores within the granule. After that, the porosity is calculated by selecting an area within the granule image and dividing the number of air pixels by the total number of the pixels of the selected area.

3.7 Surface area measurement

The outer surface area is one of the significant "morphological" parameter that could affect the granules properties namely the dissolution time in water. Therefore, it is important to measure the surface area of the granules before implementing the dissolution test. The specific surface area SSA (units: mm^{-1}) which is known as the available surface area per unit volume (or per unit mass) of the granules is usually used to quantify the interfacial surface area of the granules (Punmia and Jain, 2005).

Different techniques are used to characterize the surface area of the granules Brunauer–Emmett–Teller (BET), Accupic and microscopy. A digital microscope (KEYENCE VHX-5000) was used in this work to quantify the SSA of the granules. This microscope is able to produce 3D images (fully-focused) in which the surface topography could easily be observed, and the geometrical information (e.g. surface area, volume and surface profile) could be taken numerically and the data could be recorded as well, This method was tested by using a known size metallic sphere and accurate results were obtained, see Appendix (A).

If the object to be characterized was a sphere, then KEYENCE microscope can see only a hemisphere (the upper part of that object) and it can give the surface area and the volume of that part. If the object is not identical in all directions (the two hemisheres are not identical), then the accurency of the measurement could be affected. By dividing the surface area by the volume, the SSA will be obtained. The SSA of 20 granules of similar

size was measured by this method and the average was considered (Tan et al., 2014). The 20 granule were taken from different positions of a small batch of sieved granules of size class 0.85-1.4 mm. This small batch was obtained by dividing the sieved granules (0.85-1.4 mm) using sample divider.

3.8 Dissolution test

3.8.1 Dissolution

The dissolution measurement is the measure of the amount of the solute (granule) released in a solvent (water). The way to present the dissolution results could be found to be different in the literature. Many workers presented and discussed their dissolution results as the time needed to dissolve a certain amount of the material. In the current work, The time needed to dissolve 90% of the granule quantity in a solvent is considered to be the dissolution time for that product and named as t_{90} . While the dissolution curve which represents the percentage of the dissolved material is presented based on the following equation (Mangwandi et al., 2010):

$$D = \left(\frac{C - C_0}{C_\infty - C_0}\right) \times 100 \qquad \text{Equation 3-3}$$

Where D is the fraction of the material dissolved, C, C_0, and C_∞ represents the conductivity of the solution at any time t, at time=0 sec (initial conductivity), and at time=∞ (final conductivity), respectively.

3.8.2 Methods

There are varity of methods by which the granule dissolution could be quantified based on the way of detecting the changes happening in the solvent (water) properties. Spectrophotometry and electrical conductivity are popular ones. In the first method, UV/VIS spectrophotometers are usually used and the measurement is based on how much light will be absorbed by the materials released in the liquid. Whereas the second method is based on measuring the electrical conductivity of the solution with time. The conductivity method is the one which is used in this work. This method is been used by many workers (Gabbott, 2007; Le, 2008; Mangwandi et al., 2010).

3.8.3 Dissolution set-up.

The experimental work included measuring the conductivity of the solution of 600 ml distilled water in 1 littre beaker while 1 gram of granules was dissolving in it. Granules of size class 0.85-1.4 mm diamter was used in this test. This size class was obtaind by seiving of a whole batch. The solution was gently mixed using magnetic stirrer (600 RPM) on a hot plate and the temperature of the solution was fixed at 20 ºC (± 1º C). These conditions are similar to the conditions used by Le et al. (2011) and Gabbott (2007). The values were chosen so that it will provide good mixing of the solution without causing any mechanical breakage and erosion of the granules. The conductivity meter which is used in the current work was Jenway (provided by Bibby Scientific) is able to measure the conductivity and the temperature of the solution simultaneously. It was connected to a PC in order to record the data (conductivity and temperature) over the time every 2 seconds via a software provided from the same manufacturer.

3.9 NIR Chemical Imaging

Chemical imaging is a technique used to characterize the products of the granulation process. It has the advantage of non-destructive characterization and efficiently can give the distribution of materials on the surface of the granules.The characterization could be done at macro-scale and micro-scale depending on the lens of the equipment used (Koide et al., 2013).

The principle of this analysis method is simply explained here. It is based on illuminating the surface of the granules with a light source which includes near infrared electromagnetic waves (NIR) and analysing the reflected spectrum (NIR) from the surface of the granules by a detection system which include electromagnetic wave analyzer and detector, see Figure 3-11.

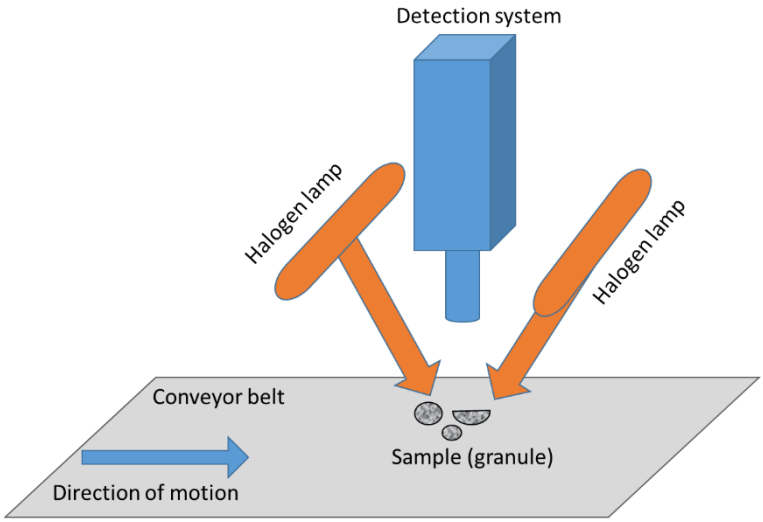

Figure 3-11: Schematic diagram for the NIR measurement system

The equipment used in this work was EVK Helios (EVK DI Kerschhaggl GmbH, Austria). In this equipment there are two halogen lamps used for illumination. The detection system consists of a diffraction grating for dispersing the reflected light (of the range 1.3-2.3 μm) on the detector sensors (320X256 pixels). This equipment uses the push-broom method (scanning line by line) to produce an image of the samples. Each line consists of 320 pixels and the coming light from the diffraction grating disperses to the width of 256 pixels. The spectral resolution of the detection system is 9 μm. The frame rate is calibrated with speed of the conveyor so that to avoid image stretching or compression. The lens of the detection system collects light from an area of width ~9mm. The spatial resolution was ~30 μm/pixel.

3.10 PIV technique

The flow of a fluid and/or a moving particles is usually monitored and tracked by using the technique of Particle image velocimetry (PIV). This technique is frequently used in the granulation studies during the last decades. Using the PIV technique in the current work can help to visualze and understand the mechnisim of the granulation process such as growth or breakage. These mechanisims are most likley to happen during the granulation process namely for the MSG process because the impeller speed changes during the single process. The PIV can also add information about the flow behavoiur in the Eirich mixer, such as velocity distribution of the granlar bed, as there is limited

information avialble in the litrature about it. Depending on the accuracy of the technique used, a precise velocity vectors could be obtained for a moving granules in a granulator.

The measurement technique starts with taking a sequence images for the moving granules with a high speed camera and the frame rate should be chosen properly. Then, these images will be analyzed by using any image processing softwares which contains a PIV algorithm to produce the velocity vectors for the moving object. Any two consecutive images can produce one frame of (2D) velocity vectors. The analysis implies divided the images into a number of calculation areas called interrogation areas. Each area includes a number of pixels, either 8x8, 16x16, 32x32 or 64x64, etc. The time and displacement of each area in the images will be checked with PIV algorithm and the velocity vector will be concluded. Decreasing the size of interrogation area increases the number of arrows. Different settings are used by different workers, see Table 3-5.

Table 3-5: Different PIV setting used by authors.

Author	**The frame rate of the images (fps)**	**Image Resolution (pixels)**	**Interrogation area (pixels)**	**Algorithm Method**
(Reynolds et al., 2008)	1125	1024 × 512	16×16, 32×32, 64×64	MQD
(Chouk et al., 2009)	2000	100 x 100 by crop		MQD
(Dhenge et al., 2013)	60	512 × 512	32 × 32	MQD
(Chan et al., 2013)	1000 at 50 RPM 1500 at 350 RPM	512 x 256	64x64	MQD
(Saleh et al., 2015)	60	512 × 512	32 × 32	MQD
(Omar et al., 2016)	60	1024 x 1024	32 × 32	DCC/FFT
The present work	1000	765x567,	64x64	DCC/FFT

3.10.1 Experimental apparatus

In this work, the experimental setup that is used to monitor the flow of the granules in a high shear mixer (Eirich-EL1) is given in Figure 3-12. In this set up, a high speed camera (Photron Fastcam 1024 PCI, Itronx Imaging Technologies, CA) was used to take images for the moving materials inside the mixer. The camera was fixed on a steel frame to be kept at the same position during the experiments and it was connected to a PC for setting up the resolution and frame rate of the images through a software provided by the same manufacturer and the images were saved in the same PC.

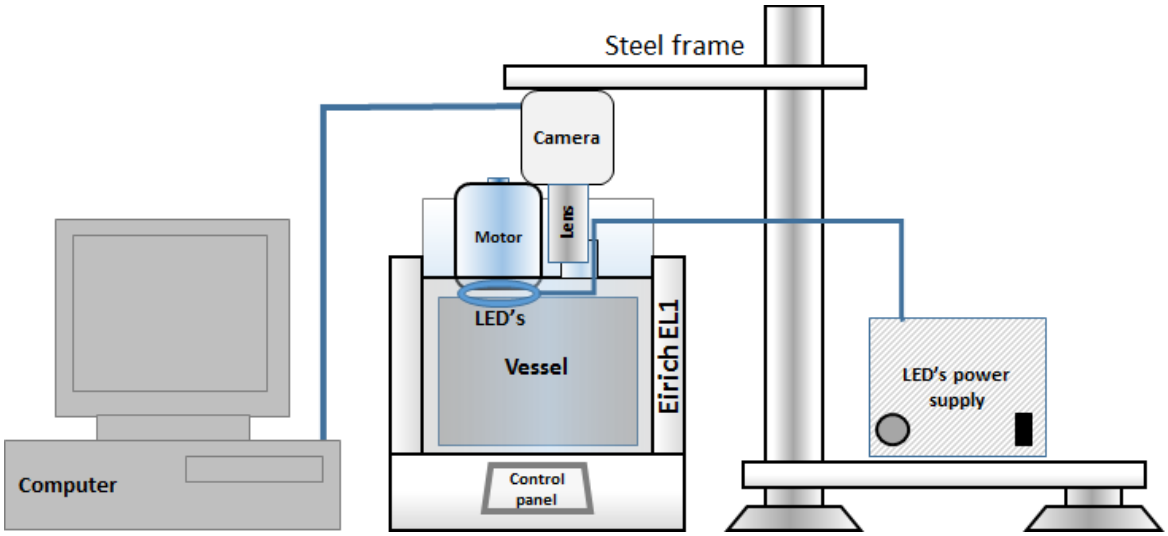

Figure 3-12: PIV experimental set-up.

The surface of the granular bed was illuminated via a custom-built light source composed of 8 LEDs fixed on the lid from inside of the mixer provided with a control box to change the light intensity as required. The LEDs were arranged appropriately with an equal distance from each other in a circular bracket of diameter = ~ 75 mm. This system of lighting has various advantages. As well as controllable light intensity, the arrangement gives the advantage of better light distribution and illuminating the surface of single granules from different angles which improves the visualization more and decreases the influence of shadow.

The camera is situated vertically from the top of the vessel and the position of the lens was fixed at the available opening window which was 4 cm diameter. The camera is

tilted with an angle 20° to the horizontal axis. This gave better viewing for the granular bed after impact by the impeller and the impacted granules were able to be visualized in a better way.

3.10.2 Analysis

There are two algorithms used frequently for analysing the images, the cross-correlation algorithm and minimum quadratic difference (MQD). In the cross-correlation method, an algorithm of PIV (Mori & Chang 2006; Willert & Gharib 1991) is conventionally used to correlate the interrogation areas for a constant time interval (Δt) of successive images. The displacement (Δx and Δy in the image) will be calculated according to the cross-correlation algorithm.

The minimum quadratic difference (MQD) algorithm computes the difference in the pixel value between the search areas. In this case, the displacements (Δx and Δy in the image) are determined from the minimum of the quadratic difference in the pixel values of search window between consecutive images.

In the current work a technique called Digital Particle Image Velocimetry (DPIV) is used. The technique quantifies and qualifies the flow visualization very satisfactorily. The interrogation areas of any image pairs, in this technique, are cross-correlated to obtain the most feasible granule displacement in the small interrogation areas. The cross-correlation function, given in Equation 3-4, could implement the statistical analysis needed in this technique (Thielicke and Stamhuis, 2014):

$$C(m,n) = \sum_{i}\sum_{,} A\,(i,j)\,B(i-m,j-n) \qquad \text{Equation 3-4}$$

Where A and B represent the sub images (interrogation areas) of any consecutive images, for instance image A and image B. The approach which was used to solve the Equation 3-4 was Direct Cross-Correlation approach (DCC) and it was evaluated by Fast Fourier Transform (FFT). Detailed explanation about the mentioned approaches could be found in (Raffel et al., 2007). The DPIV tool used in this work was PIVlab 1.35 (Thielicke and Stamhuis, 2014) to analyse the images. The PIVlab 1.35 software is a matlab toolbox that was used in Matlab R2014b. A certain region of interest (ROI) from the images of

the granular surface was chosen and some parts of the image were excluded from the analysis.

The image of the impeller was excluded from the analysis. This is because, the surface of the blade was reflecting light due to its shiny surface. The shiny surface could cause some problem while analysing the interrogation areas, due to the gray scale of the pixcels will be close to each other. As a consquence, this will cause bias in the analysis and incorrect velocity measurement. The other reason is that, the displacement of the impeller blade tip is much higher than granule bed displacement which could cause an extra error in velocity calculation. Where, if the displacement of an objects in the images is larger than the size of half of the interrogation area this could cause error in velocity calculations (Thielicke, 2014). The area after the scrapper was also excluded because limited number of granule exists there. An example of the PIV result was givenin Figure 3-13.

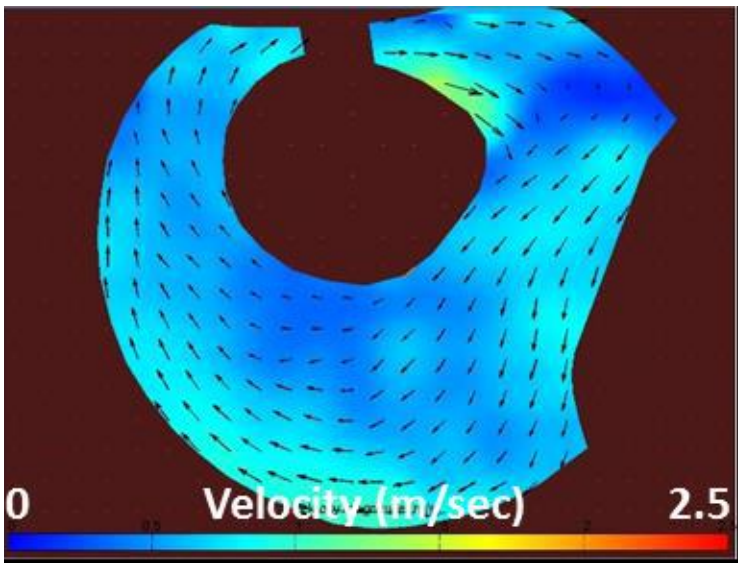

Figure 3-13:An example of PIV results In the image, there are two areas which are excluded from the calculations by applying mask.

3.10.3 Validation of the measurement technique

In PIV measurements, the resulted velocity vectors are usually examined by changing the parameters of the PIV technique and comparing it with the theoretical one (ideal case). The most important parameters are the interrogation area and the frame rate of the images. Hence, the effect of these parameters on the resulted velocity vectors was examined, here.

Two interrogation areas (32X32 pixels and 64X64 pixels) were examined using three frame rates of camera (500 fps, 1000 fps, and 2000 fps). A batch of granules was distributed as a flat surface and fixed in the mixing vessel of Eirich mixer and the position of the granules was immobile, i.e. the real velocity of each individual granule is the same as vessel's base at that point. The velocity profile was measured at two different vessel speeds (85 RPM and 170 RPM). The surface velocity of the granular bed was calculated along three line (vertical, horizontal and oblique at 45°) see Figure 3-14 and compared with the real velocity which can be obtained theoretically from the angular velocity of the vessel.

Figure 3-15 and Figure 3-16 show the velocity vectors (distribution) at the vessel speed of 85 RPM and 170 RPM, respectively. The figures show that the magnitude of the velocity vectors (arrows) increases by moving from the centre of the vessel towards the wall. In addition, the colour of the of the velocity field in the Figure 3-15 is more blueish compared to the Figure 3-16 which is consistent with speed of the vessel in the both cases.

Figure 3-17 and Figure 3-18 show the value of the velocity vectors obtained by the PIV measurement along three lines in the Figure 3-14 and compared with the real velocity (calculated theoretically from the vessel speed, 85 RPM and 170 RPM). From the figures, it could be noticed that the small interrogation area (32x32) gives the lowest compatibility between the measured value and the actual value, namely at low vessel speed (85 RPM) as in Figure 3-17. While the compatibility is better in case of high vessel speed (170 RPM).

Although, most of the settings of the PIVlab give satisfactory results the frame rate 1000 fps and the interrogation area 64x64 pixels are giving the best fit to the real value. Hence, these settings were used in the calculations of the velocity vectors in the current work.

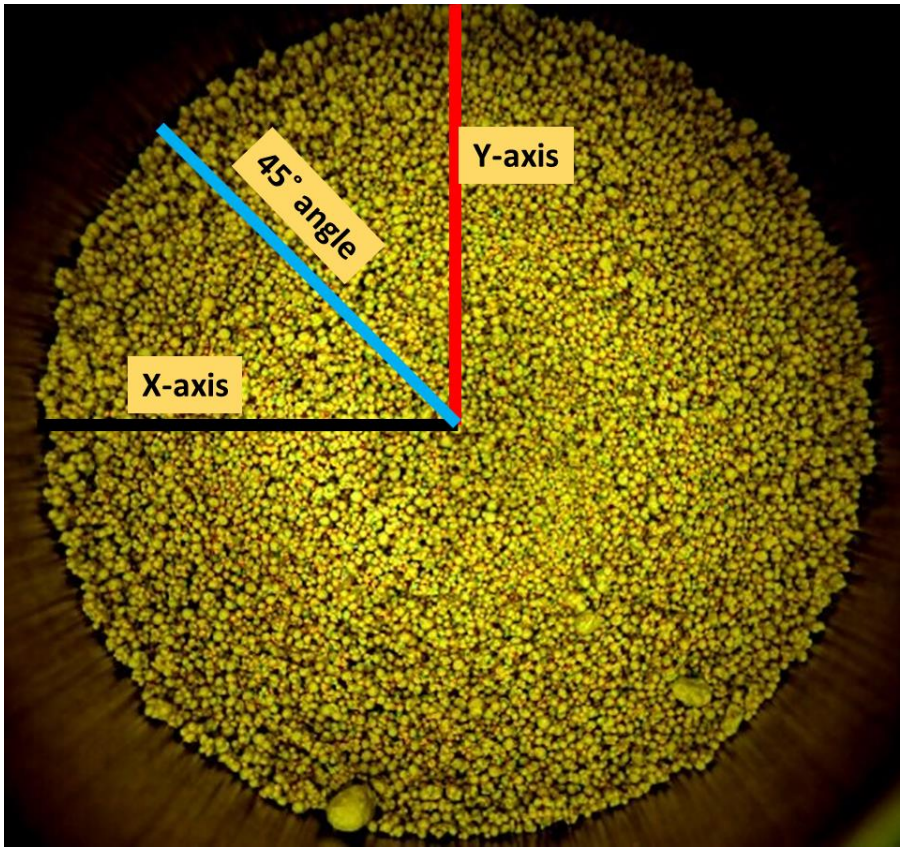

Figure 3-14: Granular bed distributed as a flat surface inside Eirich mixer. The velocity was calculated along the black, blue, and red lines.

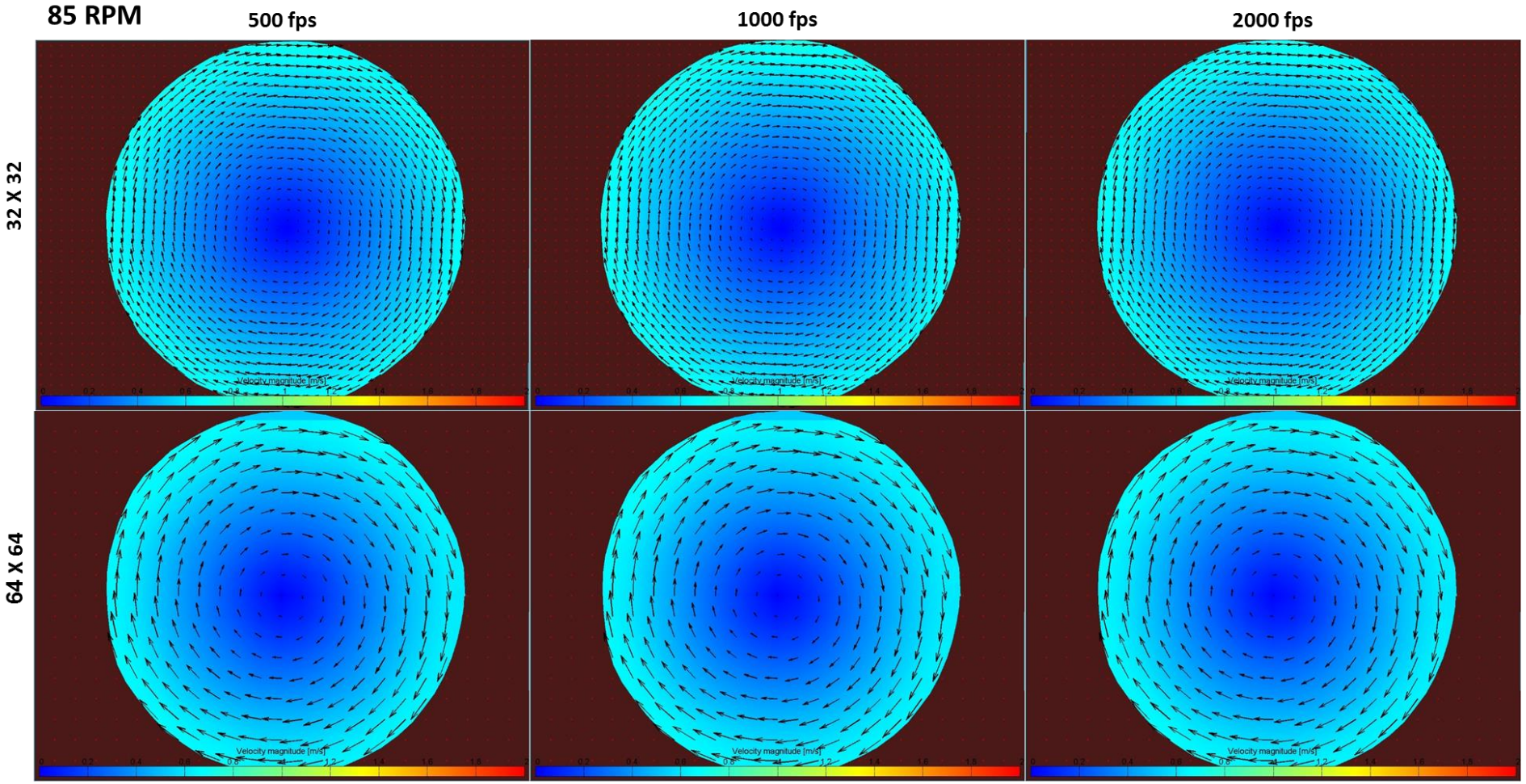

Figure 3-15: The velocity field vector. Three frame rates of camera are used (500 fps, 1000 fps, and 2000 fps) and two interrogation areas (32x32 and 64x64) pixels. The vessel speed = 85 RPM. Note: The colour bar scale is 0-2 m/sec.

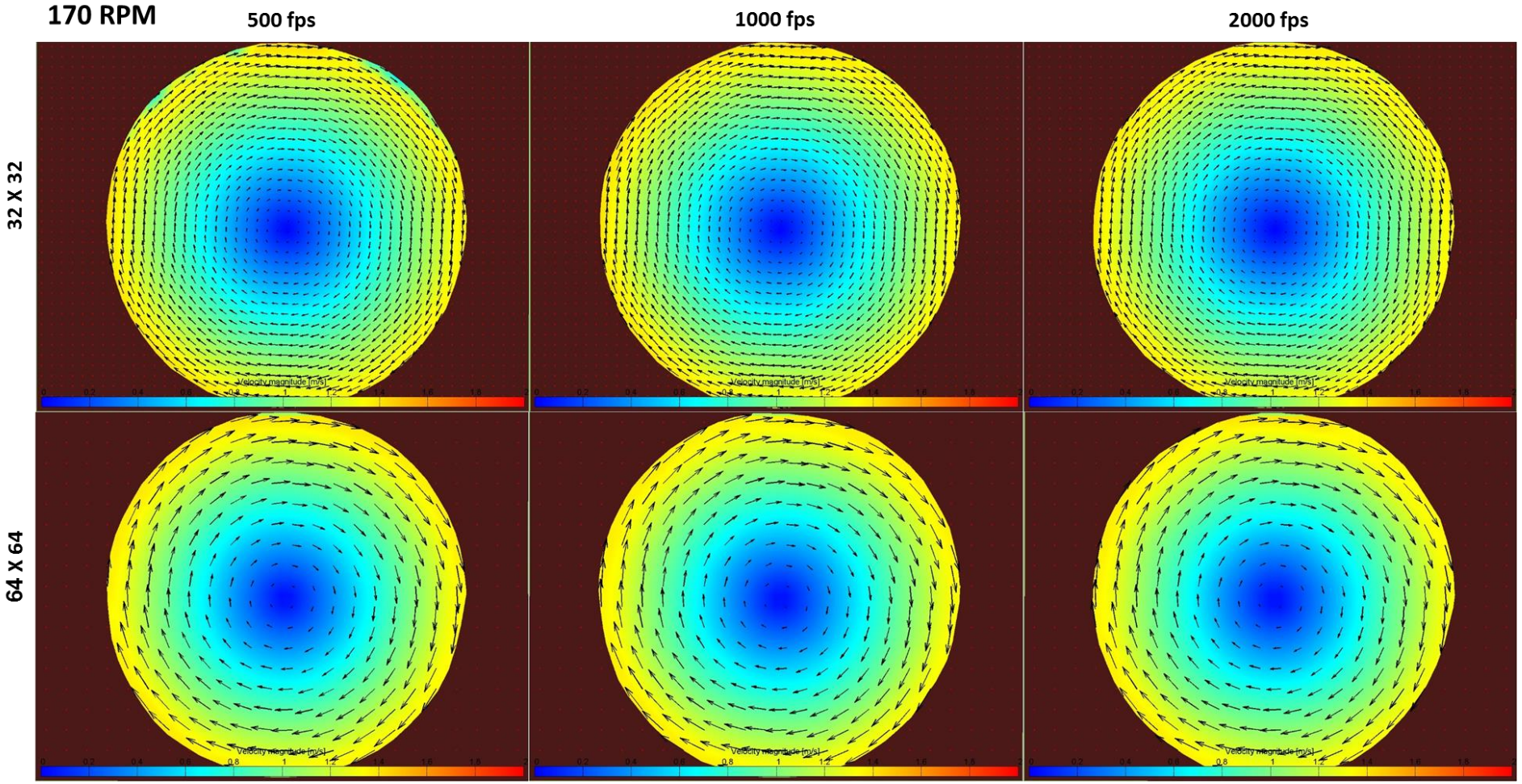

Figure 3-16: The velocity field vector. Three frame rates of camera are used (500 fps, 1000 fps, and 2000 fps) and two interrogation areas (32x32 and 64x64) pixels. The vessel speed = 170 RPM. Note: The colour bar scale is 0-2 m/sec.

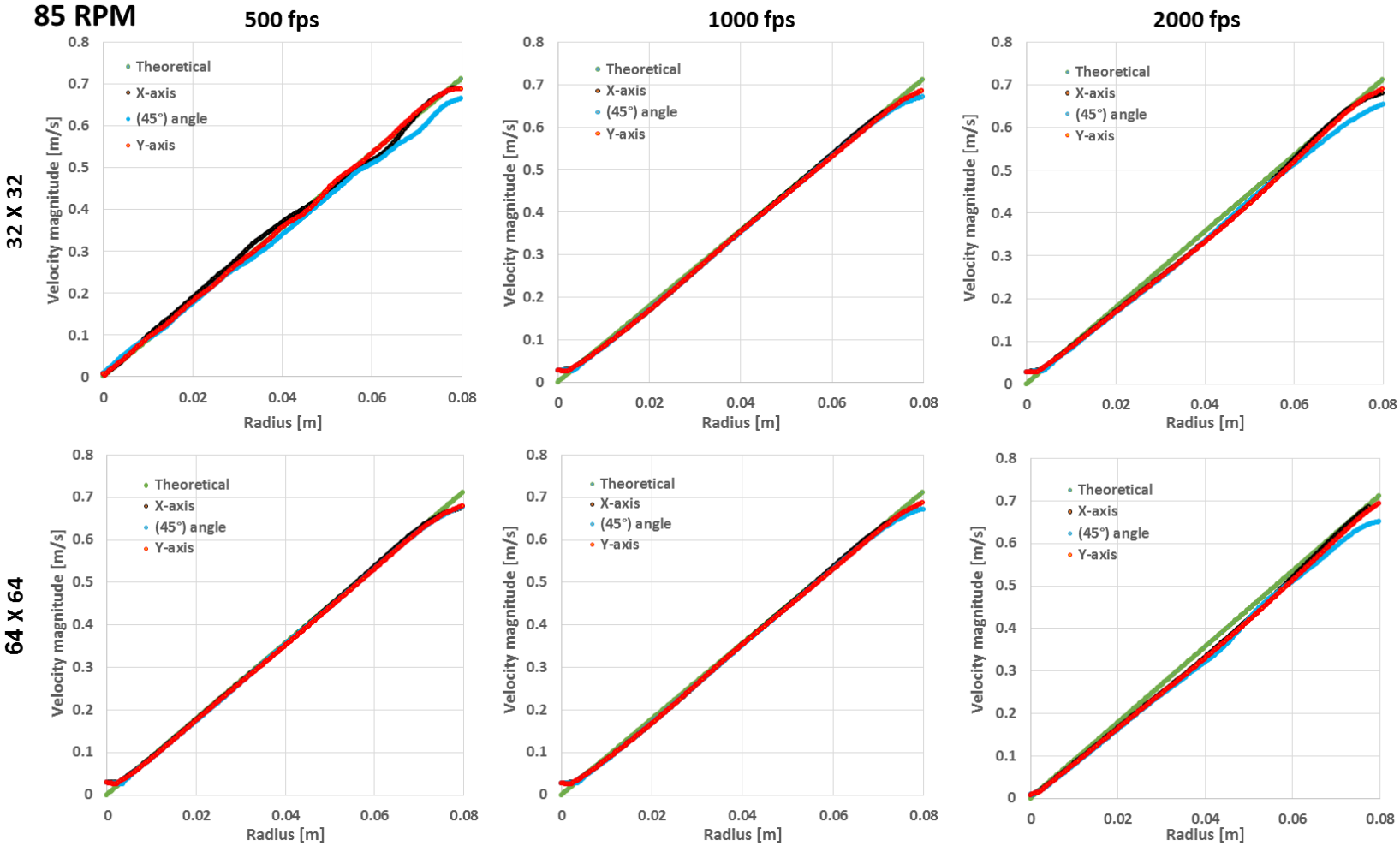

Figure 3-17: The velocity values along the three lines in Figure 3-14, compared with theoretical one (green line). Three frame rates of camera are used (500 fps, 1000 fps, and 2000 fps) and two interrogation areas (32x32 and 64x64) pixels. The vessel speed = 85 RPM.

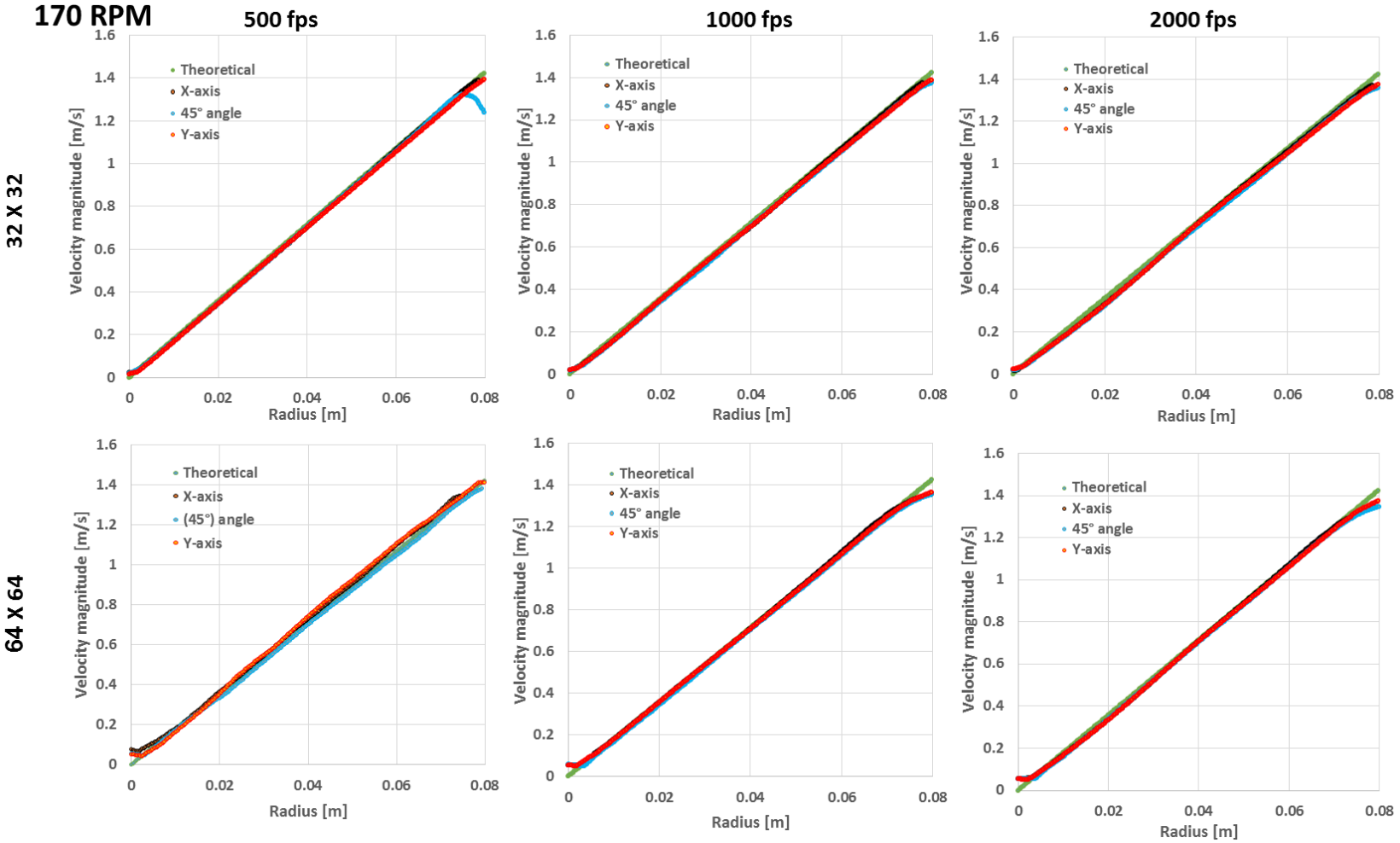

Figure 3-18: The velocity values along the three lines in Figure 3-14, compared with theoretical one (green line). Three frame rates of camera are used (500 fps, 1000 fps, and 2000 fps) and two interrogation areas (32x32 and 64x64) pixels. The vessel speed = 170 RPM.

CHAPTER 4 NORMAL GRANULATION (NG)

4.1 Introduction

Investigating the wet granulation process in Eirich mixer using normal granulation process (NG) is an important step before commencing with MSG granulation process. This is because the behaviour of granulation process in this type of mixer is still not well established. In contrast to other types of high shear mixers, e.g. Roto Junior and Diosna, the wet granulation process is extensively studied, and abundant information is available in the literature about it. On the other hand, studying the wet granulation under normal condition (NG) will provide useful information about the effect of the process parameters and the formulation on the granules properties. This, in consequence, will be useful while investigating the new granulation method, i.e. the Multi-Stage Granulation process (MSG) which will be illuminated in the next chapter.

The normal granulation in Eirich mixer was examined using different process parameters, at two different impeller speeds (2000 and 7000 RPM) and two liquid to solid ratios (0.14 and 0.15), for different granulation durations (200, 300, 400, 500, 600, and 650sec). Subsequently, the produced granules were characterized and the change in the granule attributes was explained. The granulation process, in brief, was started by premixing of the powder. Then the binder was added gradually onto the moving powder bed. Then the granulation continued for the time durations mentioned formerly, and samples were collected and characterized.

4.2 Granule size evolution

The normal granulation process (NG), as explained in the chapter of the experimental work, commenced by pre-mixing the dry powder for 100 sec and then the binder was added onto the moving powder bed. The duration of the pre-mixing and the binder addition was less than 200 sec for all cases of the granulation in this work. During this period, the nuclei were created. Some of the nuclei were big, relatively irregular in shape and full of binder and many others were small granules neighbouring the big ones, for

example see the real image given in Figure 4-1. This usually occurs in the case when a low impeller speed (2000 RPM) is used, i.e. at low shear mixing. Whereas in the case of high impeller speed (high shear mixing), the created big nuclei were breaking into small ones, as the real image shown in Figure 4-2 illustrates. Afterwards, the created nuclei and small granules started to stick to each other making bigger granules with prolonging the granulation process. The granule median size was measured at each 100 sec of the granulation time after the first 200 sec.

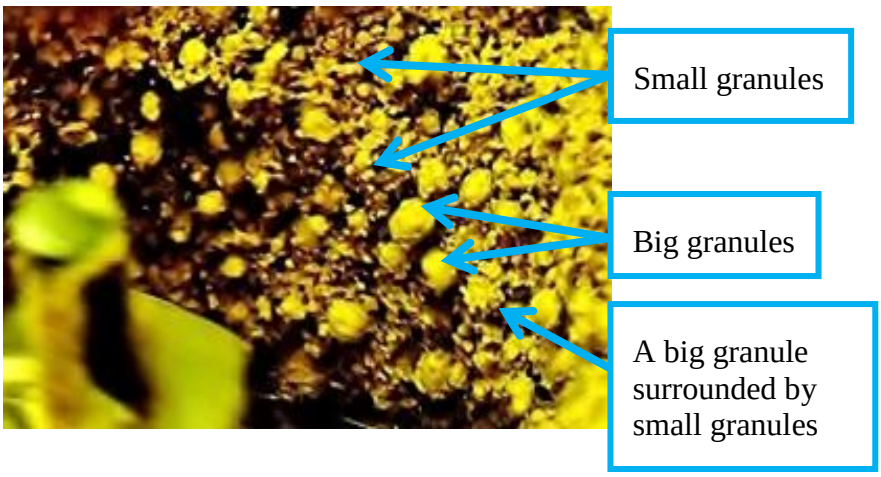

Figure 4-1: Big and small granules at 200 sec after binder addition completion, L/S = 0.15 and impeller speed = 2000 RPM

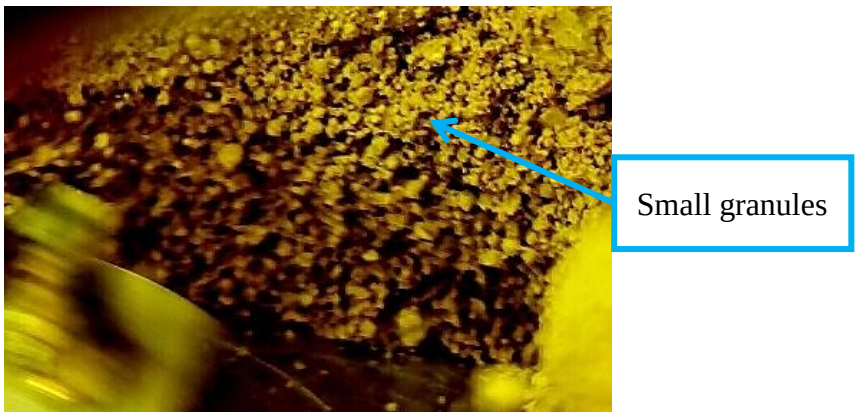

Figure 4-2: Small granules at 200 sec after binder addition completion, L/S = 0.15 and impeller speed = 7000 RPM

Figure 4-3 shows the change in the granule median size over the granulation time for the case of L/S = 0.14. The results shown here are for two cases of impeller speed, low speed (2000 RPM) and very high speed (7000 RPM). The figure suggests that the granule size was increasing steadily with increasing the granulation time for both cases of the impeller speed. Similar behaviour was noticed by Hoornaert et al., 1998 and Sochon et al., 2005.

However, the tendency of change is different. From the figure it is clear that the tendency is high in the case of low impeller speed, i.e. 2000 RPM. While, the granule size was increasing in lower rate in the case of higher impeller speed, i.e. 7000 RPM.

Similarly for the case of L/S = 0.15, the granule size was increasing with increasing the granulation time, and it was in higher rate in the case low speed (2000 RPM) than high impeller speed (7000 RPM), see Figure 4-4. In Addition, it can be noticed that the granule size in the case of higher binder content (L/S = 0.15) is, in general, is bigger than lower binder content (L/S = 0.14). This is may due to the existence of more binder, in which it tends to increase the growth rate. Knight (1993) reported similar results.

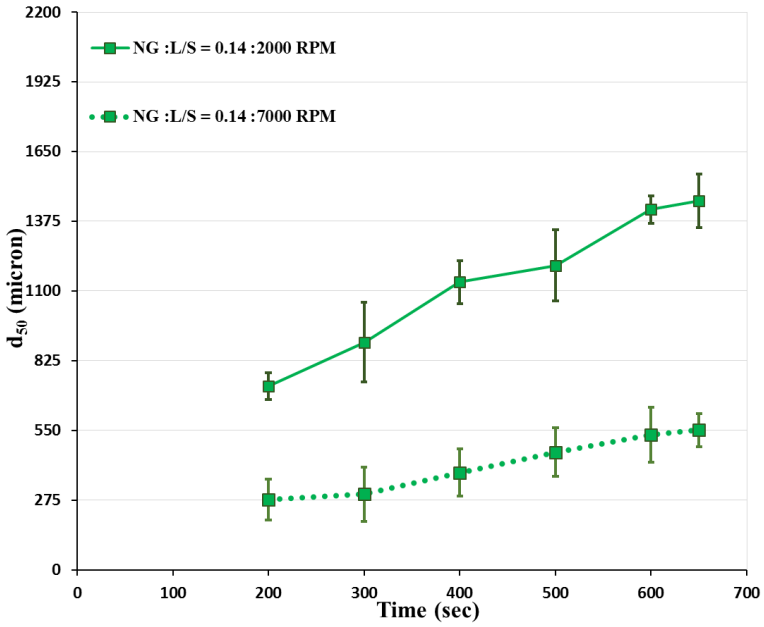

Figure 4-3: Granule median size (d_{50}) versus granulation time, L/S = 0.14.

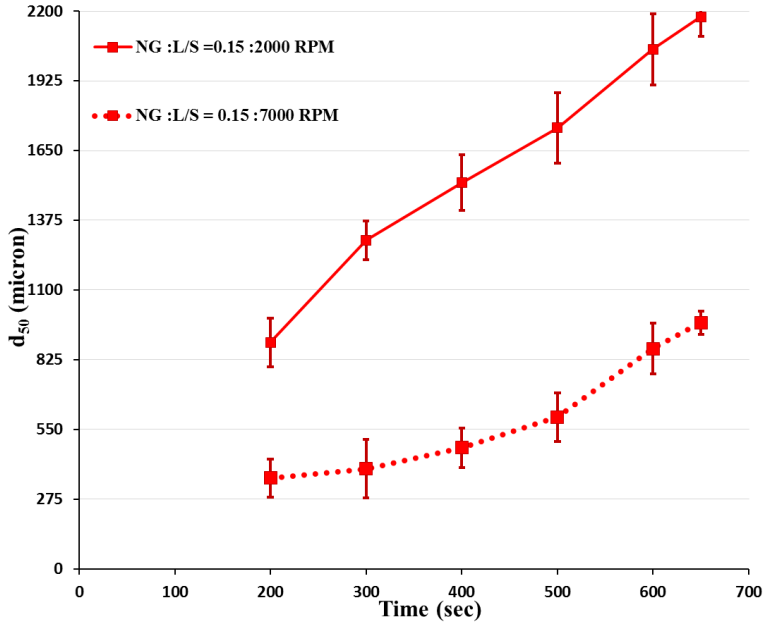

Figure 4-4: Granule median size (d_{50}) versus granulation time, L/S = 0.15.

4.3 Granule size distribution

The size distribution of the granules was measured with time and given in the Figure 4-5 to Figure 4-8 for the case of L/S = 0.14 and 0.15 and for the two impeller speeds of 2000 RPM and 7000 RPM.

At low impeller speed, as in Figure 4-5 and Figure 4-7, the granule size distribution was tending to be bimodal during the initial period of the granulation time, i.e. at 200 sec, (Knight et al., 1998). The amount of the small granules was more than the big ones, namely for the case of L/S = 0.14. However, the amount of the big granules was increasing when more binder was added to the powder bed, i.e. in the case of L/S = 0.15. This is due to the presence of more binder which always encourages the aggregation of particles, (Daumann et al., 2010). By comparing the size distribution along the granulation time, Figure 4-5 and Figure 4-7, it looks that the amount of the big granules at 200 sec was decreasing with time which is also could be resulted from the breakage process.

By continuing the granulation process, the granulation time had an influence on the granule size distribution. The small granules were disappearing gradually. They were sticking to the big ones with time making the size distribution of the granules monomodel and the size distribution was tending to be more narrower. The reduction in the size distribution with time was reported by a number of researchers (Knight et al. 1998; Knight

et al. 2000; Schaefer & Mathiesen 1996). This could be observed in all the figures from Figure 4-5 to Figure 4-8. This trend is different to the work of Knight et al. (2000). They reported that the bimodal distribution was persisting from the beginning of the granulation process till the end. They ascribed that to the contribution of the breakage process which could take place in other high shear mixers.

On the other hand, by increasing impeller speed the size distribution was noticed to change. Unlike to the size distribution at low impeller speed, the size distribution was mostly monomdel at the high impeller speed during the initial period of the granulation time, i.e. 200 sec. This due to the high impeller speed was breaking most of the nuclei created during binder addition period and most of the granules were small in size compared to corresponding granules at the low impeller speed. This occurs for both cases of the liquid to solid ratios, 0.14 and 0.15, see Figure 4-6 and Figure 4-8. The effect of time, at high impeller speed, has less influence on the size distribution compared with the low impeller speed. This is due to the growth rate at high impeller speed was less than the low impeller speed. As high speed of impact could encourage the breakage process at the expense of the growth process.

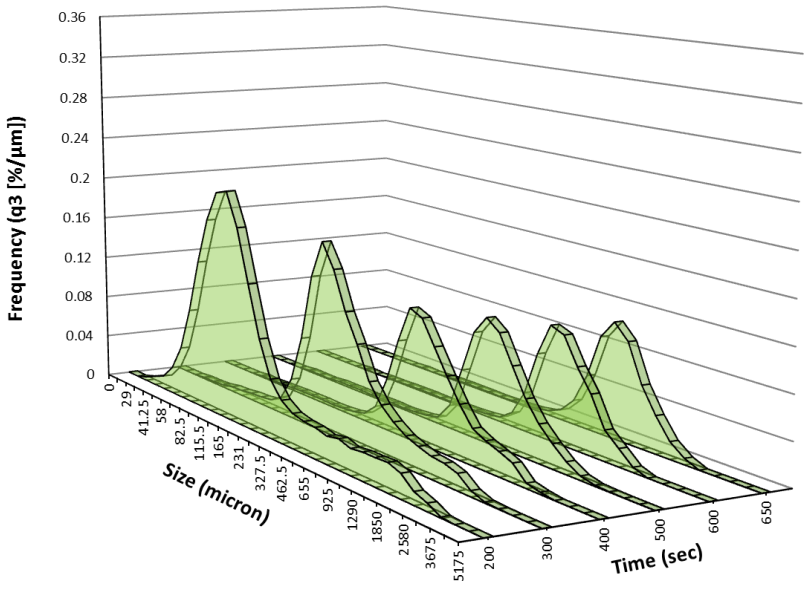

Figure 4-5: Granule size distribution at different interval of time for the case of L/S = 0.14, impeller speed = 2000 RPM, NG.

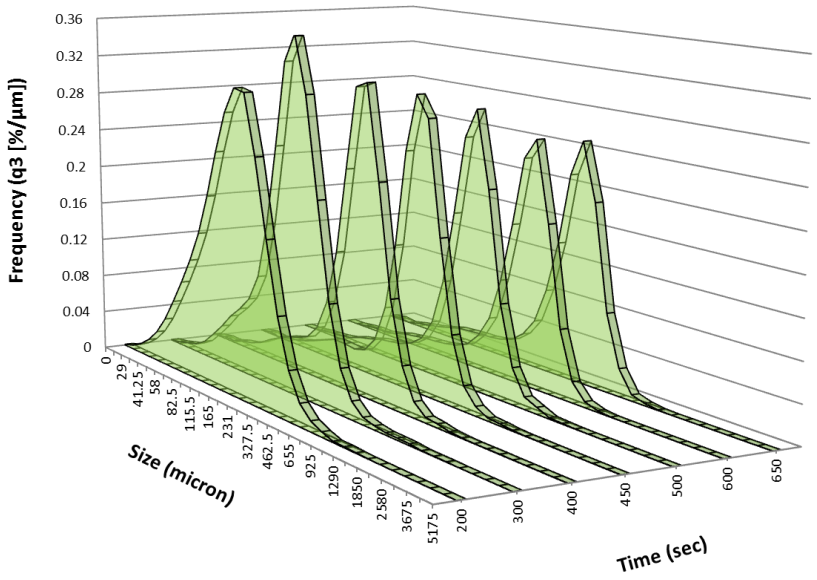

Figure 4-6: Granule size distribution at different interval of time for the case of L/S = 0.14, impeller speed = 7000 RPM, NG.

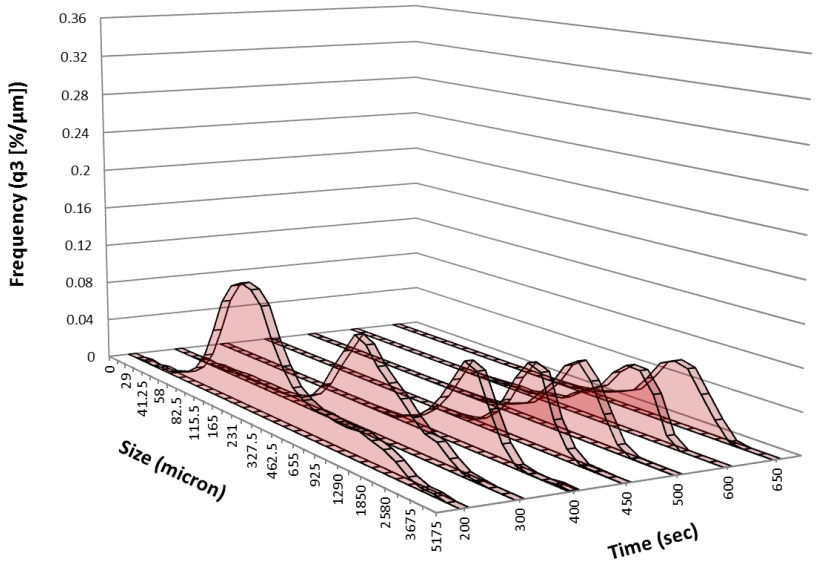

Figure 4-7: Granule size distribution at different interval of time for the case of L/S = 0.15, impeller speed = 2000 RPM, NG.

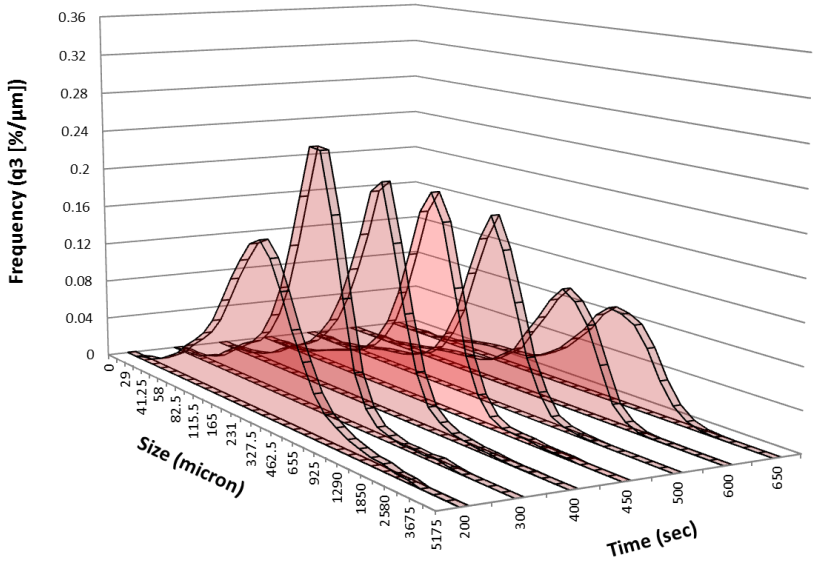

Figure 4-8: Granule size distribution at different interval of time for the case of L/S = 0.15, impeller speed = 7000 RPM, NG.

The span of the size distribution was frequently used to quantify homogeneity of the size distribution. Figure 4-9 and Figure 4-10 presents the span of the size distribution for the two of the liquid to solid ratios 0.14 and 0.15, respectively. As both of the figures show that, the span is the highest at 200 sec of the granulation time which is the moment just after binder addition finishing point all the cases of the impeller speed and the binder content. Most probably, this was due to the existence of fine granules and coarse granules at this moment which could be the result of non-even binder distribution. The same reason is believed to be responsible for the wide size distribution at the beginning.

The general behaviour that could be noticed here is the span deceases with the granulation time but with different tendencies depending on the granulation conditions. In the case of L/S=0.14 the span decreases gradually till 500 sec of the process time for the both cases of impeller speed. Whereas, in the case of L/S=0.15 the span deceases clearly at the beginning, however, the change will be trivial after 400 sec of the process time. The figures of the span also show that the span at low impeller speed is always higher than the high impeller speed. In addition, by comparing Figure 4-9 and Figure 4-10, it could be noticed that the span is slightly higher in the case of L/S=0.14 than L/S=0.15 particularly at low impeller speed, i.e. 2000 RPM. For example (in the case of 2000 RPM), at 400 sec the span is about 1.47 for the case of L/S=0.14 and 1.20 for the case of

L/S=0.15, while at 600 sec, the span is about 1.26 for the case of L/S=0.14 and 1.12 for the case of L/S=0.15.

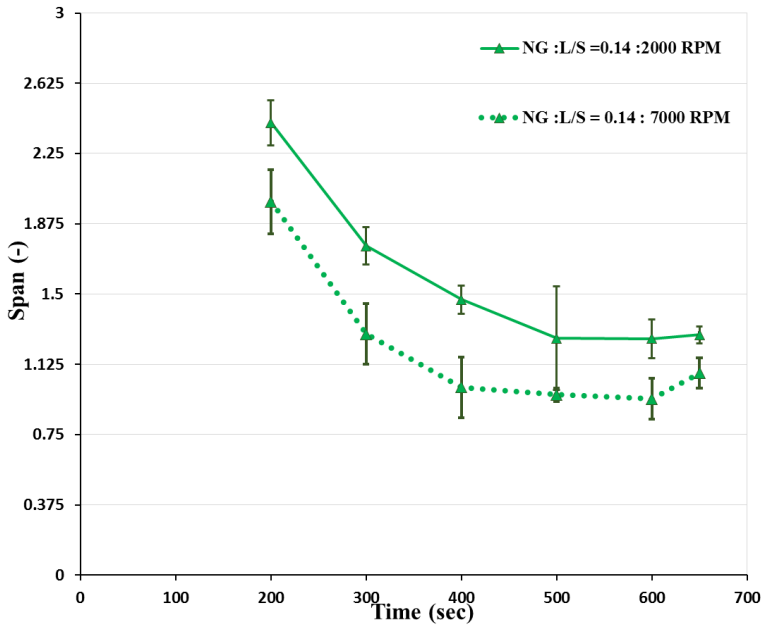

Figure 4-9: The span of the granule size versus time at two impeller speeds (2000 and 7000) RPM, L/S = 0.14, NG.

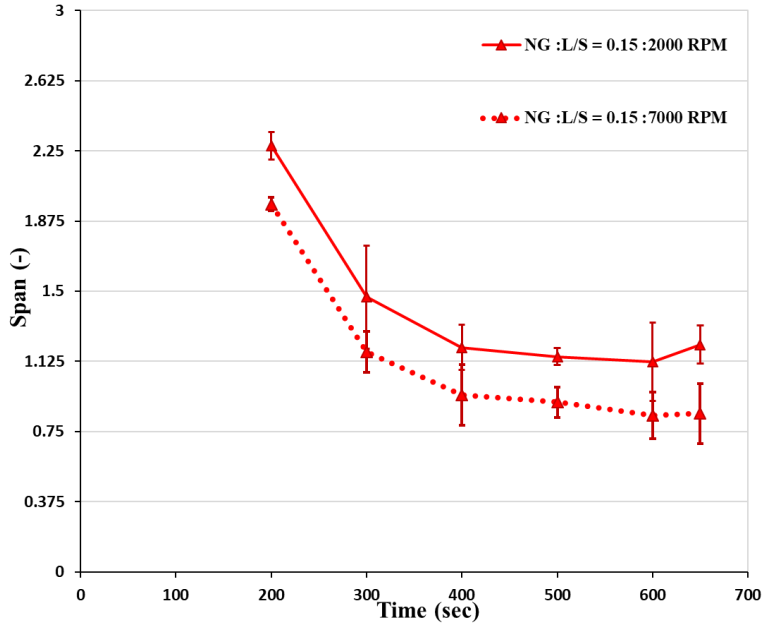

Figure 4-10: The span of the granule size versus time at two impeller speeds (2000 and 7000) RPM, L/S = 0.15, NG.

4.4 Granule shape

The shape of the granules produced by high shear mixer is usually spherical. However, it may be affected by the impeller speed. Knight et al. (2000) reported that the granules produced at low impeller speed have more spherical shape than the granules produced at high impeller speed. They ascribed that to the granule breakage that may happen at high impeller speed. Similar results were found by Eliasen et al. (1999). They stated the granules had a higher shericity and smoothness at low impeller speed in comparison to granules produced at a high impeller speed.

In this work, the shape of the granules was broadly spherical. But to be more precise, it was increasing in sphericity and smoothness with increasing the granulation time for the both cases of liquid to solid ratios (0.14 and 0.15), see Figure 4-11 and Figure 4-13. From the figures, it could be noticed that the granules at 600 sec are slightly more spherical and smooth compared with the granules at 200 - 400 sec. This is because at early stage of the granulation time the created nuclei are usually having irregular shape. Then with time the granules will gain more sphericity as they will roll over within the granulator.

At higher impeller speed i.e. (7000 RPM) the shape of the granules was more irregular compared to the low impeller speed (2000 RPM), see Figure 4-12 and Figure 4-14. The figures suggest that the granules have less sphericity to some extent at 7000 RPM compared with the corresponding granules at 2000 RPM. This may due to high impact speed of the impeller that might continuously affect the surface of the granules. As a result, the granules lose its smoothness and sphericity. By examining the images of the granules in all the cases, it could be noticed that sometimes there are some small granules are attached and partially embedded into the bigger granules, which makes them to look like satellites. These satellites are more remarkable in the case of higher binder content. As more binder content enhances the liquid bridges between the particles.

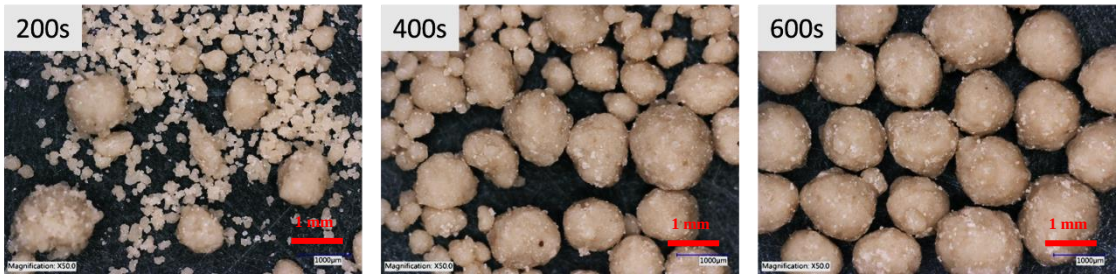

Figure 4-11: Image of the granules at different times for the case of L/S = 0.14, 2000 RPM, NG (using KEYENCE digital microscope). See Appendix (B) for more images.

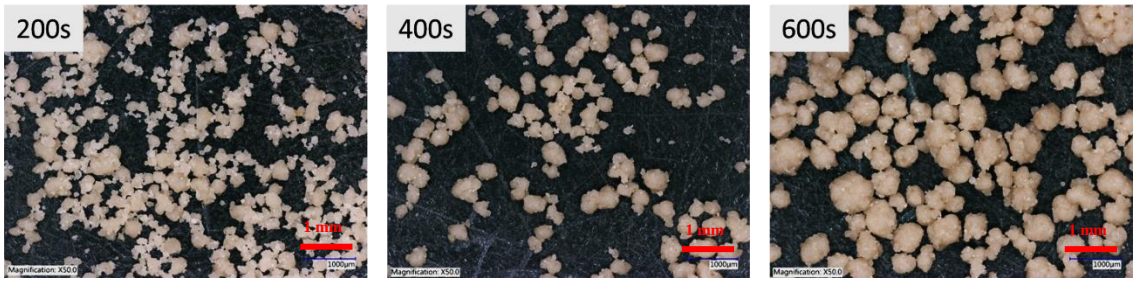

Figure 4-12: Image of the granules at different times for the case of L/S = 0.14, 7000 RPM, NG (using KEYENCE digital microscope). See Appendix (B) for more images.

Figure 4-13: Image of the granules at different times for the case of L/S = 0.15, 2000 RPM, NG (using KEYENCE digital microscope). See Appendix (B) for more images.

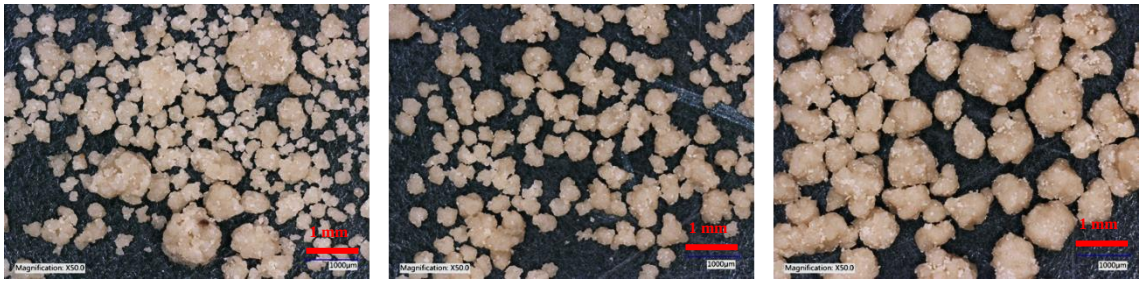

Figure 4-14: Image of the granules at different times for the case of L/S = 0.15, 7000 RPM, NG (using KEYENCE digital microscope). See Appendix (B) for more images

4.5 Granule Porosity

The porosity of the granules in high shear granulation has been reported to decrease with time (Oka et al., 2015; Schæfer et al., 1993). In the current work, a similar trend was observed. The porosity of the granules was going down continuously with progressing granulation time. Figure 4-15 and Figure 4-16 show the porosity of the granules over the granulation time for the case of L/S = 0.14 and 0.15, respectively. The figures suggest that the granules were densifying with time. This could be resulted from the primary particle movement within the granules towards its centre. The densification could also results from the stresses applied on the granule bed while it moves around the vessel.

In Figure 4-15, it can be noticed further, that the granule porosity in the case of higher impeller speed is less than the case of lower impeller speed. This is consistent with previous findings which states that more intensive motion of the granular bed could lead to more dense products. This could also be noticed by examining the X-ray images of a sample of granules in case of high impeller speed compared with the low impeller speed, comparing Figure 4-17 with Figure 4-18 and Figure 4-19 with Figure 4-20. The figures show that the number of pores in the case of low impeller speed is higher than the high impeller speed. The results obtained here are comparable with what was found by Knight et al., (1998) in which they used similar material but their granulator was a vertical axis machine. There is some difference in the trend of the decrease in the porosity. In their work the porosity was decreasing more rapidly at the initial time of the granulation compared to the end. They ascribed that to the asymptotic decrease in the number of the open pores with time.

At higher liquid to solid ratio the porosity was lower, Figure 4-16 compared with lower liquid to solid ratio, Figure 4-15. This could be resulted from more filling more interstitial volume between the primary particles due to existence of more binder which increases the coalescence rate (Ramachandran et al., 2008). This could also be noticed by examining the x-ray images, especially for the case of low impeller speed i.e. comparing Figure 4-17 and Figure 4-19. In which more pores could noticed in the Figure 4-17 indicating to higher porosity granular products.

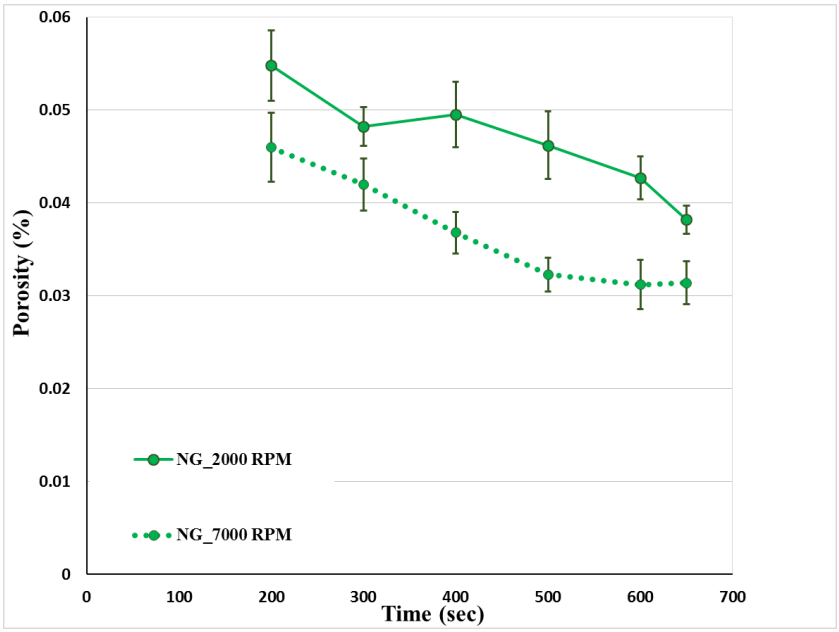

Figure 4-15: Granule porosity variation with granulation time, L/S = 0.14, NG.

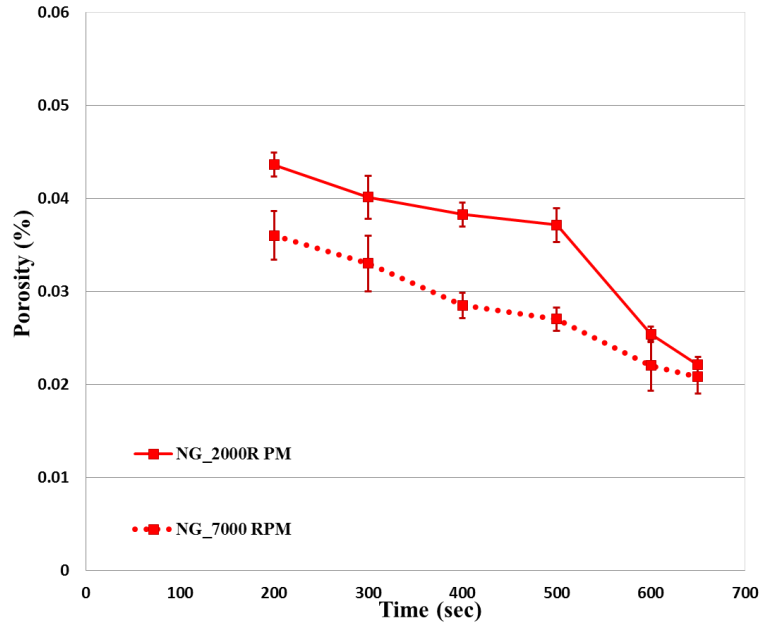

Figure 4-16: Granule porosity variation with granulation time, L/S = 0.15, NG.

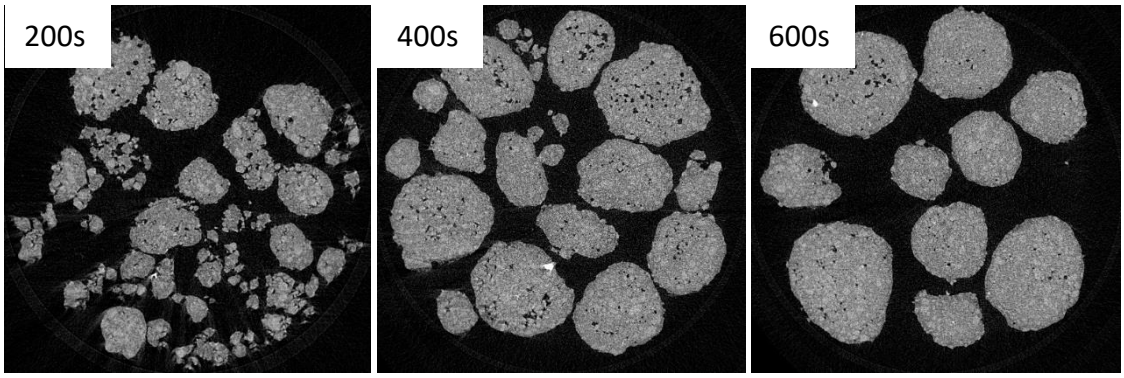

Figure 4-17: X-ray tomography for the granules of NG, L/S = 0.14, 2000 RPM, at different time intervals. See Appendix (C) for more images.

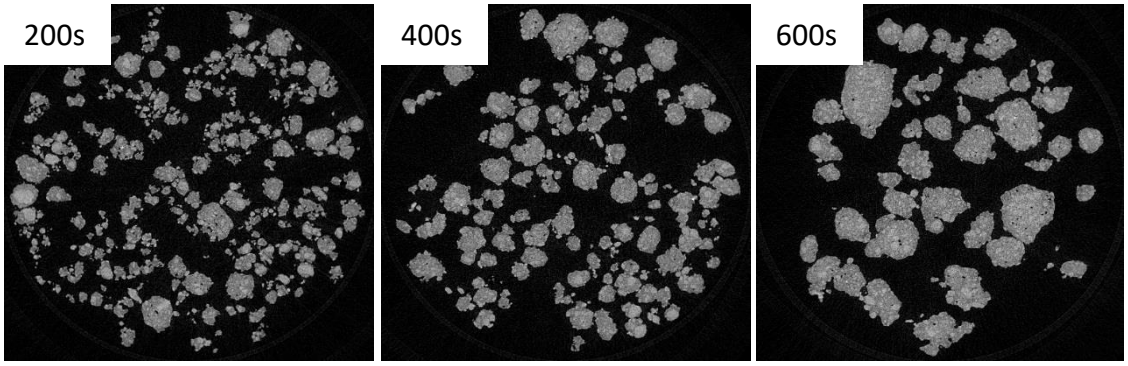

Figure 4-18: X-ray tomography for the granules of NG, L/S = 0.14, 7000 RPM, at different time intervals. See Appendix (C) for more images.

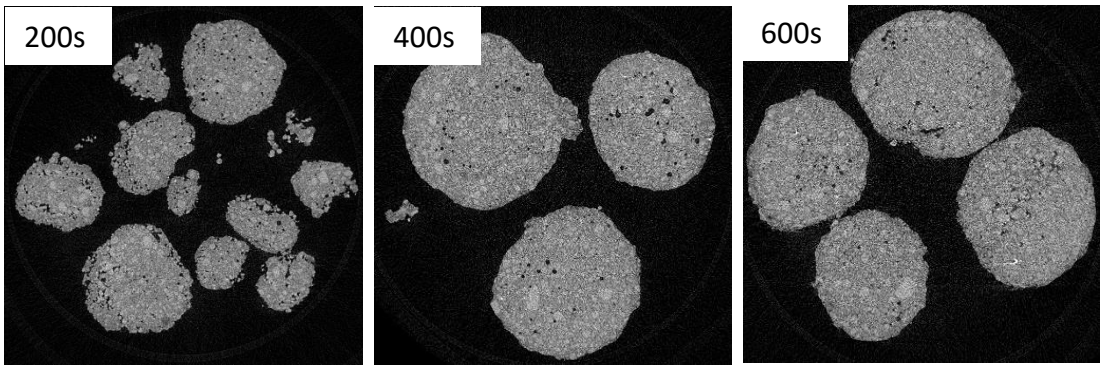

Figure 4-19: X-ray tomography for the granules of NG, L/S = 0.15, 2000 RPM, at different time intervals. See Appendix (C) for more images.

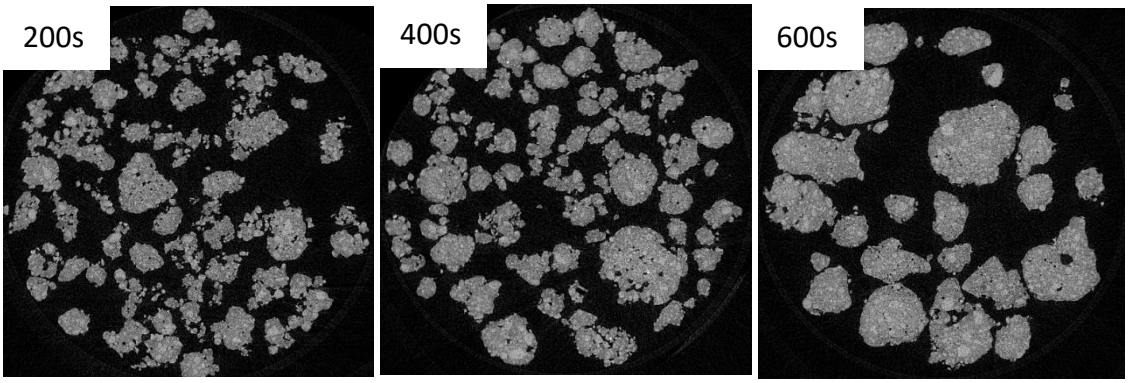

Figure 4-20: X-ray tomography for the granules of NG, L/S = 0.15, 7000 RPM, at different time intervals. See Appendix (C) for more images.

4.6 Specific surface area

Figure 4-21 and Figure 4-22 show the specific surface area of the granules measured over the granulation time for different impeller speed and liquid to solid ratio. The figures show that the surface area of the granules were reducing continuously with time. This means the surface of the granules were tending to be smoother and losing the surface pores with prolonging the granulation time. This result is consistent with what was mentioned previously about the granules shape. Where the granule shape was tending towards more spherical with time, see Figure 4-11 and Figure 4-13. The decrease of the surface area could be resulted from continuous rolling of the granules within the granulator and embedding small granules into the surface of the big granules which tends to decrease the tortuosity of the granule surface. Furthermore, Figure 4-21 and Figure 4-22 suggest that the SSA increases with increasing the impeller speed. The SSA is high at 7000 RPM compared to the 2000 RPM for the both cases L/S=0.14 and L/S=0.15. The increase in the surface area could be resulted from the breakage and attrition of the granules at high impeller speed.

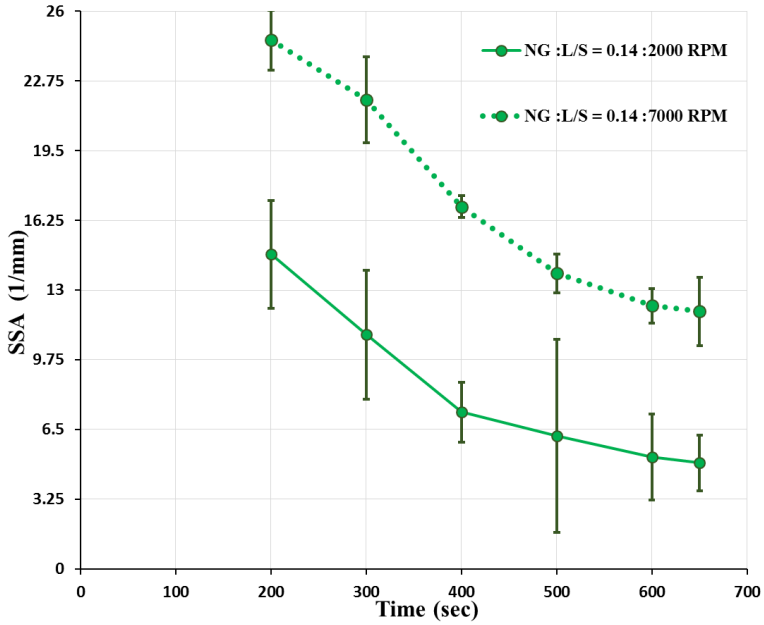

Figure 4-21: The change in the specific surface area of the granules with granulation time, impeller speed = 2000 and 7000 RPM, L/S = 0.14, NG.

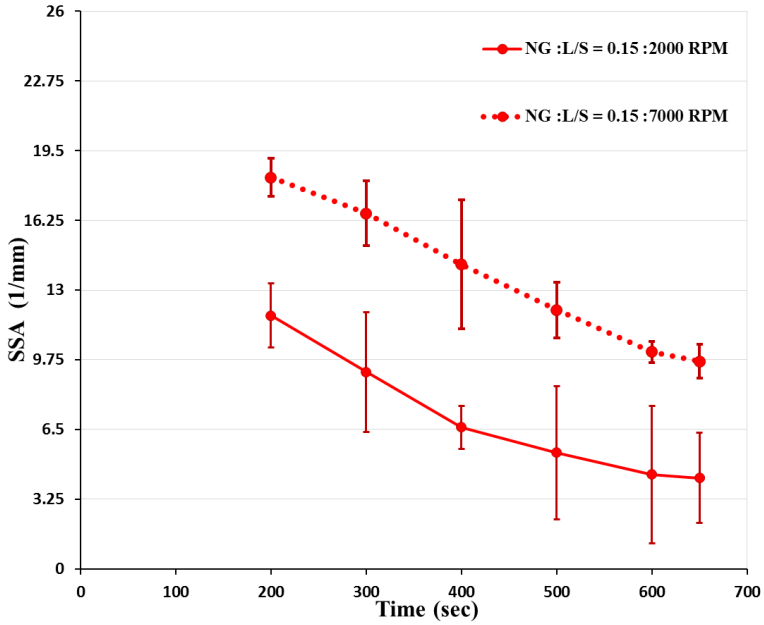

Figure 4-22: The change in the specific surface area of the granules with granulation time, impeller speed = 2000 and 7000 RPM, L/S = 0.15, NG.

4.7 Proposed mechanism for the NG

Based on what have been observed from the experimental work and the obtained results which are explained formerly, a mechanism for the normal granulation could be deduced and shown in Figure 4-23.

The mechanism of the normal granulation was divided into two parts. The first part is introducing the binder to the powder bed, which includes the premixing (100 sec), the binder addition (70 – 75 sec) and the binder distribution (30 – 25) sec. This part was short, not longer than 200 sec and it is considered to be as nuclei creation part. In this part, most of the dry powder turns into small and big granules after 200 sec, as it was shown previously in Figure 4-1 and Figure 4-2 (section 4.2). This could also be noticed by examining the granule size distributions at 200 sec, Figure 4-5 to Figure 4-8. Where, negligible portion of the size distribution is less than the d_{90} of the primary powder particles (75 µm) which confirms that most of the powder particles are turned into granules. It is also considered that when the powder and binder were coming in contact to each other, as paste-like lumps were most likely created, see Figure 4-23 (the nuclei formation part). Then these lumps were susceptible to break when they were contacted with the impeller. The probability of the breakage could be higher in the case of high impeller speed, i.e. 7000 RPM, where the nuclei could break into small fragments due to breakage. While in the case of low impeller speed, the nuclei were breaking into big and small granules.

Afterwards, the granule growth process was dominating, more clearly, in the case of low impeller speed. The granule sizes was probably increasing by coalescence of the small granules and relatively big ones with each other making bigger size granules (Knight, 1993), see Figure 4-23 for illustration. This mechanism was also suggested by Realpe and Velázquez, (2008). The granule size could also increase by the layering mechanism in which the small granules stick on the big ones making them bigger with time. An example of online image is given in Figure 4-24, where the image shows that small granules stuck on big one and this could lead to granule growth by layering. Similar mechanism was proposed by Sastry and Fuerstenau, (1973) and Hoornaert et al., (1998), in which they named this mechanism as snowballing. The possibility of existence of both of the growth mechanisms concurrently (coalescence and layering) was reported also by Schæfer, (2001). The increase in the granule size with time could lead to the granule consolidation,

as it will be denser with time. In the meantime, the binder squeezes to the surface of the granule.

The process is different in the case of high impeller speed, i.e. 7000 RPM. Although the granule size was increasing with time, the rate of growth was not high. This is because the high impeller speed was constantly tending to reduce the growth rate by breaking the coalesced aggregates that could make bigger granules with time. In addition, at high impeller speed, the granules were denser and less porous than the case of low impeller speed as it was discussed previously in section 4.5, see figures from Figure 4-15 to Figure 4-20. This will also imped the growth rate as the dense granules will not deform easily. The granule growth process in the case of high impeller speed was considered to be due to coalescence process, as presented in Figure 4-23.

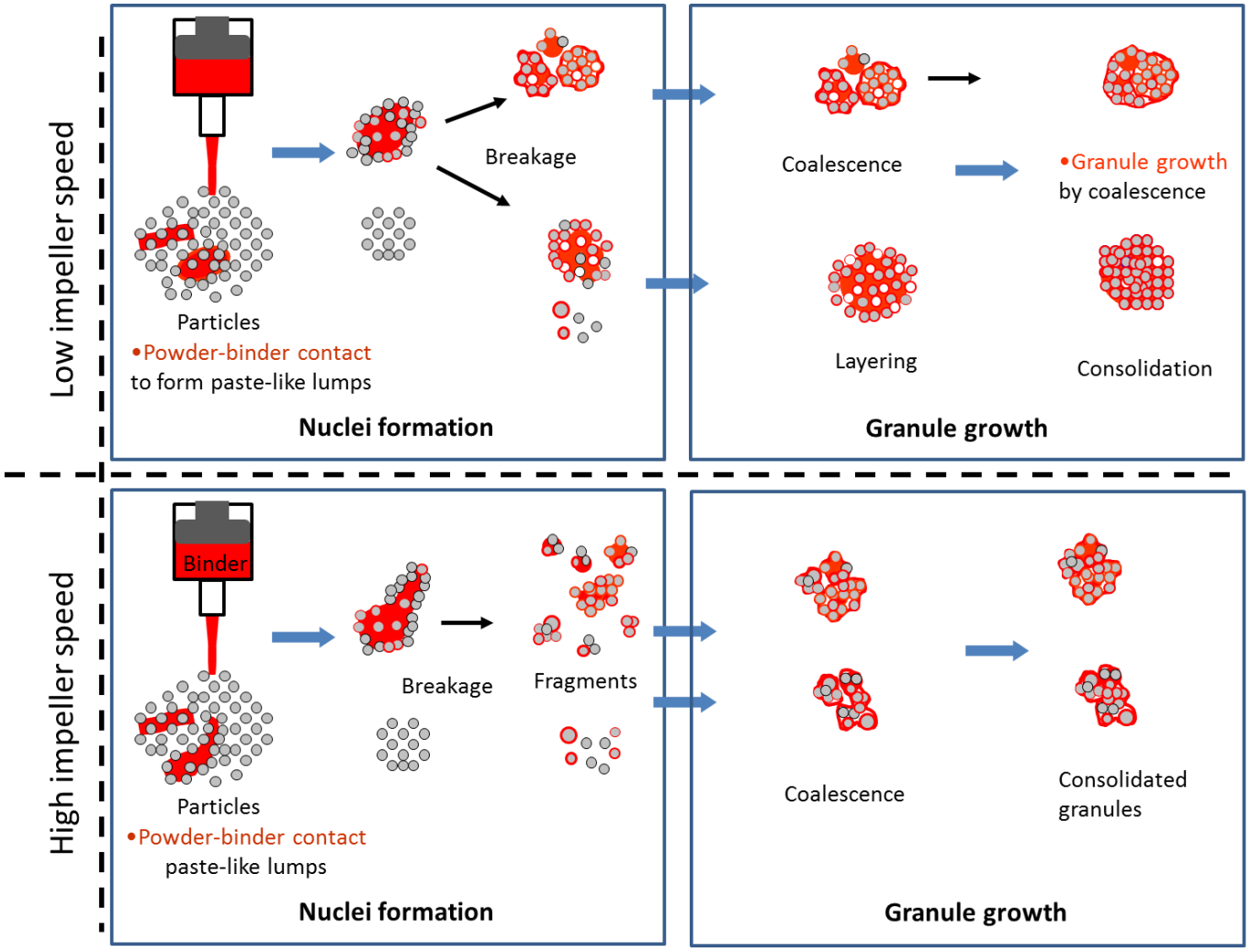

Figure 4-23: Proposed mechanism for the normal granulation process

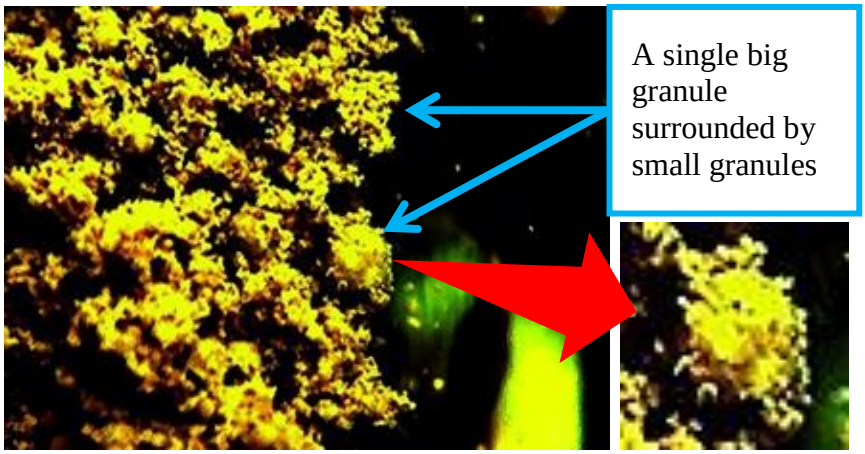

Figure 4-24: Online image of the granule bed (at 300 sec, L/S = 0.14, 2000 RPM, NG), showing small granules sticking on the big granules.

4.8 Conclusions

The goal of this chapter was to study the wet granulation in an intensive small scale laboratory mixer (Eirich EL) following normal granulation process. This process was named here as normal granulation (NG) to be distinguished from the Multi-Stage Granulation (MSG), which will be explained in the next chapter. It was necessary to study the effect of the process parameter using NG on the granule properties, as limited number of literature available about this mixer using the pharmaceutical products. The effect of the process parameters, such as impeller speed, granulation time, and liquid to solid ratio, on the granules properties was investigated.

The granule size was found to increase with granulation time, regardless the speed of impeller. However, the granule size was increasing in higher rate in the case of low impeller speed (2000 RPM) than the high speed (7000 RPM). This is because the breakage rate at the high speed was impeding the tendency of the growth rate. The shape of the granules was noticed to be more spherical at low impeller speeds rather than high speed. The size distribution was noticed to be as bimodal at 200 sec when the impeller speed was low, but it was tending to be monomodal for the high impeller speed. With time, the granule size distribution as well as the span was declining and getting narrower. At low L/S ratio, the span was higher, where it was 1.47 and 1.16 when the L/S was 0.14 and 0.15 respectively, at 400 sec. While it was 1.26 and 1.17 for L/S=0.14 and L/S=0.15,

respectively, at 600 sec. The granule porosity and the specific surface area were observed to decrease with time for the both cases of liquid to solid ratios, 0.14 and 0.15. The porosity was higher in the case of low impeller speed but the SSA was higher in the case of high impeller speed. The tendency in porosity decrease was slightly different with was found by Knight et al., (1998), in which they used the same materials and a typical high shear mixer (vertical axis). The porosity was decreasing progressively with time in the current work, while in their work the decrease in the porosity at the initial period of the granulation process was higher compared with end of the process.

CHAPTER 5 MULTI-STAGE GRANULATION (MSG)

5.1 Introduction

Most of the granulation studies in high shear mixer were carried out by applying constant process parameters throughout the granulation time. This means that the granules were exposed to a fixed process parameter from the starting point to the end point of the granulation process. This type of process is referred to as normal granulation (NG) in the present work and as explained in the previous chapter, the granualtion process was conducted in a single stage using lab scale Eirich mixer. However, there is some work in the literature, which implies carrying out the process in steps. For instance, (Rahmanian et al., 2011) while they were investigating the wet granulation in high shear mixer, they changed the impeller speed during the initial period of the granulation process for the sake of binder dispersion. However, they did not change it during the granulation process. Hence, their granulation method was also considered, here, as a normal granulation process.

A new method in a high shear wet granulation process was implemented to enhance the final granule attributes. The granulation process in this method is divided into stages. At each stage, different impeller speeds were used. For this reason, this method of wet granulation is named here as Multi-Stage granulation (MSG) to distinguish it from the conventional Normal granulation (NG) in which the impeller speed is fixed throughout the granulation process. The methodology of the experimental work for the MSG process was explained in chapter 3. The experimental work revealed that by following the multi-stage granulation a noticeable change in the granule attributes has been observed. The speed of impeller was changed in a pulse mode throughout the granulation process from moderate speed to high speed for different intervals of time. Analysis of the produced granules showed that the granule characteristics with the multi-stage granulation were different to that with the normal granulation process. The granule median size was affected clearly during the process. However, the granule porosity was not influenced enormously during the process. The surface area of the granules also increased to some extent after the pulse change in the impeller speed. This increase in the surface area is reflected on the granule dissolution process. The collected granules after the pulse change

were dissolving faster than the granule samples before the pulse change. This may due to the increase in the surface area of the granules. The granule size distribution was changing throughout the whole MSG process.

5.2 Results

5.2.1 Granule median size

Figure 5-1 and Figure 5-2 show the granule median size variation with time throughout different stages of granulation processes of the early pulse (EP) and late pulse (LP) processes for both cases of L/S=0.14 and 0.15. The experimental results revealed that the granulation process proceeded normally for the first stage, for the both of the liquid to solid ratios 0.14 and 0.15, after binder addition completion. In this stage, the granule size was increasing with time while the impeller speed was fixed at 2000 RPM, as it is clear in Figure 5-1 and Figure 5-2. This behavior confirms what many researchers reported, that is by prolonging the time of the granulation process the granule size will increase, i.e. growth process domination (Knight, 1993; Tu et al., 2009). The increase in granule size could be attributed to the coalescence process which results from the collisions between the granules themselves or by the layering process in which the small granules begin to stick on the big ones leading to the granule growth. The growth process could also be enhanced by the existence of more binder on the surface of the granules.

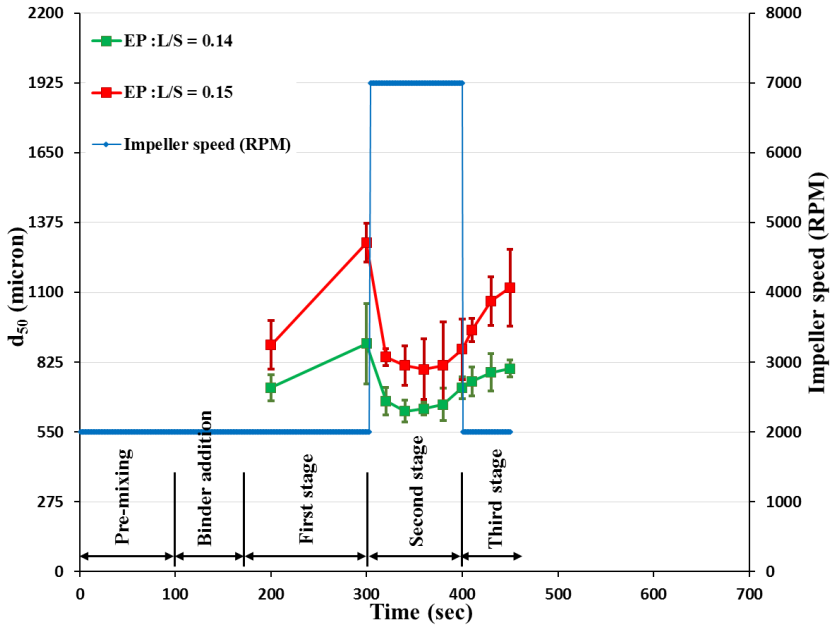

Figure 5-1. Granule median size vs granulation time for L/S=0.14 and 0.15, EP process.

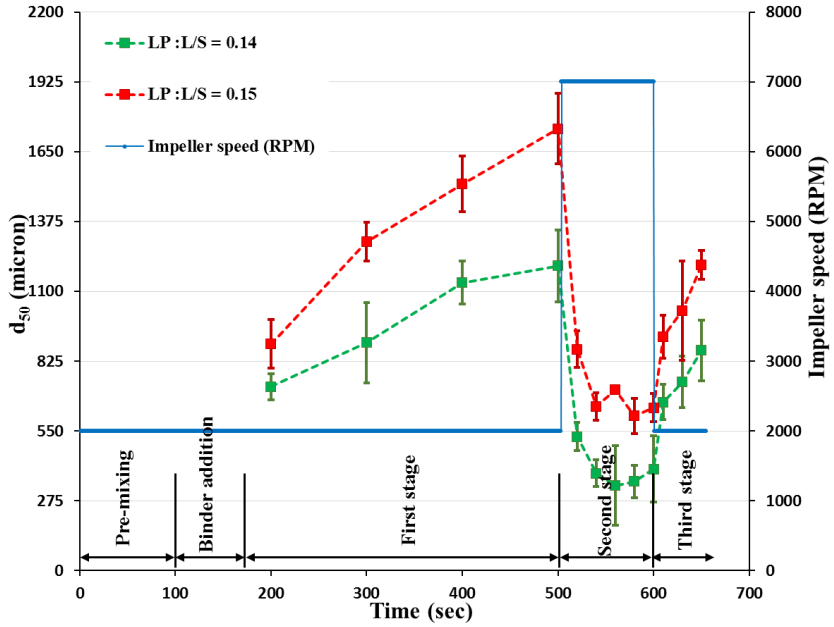

Figure 5-2. Granule median size vs granulation time for L/S=0.14 and 0.15, LP process.

The first stage of the late pulse (LP) process ended after 500 sec which is longer than the first stage of the early pulse (EP) process by 200 sec. As a result, the median granule size at the end of first stage of the LP process (Figure 5-2) is bigger than that of the EP process (Figure 5-1).

In the second stage, which persists for about 100 sec, the speed of impeller is rapidly increased from 2000 RPM to 7000 RPM for the both processes of EP and LP. The median size of the granules, as a result, decreased markedly for the both cases of L/S=0.14 and 0.15 especially for the process of the late pulse LP, see Figure 5-2. This means that this condition led to the domination of granule breakage. At this stage, the granules could be compacted more by virtue of high speed impact delivered by the impeller on the granules. As a result, the binder may move within the granule structure and will redistribute. Figure 5-1 and Figure 5-2 suggests further that the granule breakage rate in the case of the EP process is less than the breakage rate in the case of the LP process.

The third stage of this MSG process starts after the moment 400 sec for the EP process and after 600 sec for the LP process, where the speed of the impeller is decreased to 2000 RPM. During this stage (approximately 30 sec), the small granules of the second stage have more chance to stick to each other and grow once again, since the stresses applied by the impeller on the granules is much less than the previous (second) stage, which leads to a decrease in the breakage rate. As a consequence, the size of the granules increased with time once again, particularly for the LP process. The change in the granule size in all the stages of MSG process was different to some extent when more liquid binder was added to the powder, i.e. liquid to solid ratio = 0.15. Figure 5-1 and Figure 5-2 show that the granule size is generally larger in the case of more binder (L/S=0.15) through all the stages. This is most probably due to the existence of more binder that may give rise to increasing the stickiness between particles leading to increasing the coalescence rate.

5.2.2 Online images of the granular bed

Figure 5-3 shows actual images of the granules motion in the Eirich mixer taken by the high-speed camera (2000 fps) for the case of LP process. The figure confirms that the size of the granules in the case of L/S=0.14 is smaller than the case of 0.15 at the end of the first stage. This is consistent with the results in Figure 5-2, where the red points (L/S=0.15) is above the green points (L/S=0.14). This is because of the existence of more binder which encourages the growth rate. In addition, the granule shape appears to have a high sphericity at this moment, which is the end of the first stage for the both cases, see also Figure 5-4 for the microscope images. The bed of the granules was moving around the vessel and the impeller was touching the bed mainly at its tip.

Moving on to the second stage, the process of wet granule breakage dominated here by virtue of high impact speed of the impeller on the granules which turned the granules of the first stage to small pieces and fragments, as it could be seen in Figure 5-3, the snapshot was taken at the middle of the second stage. The granular bed in this stage moves faster than the first stage and the impeller touches the bed with less area compared with the first stage.

By decreasing the speed to 2000 RPM in the third stage, the small granules and fragments of the second stage started to stick to each other and resulted in regrowth again. The granule shape loses its sphericity, namely after about 30 sec of the third the stage start, since they are composed of aggregates of small granules, as Figure 5-3 and Figure 5-4 shows. In fact, the shape of the granule was changing throughout the whole granulation process as it could be noticed also in Figure 5-4. Where the granule shape was more spherical in the first stage. Then small fragments in the second stage. Followed by agglomerating the small granules forming bigger size and tortuous surface granules. More images about the granule shape at different moments and stages of the MSG process are available in Appendix D.

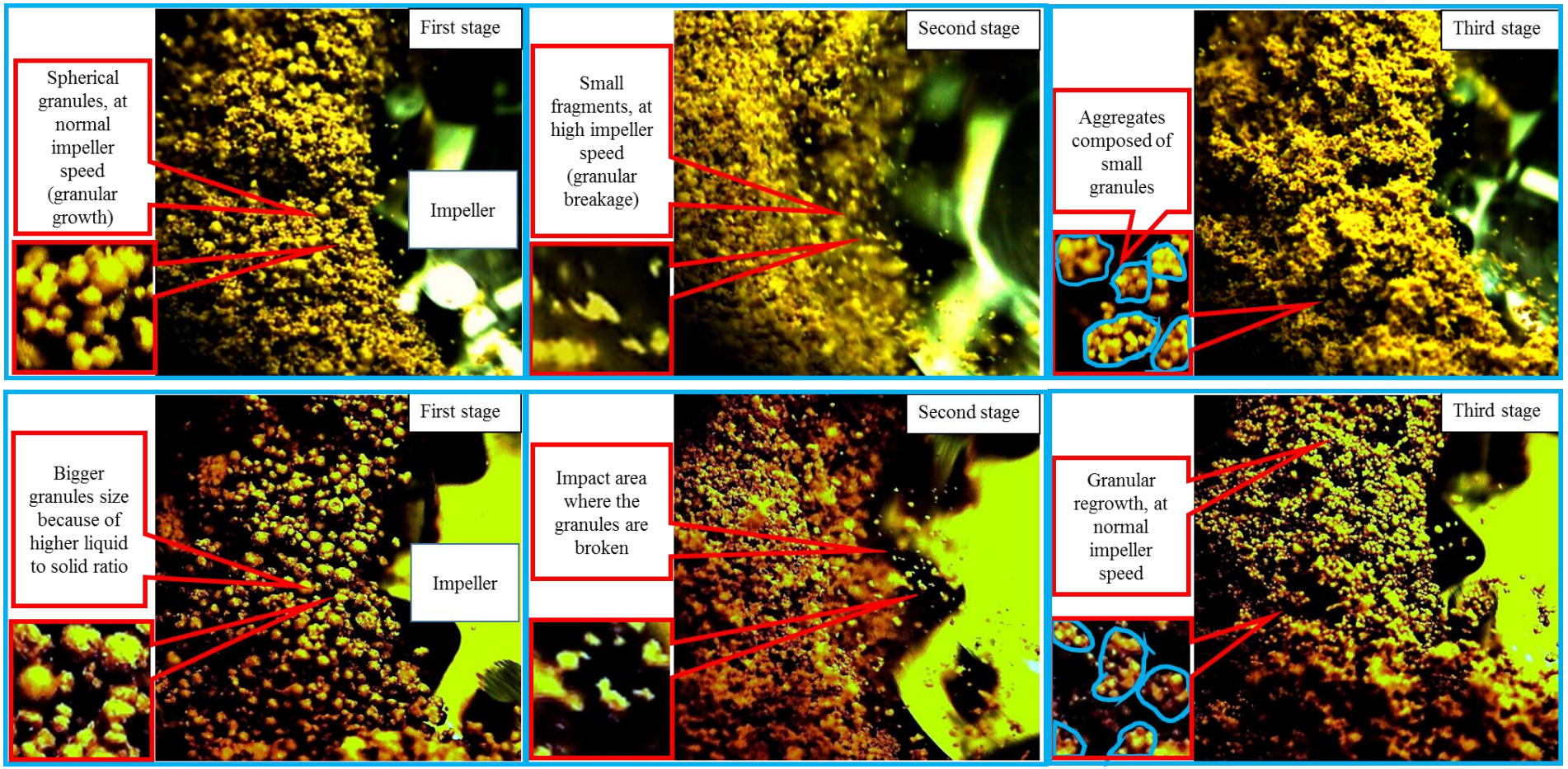

Figure 5-3. Granule bed near the impeller in Eirich mixer throughout different granulation stages, L/S=0.14 and 0.15, Late pulse (LP) process. Images were taken by high-speed camera at a rate = 2000 fps.

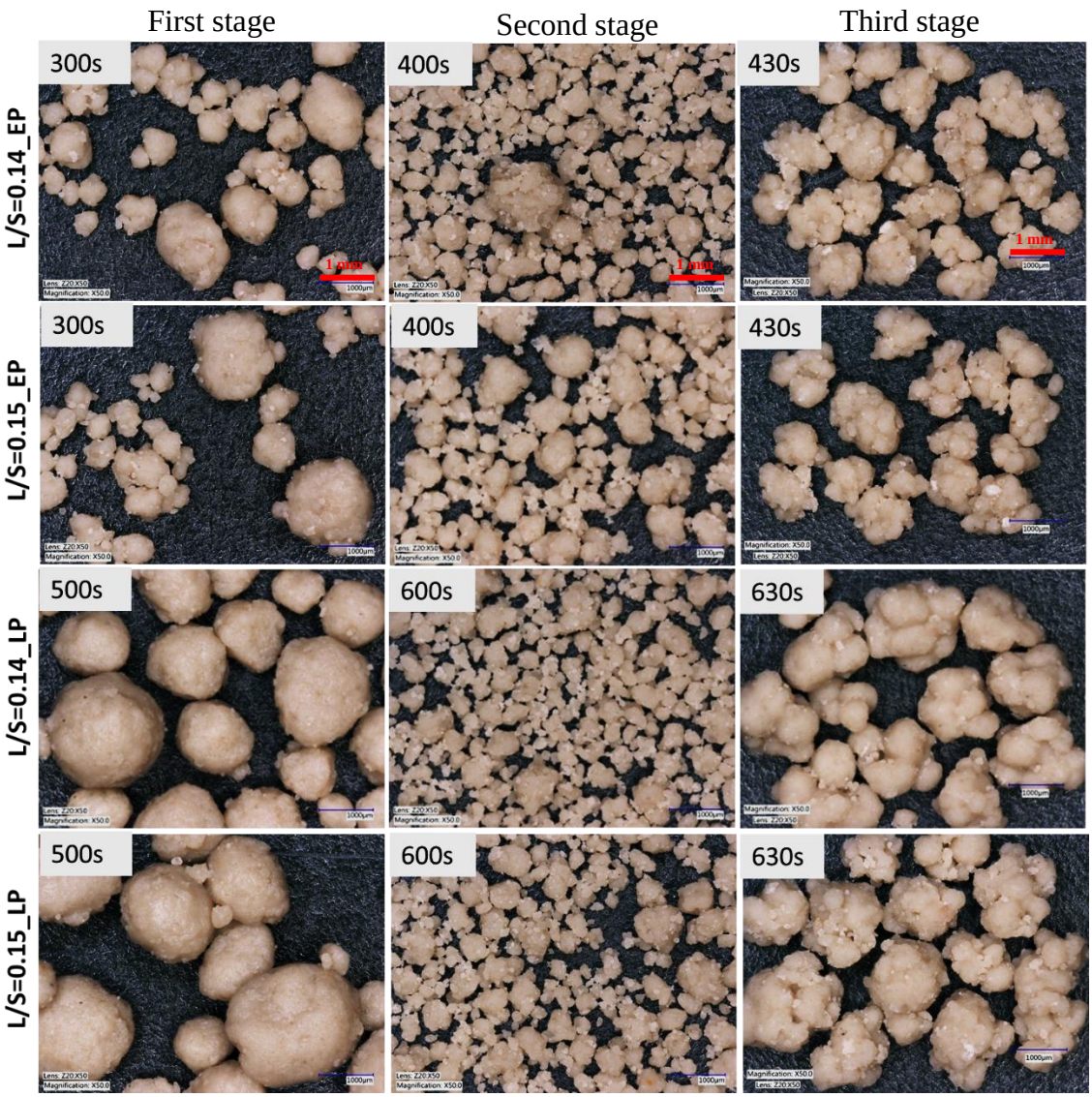

Figure 5-4. Granule shape during MSG process in different moments and stages (Keyence microscope images).

5.2.3 Size comparison between NG and MSG processes

A comparison between granule median size of (NG) process and (MSG) process could be observed from Figure 5-5 and Figure 5-6. It can be seen that the granule size keeps growing with time in the case of NG process. This is because of the growth rate domination during the whole process. While in the MSG process the granule size tendency varies through different stages, which is growth then reduction then growth once again. The reason behind this, as it is explained formerly, is because of different granulation processes occurrence in each stage. Figure 5-5 and Figure 5-6 show further that granules size in the case of L/S=0.15 is higher than L/S=0.14 for the NG process.

This is due to higher liquid to solid ratio, in general, leads to increasing coalescence rate (Reynolds et al., 2007).

In addition to the difference in the granule size, the granule shape also differs. This could be noticed by comparing the granule shape in Figure 5-4 and Figure 4-11 (in the previous chapter, section 4.4). Where the granule surface is smooth and spherical in the case of NG process throughout the granulation process while in the case of MSG process the granule shape and size are less spherical and irregular shape especially in the second and third stages.

By comparing the granule size in the case of EP and LP in Figure 5-6, it appears that the small granules at the end of the second stage of LP were growing slightly faster than the case of EP. This could be as a result of the binder distribution which was better in the case of LP compared to the EP as LP is a longer process in comparison to EP. Hence, the final granule size in the case of EP and LP looks to be insignificant statistically. Figure 5-6 shows further that the reduction in the granule size in the case of LP is more than the case of EP during the second stage. This is because the granule in the case of LP were bigger than the granules in the case of the EP at the end of the first stage.

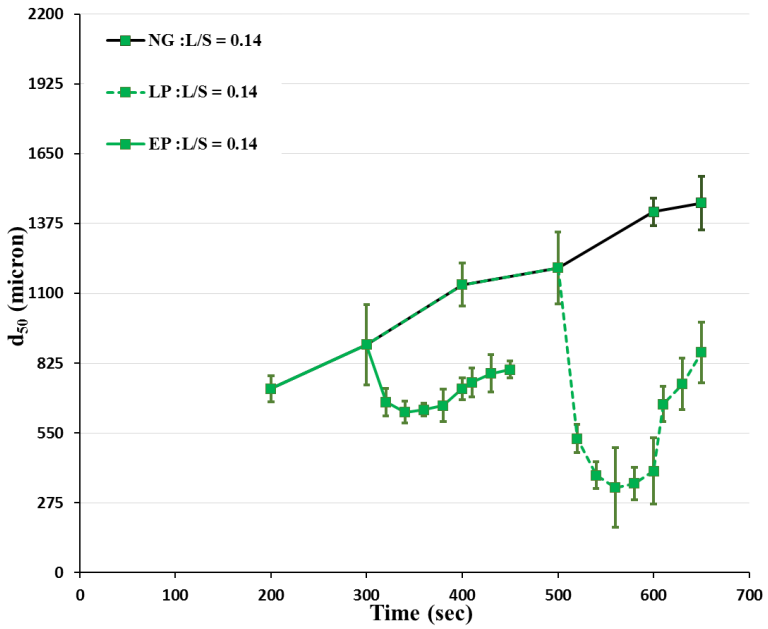

Figure 5-5. Granule median size as a function of time of NG and MSG processes for both of EP and LP, liquid to solid ratio = 0.14.

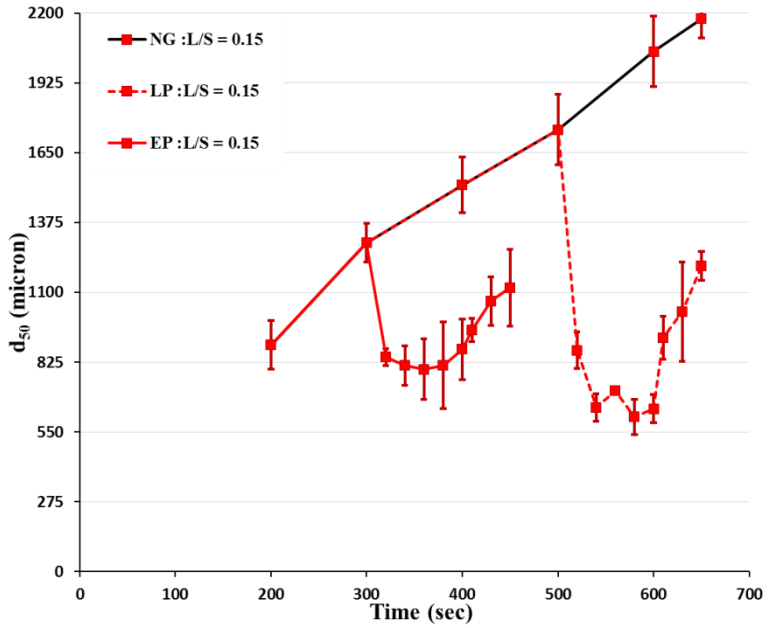

Figure 5-6. Granule median size as a function of time of NG and MSG processes for both of EP and LP, liquid to solid ratio = 0.15.

5.2.4 Granule porosity

The porosity of the produced granules was measured by liquid displacement method which is based on measuring the envelope density of the granules (Ohno et al., 2007; van den Ban and Goodwin, 2016). The envelope density depends on measuring the volume of an imaginary envelope that surrounds a single granule including the pores in the granule structure. Where a single granule could have two types of pores in its structure, open pores and closed pores (Webb, 2001). The open pores have access to the surface of the granule while the closed pores are blind pores and have no connection to the granule surface. If the surrounding liquid intruded into the open pores, the results will be biased as a consequence (Iveson et al., 1996; Le et al., 2011). Hence, this issue needs to be considered when the porosity is measured by liquid displacement method.

The experimental result for the granules porosity of MSG process for both of the EP and LP processes of liquid to solid ratio of 0.14 and 0.15 is shown in Figure 5-7 and Figure 5-8, respectively. Both figures show that the granule porosity at the first stage, in which the impeller speed is 2000 RPM, decreased with increasing granulation time. This is often the case since the extended time of granulation could lead to more consolidation of granules (Ohno et al., 2007). In the second stage (duration 300-400 sec for the EP process

and 500-600 sec for the LP process), where more aggressive conditions are applied (impeller speed 7000 RPM), the granule porosity reduced further. The reason behind this, as stated by Benali et al (Benali et al., 2009), could be as a result from the compaction and densification of the granule that may be caused by the excessive mechanical stresses imparted by the impeller to the granule while they move closer to the impeller. However, in the third stage, by reducing the applied stress to the granular bed, the porosity of the granules increased to some extent, as it can be noticed in Figure 5-7 and Figure 5-8 for the all the cases. This may due to the granules in the third stage are composed of aggregates of small fragment in which some air may be entrapped between these small granules while they were aggregating.

The change in the granule porosity during the MSG process could be observed by examining the X-ray tomography images of the granule samples taken from different stages of MSG / LP process and given in Figure 5-9 and Figure 5-10 for L/S=0.14 and 0.15, respectively. The images displayed are taken from approximately the center of the granules. They illustrate how the pores are distributed within the granules structure. It could be noticed from the images that the number of the closed pores at the time 600 sec which is the end of the second stage is lower than the other two stages. This suggests that the granules are more compacted and densified during this stage. It could be observed further, that some granules in the third stage have some open pores which may not be considered as pores during the measurement with liquid displacement method. This means that the granules at the third stage may have higher porosity than the measured one.

Figure 5-7 and Figure 5-8 show further that the granules porosity is higher in the case of L/S=0.14 than L/S=0.15 for the both of the granulation process, EP and LP. This may due to the granule interstitial volume is more saturated by more binder. In addition, the effect of the pulse in the impeller speed on the granule porosity seems to be higher in the case of lower liquid to solid ratio, i.e. the porosity variation in case of L/S=0.14 is higher than L/S=0.15. It is worth noting here that the size class of the granules used in the porosity measurement was 0.85-1.4 mm, as mentioned previously in section 3.6.2.

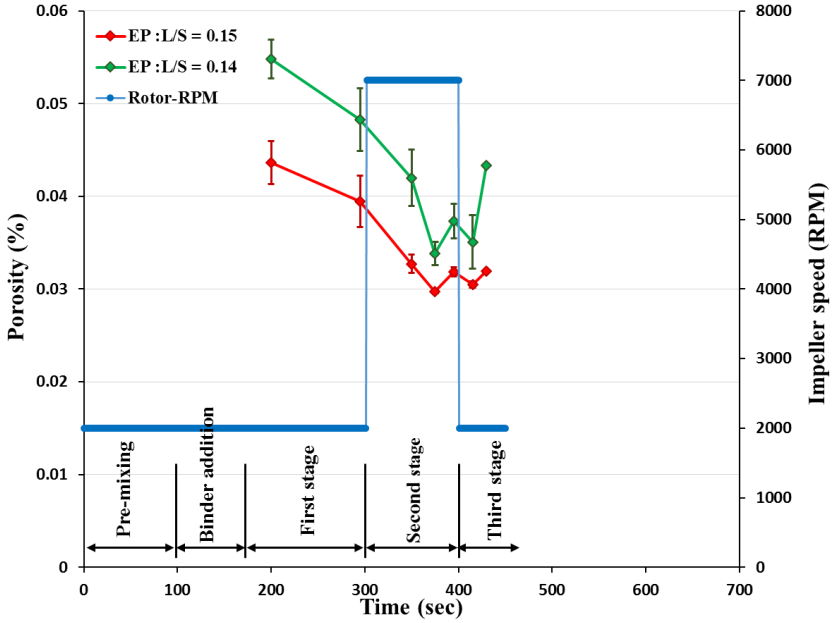

Figure 5-7. Granule porosity variation with granulation time, MSG / EP process, L/S = 0.14 and 0.15.

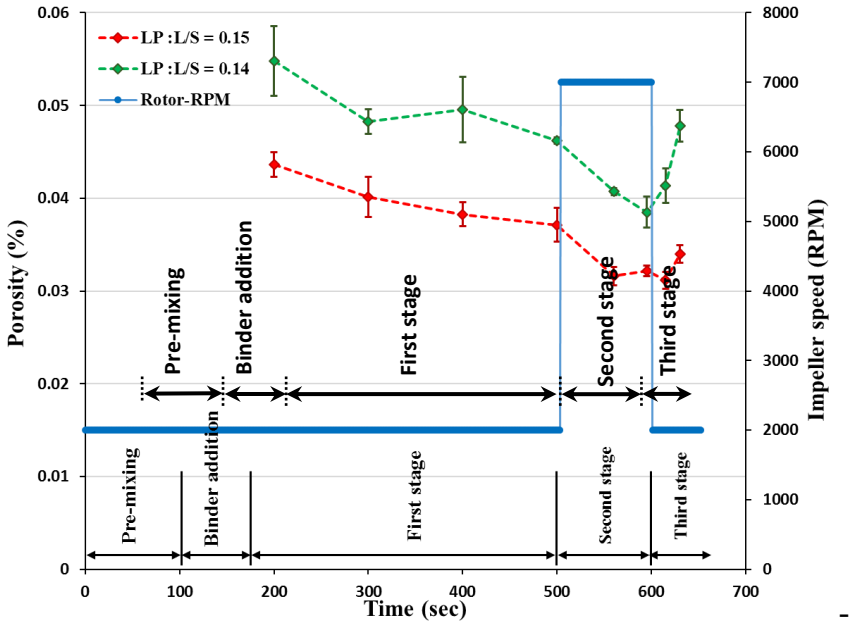

Figure 5-8. Granule porosity variation with granulation time, MSG / LP process, L/S = 0.14 and 0.15

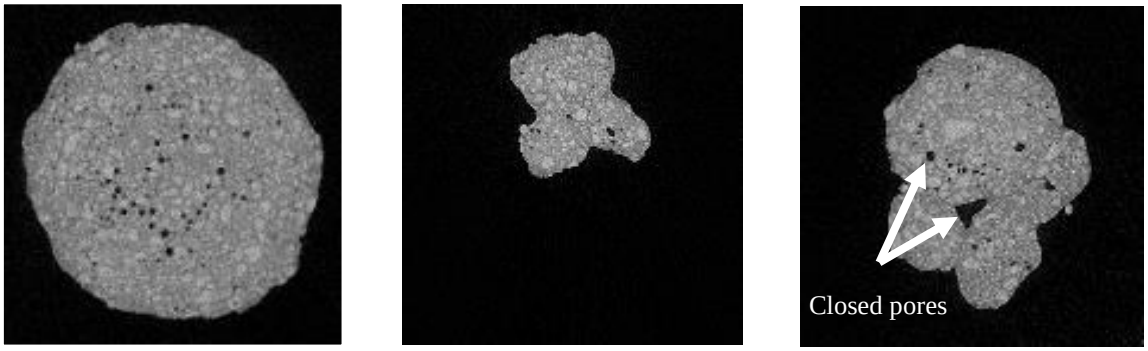

Figure 5-9. X-ray tomography images throughout the center of the granules of MSG / LP process, L/S=0.14

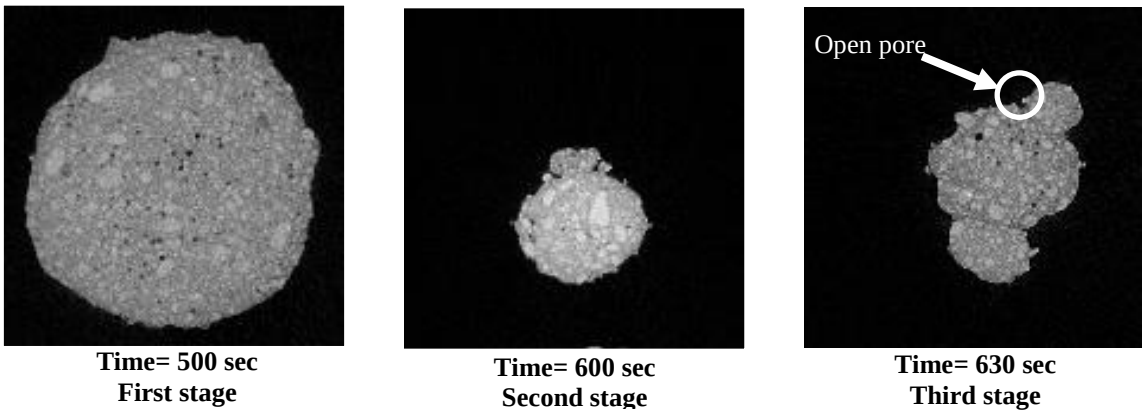

Figure 5-10. X-ray tomography images throughout the center of the granules of MSG / LP process L/S=0.15.

5.2.5 Specific surface area (SSA)

As explained in the literature review (section 2.6.5) that the specific surface area of wet granules in a high shear mixer could be affected by the granulation time. The results of the variation of SSA with the granulation time for the process of EP and LP are given in Figure 5-11 and Figure 5-12, respectively. Both of the figures shows that the SSA was decreasing with increasing the granulation time and the higher binder content in the granules leads to a decrease in the SSA. This means both of the parameters (time and high L/S) leads to make the surface of the granules smoother.

In the second stage of EP LP process, the SSA increased clearly. This is because of the breakage process which turned the big and smooth granules of the first stage to small and irregular shape fragments. By examining the Figure 5-11 and Figure 5-12 it could be noticed that the SSA was decreasing after a while during the second stage. This may due to the granules transforming towards spherical as the time progresses, although the impeller speed was relatively high (7000 RPM).

In the third stage (immediately after the second stage), the SSA was similar to the end of the second stage. However, it increased noticeably after about 30 sec in all case of MSG, notice Figure 5-11 and Figure 5-12. This may due the generation of aggregates from the small granule under low shear process (impeller speed = 2000 RPM). Then those aggregates were turning to spherical shape with time which leads to decrease in the SSA. By comparing the MSG process with NG process, it could be noticed that the SSA is always higher in the case of MSG process (in the second and third stages), which may be due to the breakage process in the second stage and the creation of the aggregates of irregular shape.

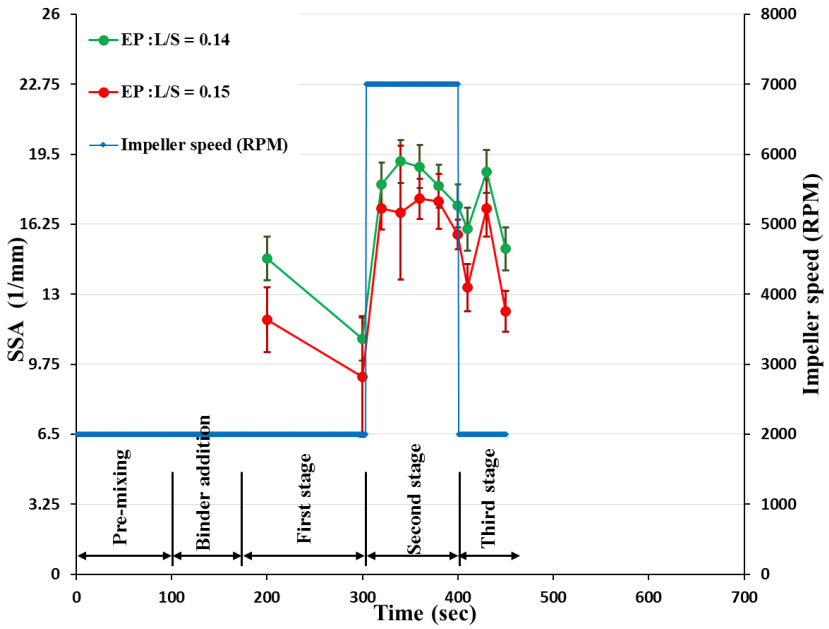

Figure 5-11: The specific surface area over the granulation time, EP process.

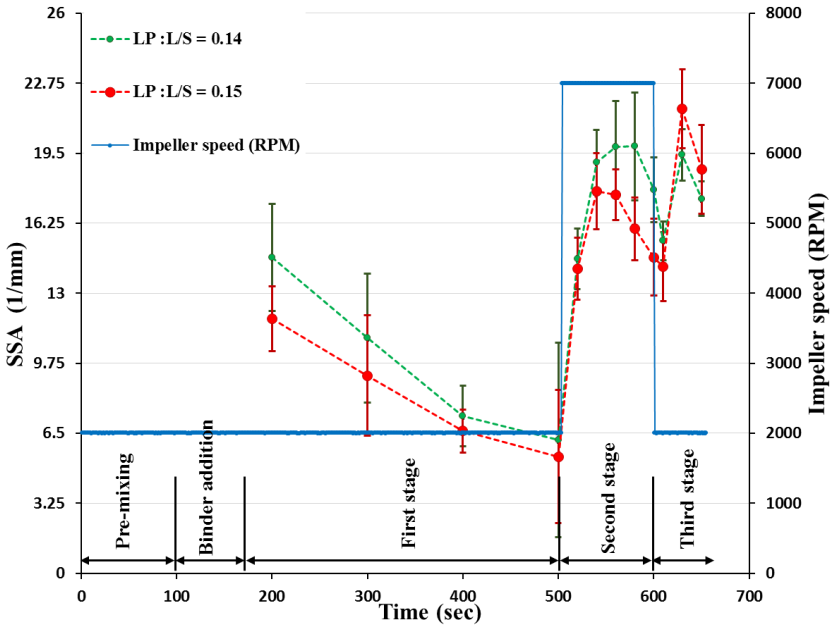

Figure 5-12: The specific surface area over the granulation time, LP process.

5.2.6 Dissolution and surface area

The rate of granules dissolution depends on the process condition of the dissolution as well as the granule properties such as porosity, surface area, and type of the constituent materials. Therefore, to eliminate the effect of the dissolution condition, the dissolution process was conducted under the same conditions using the same amount of granules, see the chapter of materials and methods (section 3.8). It is worth mentioning here that the granules disintegrate first when the binder (PEG1000) starts dissolving in the liquid solution and the powder constituents will dissolve in the solution simultaneously. Samples of granules from the first and third stage of the multi-stage granulation process are examined and their conductivity recorded with time.

For the case of LP process experiments and L/S=0.14, the dissolution profiles for the granules samples at 500 sec and 630 sec, which are the end of the first and third stage respectively, are given in Figure 5-13. The figure shows that the granules from the first stage require a longer amount of time to dissolve in comparison to the granules of the third stage. This is emphasised clearly by comparing the t_{90} for the both samples. The t_{90} represents the time needed to dissolve 90% of 1 gram of granule sample of a certain size range. The t_{90} for the both samples are given in Figure 5-13.

Figure 5-13 suggests that the difference in the dissolution time (t_{90}) between the first stage and the third stage is about 35 sec. This shows that the granules at third stage dissolve faster than the first stage, in contrast to what is generally expected when a longer granulation time is sued, which usually leads to granule consolidation and therefore longer dissolution time will be needed as a consequence. This difference in dissolution time most probably results from the difference in the granule surface area of the first stage and the third stage. Meanwhile, the dissolution process is governed by the contact surface area available between the granule and the liquid solvent. Consequently, increasing the granules surface area means decreasing dissolution time. The specific surface area (SSA) of the granules were 6.1 mm^{-1} and 19.4 mm^{-1} for the end of the first stage and the third stage respectively. This change in the surface area was by virtue of the different stages of the granulation process that the granules went through. The difference in the surface area is more apparant by examining the SEM images, shown in Figure 5-14, of the granules at the different stage and different moments. It is clear that the granule at the moment 630 sec is more tortuous and has more surface area than the granule at the moment 500 sec (end of the first stage).

The dissolution test was also conducted for granules of LP process and L/S=0.15. The dissolution profiles for the granules at the end of the first stage and third stage are given in Figure 5-15. The dissolution time (t_{90}) for the first stage and the third stage was 192 sec and 151 sec respectively. This difference in the dissolution time may, also, due to the higher surface area of the granules at the third stage than the first stage. The specific surface area for the granules at the moments 500 sec (first stage) and 630 sec (third stage) was 5.4 mm^{-1} and 21.5 mm^{-1} respectively. This difference could be more recognizable by observing Figure 5-16, in which it suggests that the granule at the 500 sec is more spherical compared with the granule at 630 sec.

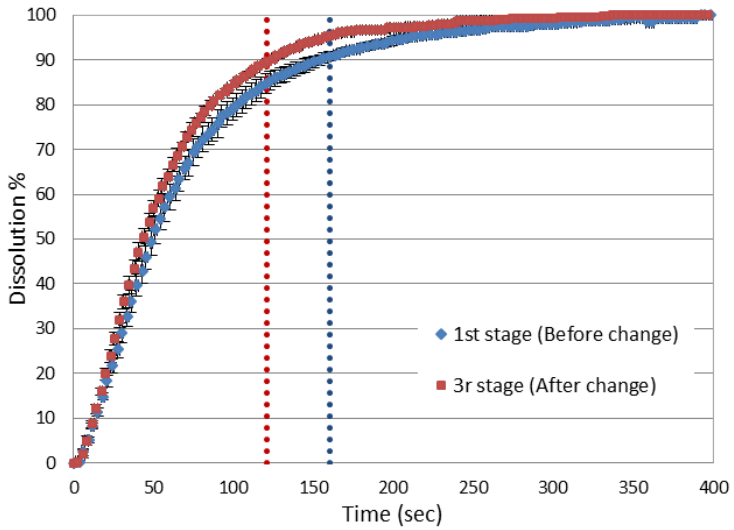

Figure 5-13. Granule dissolution of first and third stages. (LP process, L/S=0.14). t_{90}=154 sec for the 1st stage and t_{90}=119 sec for the 3rd stage.

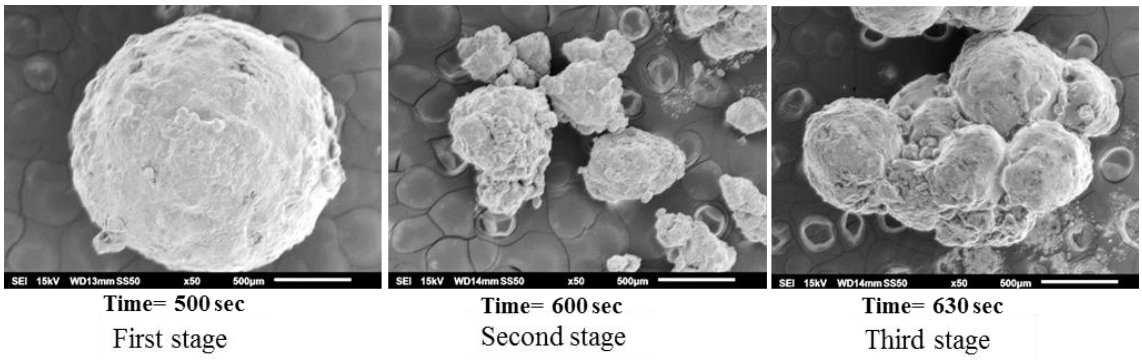

Figure 5-14. SEM images for the granules at different moments. (MSG / LP process, L/S=0.14).

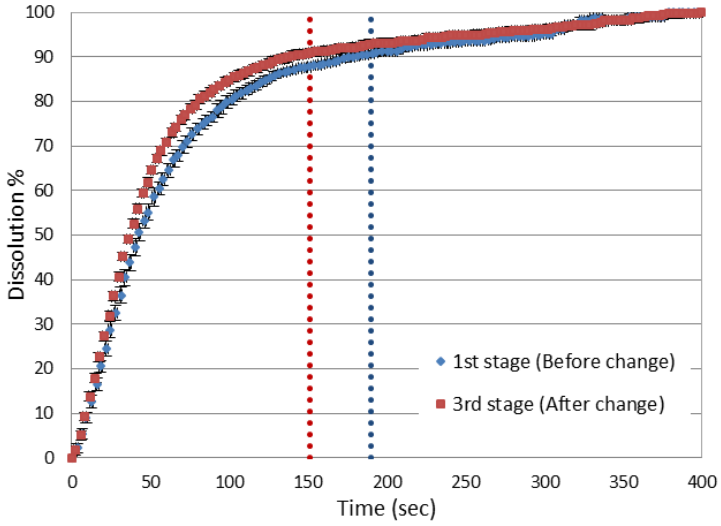

Figure 5-15. Granule dissolution of the first and third stage. (LP process, L/S=0.15) t_{90}=192 sec for the 1st stage and t_{90}=151 sec for the 3rd stage.

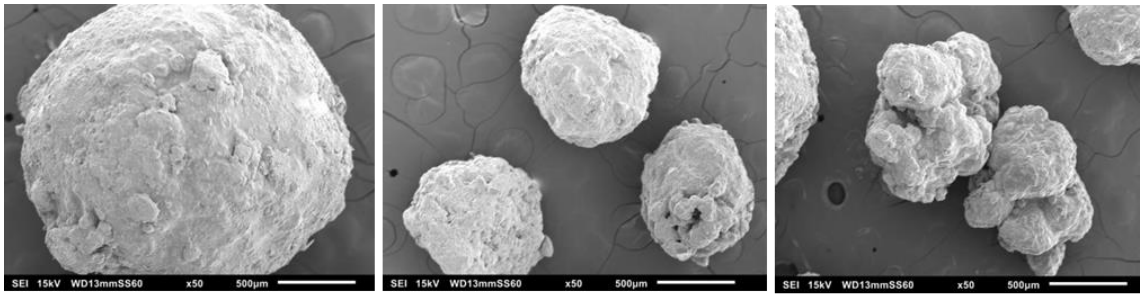

Time= 500 sec
First stage

Time= 600 sec
Second stage

Time= 630 sec
Third stage

Figure 5-16. SEM images for the granules at different moments, (MSG / LP process, L/S=0.15).

On the other hand, the dissolution profile for the granules produced by EP process and L/S= 0.14 is shown in Figure 5-17. Similarly, the figure suggests that the granules of the third stage have a higher dissolution rate in comparison to the granules of the first stage (before the change), since there is a 39 sec difference in the dissolution time (t_{90}) between them. This is also ascribed to the difference in the surface area. Where the specific surface area (SSA) was approximately 10.9 mm^{-1} and 18.7 mm^{-1} for the first and third stage respectively. A similar approach has been noticed in the case of L/S=0.15, see Figure 5-18. Where the difference in the dissolution time (t_{90}) between the first stage and the third stage was in the region of 33 sec owing to the difference in the granules specific surface area, which was 9.17 mm^{-1} for the first stage and 16.9 mm^{-1} for the third stage. It is worth noticing here that the effect of granule surface area, as suggested, was a significant parameter in the dissolution process.

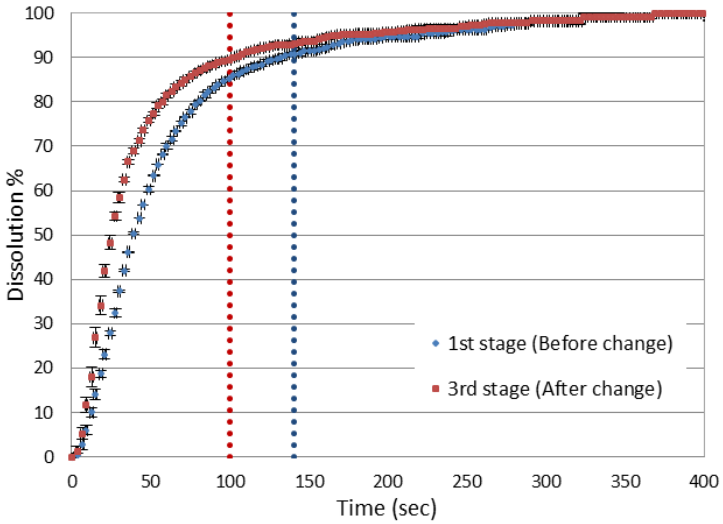

Figure 5-17. Granule dissolution of first and third stage. (EP process, L/S= 0.14). t_{90}=141 sec for the 1st stage and t_{90}=102 sec for the 3rd stage.

By plotting the dissolution time (t_{90}) against the specific surface area (SSA) for the all cases explained formerly, the difference between the granules of the first stage and the third stage could be observed more clearly, see Figure 5-19. Where the granules of the third stage have higher SSA and lower t_{90} than the corresponding granules of the first stage. By comparing the dissolution time (t_{90}) of EP and LP, Figure 5-19 shows that the difference between EP and LP is relatively more pronounced in the case of higher L/S ratio, i.e. L/S=0.15. This could be ascribed to the difference in the surface area which is higher in the case of L/S=0.15 than in the case of L/S=0.14.

To further explain the change in the dissolution time t_{90} of all cases of the EP and LP, the percentage of dissolution time reduction is calculated (based on comparing the t_{90} of the granules of the 3rd stage to the 1st stage) and showed the following; (LP/0.14)=22.72%, (LP/0.15)=21.35%, (EP/0.14)=27.66%, and (EP/0.15)=22.29%. Although the difference appears not to be significant between all the cases, there is at least 21.35% change which is not a trivial change. This could be exploited in many fields, e.g. in pharmaceutical products, in which the product dissolution time is an important issue.

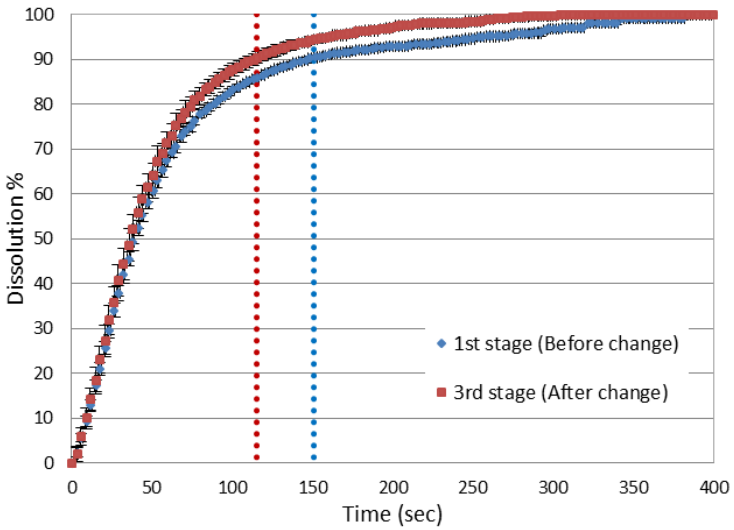

Figure 5-18. Granule dissolution of the first and third stage. (EP process, L/S=0.15) t_{90}=148 sec for the 1st stage and t_{90}=115 sec for the 3rd stage.

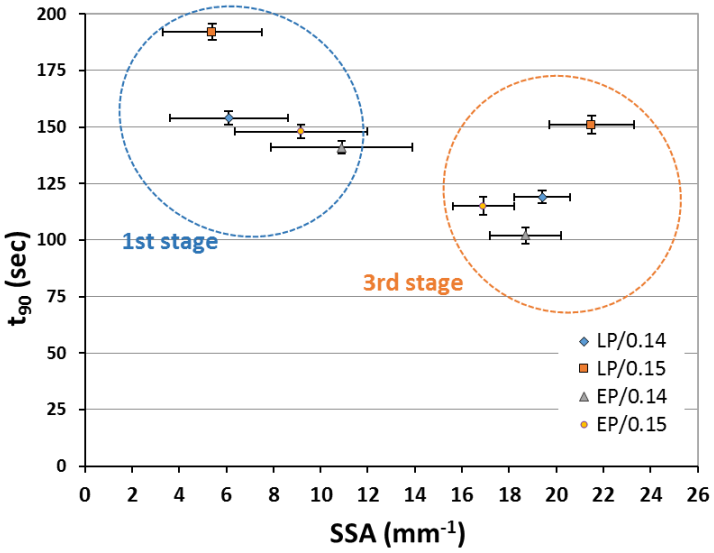

Figure 5-19. The dissolution time (t_{90}) versus specific surface area (SSA).

5.2.7 Size distribution and span

One of the important characteristics of the granular products is the size distribution and the width of the size distribution. The evolution of granule size distribution for the MSG processes with the time are shown in Figure 5-20 to Figure 5-23. Different trends in the size distribution were noticed at different stage of the MSG. The size distribution during the first stage was tending to be narrower with time for the all cases of MSG. This part

was discussed in the previous chapter (section 4.3) and will not be explained here, as the first stage of MSG is similar to the process of the NG.

While during the second stage (impeller pulse duration) the evolution of the size distribution was relatively different. At the early time of the second stage the size distribution was wide. Most possibly, this was due to the breakage of all the granules was not accomplished, yet. Meaning that there was big granules and small granules present at the same time which resulted in a wide distribution. This will be clearer by observing the span of the granule in the Figure 5-24 and Figure 5-25 for EP and LP process, respectively. Where, during the second stage the span was increased at 320 sec in case of EP and at 520 sec in case of LP process. Then after that, the span decreased with time due to the progress of the breakage process which tends to increase the uniformity of the size distribution, see Figure 5-20 to Figure 5-23.

The figures of the span and size distribution, also, suggests that the narrowest size distribution was at the end of the second stage and the beginning of the third stage. At the beginning of the third stage, the size of the granule was small and close to be monosized granules. Then after that the size distribution transitioned towards a wider range and the span started to increase with time, which is opposite to that seen during the first stage in which the size distribution was getting narrower with time and the span was decreasing with time.

It could be concluded out of these results, that if a narrow granule size distribution is preferred, then it will be better to stop the granulation process right after the second stage. In other words, short duration time of the third stage could lead to produce monosized granules. However, this will also depends on the materials used in the granulation process. It is interesting to compare, here, the span between the third stage of MSG (EP and LP) processes and NG process at 2000 RPM impeller speed. In the case of L/S=0.14, the span at the beginning of the third stage of MSG was about 0.99 and 0.88 for the case of EP and LP respectively, and at the equivalent points of the NG process, i.e. at 400 sec and 600 sec, the span was 1.47 and 1.26 respectively. While, in the case of L/S=0.15, the span at the beginning of the third stage of MSG was about 0.82 and 0.77 for the case of EP and LP respectively, and at the equivalent points of the NG process, i.e. at 400 sec and 600 sec, the span was 1.20 and 1.12 respectively. In other words, it means that the span of size distribution was reduced at least 30% when using MSG process compared to the NG

process. These values highlights the advantages of the MSG process compared with the NG process in which it is possible to obtain a narrower size distribution if desired.

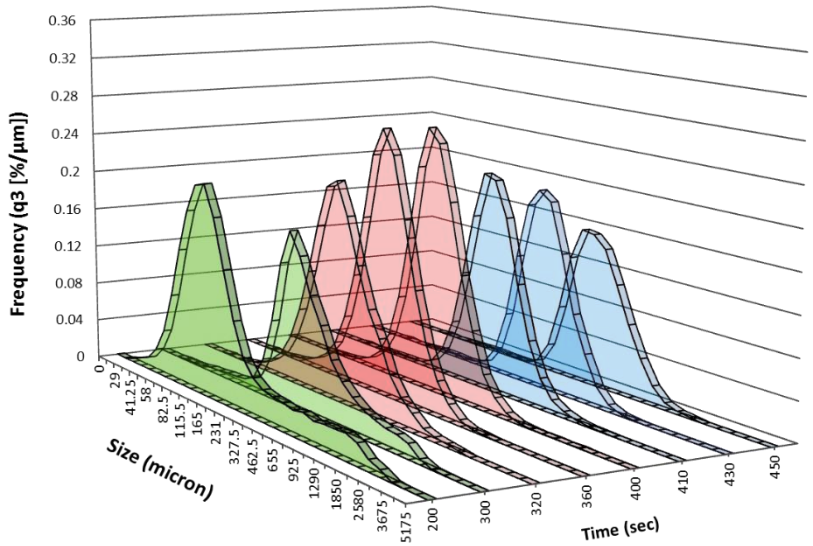

Figure 5-20: Granule size distribution over MSG, EP, L/S = 0.14. The green colour for the 1st stage, the red colour for 2nd stage, and the blue colour for the 3rd stage.

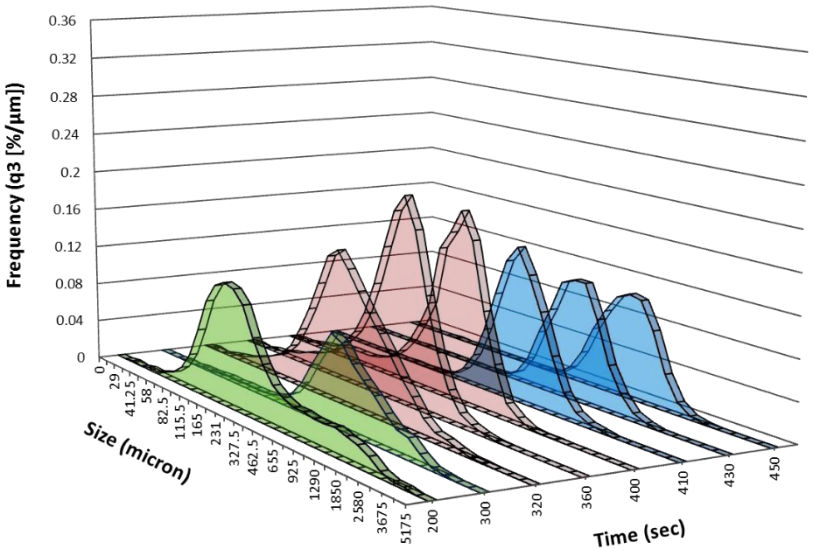

Figure 5-21: Granule size distribution over MSG, EP, L/S = 0.15. The green colour for the 1st stage, the red colour for 2nd stage, and the blue colour for the 3rd stage.

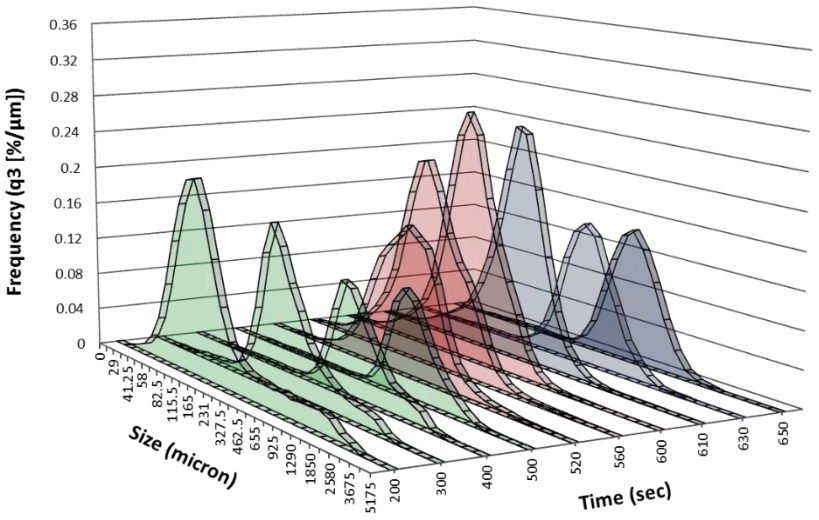

Figure 5-22: Granule size distribution over MSG, LP, L/S = 0.14. The green colour for the 1st stage, the red colour for 2nd stage, and the dark blue colour for the 3rd stage.

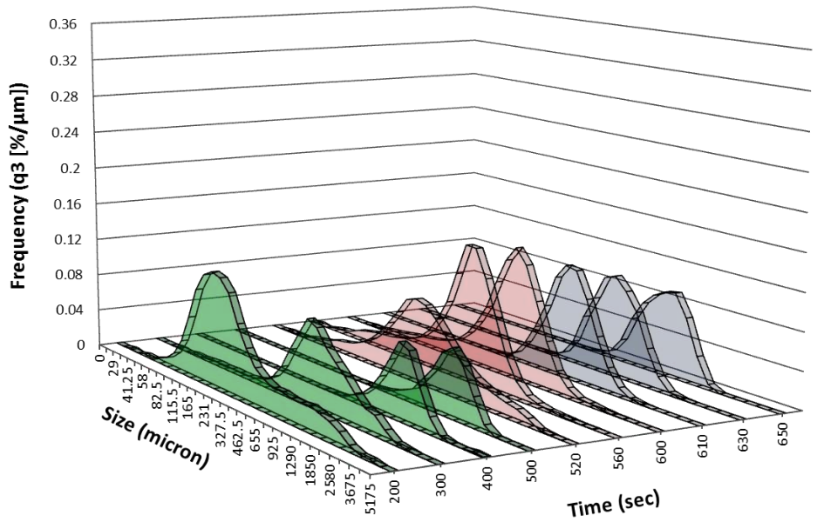

Figure 5-23: Granule size distribution over MSG, LP, L/S = 0.15. The green colour for the 1st stage, the red colour for 2nd stage, and the dark blue colour for the 3rd stage.

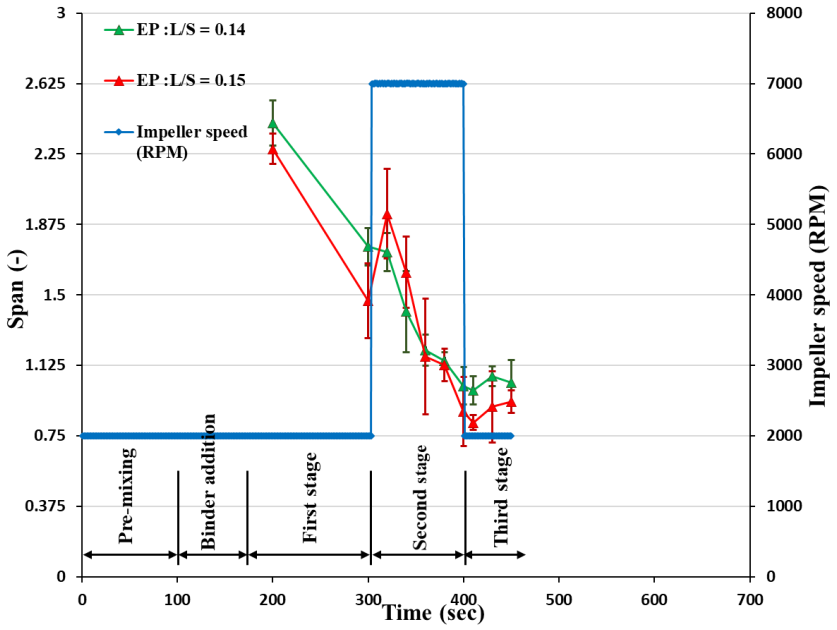

Figure 5-24: Span of the granule size over granulation time, EP process.

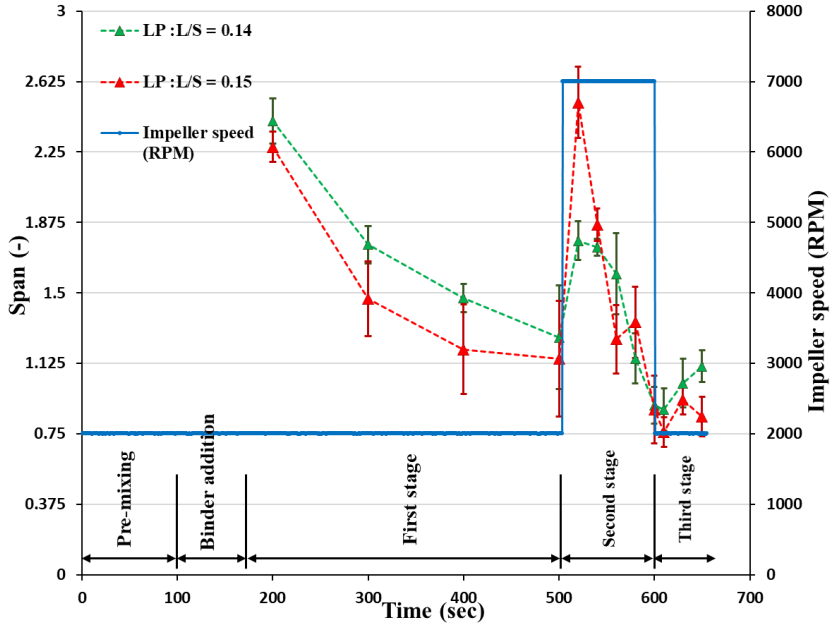

Figure 5-25: Span of the granule size over granulation time, LP process.

5.2.8 Proposed mechanism for the MSG

A certain mechanism for the MSG was proposed depending on the experimental results explained formerly, see Figure 5-26. Three mechanisms were proposed equivalent to the number of stages of the MSG process. The first mechanism is for the first stage which identical to the normal granulation process (NG) at low impeller speed (2000 RPM). This mechanism was explained in the previous chapter (section 4.7), hence it will only be explained briefly here. As mentioned previously, the nucleation process is started by adding the binder onto the moving powder bed. Then the binder is distributed by virtue of the shear within the powder bed which is imparted by the vessel and impeller movement. Then the granule size started to increase by coalescence and layering. The granules were densifying due to a longer granulation time. It was expected that the binder was moving from the centre of the granule towards its surface while it densifies with granulation time. Samples of binder distribution within the granule are given in Figure 5-27. The figure illustrates how the binder is distributed within the granule (section from middle). This figure is for a broken granule from the central area.

In the second stage, where the impeller speed was increased from 2000 RPM to 7000 RPM, the granules started moving more intensively especially at the point where the impeller hits the granular bed. As a consequence, the granules started to break into small pieces with time, see Figure 5-28. The breakage persisted with time until most of the big granules were broken to fragments. This process was represented by a breakage process which is illustrated in the second stage in the Figure 5-26. Most of the granules at this stage have the lowest porosity, see Figure 5-7 and Figure 5-8, and the shape of the granules was irregular during the initial period of this stage, see the middle images of the Figure 5-3. However, the granules shape will become more spherical with time, see the images of the second stage of the Figure 5-4 taken by the microscope. At the end of this stage, the binder was expected to be distributed more evenly in the granules.

Finally, in the third stage when the impeller speed was decreased, the size distribution was uniform and the granule size was small at the start point of this stage. However, if the granulation proceeded for longer time, the small granules from the second stage start to aggregate again and re-growing with time. The mechanism for this growth most likely is the coalescence process. As the granules from the second stage were small and the binder is well distributed, this will encourage the coalescence process.

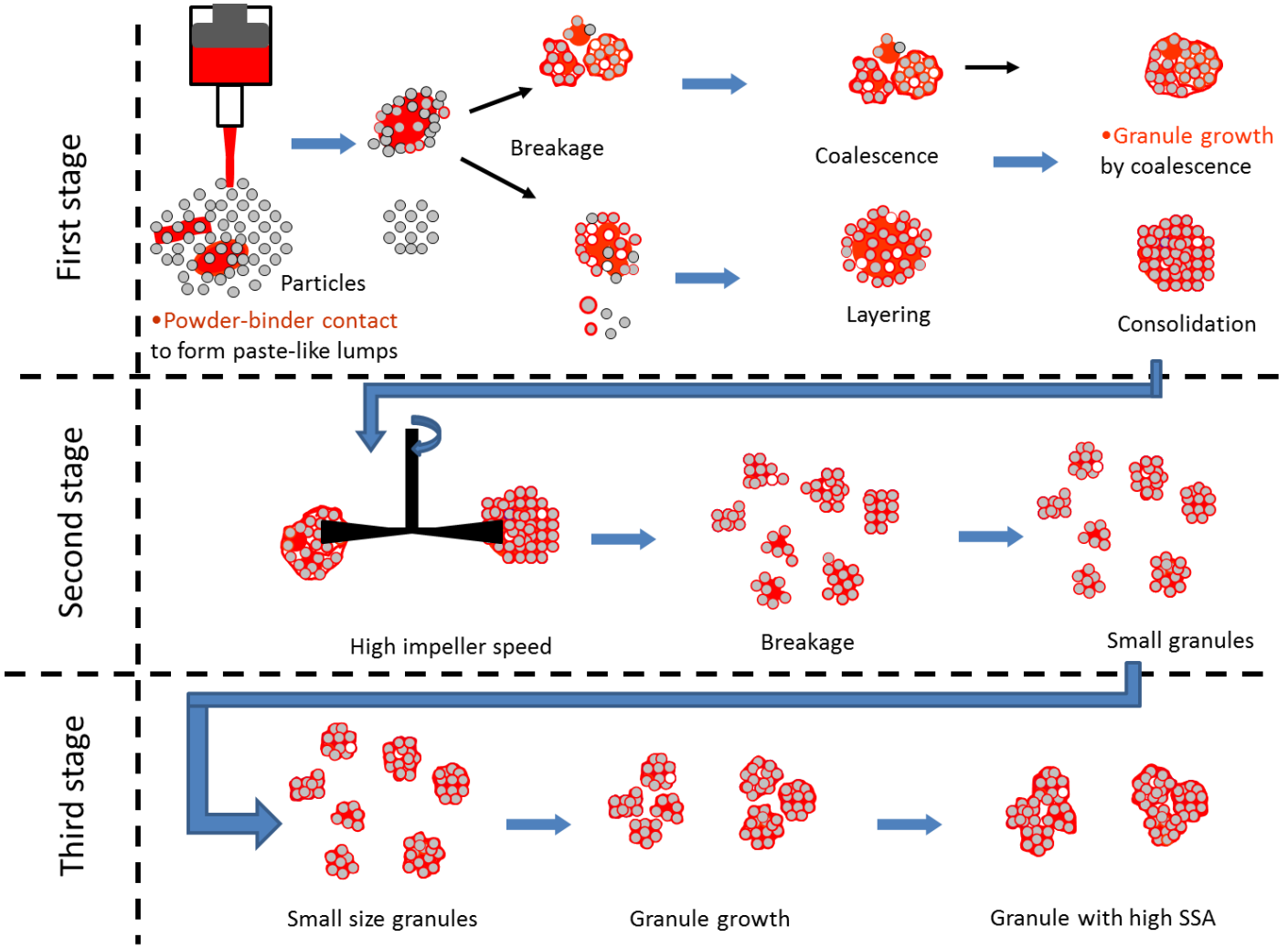

Figure 5-26: Proposed mechanism for the Multi-Stage Granulation process.

This means, if the period of the third stage is short, anarrow granule size is attainable. Whereas, if the granulation time is prolonged, granules with high specific surface area could be obtained, since the granule will form aggregates of small granules and the surface of the granules will be tortuous, notice the images of the granules of the third stage in Figure 5-4, Figure 5-14, and Figure 5-16.

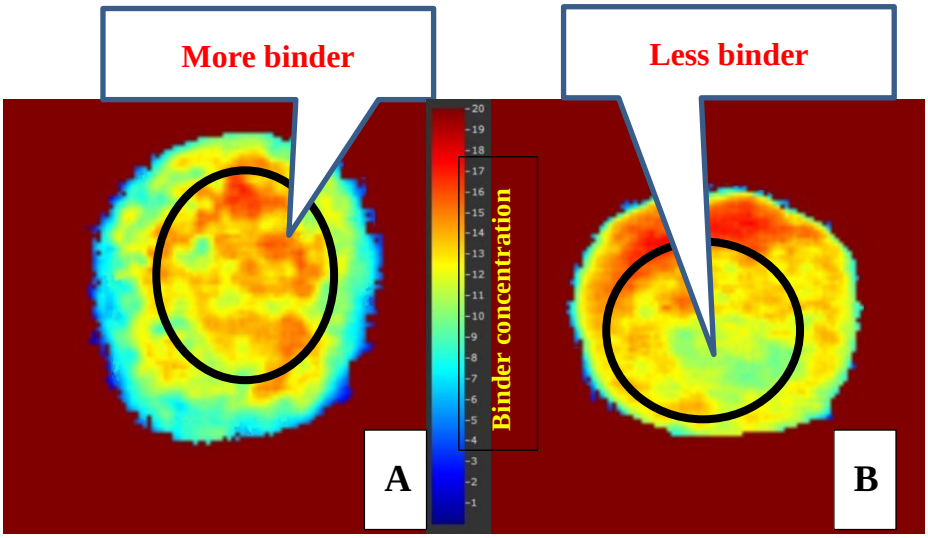

Figure 5-27: The binder distribution within the granule at the first stage. A) At 200 sec, B) At 500 sec.

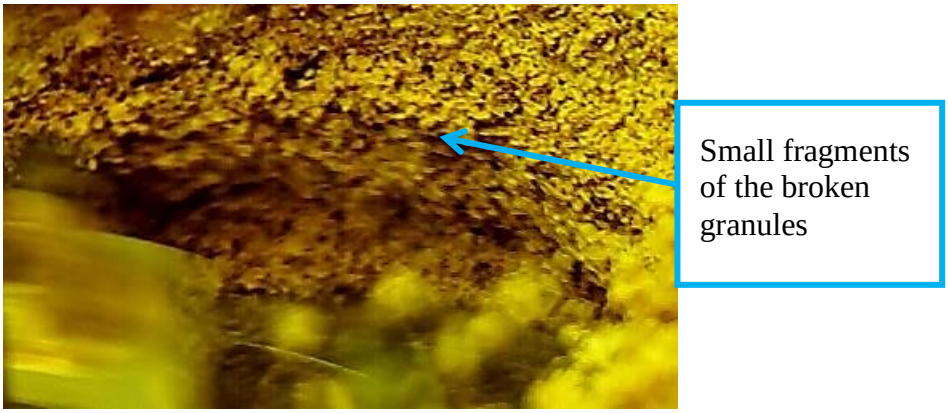

Figure 5-28: Image of the granular bed after been impacted by the impeller, Impeller speed = 7000 RPM, L/S = 0.14.

5.3 Conclusions

The majority of research available in the literature, which is concerned with improving the final granules properties in terms of granules ability to dissolve fast and survive during handling and storage, have revealed difficulties in producing such preferred typical granules. In the current work, an attempt is made to get an approach to enhance the final granule attributes via a non-conventional granulation method named as multi-stage granulation.

It could be noticed from the results of this chapter that the granules characteristics are apparently influenced by the process variables. Where the granule size, porosity, shape, and dissolution have changed with changing the process variables which is compatible with what many researchers have reported in the literature.

The experimental results of the multi-stage granulation (MSG) process, which is granulation procedure followed in the current work, has showed that granules median size was changing by varying the impeller speed throughout the different granulation stages and with the granulation time. This change is the consequence of different granulation mechanisms that the granules may undergo during the granulation process, particularly growth, breakage, and coalescence. The change in the granule size was more obvious when the pulse change in the impeller speed was late (LP) rather than early pulse (EP) condition.

Although the porosity of the granules did not improve valuably a narrow size of granule was achievable. Where the size distribution was more uniform at the beginning of the third stage, then the span was increasing slightly with time. The span was reduced to about 30% in the third stage of MSG process compared with equivalent points of NG process. These results could be interesting and relevant for certain industrial application, e.g. catalyst and pharmaceutical products, in which a narrow size distribution is important property.

The dissolution rate of the granules was observed to improve, as well, to some extent at the third stage. Where granule samples which are collected after the pulse change (i.e. granules of the third stage) were noticed to dissolve at a higher rate than granules before change (i.e. granules of the first stage). The dissolution time improved by at least 21%,

which is not a trivial change that could be exploited in some applications in which the dissolution time is important, e.g. pharmaceutical industry. This difference in the dissolution time (t_{90}) is most probably as a result of the difference in the granules surface area and the SSA of the granules was the main parameter influencing the dissolution time. It has been noticed that the granules surface area increased when the multi-stage process is implemented, which is not achievable via normal granulation process.

It is worth mentioning that the mechanism of MSG was utilized for an industrial project to improve the granule size distribution. The yield of a certain size class of a product was improved from 30-35 % to 50-55 % in an industrial Eirich mixer.

CHAPTER 6 FLOW CHARACHTERISTICS IN MSG USING PIV TECHNIQUE

6.1 Introduction

In this chapter, the behaviour of the flow of the granular material inside the high intensive mixer (Eirich mixer) and the mechanism of generation of particle motion inside the mixer was investigated. This is an important because the flow pattern of the granular flow and the velocity field has a curial effect on the different granulation mechanisms, especially growth and breakage, in which it has an impact on the properties of the granules and changes in the size of the granules during the granulation process. The growth and breakage processes were clearly taking place in the same granulation process in this work, namely in MSG process as explained in chapter five. Hence, this chapter will give insights and interpretations on how the granule properties, namely the size, was affected during the MSG process. In addition to the above motivation, the PIV study is also important to validate the simulation work which is related to the particle motion and will be explained in detail in the next chapter. For this reason, experimental work was carried out in the current work to investigate the velocity distribution of the granules in the whole mixer. The velocity distribution of the granule movement was obtained using a technique called Particle Image Velocimetry (PIV), which is outlined in Chapter 3. Since this technique is based on using optical high-speed camera, which takes images from surfaces reflecting the light, the surface velocity of the granule bed could be monitored.

It is important to mention here that studies in relation to the granular flow in the Eirich mixer is limited in terms of the published literature available. However, some explanations have been reported in some articles (Nold et al., 2008; Serkowski Habil and M, 2004) showing the general flow directions of the materials in the Eirich mixer without illustrating the technique used to infer the flow direction. Although the Eirich mixer consists of three main parts (impeller, scraper and the vessel), the granular flow inside it is, in fact, more complex than other high shear mixers (e.g. Roto Junior). This may due to the difference in the arrangement and geometrical shape of the mixer's parts.

The experimental results demonstrated here are for the cases of MSG of LP and EP for different impeller speeds, 2000 RPM and 7000 RPM and for the both cases of L/S=0.14

and L/S=0.15. Some areas in the images were excluded from the region of interest of analysis as indicated in the Figure 6-1. This is because of either the granules were covered from the camera by an obstacle, e.g. impeller shaft, or there were limited number of granules in the examined area, e.g. area behind the scraper.

The flow characteristics will be explained in term of general features of the granule flow and the velocity vectors in a specific region within the mixer.

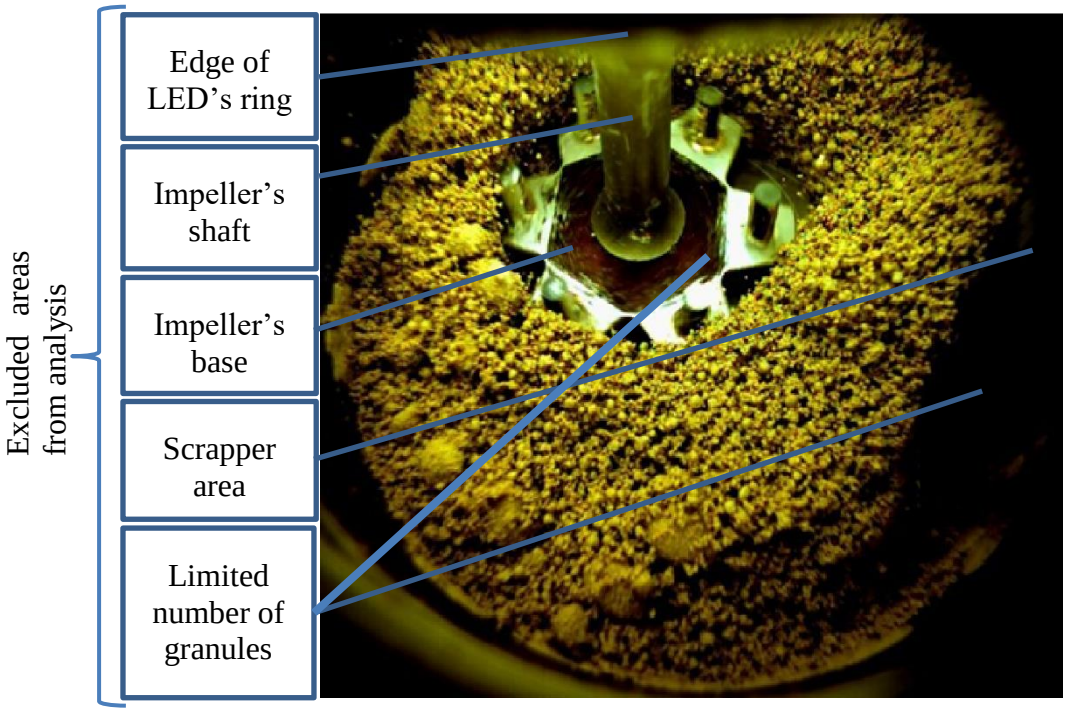

Figure 6-1: Image of the granular bed showing the areas excluded from analysis

6.2 General flow characteristics

An example of the velocity vectors of the granular flow inside the mixer is given in Figure 6-2 for a certain granulation conditions. The flow vectors illustrate that the flow of the granules in the mixer is not in a regular way (asymmetric in angular direction). Which means that the motion is not in a circular lane neither around the impeller nor around the circumference of the vessel. This is dissimilar to what is usually noticed with other mixers like Roto Jounior (Vertical type mixer), where the granules, usually, move symmetrically in the angular direction in the circumferential direction of the mixer vessel. The granular bed in the Eirich mixer, however, could be described to move in a semi-circular lane

around the impeller with different speeds and direction depending on which zone they are moving in. This is mostly due to the eccentricity of the impeller position from the centre of the vessel and the existence of the scrapper that deflects the trajectory of the motion direction.

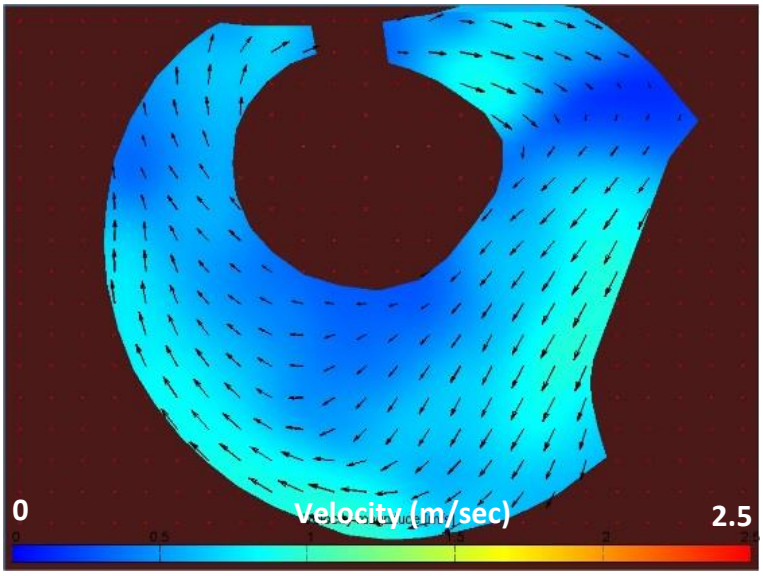

Figure 6-2: Typical example for the velocity vectors in Eirich mixer

Because of this asymmetric motion and the variation of the granules velocity vectors in different zones inside the mixer, the granules will be subjected to different shear forces and stresses within the mixer depending in which zone they are present. This, in consequence, will lead to different granulation mechanisms occurring, e.g. growth and breakage, in the mixer simultaneously in different zones of the mixer. Accordingly, the vessel of the mixer is divided to a number of zones, see Figure 6-3.

Zone 1, which is the zone before the impact of the impeller to the granular bed. In this zone, the granules have the velocity magnitude and direction similar to the vessel's base. This is because of the motion of the granules is mainly driven by the motion of the vessel of the mixer. Within this zone, the relative velocity between the granules most probably is the minimum velocity compared to the other zones of the mixer, as the granules in this region are not exposed to any other external applied forces rather than the wall of the vessel. In other words, it means that the granules are subjected to the less stress and shear within this region.

Zone 2 is the region to the right side of the impeller in the Figure 6-3. In this zone, the granular bed moves faster than the zone1 as a result of the impeller which impacts on the bed. Some of the granules, which are not subjected to direct impact by the impeller, will have a lower velocity. However, the velocity of the granules will reduce, as they will be close to the scrapper, which tends to change the trajectory of the particle pathway.

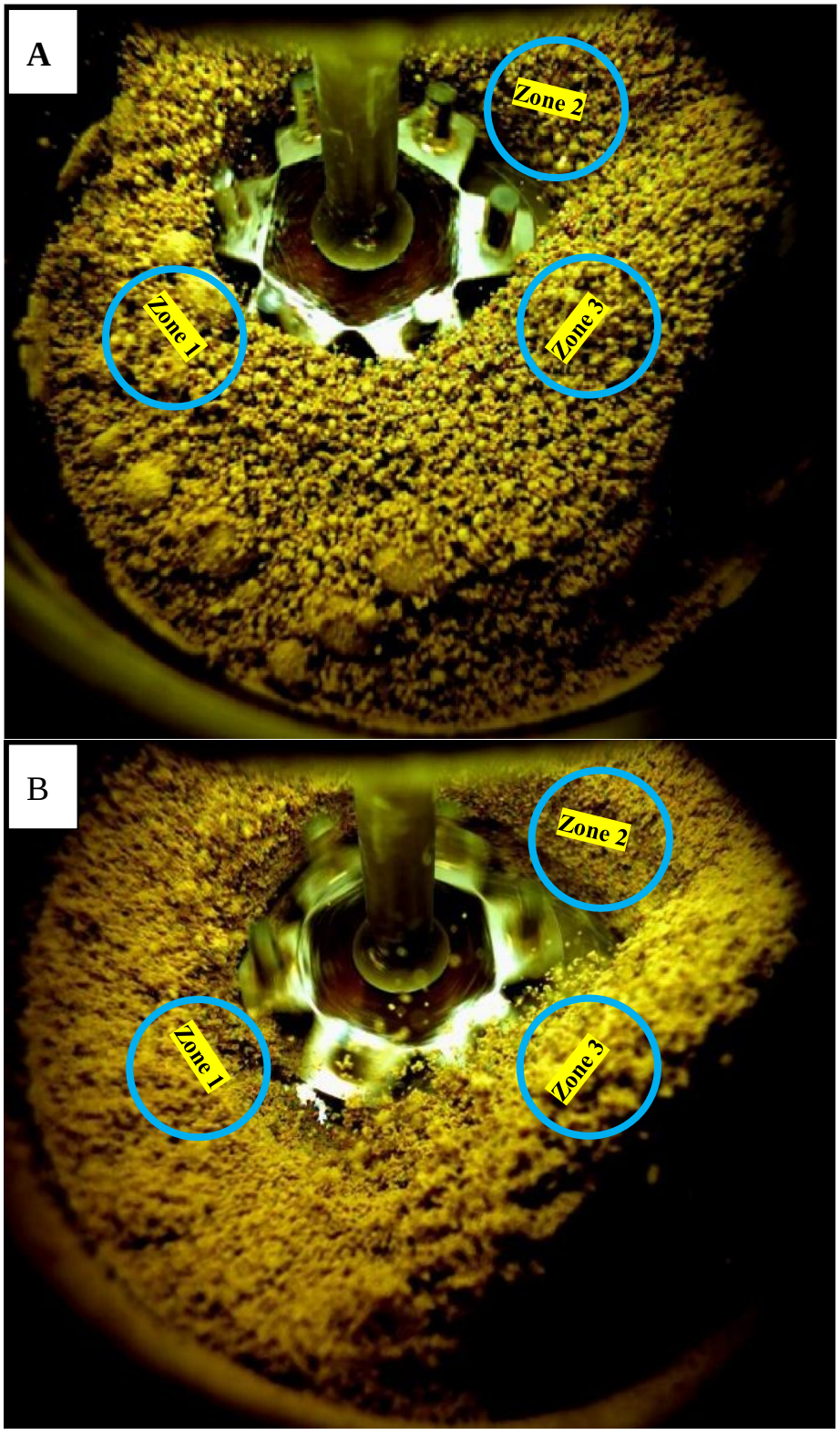

Figure 6-3: Zones of the bed of the granules in the vessel. A: First stage, impeller speed = 2000 RPM and the vessel speed = 85 RPM. B: second stage, impeller speed = 7000 RPM and the vessel speed = 170 RPM

As a result, zone 2 was considered as the most intensive zone, as the granules have the highest kinetic energy (highest velocity). This could affect the granule properties but depending on the speed of the impeller. If the impeller speed was moderate, most probably, the granules will gain more velocity that could lead to encourage the growth process of the granules and the granule size will increase with time. Conversely, if the impeller speed was very high compared with the bed velocity, granule breakage may take place and as a consequence, it will lead to a decrease the granule size. The fast granules (after impact) were hitting the scrapper. This region is the granule collision region, where the granules collide primarily with each other and collide with the scrapper.

After the granular bed impacts with the scrapper, the granules now move into zone 3. This zone was designated to be after the scrapper. The interspace between the granules and aggregates in this region was high and the granules are in less contact with each other and moving more freely. This means that the instantaneous bulk density of the granular bed in this zone is the minimum, compared with the other two zones, (zone 1 and zone 2).

The velocity of the granules in this zone is less than the velocity at the zone 2, this is because some of the granule kinetic energy will be dissipated during the granules collision with each other and with the scrapper at the end of the zone 2. In addition, the shear within the bed of the granules is less compared with the other zones, as the granules are in less contact with each other in this zone. The granules at the end of the zone 3 were looking to fall on the granular bed at the beginning of zone 1 from a higher level in which granule coalescence may take place there. As the velocity of the granules decreases, this means there is a reduction in the kinetic energy of the granules.

There are some differences in the area of each zone at different stages namely for the zone 2 in the second stage of the MSG. The area of the zone 2 will be slightly smaller when increasing the speed of the impeller. This will be raised form the high impact speed of impeller to the bed, which will lead to accelerate the granules towards the direction of the flow. This means the granules were leaving zone 2 faster, when the impeller speed was higher. Notice that the granular bed was more fluidized at high impeller speed. In zone 1 and zone 3, there was no big difference in the area of the granular bed by changing the impeller speed.

6.3 Surface velocity and the flow pattern

6.3.1 Velocity in NG

The vector field of granule velocity (surface velocity) for the case of NG processes was not explained, here. This is due to the general flow conditions in the NG process at low speed (impeller speed = 2000 RPM, and the vessel speed = 85 RPM) is analogous to the first stage of the MSG (LP process) and at the high speed (impeller speed = 7000 RPM, and vessel speed = 170 RPM) is analogues to the second stage of the MSG.

6.3.2 Velocity in the MSG (qualitative)

The velocity vector of the granules in the Eirich mixer was varying in magnitude and direction inside the mixer dependent on the position of the granule within the mixer. Figure 6-4 and Figure 6-5, show the granular flow vector for the case of EP (L/S = 0.14 and L/S = 0.15) and LP (L/S = 0.14 and L/S = 0.15), respectively, at different intervals of time (different stages). The figure represents the average velocity profile of the surface of the moving bed. The average velocity was obtained via PIV technique by averaging each interrogation area over 193 frames (each frame resulted from two consecutive images) which is equivalent to 0.386 sec of the measurement. Averaging the velocity vectors over granulation time thoroughly damps the variation in the velocity vector of any local point. At the same time, the time averaged velocity vector is a more representative parameter for the granules motion in the mixer. Therefore, it is the parameter which the granular flow vectors are usually presented (Börner et al., 2016; Hassanpour et al., 2011).

By quick inspection of the Figure 6-4 and Figure 6-5 for all the cases of MSG processes, it could be inferred that the colour of the velocity field vector for the granular bed surface is mainly blue during the first and the third stage of the granulation while it is yellowish-red during the second stage of the granulation. This is most probably as a result from the change of the both of the impeller speed and the vessel speed during the second stage. Where, the vessel speed increases the bed velocity overall, while the impeller speed changes the bed velocity locally. Further inspection of the figures, namely in zone 2, could lead to conclude that the granular bed was subjected to a higher shear in that area as the velocity field has a higher gradient there. It was changing from high speed (average

velocity ~1.2 m/s) to low speed (average velocity ~0.4 m/s) in the first and third stage, whereas it was changing from about 2 m/s to 1.2 m/s in the second stage. Less gradient in the velocity vector was observed in zone 1 and zone 3. In zone 1, however, the velocity of the granules was bit higher when it was close to the vessel's wall and it was less in radial direction towards the centre of the vessel. However, the velocity magnitude, in general, was lower than zone 3. Moreover, at the end of the zone 1, the granular bed was subjected to the impeller impact in which it started accelerating and moving towards zone 2.

It is also interesting to focus here at the points in which the zones meet with one another. This is because the magnitude and direction of the granular bed velocity were changing at the meeting area namely at the area between zone 2 and zone 3. At the transition point in which the granular bed leaves zone 2 and enters into zone 3 (notice the blue colour in the figures), the granules were looking to lose part of their kinetic energy, as their velocity was changing in magnitude and direction, notice the vector arrows in the Figure 6-4 to Figure 6-5. Similarly when the granules moved from zone 3 to zone 1, the bed velocity changed. The bed height was the higher in zone 3 compared with zone 1, see

Figure 6-3.

The former explanation of the flow features was noticed to be applicable for all the processes of the MSG, except there are some differences in the velocity magnitudes between the each process. The values of the velocity vectors will be explained in the next section.

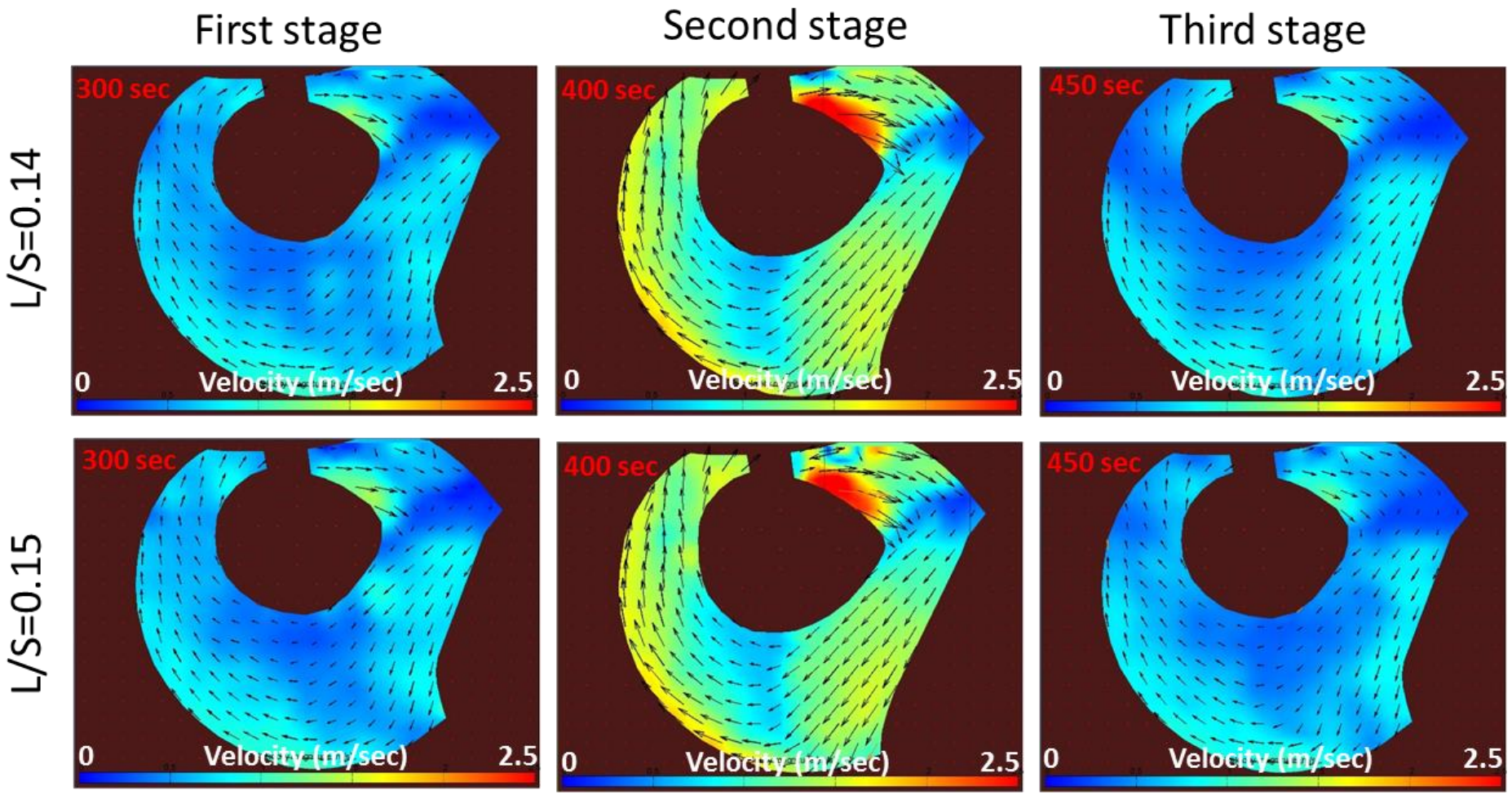

Figure 6-4: The velocity profile for MSG, EP process for the case of L/S = 0.14 and L/S = 0.15. See appendix (E) for more profiles at different time.

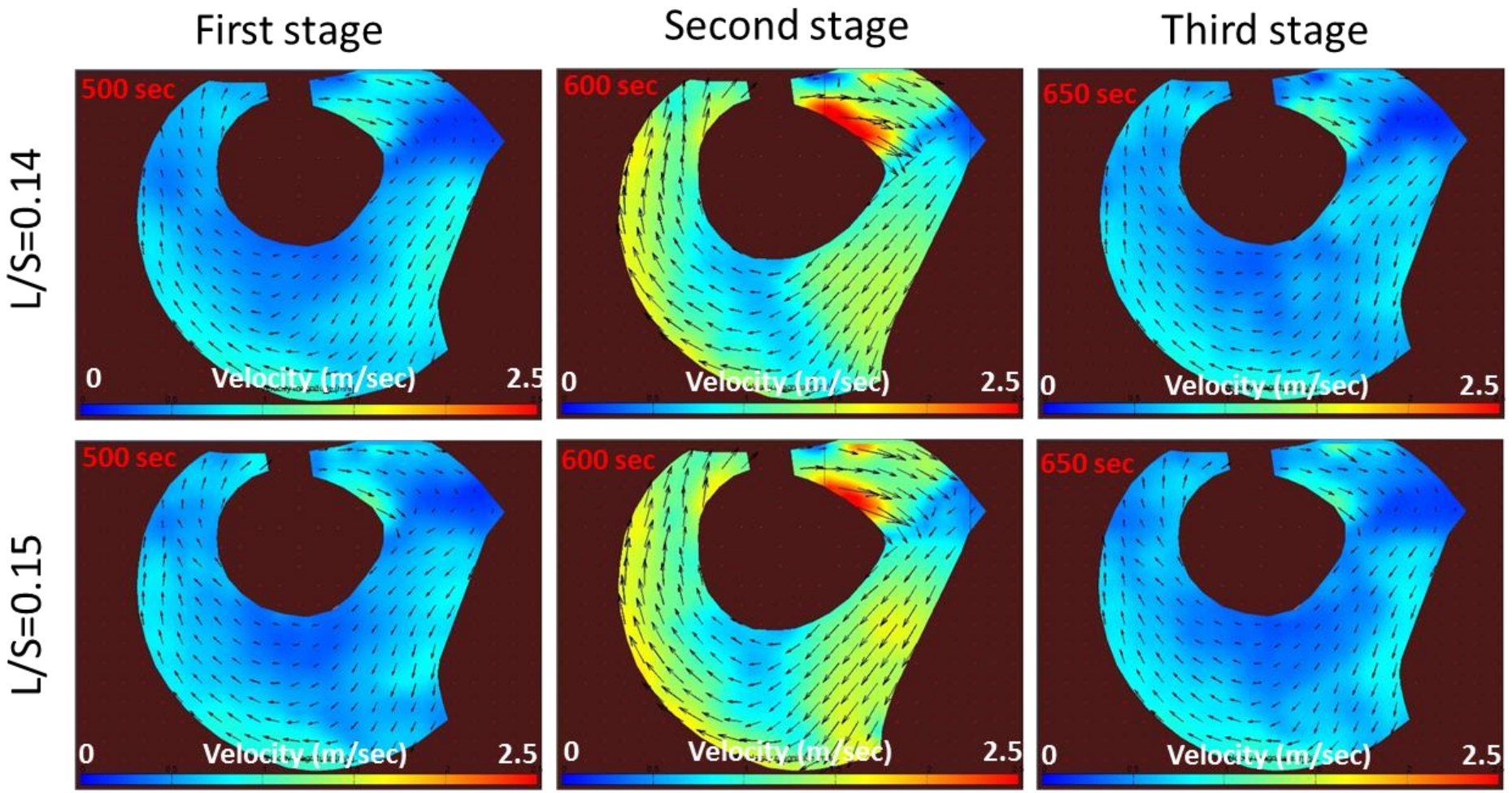

Figure 6-5: The velocity profile for MSG, LP process for the case of L/S = 0.14 and L/S = 0.15. See appendix (E) for more profiles at different time.

In all of the figures of the velocity field vector, the colour scale was fixed from 0 m/sec to 2.5 m/sec. The upper limit was set as the majority of the velocity vectors did not exceed 2.5 m/sec in all cases, despite velocity of some individual granules might be more than 2.5 m/sec especially after being impacted by the impeller at high speed, i.e. in zone 2 during the second stage of the MSG process. However, by averaging the velocity vectors over certain number of frames (in PIV) will diminish this exception. This was supported by plotting the scatter of the components "u" and "v" of the velocity vectors of the granules. Where "u" is the component in the direction of x-axis and "v" is the component in the direction of the y-axis. Samples for different cases of the granulation process are given in Figure 6-5 . The scatter plot for all the cases shows that the great part of the velocity components were less than 1 m/s in the case of A and B in the Figure 6-5 (which are the first and third stage of MSG), while they were less than 1.7 m/s for the cases of C and D (which are the second stage of MSG). In all cases, the velocity vectors were recorded to be less than 2.5 m/s. This scale was also useful to give better visualization for the gradient in the velocity field.

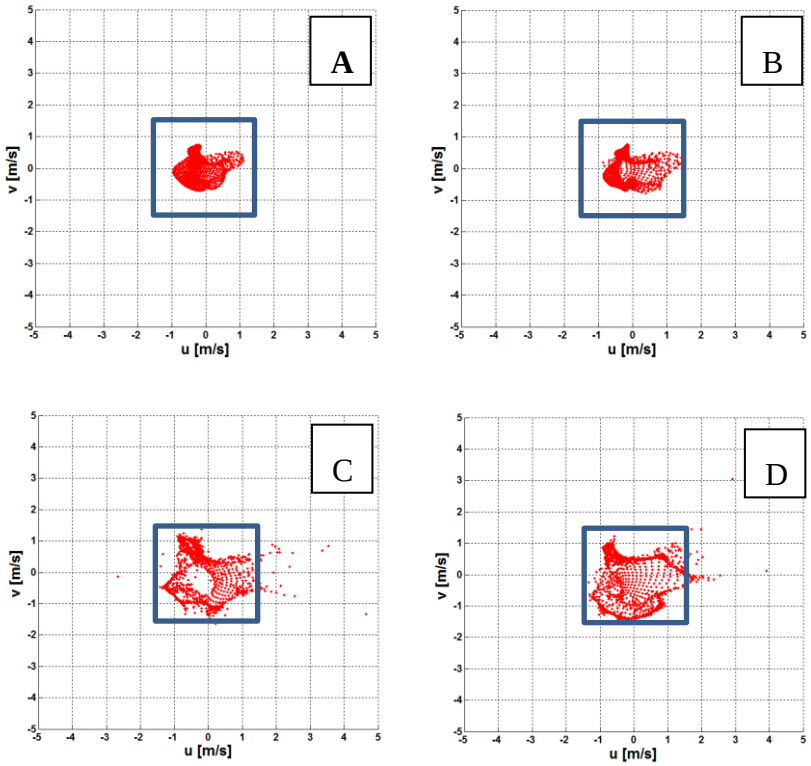

Figure 6-6: The scatter of the "u" and "v" components of the velocity vectors: A: At 1st stage, EP, L/S = 0.14. B: At 1st stage, EP, L/S = 0.15. C: At 2nd stage, EP, L/ S = 0.14. D: At 2nd stage, EP, L/S = 0.15.

6.4 Local surface velocity (quantitative values)

The surface velocity of the granular bed at two local areas (area 1 and area 2 in the Figure 6-7) was extracted from PIV measurements and plotted as a function of time. These two areas are localized in the positions illustrated in Figure 6-7. Area 1 is the blue dotted circle and area 2 is the red circle. These areas were selected as they represent the most effective areas to change the granule flow characteristics, where the change in the granule velocity is the highest between these two areas (explained in the previous section). As a result, it is a logical consequence to expect that different granulation mechanism could take place in these areas, namely the breakage process. The bed velocity in the zone 3 was neglected.

It is important to mention here that, the linear velocity at the centre of the circles for the base of the vessel is 0.57 m/s and 0.5 m/s for the area 1 and area 2, respectively, during the first and the third stage of MSG process. While it is equal to 1.14 m/s and 1 m/s for the area 1 and area 2, respectively, during the second stage of the MSG. These values are illustrated as horizontal green lines (solid and dotted) in Figure 6-8 to Figure 6-11.

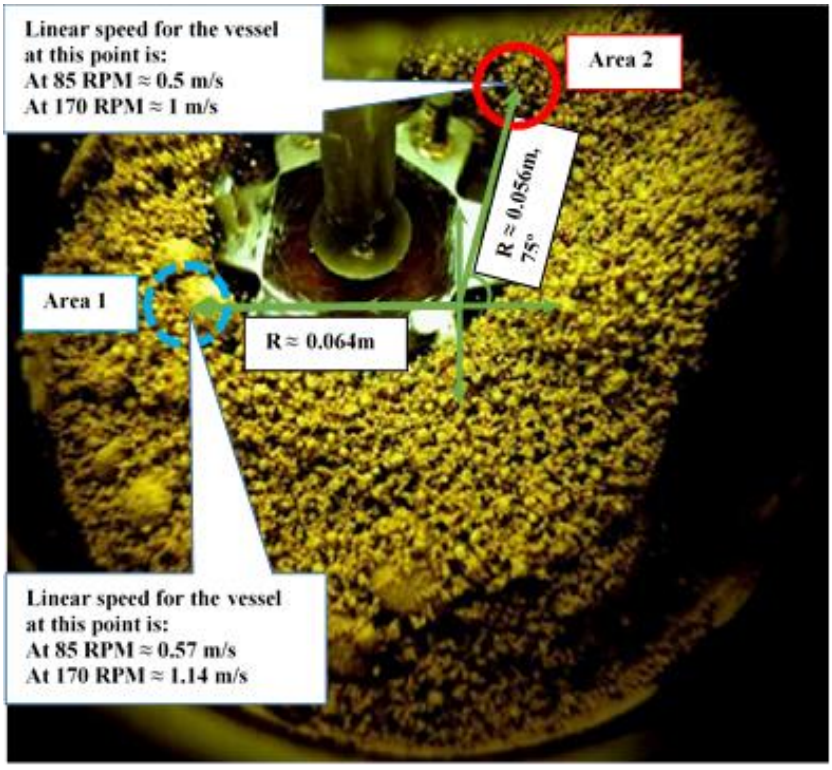

Figure 6-7: Shows the position of the measured local velocity

The surface velocity in area 1 during the first stage of the granulation was close to the velocity of the vessel's base in all cases of the MSG processes; see Figure 6-8 to Figure 6-11. This is due to the driving force for the granular bed motion is primarily motivated by the vessel walls at that point; compare the blue dotted line with the green dotted line in Figure 6-8 to Figure 6-11. However, the value of the mean velocity was slightly less than the vessel's velocity namely for the case of (EP, L/S=0.14), as in Figure 6-8. This leads to conclude that there was slight gradient in the granule velocity from bottom (base of the vessel) to the top (free flowing surface). The flowablity of the granular bed could be behind of this gradient. Where the cohesion forces between the granules was the less in this stage, as the binder was newly introduced to the powder bed during this period. If there was more binder, the gradient will diminish, see Figure 6-9, in which L/S = 0.15. Moving on to area 2 during the first stage, the velocity of the granules at the bed surface increases rapidly compared with area 1 due to the impact of the impeller to the granule. This is for all cases of the MSG process. For the same reason as in the area 1, the velocity was recorded to be higher when the L/S ratio was lower. However, it was slightly reducing with longer granulation time, as in the case of LP, see Figure 6-10 and Figure 6-11. This may due to an increase in the bed cohesiveness with time as the binder content on the granule surface was increasing with time.

In the second stage of MSG, which is the intensive mixing condition, the velocity of the granules clearly increased to a high level particularly in the area 2, for all the cases of the MSG. As explained formerly, this is believed to be due to the impact of the impeller in addition to the increase in the vessels speed during the second stage. The velocity was noticed to be the highest when amount of the binder was low (L/S = 0.14, EP, see Figure 6-8). Where the highest average velocity was 2.37 m/sec in the area 2 at the end of the second stage. At the same time, the velocity decreases in the case of LP compared with EP, compare Figure 6-10 and Figure 6-11 with Figure 6-8 and Figure 6-9, respectively. As more binder could exist at the granule surface in the case of LP compared to the EP which decreases the flowablity. Furthermore, the figure suggests that the velocity of the granules, at area 2, was increasing with time in the second stage. This is due to the granules which will move more freely with time as breakage of the granules proceeds with time. On the other hand, by examining all of these figures, it could be observed that the velocity of the bed at the area 1 was close to the velocity of the vessel's base.

In the third stage as the impeller speed and the vessel speed was set to low similar to the first stage, the velocity of the granules was similar to that of the first stage. However, the velocity of the bed at the area 2 was noticed to be less in the third stage compared with the first stage. This could be due to the increase of the granular bed cohesiveness and the motion appeared to be sluggish during this stage.

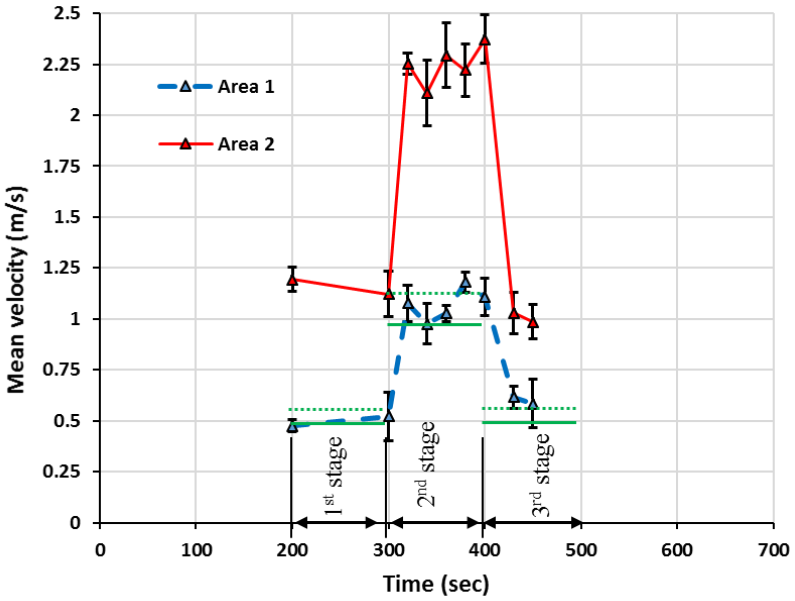

Figure 6-8: Surface velocity of the granular bed, MSG, EP, L/S = 0.14. The green lines represent the vessel's base velocity, dotted line at area1; continuous line at area 2.

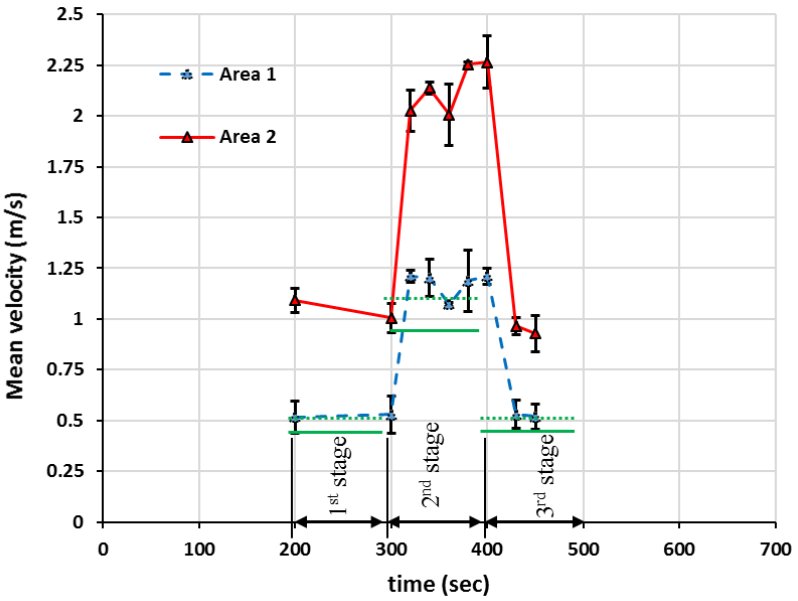

Figure 6-9: Surface velocity of the granular bed, MSG, EP, L/S = 0.15. The green lines represent the vessel's base velocity, dotted line at area 1; continuous line at area 2.

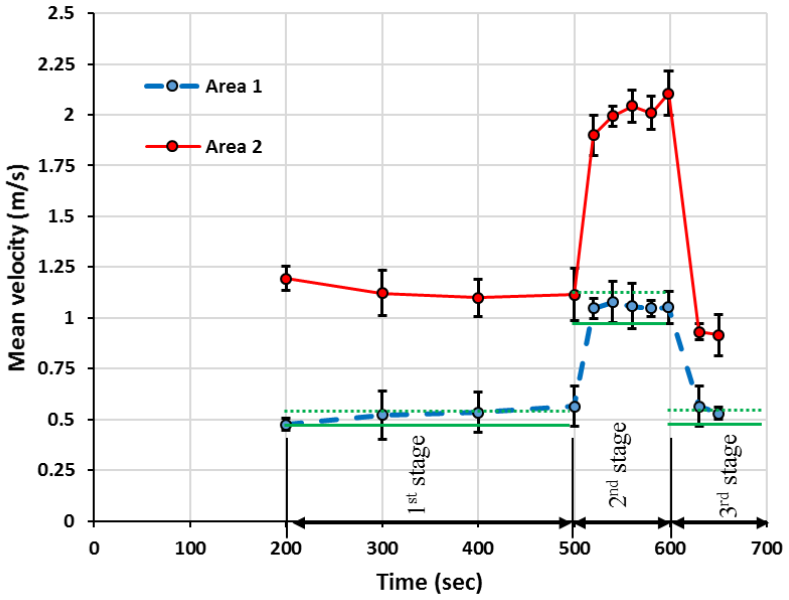

Figure 6-10: Surface velocity of the granular bed, MSG, LP, L/S = 0.14. The green lines represent the vessel's base velocity, dotted line at area1; continuous line at area 2.

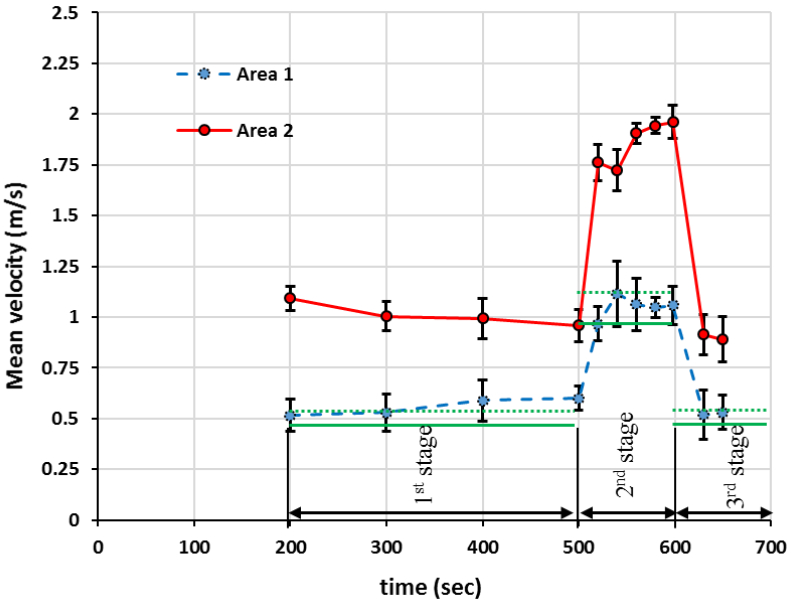

Figure 6-11: Surface velocity of the granular bed, MSG, LP, L/S = 0.15. The green lines represent the vessel's base velocity, dotted line at area 1; continuous line at area 2.

6.5 Power consumption

It is widely reported that by adding the binder to the powder bed the power consumption will increase. It was also claimed that the power consumption depends on the ability of the aggregated wet particles to be strained (Holm et al., 1985).

The power consumed during the MSG for the process of EP and LP is given in Figure 6-12 and Figure 6-13, respectively. For the both of the processes of EP and LP, the power profile form the starting point till the second stage is quite similar to the what could be found in the literature (Hansuld and Briens, 2014; Pepin et al., 2001; Saito et al., 2011). The first 100 sec (premixing of powder) the power consumed is very low because the dry particles of the $CaCO_3$ powder were moving easily in the mixer and minimal cohesion forces exist between the particles. Then at 200 sec the binder is introduced to the powder bed, nuclei started to create and the power consumption at the first moments was also low. However, the power started to increase alongside with more binder addition. This is most likely due to the existence of the binder (PEG1000) between the particles increases the attraction forces between them. Meanwhile, some power will could be consumed when big nuclei start to break up due to impact with the impeller. After the binder addition completion, no significant change in the power consumption was noticed (plateau in the

power profile) during the first stage of the MSG for the both processes of EP and the LP. At this time the power delivered to the granules was likely encouraging the steady growth of the granule size. The profiles also shows that the power consumption was higher in the case of more binder content, i.e. L/S = 0.15, compared with lower binder content (L/S =0.14). Most probably, this resulted from an increase in the attraction force between the particles.

In the second stage when the impeller speed was increased abruptly from 2000 RPM to 7000 RPM, the power consumption increased, accordingly. Possibly, the increase in the power was to overcome/break the liquid bridges between the aggregated granules tending to fluidize the granular bed. At the same, the increase in the power could result from consuming more energy to break the granules which will encounter the impeller. Then the consumed power decreased gradually with time making the profile of the power to looking like exponential curve. The decrease in the consumed power is expected to be as a result from the decrease in the granule size and fluidization of the granular bed with time. Figure 6-12and Figure 6-13 show that the power consumption in the case of LP was more than the case of EP. This could be ascribed to the properties of the granules in which the granules in the case of LP were less porous and denser (consolidated) than the EP, as explained in Chapter 5. Where, high porous granules usually need less power to break than the low porous granules. In addition, as in the first stage, the higher L/S the more power consumed. This is also because of existence of more binder.

For stage three, the power consumption was analogous to the first stage for the both processes EP and LP. However, less power was recorded comparing with the first stage. This could lead to conclude that the granular bed was moving more freely during this stage compared to the first stage, as the less resistance was faced by the impeller. This, in consequence means less compaction could happen to the granule in the stage, as less energy is imparted to the granular bed.

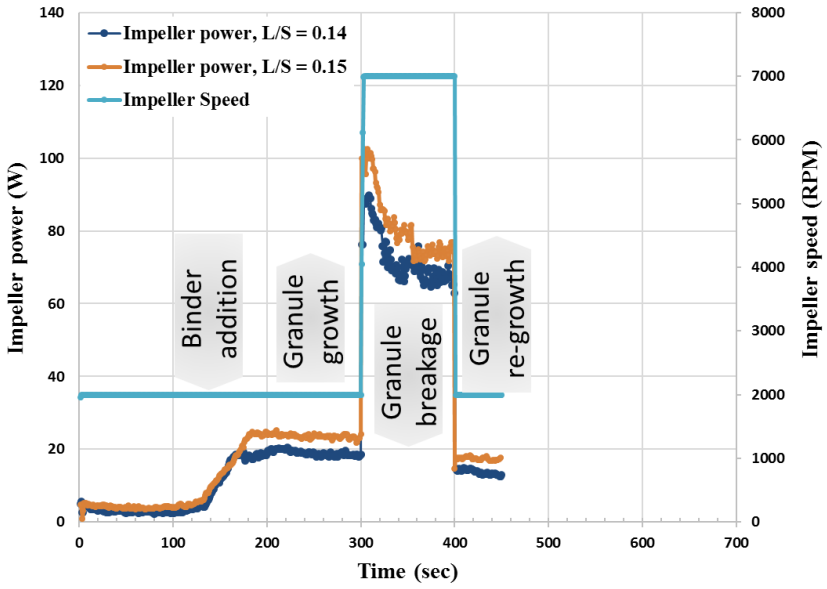

Figure 6-12: The profile of the power consumption during the MSG of the EP process

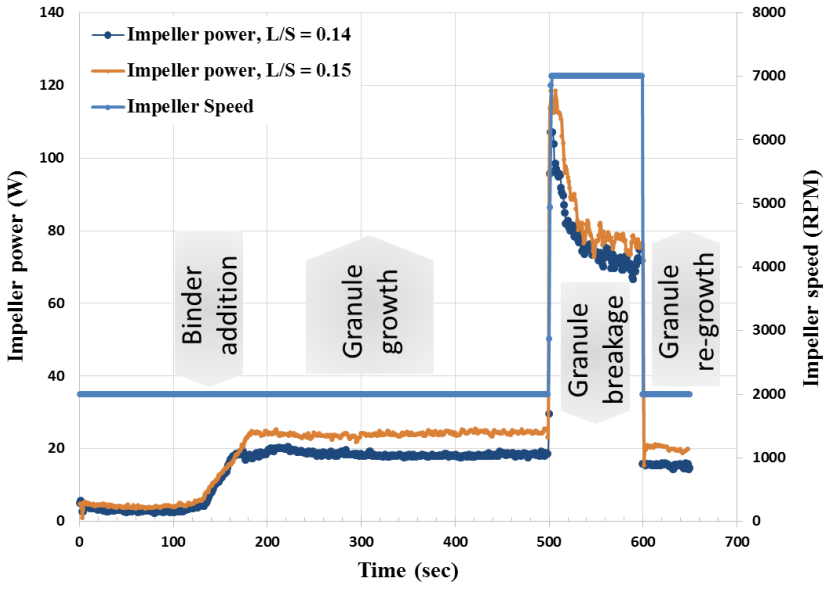

Figure 6-13: The profile of the power consumption during the MSG of the LP process

6.6 Conclusions

The granular flow within the Eirich mixer is more complex in comparison to conventional mixers like the Roto junior. Dissimilar to the vertical types of higher shear mixers, the flow pattern is asymmetric around the impeller and either around the vessel. For this reason, the area inside the mixer was divided to zones to better understand the flow patterns taking place within the mixer. Zone 1 was designated as the granular bed before the granules come in contact with the impeller. Zone 2 was denoted as the area after the granules come into impact with the impeller. While the area after the scrapper was denoted as zone 3.

The surface velocity of the granular material was calculated for zone 1 and zone 2, while the zone 3 was ignored. This is because the highest change in the granule velocity was occurring within these two zones, and the most changes in the granule attribute was expected to take place there. In Zone 1, the surface velocity was close to the velocity of the vessel's base at that point in most of the cases, except in the case of EP at low L/S (0.14), where it was slightly less than the vessel's velocity. In zone 2, the magnitude of the velocity of the granules was higher than the vessel's base. The magnitude of the velocity was dependent on the impeller speed. Since the impeller speed was the highest in the second stage, the velocity of the granular material within zone 2 was the highest. The maximum velocity was noticed to be in the case of EP and L/S = 0.14 and it was 2.37 m/sec at the zone 2.

The power consumed during the MSG granulation increased with binder addition. Then, during the first stage the consumed power was mainly constant (a plateau in the power profile was noticed) in the meantime the granule growth was proceeding. During the second stage the power increased due to increasing the impeller speed. However, the power profile went down exponentially due to the reduction in the granule size which was as a result from the breakage and the granular bed was more fluidized. At the third stage, when the small granules started to grow again, the power profile was similar to the first stage, though the overall power consumption was lower than the first stage.

CHAPTER 7 DEM SIMULATION

7.1 Introduction

The dynamics of the moving granules in the granulator have a significant effect on the granule attributes. Therefore, studying the particle motion during the mixing process in the high shear mixer is a required step for comprehending the granulation process (MSG process in the current work). Although the granule velocity distribution was explained in the previous chapter, no information was provided about the velocity of the granule within the bed, as the PIV technique is only surface measurement technique. Hence, this chapter is dedicated to obtaining more information about the granule velocity inside the particle bed in the Eirich mixer as well as to analyse the mixing process in the Eirich mixer namely for the MSG process. The velocity distribution inside the particle bed will elucidate the role of the impeller in the MSG process and the velocity probability distribution function (PDF) and Lacey's mixing index (LMI) will be used to evaluate the MSG process. This was achieved by using the Discrete Element Method (DEM) simulation. This simulation technique was first used to study the granular material by Cundall and Strack, (1979) and currently it is widely used to simulate particulate systems in many fields, e.g. Pharmaceuticals, Metallurgical, and chemical engineering processes.

One of the historical major drawbacks of DEM is that it is extremely time consuming, as it conducts the calculation for each individual particle created in the simulation. However, this problem is mitigated nowadays by using high computational power machines. In the present chapter the principles of the DEM will be explained including the contact model employed. Then the geometry of the mixer parts and the simulation parameters will be explained. Followed by the validation of the technique and comparing with PIV technique. Finally, the results will be presented and discussed.

7.2 Previous works

Studying the flow of particles in the mixers is a fundamental step in designing, scaling up, and optimization in numerous applications such as detergent, food, and pharmaceutical manufacturing. Hence, considerable work has been conducted to study

the flow of particles in different types of mixers (Brenda et al., 2009; Chan, 2012; Chandratilleke et al., 2009; Hassanpour et al., 2011, 2009; Nakamura et al., 2013; Remy et al., 2010; Sato et al., 2008; Stewart et al., 2001; Zhou et al., 2004). This is due to the advantages that DEM simulation offers in comparison to other alternative methods. Where the flow of the particles inside the particle bed can be visualized and analysed. In addition, more detailed information can be collected which is not possible via alternative means. These studies were covering different characteristics of the particle flow, e.g. the velocity vectors, mixing index, and the stress distribution within the granular bed.

The powder flow in a vertical cylindrical high shear mixer was studied by Stewart et al., (2001) using the DEM simulation (soft-shere model). They compared their simulation results with the experimental data, which was obtained by PEPT method. There was good agreement between the simulated and experimental data. The results of overall motion of the particle bed was well predicted. However, there was different accuracies in the results in different areas of the particle bed. The effect of different impeller speed on the particle flow in a high shear mixer was investigated by Sato et al. (2008). They accompanied this study with computing the force acting on the particle and the agitation torque. Their results revealed that the particles at the bottom of the mixer were experiencing a greater amount of force compared with the middle or upper parts. The velocity profile of the particles was noticed to be different by changing the rotational speed of the agitator and there was a linear relationship between the total torque of agitation and the impeller speed. Chan et al. (2012) studied the particle velocity and the stress, which named as “Blade-Granule Bed Stress”, in a high shear granulator using soft-sphere DEM model. They found that the surface velocity of the particle bed was steadily increasing with the Froude number. While the stress of the blade-bed was not remarkably changed by changing the Froude number.

The velocity probability distribution of particles is one of the important parameters, which is usually studied in the field of particle mixing. Remy et al. (2010) studied the flow behaviour of cohesionless, monodispersed spherical particles in a four-bladed high shear mixer using DEM simulation. They found that the high wall friction has an influence on the diffusive and convective particles mixing. By studying the velocity probability distribution function, they noticed that most of the particles possess tangential velocities that are significantly higher than the vertical or radial velocities.

7.3 Basics of the Discrete Element Method (DEM)

The motion of the particles inside a container is determined by the action of the forces and the moments applied on the particles, whether it was applied externally by the wall of the container and by any other objects (particle-wall interaction) or it was applied internally (particle-particle interaction). The motion of a particulate system could be translational and rotational. The translational will be determined by the some physical quantities such as velocity, acceleration, and the position. While, the rotational motion is determined by the angular velocity and the acceleration. Newton's law of motion is usually used to describe these types of motions (Cundall and Strack, 1979).

If there was particle-particle and particle-wall interaction in any assembly of particles, the equation of motion for an individual particle "*i*" is given by:

$$m_i \frac{dv_i}{dt} = m_i g + Fc_i \qquad \text{Equation 7-1}$$

$$I_i \frac{d\omega_i}{dt} = Mc_i \qquad \text{Equation 7-2}$$

Where, m_i = the mass of the particle

v_i = the translational velocity

I_i = moment of interia

ωi = rotational velocity

g = the gravitational velocity

Fc_i = the total force (contact force) on the particle including particle-particle and particle-wall interaction forces

Mc_i = total torque applied on the particle, which could be due to the tangential forces applied on the surface of the particle.

If the above equations (Equation 7-1 and Equation 7-2) are discretized to small time step (Δt) and simplified, the translational and the angular velocity as well as the position of the particle "*i*" could be deduced, as in the following:

$$v_i = v_i^0 + \left(\frac{Fc_i}{m_i} + g\right) \Delta t \qquad \text{Equation 7-3}$$

$$x_i = x_i^0 + v_i \, \Delta t \qquad \text{Equation 7-4}$$

$$\omega_i = \omega_i^0 + \frac{Mc_i}{I_i} \, \Delta t \qquad \text{Equation 7-5}$$

Where, x_i gives the position of the particle and the v_i^0, x_i^0, and ω_i^0 are the values at the initial condition in which it will be the values in the previous time step during the simulation.

Providing a solution of the above equations (Equation 7-3 to Equation 7-5) is not an easy task, as all the force and torque interactions of the particle-particle and the particle-wall should be taken in consideration during the calculations. Two types of models are commonly used to consider the equation of force and toque for the particle-particle and the particle-wall interaction in the DEM simulations. These models are the hard sphere and the soft sphere contact model. Each of which are used dependent on the suitability for the model with the experimental data..

In hard sphere, binary collisions are only allowed between the particles and assumes the nature of the particles to be rigid which results instantaneous collisions between the particles (Hassanpour and Pasha, 2015; Hoomans et al., 1996). While the soft sphere model, allows multiple contacts to occur between the particles instantaneously and considers the particles to be deformable in nature. Particles could overlap in this model and the interaction forces are calculated accordingly. More information about this model is available in Cundall and Strack, (1979). Since this model allows for multiple contacts between the particles, in contrary to the hard sphere model, it is usually used to simulate

dense particles assembly. This model was used in the current work, as the particle bed in the high shear mixers are generally densely packed.

7.3.1 Soft sphere model

Soft-sphere model which is used in the current work, was first developed by Cundall & Strack (1979). It is primarily used to model the mixing of particles in different types of granulators. This model takes into account some models like dashpot, spring and frictional slider model to consider the particle-particle and the particle wall interaction. Tsuji et al. (1992) applied the models of Cundall & Strack (1979) to study the flow of cohesionless particles inside a tube. Their representation of the particle-particle and the particle wall interaction is shown in Figure 7-1. In the case of the normal direction (Figure 7-1,A), the dashpot (viscous damping) describes the plastic energy dissipation and the spring describes the force of the elastic repulsion. While in the case of the tangential direction (Figure 7-1,B), the dashpot and the spring models calculates the force if the deformation of the particle was small in the tangential direction. This case represents the static friction, however, if the deformation was high, the frictional slider calculates the force and this case represents the dynamic friction.

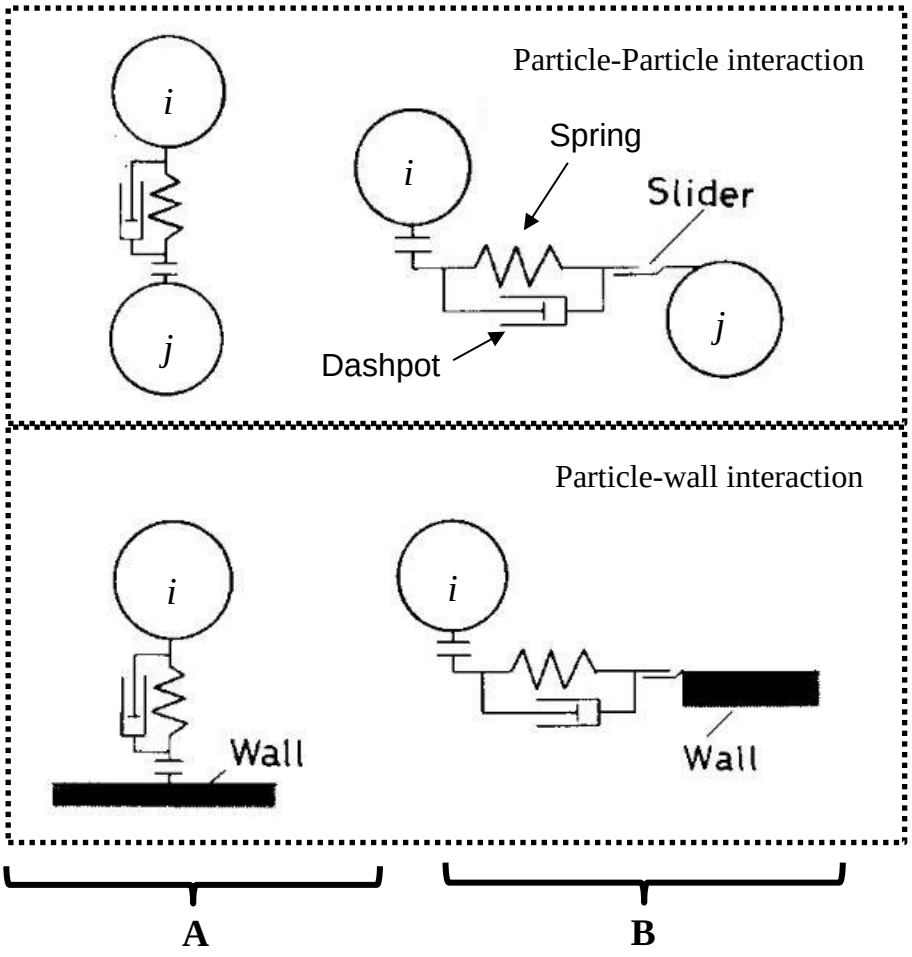

Figure 7-1: The model of soft-sphere for the particle-particle and particle wall interaction A) normal force interaction, B) tangential force interaction. Modified from Tsuji et al. (1992).

7.3.2 The collision force model

According to Tsuji et al. (1992), if the particle *i* contacts the particle *j*, the contact force f_{Cnij} (normal component) that acts on the particle *i* is given by :

$$f_{Cn,ij} = \left(-k_n\, \delta_{nij}^{3/2} - \eta_n\, v_{r,ij}\, n_{ij}\right) n_{ij} \qquad \text{Equation 7-6}$$

Where, k_n = the normal stiffness

δ_{nij} = particle displacement (in normal direction) due to the normal force

η_n = the damping coefficient (for the dashpot)

$v_{r,ij}$ = the relative velocity of the particle *i* with respect to the particle *j*

n_{ij} = the unit vector directed from the centre of first particle *i* to the centre of the other one *j*

Note that the exponent (3/2) represents non-linear relationship between the force and displacement which is the Hertzian contact theory. Figure 7-2 illustrates all the physical quantities.

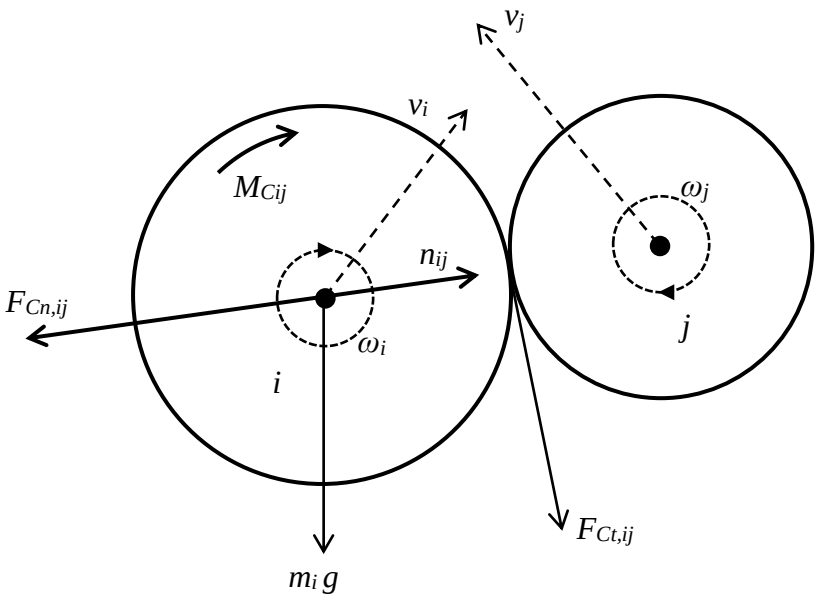

Figure 7-2: The types of the interacted forces and torques on the particle *i* and *j*.

On the other hand, the tangential component of the collision force is given by the following equation:

$$F_{Ct,ij} = \begin{cases} -k_t \delta_{t,ij} t_{ij} - \eta_t \, v_{rt,ij} \; ; if \left| -k_t \delta_{t,ij} t_{ij} - \eta_t \, v_{rt,ij} \right| \leq -\mu_f \left| F_{cn,ij} \right| \\ -\mu_f \left| F_{cn,ij} \right| t_{ij} \; ; \qquad if \left| -k_t \delta_{t,ij} t_{ij} - \eta_t \, v_{rt,ij} \right| > -\mu_f \left| F_{cn,ij} \right| \end{cases} \qquad \text{Equation 7-7}$$

Where,

$$t_{ij} = \frac{v_{rt,ij}}{\left|v_{rt,ij}\right|} \qquad \text{Equation 7-8}$$

$$v_{rt,ij} = \left[v_{r,ij} - \left(v_{r,ij}\, n_{ij}\right) n_{ij}\right] + \left[r_p \left(\omega_i + \omega_j\right) \times n_{ij}\right] \qquad \text{Equation 7-9}$$

Where, k_t = the tangential stiffness

δ_{tij} = the tangential displacement

t_{ij} = a unit vector towards the tangential motion (given in the Equation 7-8)

$\eta_{t,}$ = the damping coefficient

μ_f = the sliding friction respectively

$v_{rt,ij}$ = the relative velocity in the tangential direction which includes the rotational and the translational velocities (given in the Equation 7-9)

r_p = the radius of the particle

ω_i, ω_j = are the rotational velocity for the particle *i* and *j* respectively. If the interaction was with the wall, then $|v_j| = |\omega_j| = 0$.

In the right hand side of the Equation 7-7, the upper quantity is for the combination of the spring and the dashpot, while the lower quantity is for the frictional slider. If the former one dominates, then the particle *i* will commence sliding over the contact plane (slip) and the frictional slider will be responsible to model the force. Whereas, if the particle was not able to slip (non-slip case) the spring-dashpot model will be responsible to model the force.

Since in the soft-sphere model multiple particles are allowed to interact with a single particle (particle *i*), the total force of the collisions and the applied torque on the particle *i* (for particle-particle and particle-wall interactions) could be obtained by summing all the forces and torques as in the following equations:

$$F_{Ci} = \sum_{j} \left(F_{Cn,ij} + F_{Ct,ij} \right)$$ Equation 7-10

$$M_{Ci} = \sum_{j} \left(r_p \, n_{ij} \times F_{Ct,ij} - \mu_r \left| F_{Cn,ij} \right| r_p \left(\frac{\omega_i}{|\omega_i|} \right) \right)$$ Equation 7-11

Where, μ_r is the rolling friction coefficient. The last term in the Equation 7-11 represents the torque that is generated due to the rolling friction (Ai et al., 2011; Zhou et al., 1999).

7.3.3 Stiffness

In the Hertzian contact model (non-linear contact model), if two particles (spherical, isotropic, and ideal smooth surface) collide with each other, the force will be proportional to the deformation (δ_n) raised to the power (3/2) and the proportionality factor in the normal direction (k_n), which is stiffness is given by Goldsmith, (1960) and Tsuji et al., (1992):

$$k_n = \frac{\sqrt{2r_p}\, E_p}{3\left(1 - \upsilon_p^2\right)}$$ Equation 7-12

Where, υ_p = Poisson's ratio for the particle

E_p = Young's modulus of the particle

While the stiffness in the tangential direction (k_t) for a two colliding particles in the non-slipping case, see Equation 7-7, is given by Tsuji et al., (1992):

$$k_t = \frac{2\sqrt{2r_p}\, G_p}{2 - \upsilon_p} \, \delta_{n,ij}^{1/2}$$ Equation 7-13

Where, G_p = is the particle's shear modulus, and is given by:

$$G_p = \frac{E_p}{2\left(1 + \upsilon_p\right)}$$ Equation 7-14

7.3.4 Damping coefficient

Tsuji et al. (1992) solved the equation of motion (Equation 7-15) for the spring-dashpot system to obtain an expression for the normal damping coefficient (η_n).

$$m_p \left(\frac{d^2x}{dt^2}\right) + \eta_n \left(\frac{dx}{dt}\right) + k_n x^{3/2} = 0$$ Equation 7-15

Where, m_p = the mass of the particle

x = displacement

They solved the above equation by assuming that the "*e*" the restitution coefficient is independent of the velocity of the impact and they suggested the following equation for the normal damping coefficient:

$$\eta_n = \beta \left(m_p\, k_n\right)^{1/2} \delta_{n,ij}^{1/4}$$ Equation 7-16

In the above equation, β is related to the restitution coefficient *e* as shown in the (Figure 7-3). On the other hand, Tsuji et al. (1992) assumed that the damping coefficient in the tangential direction (η_t) to be same as in the normal direction (η_n).

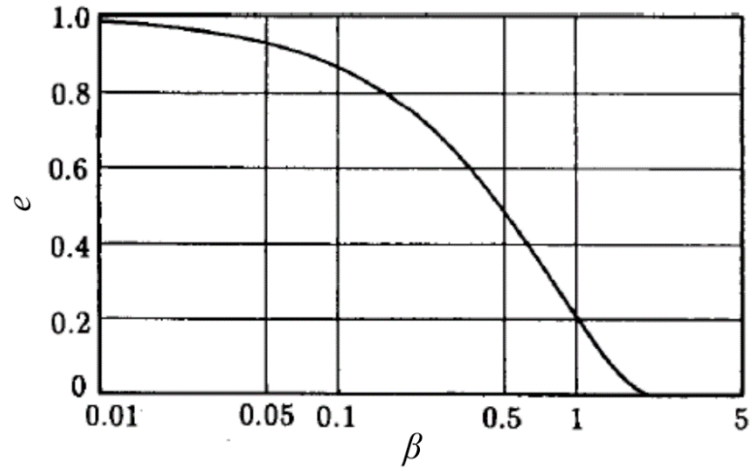

Figure 7-3: The relation between β and *e*, taken from (Tsuji et al., 1992).

Many researchers used the above discussed models for studying the flow and mixing characteristics in different types of granulators, namely in high shear mixer (Brenda et al., 2009; Chan, 2012; Stewart et al., 2001; Washino, 2011; Zhou et al., 1999).

7.4 The geometry of the Eirich mixer

In order to simulate the particle motion in a granulator, a computer CAD for geometry of the granulator (the walls of the vessel, the impeller and the scrapper of the Eirich mixer) was required. All the parts of the Eirich mixer was generated using FreeCAD 0.16. The dimensions related to the parts of the Eirich mixer was given previously in the experimental chapter (Chapter 3, section 3.1.3). Using the same software, i.e. FreeCAD 0.16, a surface meshes (triangular mesh) were created and exported to the simulation. Figure 7-4 shows the geometry of the parts of the Eirich mixer. Where, A is the experimental image and B is the generated geometry in which the mesh triangles can be observed.

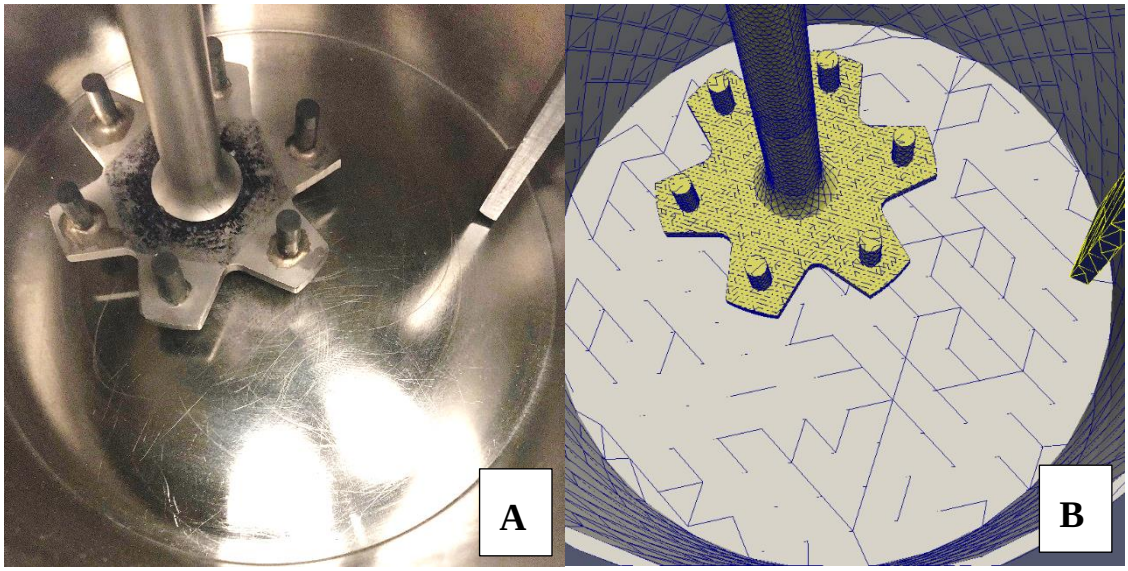

Figure 7-4: The geometry of the Eirich mixer: A) Experiment, B) Simulation.

7.5 DEM Simulation parameters

The calculations related to the equations mentioned previously Equation 7-1to Equation 7-11 were implemented in an open source software package which is used for the DEM simulation called LIGGGHTS (version LIGGGHTS-PUBLIC 3.6.0). This software is usually used to simulate the processes which include the granular flow.

7.5.1 Parameters

To proceed the calculations during the simulation, certain properties related to the particles (restitution coefficient, Young's modulus, Particle diameter …etc) should be provided. Table 7-1 shows the physical parameters used in the current simulation.

The number of particles was 203718 particles this number was sufficient and represented a similar value of the fill level to the experimental work inside the mixer. Where the amount of the particles/granules in the simulation/experimental work was filling the vessel to about 1/3 of the vessel's volume, see Figure 7-5. The particle diameter was assumed to be 1.5 mm as this size reside within the size range of the real granules produced. The Young's modulus value looks to be small value compared to the real one. This was chosen for the purpose of deceasing the unnecessary computational time. The same values of the coefficient of sliding friction was used for the particle-particle and the particle-wall interaction. The coefficient of rolling friction was set to 0.003. This value is a typical value, which was used by many researchers (Chan, 2012; Washino, 2011) for dense particle systems, e.g. in high shear mixer.

It is important to mention here that, for dense particle flow systems, the quantitative difference between the experimental work and the DEM simulation could only be observed if an extreme values of the restitution coefficient (1) and the coefficient of friction (0) was used in the simulation. This was reported by Kuo et al., (2002).

Table 7-1: The used parameters in the DEM simulation

Particle and particle bed parameters	Number of the particles [-]	203718
	Particle diameter [mm]	1.5
	Particle density [kg/m3]	2300
	Poisson's ratio [-][a]	0.25
	Young's modulus [MPa] [a]	7.13
	Restitution coefficient [-][b]	0.3
	Rolling friction coefficient [-][b]	0.003
	Sliding friction coefficient [-][b]	0.3
	Time step [sec]	1×10^{-5}
The mixer parameters	Impeller rotational speed [RPM]	2000, 7000
	Vessel rotational speed [RPM]	85, 170
	Type of the impeller [-]	Pin type

[a] : a similar value was considered for both of the particle and the wall

[b]: a similar value was considered for both of the interactions of particle-particle and particle-wall/impeller.

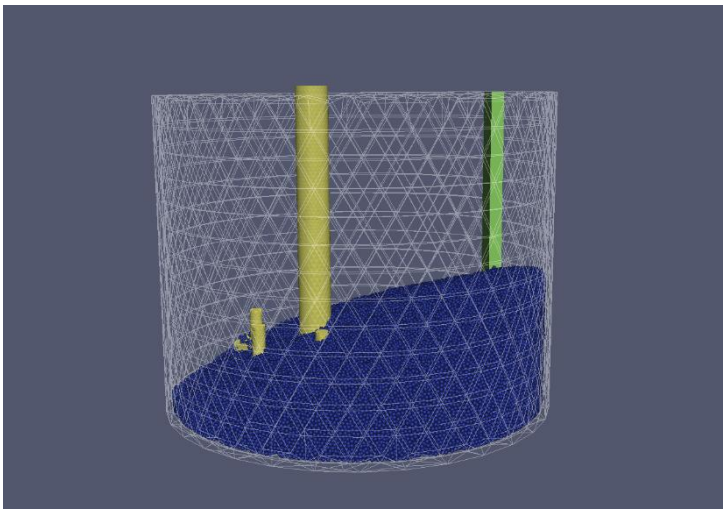

Figure 7-5: The level of the generated particles inside the vessel.

7.5.2 Time step

Selecting the time step is essential in the DEM simulation. This is because if a short time step is used, the calculation time will be extremely long, which could be unnecessary step. Besides it is also affects the stability of the simulation. Based on some studies (Cundall and Strack, 1979; Li et al., 2005), the time step should be determined according to the following equation:

$$\Delta t = \frac{\pi R}{\lambda} \sqrt{\frac{\rho}{G_p}} \qquad \text{Equation 7-17}$$

Where, R = is the average radius of the particles and it is equal to the r_p in the current work because mono-size particles were used here.

ρ = the density of the particle

λ = is a value which could be approximated and given by the following equation (Li et al., 2005):

$$\lambda = 0.8766 + 0.163\, \upsilon_p \qquad \text{Equation 7-18}$$

The value of the time step in the current work was set to 1×10^{-5} sec. This value was adequate enough to have a stable particle flow after the mixer (impeller and vessel) started moving for about 1 sec. A comparison between the current work with the literature for the time step and the other simulation parameters is given in Table 7-2.

Table 7-2: The simulation parameters used by different authors, compared with the current work.

Authors / Parameters	(Stewart et al., 2001)	(Chan et al., 2015)	(Chan and Washino, 2018)	(Nakamura et al., 2013)	(Alian et al., 2015)	(Washino, 2011)	(Sato et al., 2008)	Current work
Number of the particles [-]	16000	~1.5× 10^6 Max	-	13078-730417	Varied no.	43090	11132	203718
Particle diameter [mm]	5	1.25 - 10	0.5	4	4	1.29	2.0× 10^{-3}	1.5
Particle density [kg/m3]	2500	1250	1000	1500	2500	1058	2500	2300
Poisson's ratio [-]	0.3	0.25 / 0.3	0.3	0.30	0.3	0.25	-	0.25
Young's modulus [MPa]	2.16	10	100	2.16	2.16	7.13	-	7.13
Restitution coefficient [-]	0.3	0.4	0.3	-	0.3	0.9	0.9	0.3
Rolling friction coefficient [-]	0 - 0.05	0.1	-	2.5× 10^{-5}	0.05	0.003	-	0.003
Sliding friction coefficient [-]	0.2-0.5	0.5	0.5	0.5	0.5	0.3	0.3	0.3
Time step [sec]	5.0× 10^{-5}	1.0× 10^{-5}	-	2.0× 10^{-5}	-	1.0× 10^{-5}	1.0× 10^{-5}	1.0× 10^{-5}

7.5.3 Mixer run conditions in the DEM

It is important to mention here that, the simulation run was implemented for two case of impeller and vessel speed. Case 1: impeller speed =2000 RPM and vessel speed=85 RPM, which represent the first stage and the third stage of the MSG. Case 2: impeller speed=7000 and vessel speed=170 RPM and this one represents the second stage of the MSG. In the both cases, the particles are generated first inside the vessel while the impeller and the vessel were stationary. Then, the simulation continued while the impeller and vessel started to move. The whole simulation provides a mixing time equivalent to 12.8 sec.

7.6 Validation

Validation is one of the required steps in any simulation work. This is to make sure that the results of the simulation are close to the real case, i.e. experimental work. In this work, certain outcomes of the DEM work were compared with the experimental PIV data. The fill level of the particle bed was close to the experimental one as mentioned and shown previously in Figure 7-5. The surface velocity of the particle bed was compared between the DEM results and the PIV results at the impeller speed 2000 RPM. A snapshot of the particle flow for the both methods is shown in Figure 7-6. It could be noticed form the figure that flow characteristics of the particle bed is, fairly, similar. The maximum velocity of the particle located at the position after the impeller impacting the bed, i.e. zone 2 in PIV. While, the velocity of the particles is slower in the area of impact, i.e. zone 1 in PIV, in both methods. Furthermore, as it has been mentioned previously (in Chapter 5, section 6.3.2), the particle bed interacts with the impeller at the end of zone 1 which is similar place of interaction was noticed in DEM, see Figure 7-6. There is also analogy in the height of the bed in different areas within the mixer. By comparing figure B and C in the Figure 7-6, it could be noticed that the particles reach to highest point in the mixer in the zone 3 in the both cases, i.e. DEM and the experimental image. While in the zone 1, the level of the particle bed looks to be the lowest in the both cases as well. This comparison proves that there is qualitative analogy between the DEM results and the experimental work.

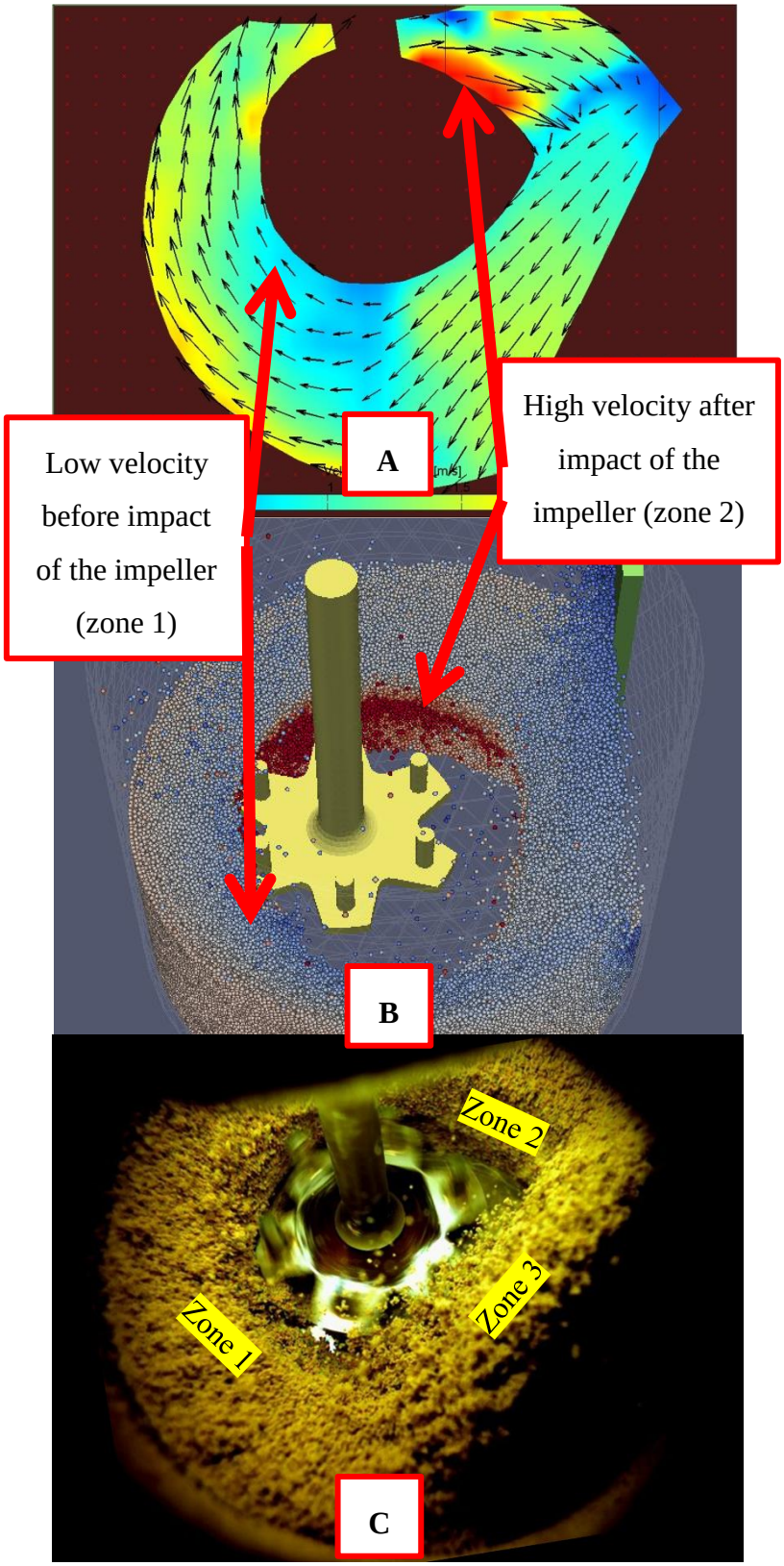

Figure 7-6: The analogy of the particle bed surface velocity, A) PIV, B) DEM, C) Experimental image

7.7 Results

The velocity of the particles at the surface of the bed and within the bed will be presented and discussed in this section. In addition, the velocity probability density function PDF and the Lacye's mixing index will be presented as well.

7.7.1 Velocity distribution and pattern

The figures in this section presents snapshots for the velocity of the particles. The particles were coloured based on their velocity. Figure 7-7 shows the surface velocity distribution for the particle bed. It could be noticed from the figure that the velocity of the particles, in general, is low in the case of first/third stage (Figure 7-7, Top) compared to the case of the second stage (Figure 7-7, Bottom). This shows a qualitative analogy with the experimental results of the PIV presented in (Chapter 5). It could be noticed from the Figure 7-7, that the change in the bed velocity is higher in case of second stage (impeller speed=7000 and vessel speed=170 RPM) compared to the first or third stage (impeller speed=2000 and vessel speed=85 RPM), by checking the variation of the colour of the particles. In other word, it means that the local velocity for individual particle at the surface of the particle bed variates more in case of the second stage than the first/third stage depending on where the particles are reside at surface of the bed. This leads to conclude that the particles, which are close to the surface, were subjected to a high shear in the second stage of the MSG comparing with the first/third stage, which seems to be in a low shear condition. This conclusion is more applicable to the particles, when they will go through the zones close to the impeller.

Figure 7-7also suggests that the velocity of the particles will reduce when they impact the scrapper. This means that the particles losses some of their kinetic energy in that area due to the impact with scrapper. By further inspecting the Figure 7-7, it could also be notice that the impeller is not in a fully contact with the particle bed, only at certain areas. The contact area in the case of low speed condition (first/third stage of MSG) is higher than the case of high speed condition (second stage of the MSG). The area of the contact is mostly located at the position in which the distance between the impeller and the vessel's wall is the smallest. At this point, possibly the highest shear on the particles is applied as the highest gradient in the particle bed velocity could take place there, see Figure 7-8.

This figure is a section taken from the particle bed and the velocity scale was changed for better comparison.

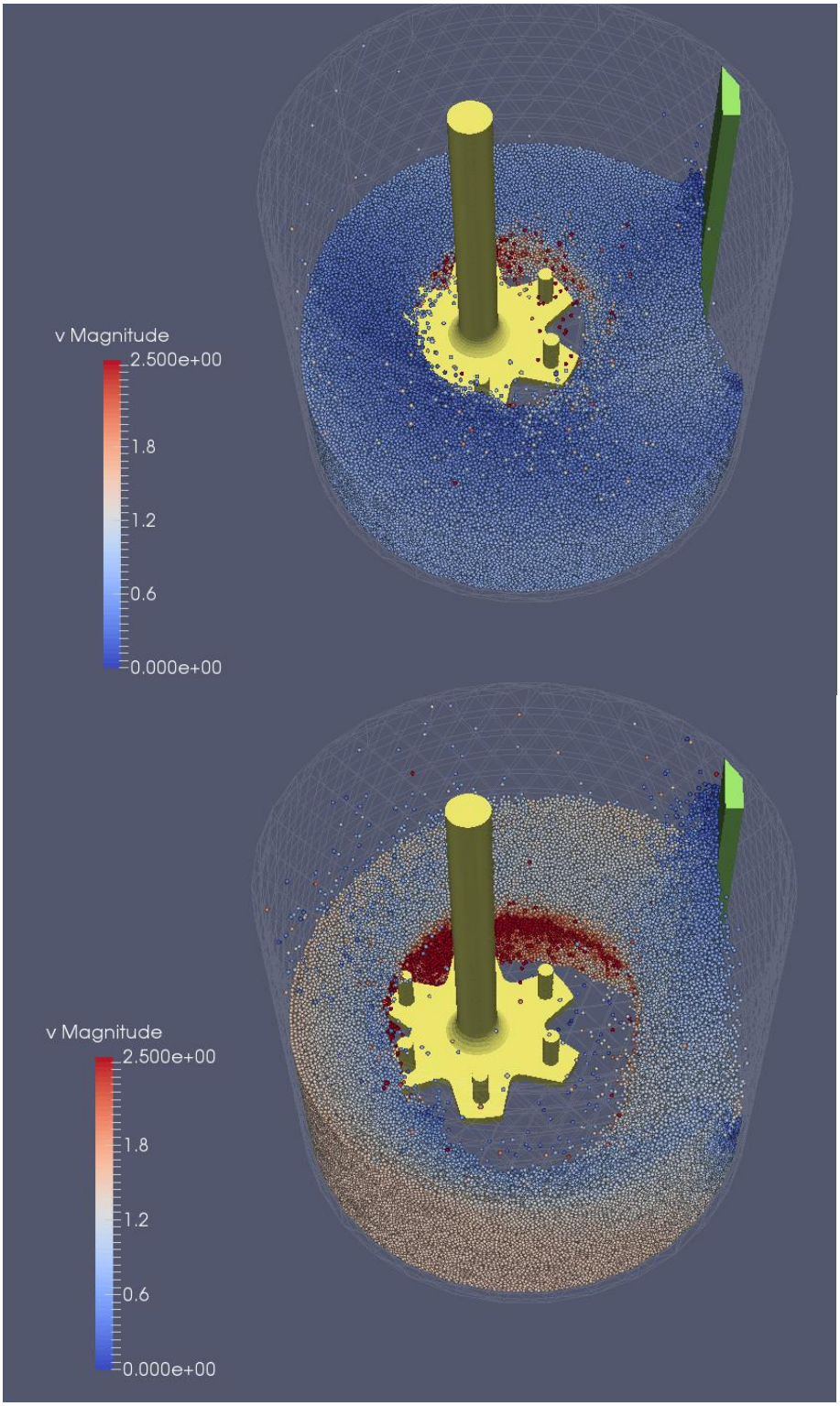

Figure 7-7: Particle bed velocity profile, view from top. Top; Impeller speed = 2000 RPM, vessel speed = 85 RPM, represent first/third stage of MSG. Bottom; Impeller speed = 7000 RPM, vessel speed = 170 RPM, represent second stage of MSG.

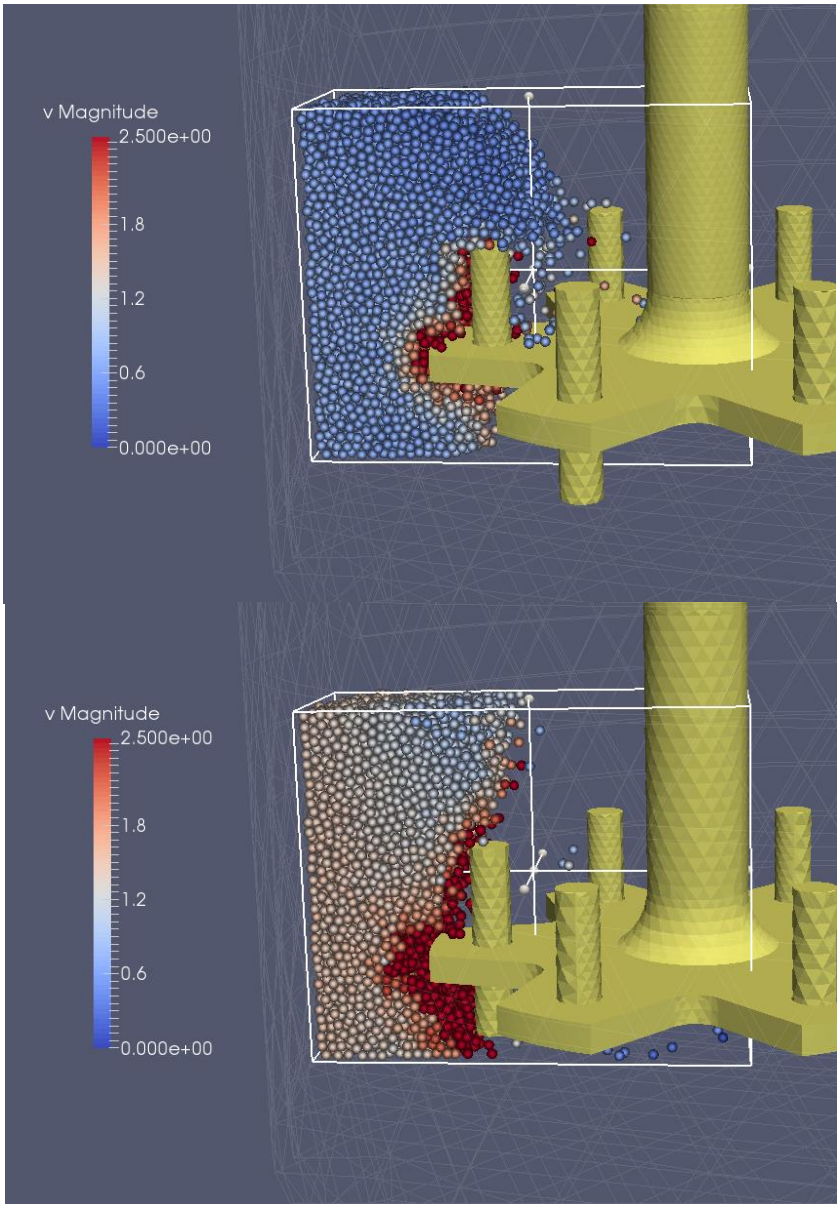

Figure 7-8: A section from of the particle bed, showing the gradient in the velocity. Top; Impeller speed = 2000 RPM, vessel speed = 85 RPM, represent first/third stage of MSG. Bottom; Impeller speed = 7000 RPM, vessel speed = 170 RPM, represent second stage of MSG.

Similar conclusions could be inferred by checking the velocity of the bed from the bottom side, see Figure 7-9. However, more influence (interaction) of the impeller on the particle bed could be noticed namely for the case of high impeller and vessel speed, i.e. second stage of the MSG.

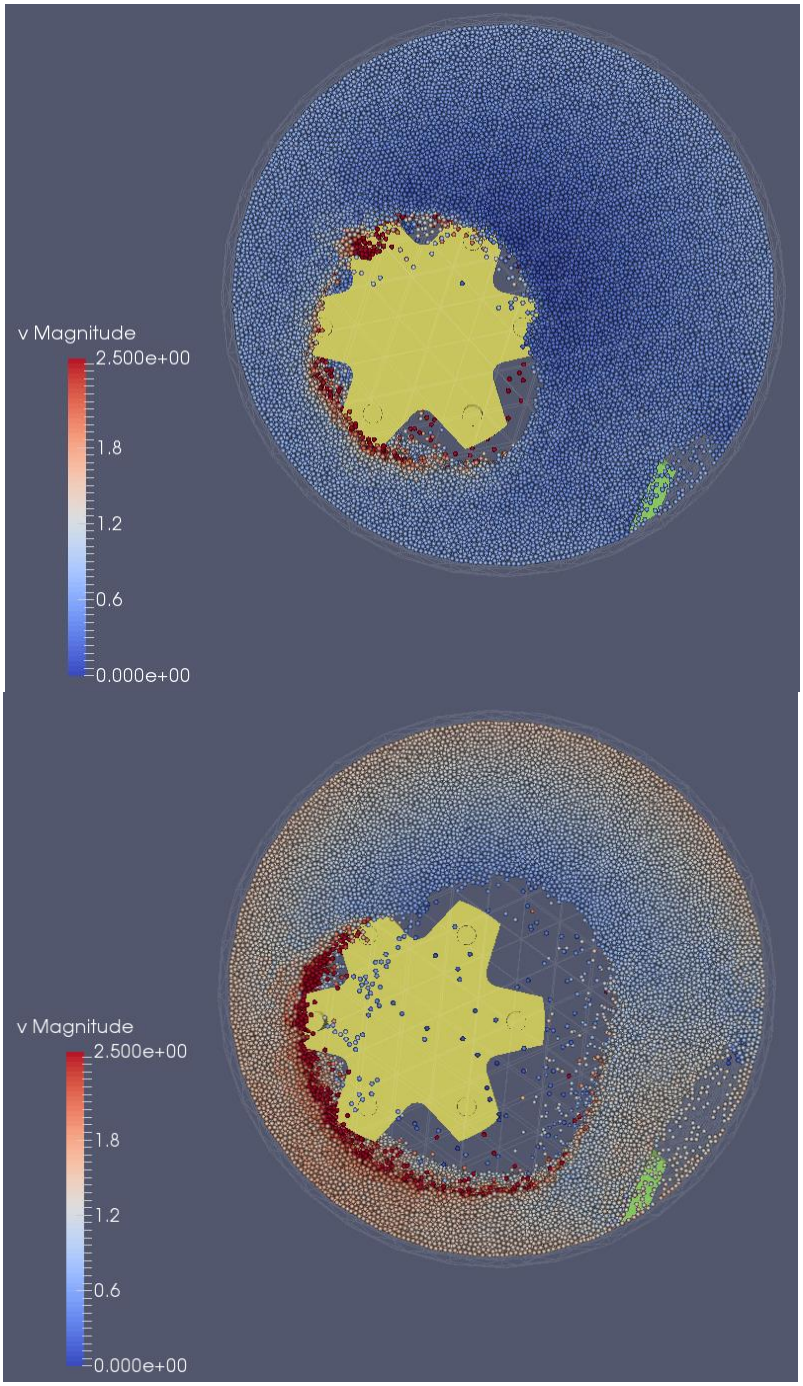

Figure 7-9: Particle bed velocity profile, view from bottom. Top; Impeller speed = 2000 RPM, vessel speed = 85 RPM, represent first/third stage of MSG. Bottom; Impeller speed = 7000 RPM, vessel speed = 170 RPM, represent second stage of MSG.

The highest velocity for the particles was expected to be around the impeller. This can be better visualized if the particles which have low velocity were removed, which can be seen in t Figure 7-10. The figure shows that the particles which have highest velocity are positioned around the impeller. This is mostly due to the impact of the impeller in which

the tip speed of the impeller (8.4 m/sec at 2000 RPM, and 29.3 m/sec at 7000 RPM) is significantly higher than the local velocity of the particles near the impeller.

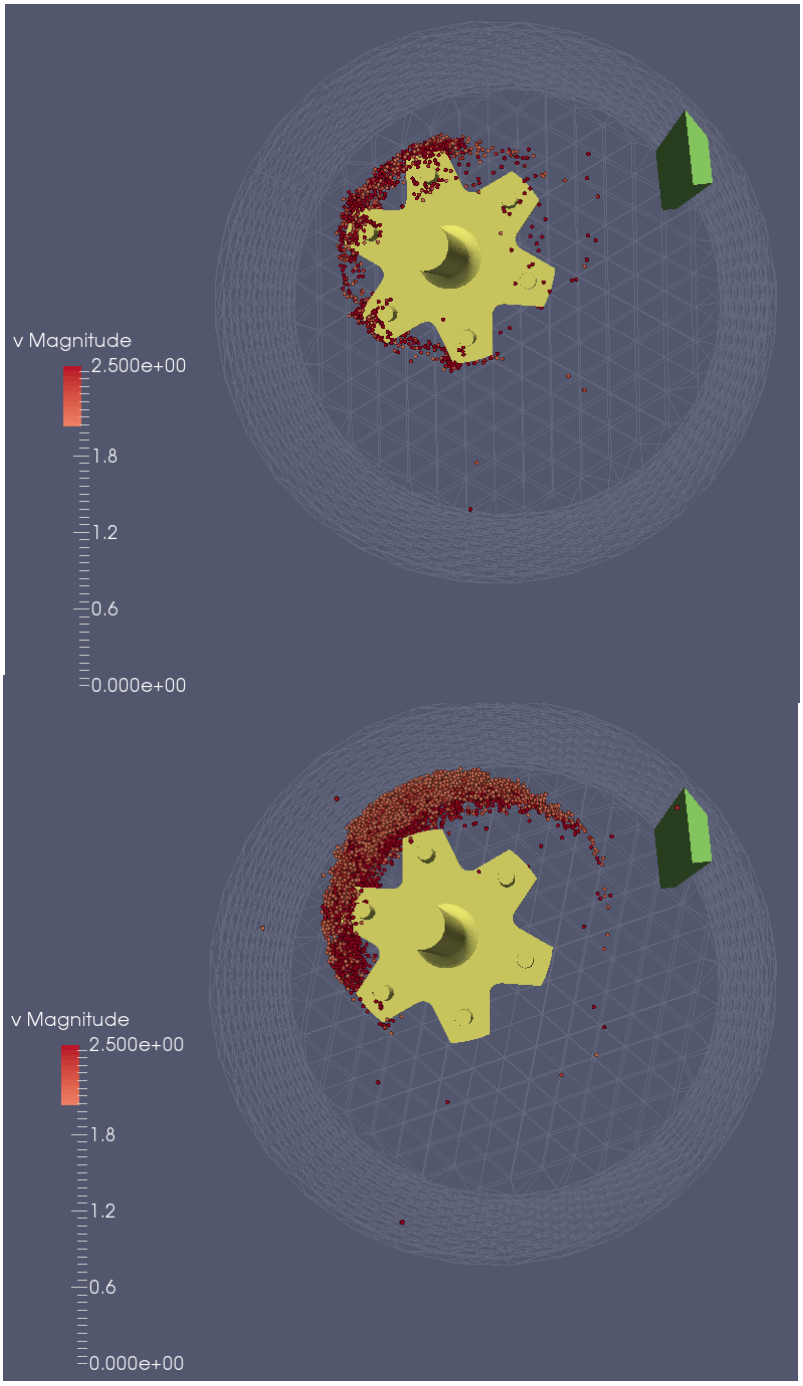

Figure 7-10: Particle bed velocity profile, particles with low velocity are removed. Top; Impeller speed = 2000 RPM, vessel speed = 85 RPM, represent first/third stage of MSG. Bottom; Impeller speed = 7000 RPM, vessel speed = 170 RPM, represent second stage of MSG.

The velocity vectors of the particles is presented in Figure 7-11. The vectors are coloured based on the magnitude of the velocity. The flow pattern in the figure suggests that, the

flow of the particles inside the mixer is primarily in the tangential (or angular) direction which looks to be analogous to the other vertical axis high shear mixer (Brenda et al., 2009). However, the structure of the flow seems to be more complex in Eirich mixer. As the impeller and the vessel move, the particles will move to the wall by virtue of the centrifugal force as a consequence of the vessel rotation, it will speed up when it will pass the region of the impeller due to the impact. Then the velocity will decrease when the particles collide with the scrapper and the particles bed level is a bit higher at this area due to accumulation of the particles. After that, the particles move away from the vessel's wall due to rebounding with the scrapper and speed in a wider area.

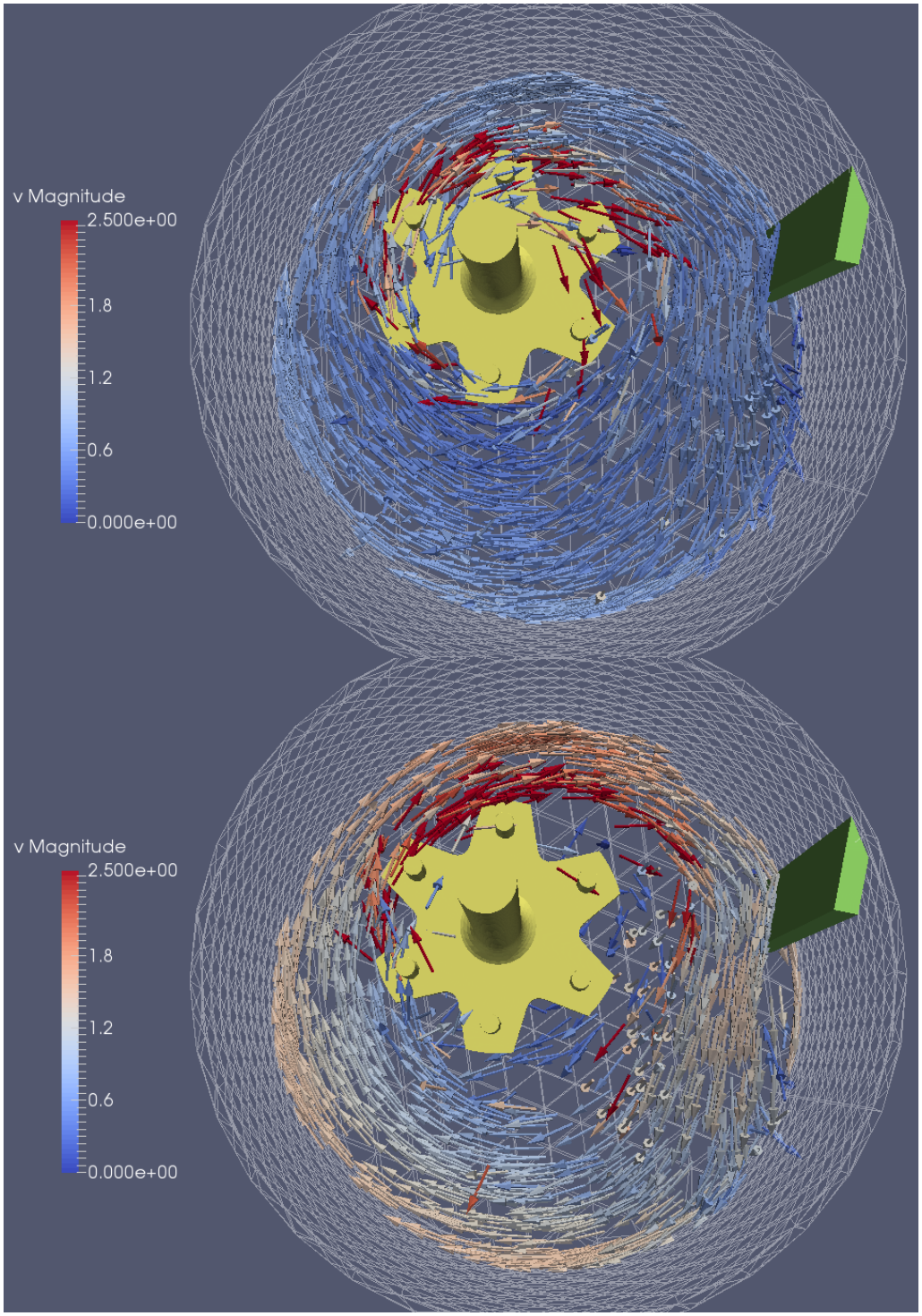

Figure 7-11: The velocity vector for the particles, view from top part of the vectors are removed for better visualization. Top; Impeller speed = 2000 RPM, vessel speed = 85 RPM, represent first/third stage of MSG. Bottom; Impeller speed = 7000 RPM, vessel speed = 170 RPM, represent second stage of MSG.

7.7.2 Velocity probability distribution function (PDF)

The probability distribution function (PDF) for the particles velocity was computed. The PDF can give more insights about the granular flow. Figure 7-12 and Figure 7-13, show the probability distribution function for the both cases of the low speed motion condition, i.e. first/third stage of MSG, and the high-speed motion condition, i.e. second stage of MSG. The figures show that, in the both cases, the distribution is left-skewed to the value of the tip speed of the vessel, which is 0.73 m/sec for the first case and 1.46 m/s for the second case with some differences. In the first case (Figure 7-12) the probability of the particles which tends to have velocity close to the velocity of the vessel's tip speed, during the "first/third stage", is higher compared to the second case (Figure 7-13). The reason behind this is that the vessel's base tangential velocity distributes from 0 m/sec (at the centre) to the 1.47 m/sec (at the vertical wall) at the second stage while it is from 0 m/sec to 0.74, respectively at the first/third stage. The velocity of the particles was distributing accordingly.

By further examining Figure 7-12 and Figure 7-13, it could be noticed that the area under the curve to the right side of the red line in the case of Figure 7-12 "first/third stage of MSG" is slightly higher than the case of the Figure 7-13 "second stage of the MSG". The percentage of the area out of the total area under the curve is 0.128 and 0.099 for the first/third stage and second stage, respectively. This leads to conclude that the probability of particles to interaction with the impeller during the first/third stage of the MSG is higher compared to the second stage of the MSG. This is by assuming that the particles, which possess velocity higher than the tip speed of the vessel (0.73 m/sec or 1.46 m/sec, depending on the stage), is by virtue of the impact of impeller to the particle bed. This will be more reasonable by checking the Figure 7-7 in which it shows that there is more number of particles interacting with the impeller in the case of first/third stage than the second stage.

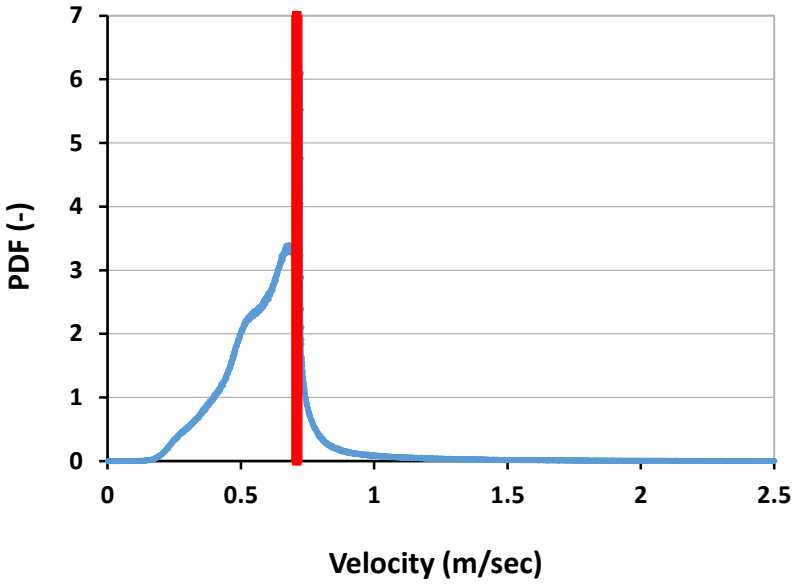

Figure 7-12: The velocity probability distribution function (PDF) for the particles, Impeller speed speed=2000RPM, Vessel speed = 85 RPM. The red line is vessel's tip speed = 0.73 m/sec.

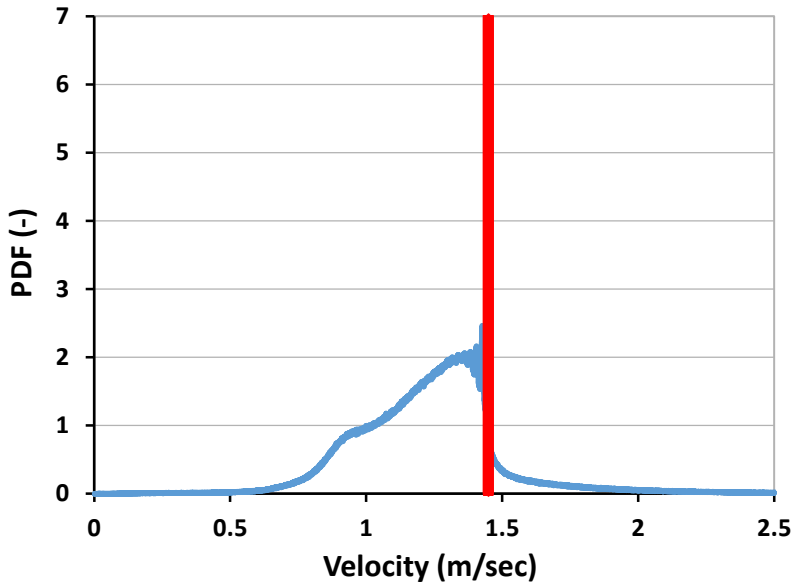

Figure 7-13: The velocity probability distribution function (PDF) for the particles, Impeller speed speed=7000RPM, Vessel speed = 170 RPM. The red line is vessel's tip speed = 1.46 m/sec.

7.7.3 Mixing in MSG

Further information about the flow of the particle bed and the mixing characteristics is presented here. Lacey's mixing index (LMI) was computed (Lacey, 1954). This parameter has been used by a number of researchers to quantify and compare how the mixing process is efficient in the mixers (Alian et al., 2015; Chan and Washino, 2018; Chandratilleke et al., 2009; Liu et al., 2013). The mixing index gives indication about the segregation, which has potential effect on the material distribution in the granulator during wet granulation (Oka et al., 2017).

The particles in the mixer, after reaching the steady state motion condition, were split into two parts and coloured as blue and red, as shown in Figure 7-14.The mixing between the two parts was computed with time using LMI (Lacey, 1954). This mixing index is the appropriate one for the monosized binary systems. The LMI is given by:

$$LMI = \frac{\sigma_0^2 - \sigma^2}{\sigma_0^2 - \sigma_R^2}$$ Equation 7-19

$$\sigma_0^2 = X_i X_j$$ Equation 7-20

$$\sigma_R^2 = \frac{X_i X_j}{N_p}$$ Equation 7-21

Where, σ_0^2, σ_R^2: are the variance of the fully segregated and fully random state, respectively.

X_i, X_j: are the mean number fraction of the component *i* and the component *j* respectively.

N_p: number of all the particles.

σ : the sample variance

The evolution of the particle mixing pattern with time is depicted in Figure 7-14. The view is from the bottom of the mixer. The figure suggests that the mixing status at the final point in both cases (first/third stage and second stage) is quite similar, although the second stage of MSG (Figure 7-14, B) shows better mixing performance and higher mixing rate. This could be ascribed to the difference in the mechanism of the mixing process between the two cases. After 4 sec of simulation time of the mixing, a snapshot is given in Figure 7-14, mechanical mixing in the first/third stage was most likely diffusive mixing, while in the case of the second stage it looks convective mixing was dominating. This may due to the impeller, which was in contact with the particle bed in high contacted area, which could speed up the local mixing process. While in the case of high mixing speed, the high speed of impeller and vessel could help to move a bulk of particles randomly meanwhile the impeller could motivate the local motion of a single particle in the particle bed. This, in consequence, resulted in better mixing performance. This leads to conclude that the mixture in Eirich mixer during the MSG process was, most probably, more homogenous in the case of second stage than the first/third stage. This will be clearer by examining the quantitative mixing characteristics of the Figure 7-14 which is shown in Figure 7-15. The figure suggests that the mixing rate in the case of first/third stage is lower than the mixing rate in the case of second stage of the MSG. This means that the particle bed reaches the homogeneity faster during the pulse change in the impeller speed.

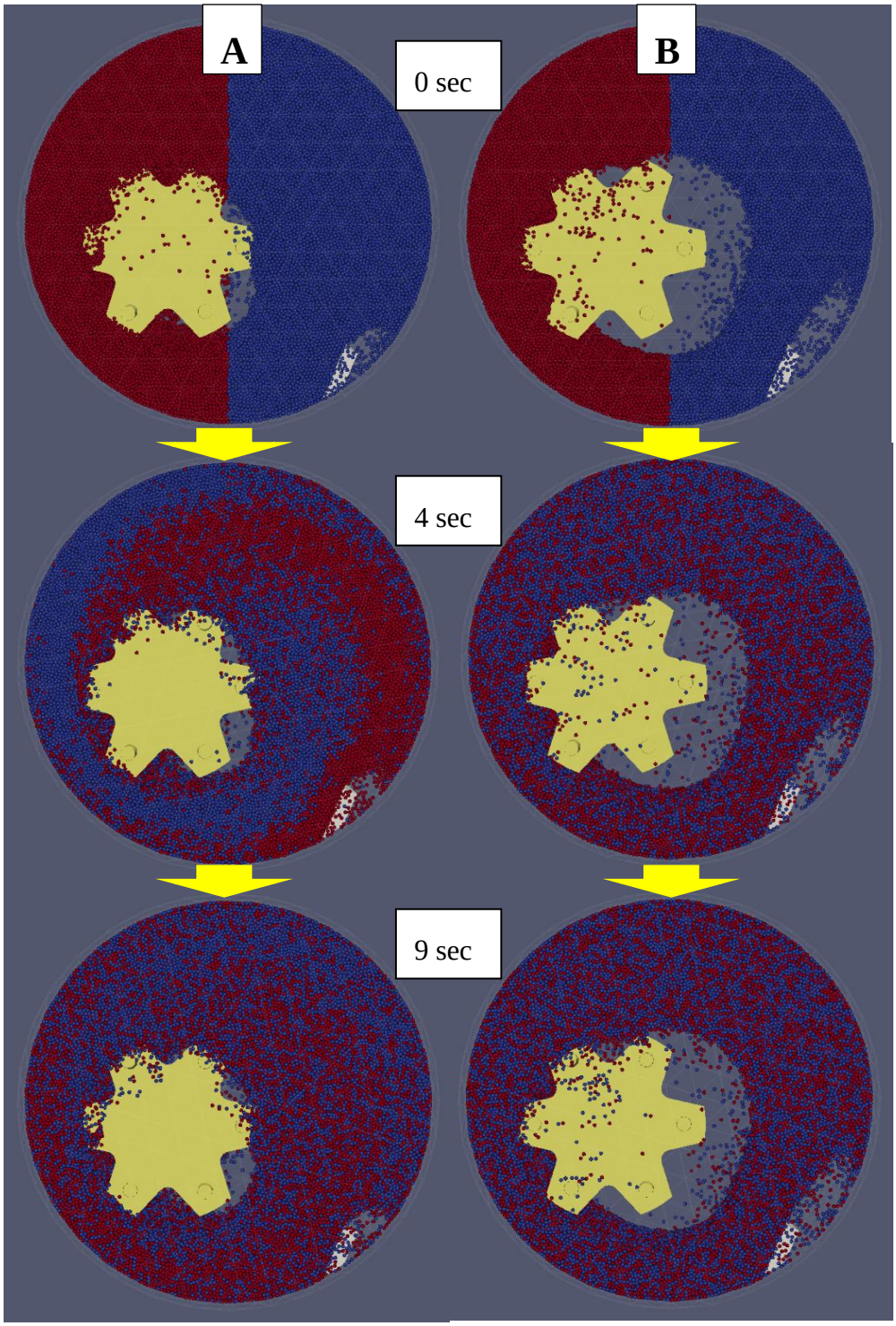

Figure 7-14: Mixing pattern evolution. A) Represents the first/third stage of MSG. B) Represents the second stage of MSG. The view is from bottom.

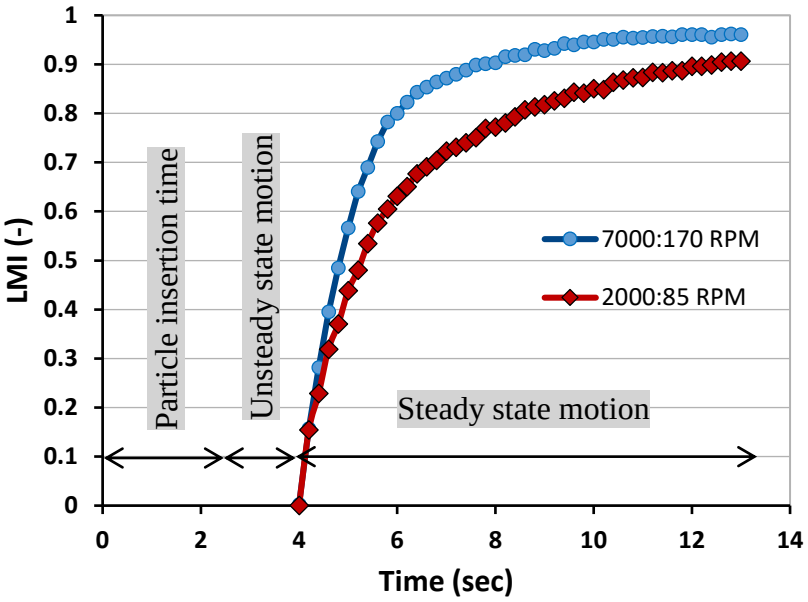

Figure 7-15: Lacey's mixing index for both cases of first/third stage of MSG (impeller speed=2000 RPM and vessel speed=85 RPM) and the second stage of MSG (impeller speed=7000 RPM and vessel speed=170RPM).

7.8 Conclusions

In this chapter, DEM simulation was employed to simulate the particle bed flow in Eirich mixer. This was one of the necessary steps in the current research as the DEM simulation is able to provide detailed information about certain parameters, such as particles velocity within the particle bed, which plays an important role in understanding the granulation process.

The results showed that the velocity distribution inside the mixer was not analogous in all the parts of the mixer. Similar to outcomes of the PIV chapter, the velocity of the particles at the free surface changes inside the mixer depending where the particle is located (similar to the zones explained in Chapter 6). The highest velocity of the particles was noticed to be in the area after the impact of the impeller, i.e. zone 2. While the velocity of the particles bed was decreasing after colliding with the scrapper and after scrapper in which the particle bed was mostly driven by the wall of the vessel.

By examining the velocity inside the bed, the highest gradient in the particle velocity was noticed to be when the impeller contacts the particles bed, as shown in Figure 7-8. This means that the highest shear was applied on the particles bed at that area. In consequence, it suggests that the granule breakage process, which was occuring during the second stage of the MSG, was most probably taking place in that area (Zone 1, in Chapter 6). Meanwhile, it was expected that the granule breakage could happen when the high velocity particles impact with the scrapper and which changes the direction of the particles motion. However, the results here show inapplicability of this proposal.

The second stage of MSG was showing better Lacey's mixing index (LMI) and the rate of mixing was looking better than the mixing rate in the case of first/third stage of the MSG. This indicates that the mixture was more homogenous in the case of second stage compared to the first/third stage and the binder was, distributing in the whole material in better way in the case of the second stage of the MSG rather than the first/third stage of the MSG. The velocity probability distribution function (PDF), showed that the number of particles affected by the impeller speed was slightly more in the first/second stage compared with second stage. This was indicated by calculating the area under the curve of the PDF in which the percentage of the particles that have velocity higher than the tip

speed of the impeller was 0.128 and 0.099 for the first/third stage and second stage, respectively..

CHAPTER 8 GENERAL CONCLUSIONS AND FUTURE WORK

8.1 Conclusions

Many researches available in the literature, which are concerned with improving the final granule properties in terms of granule size and size distribution, ability to dissolve fast, and survive during handling and storage, have revealed difficulties in producing such preferred typical granules. Hence, an effort was made to get an approach to enhance the final granular attributes via non-conventional granulation method named as multi-stage granulation (MSG). It was found that the new method (MSG) has an effect on the granule properties. The effect of the process parameters of the granule properties was studied using the new method of granulation (MSG). Nevertheless, the effect of the process parameters on the granule properties using (NG) process was also studied, as this process is also important to infer the difference between the MSG and NG processes. Meanwhile, the flow characteristics of the granular bed was also investigated employing, two techniques PIV and DEM, as it is important to understand the mechanism of the granulation process.

8.1.1 NG process

In normal granulation process, the influence of the granulation time, impeller speed, and liquid to solid ratio on the granule properties was examined. The size of the granules was noticed to increase progressively with the granulation time depending on the impeller speed and the liquid to solid ratio. The tendency of the increase was high at low impeller speed and it was low at high impeller speed. According to these results, it was inferred that the growth process was dominating on the breakage process and the breakage rate was higher at high impeller speed. Whereas the trend of the size was increasing with increasing the liquid to solid ratio. The porosity was noticed to decrease with granulation time, meaning that the granules were getting denser with time. The specific surface area was also decreasing with time. The granule size distribution was tending to be narrower with granulation time. Based on these observations, two mechanisms for the granulation were proposed for the normal granulation (NG).

8.1.2 MSG process

In MSG process three stages of the process variables (the impeller and vessel speed) were used in one granulation process and two types of processes were conducted, early pulse (EP) and late pulse (LP). The effect of these processes on the granule properties was investigated, too. The granule characteristics are apparently influenced by the process variables. Where the granular size, size distribution, porosity, shape and dissolution have changed with changing the process variables which is compatible with what many researchers have reported in literature. This proves that the granular attributes are responsive to the change in the process variables.

The experimental work showed that the granule median size was changing dramatically by changing the impeller speed throughout the different granulation stages and with the granulation time. This change was the consequence of different granulation mechanisms that the granules were undergoing during the granulation process, particularly growth, breakage and coalescence. The change in the granular size was more apparent in LP than EP. The porosity of the granules did not change significantly during the granulation processes. This may due to the amount of binder was relatively high. However, the granular porosity was increasing slightly in the third stage. This could be resulted from entrapping air inside the granule.

The size distribution and span were affected during the MSG process. Interesting results were obtained in the third stage depending on the granulation time. If the granulation time was short, then narrow size distribution of granules is attainable. For instance, the span of the granules at the beginning of the third stage of MSG/EP process was about 0.99 while at the equivalent of NG process, i.e. at 400 sec, the span was 1.47. This means that the span was reduced to about 30% in the third stage of MSG compared with equivalent points of NG process If the granulation time was relatively long, then high surface area of granules is attainable, in which it has impact on the dissolution time of the granules. However, the size distribution will be wider due to the coalescence of the small granule with each other. The dissolution time for these granules was reduced for at least 21%.

8.1.3 Granular bed dynamics

By using the PIV technique to monitor and study the granular bed flow inside Eirich mixer, it was observed that the granules were moving in the mixer with different velocity

depending on its position in the mixer. Accordingly, the whole area in the mixer was divided into zones. The velocity of the granular bed in zone 2, which is the area after impeller impact to the bed, was noticed to be the highest and the maximum velocity in this zone was 2.37 m/sec for the case of EP, L/S=0.14. In zone 3 (area after the scraper) the bed velocity was reduced after changing its trajectory by impacting the scrapper. Then the bed was moving to the zone 1 in which the granular bed had the lowest velocity. As a consequence to this difference in the bed velocity, the granules might be subjected to different shearing conditions in its bed within the mixer. The highest shear was noticed to be in the area where the impeller impacts the bed (end of zone 1) and in the zone 2. The granule breakage was expected to take place in those areas during the second stage of MSG process.

The velocity distribution obtained by DEM simulation was similar to the PIV results. Where the particles had the highest velocity after the contact with the impeller and the they had low velocity in the area before the contact with the impeller. It was, also, noticed that the mixing condition during the second stage of MSG was better than the first/third stage, as the Lacey's mixing index (LMI) was slightly higher. This means the second stage was increasing the homogeneity of the mixture in the mixer. While the results of the velocity probability density function (PDF) showed that the number of particles interacting with the impeller in the first/third stage was more than the second stage, which could indicate that the mixing in the impeller during the first/third stage was motivating the mixing by diffusion process.

8.2 Future work

- Since better binder distribution could increase the homogeneity of binder distribution, hence its worth to try the process with using spray system as a binder addition method.
- Adding the binder to the powder as batches, instead of one batch, corresponding with the stages of MSG. This could have a potential effect on the granule attributes particularly on the porosity of the granules as the porosity may change if the amount of binder will reduce between the primary particles and the interstitial volume of the air could increase. This method of binder addition could be more convenient for the granulation processes in which the binder content may change with time due to drying process.
- Using the counter-current operating mode may also lead to some interesting results, especially when elastic materials are used in the granulation process.
- As the effect of the granulation time and the impeller speed on the granule size distribution were demonstrated in this work and some interesting results were obtained, it could be, also, interesting to study the MSG process using population balance modelling to have more understanding about the MSG process.
- Regarding studying the dynamic of the flow in the mixer using DEM simulation, it is recommended to study the chain force within the particle bed. This could give good visualization about how the force affects and distributes inside the particle bed which is important to understand the dynamic of the mixing process in the Eirich mixer. In addition, using some cohesion contact model is also recommended.
- If the measurements of the granule properties were upgraded to the online measurement systems, then the process, probably, could be utilized in producing granules with controlled properties.

REFERENCES

Ai, J., Chen, J.F., Rotter, J.M., Ooi, J.Y., 2011. Assessment of rolling resistance models in discrete element simulations. Powder Technol. 206, 269–282.

Albertini, B., Cavallari, C., Passerini, N., Voinovich, D., González-Rodríguez, M.L., Magarotto, L., Rodriguez, L., 2004. Characterization and taste-masking evaluation of acetaminophen granules: Comparison between different preparation methods in a high-shear mixer. Eur. J. Pharm. Sci. 21, 295–303.

Albrecht, H., Borys, M., Damasche, N., Tropea, C., 2003. Laser Doppler and phase Doppler measurement techniques, Cryogenics. Springer Verlag, Berlin Heidelberg.

Alian, M., Ein-Mozaffari, F., Upreti, S.R., Wu, J., 2015. Using discrete element method to analyze the mixing of the solid particles in a slant cone mixer. Chem. Eng. Res. Des. 93, 318–329.

Armstrong, N., 2009. Handbook of Pharmaceutical Excipients, 6th ed. Pharmaceutical Press, London.

Ax, K., Feise, H., Sochon, R., Hounslow, M., Salman, A., 2008. Influence of liquid binder dispersion on agglomeration in an intensive mixer. Powder Technol. 179, 190–194.

Barrera-Medrano, D., Salman, A.D., Reynolds, G.K., Hounslow, M.J., 2006. Granule Structure, in: Salman, A.D., Hounslow, M., Seville, J.P.K. (Eds.), Handbook of Powder Technology (Granulation). Elsevier, Amsterdam, p. 1402.

Benali, M., Gerbaud, V., Hemati, M., 2009. Effect of operating conditions and physico – chemical properties on the wet granulation kinetics in high shear mixer. Powder Technol. 190, 160–169.

Börner, M., Michaelis, M., Siegmann, E., Radeke, C., Schmidt, U., 2016. Impact of impeller design on high-shear wet granulation. Powder Technol. 295, 261–271.

Brenda, R., Khinast, J.G., Glasser, B.J., 2009. Discrete Element Simulation of Free Flowing Grains in a Four-Bladed Mixer. AIChE J. 55, 2035–2048.

Bridgwater, J., Forrest, S., Parker, D.J., 2004. PEPT for agglomeration? Powder Technol.

140, 187–193.

Broadbent, C.J., Bridgwater, J., Parker, D.J., Keningley, S.T., Knight, P., 1993. A phenomenological study of a batch mixer using a positron camera. Powder Technol. 76, 317–329.

Cavinato, M., Artoni, R., Bresciani, M., Canu, P., Santomaso, A.C., 2013. Scale-up effects on flow patterns in the high shear mixing of cohesive powders. Chem. Eng. Sci. 102, 1–9.

Chan, E.L., 2012. High shear granulation: a study of blade-granule bed interactions. The University of Sheffield, PhD Thesis.

Chan, E.L., Reynolds, G.K., Gururajan, B., Hounslow, M.J., Salman, A.D., 2013. Blade – granule bed stress in a cylindrical high shear granulator : I — Online measurement and characterisation. Chem. Eng. Sci. 86, 38–49.

Chan, E.L., Reynolds, G.K., Gururajan, B., Salman, A.D., Hounslow, M.J., 2012. Blade-granule bed stress in a cylindrical high-shear granulator: Variability studies. Chem. Eng. Technol. 35, 1435–1447.

Chan, E.L., Washino, K., 2018. Coarse grain model for DEM simulation of dense and dynamic particle flow with liquid bridge forces. Chem. Eng. Res. Des. 132, 1060–1069.

Chan, E.L., Washino, K., Ahmadian, H., Bayly, A., Alam, Z., Hounslow, M.J., Salman, A.D., 2015. Dem investigation of horizontal high shear mixer flow behaviour and implications for scale-up. Powder Technol. 270, 561–568.

Chandratilleke, G.R., Yu, A.B., Stewart, R.L., Bridgwater, J., 2009. Effects of blade rake angle and gap on particle mixing in a cylindrical mixer. Powder Technol. 193, 303–311.

Chouk, V., Reynolds, G., Hounslow, M., Salman, A., 2009. Single drop behaviour in a high shear granulator. Powder Technol. 189, 357–364.

Conway, S.L., Lekhal, A., Khinast, J.G., Glasser, B.J., 2005. Granular flow and segregation in a four-bladed mixer. Chem. Eng. Sci. 60, 7091–7107.

Cundall, P.A., Strack, O.D.L., 1979. A discrete numerical model for granular assemblies. Géotechnique 29, 47–65.

Darelius, A., Rasmuson, A., Niklasson Björn, I., Folestad, S., 2007. LDA measurements of near wall powder velocities in a high shear mixer. Chem. Eng. Sci. 62, 5770–5776.

Daumann, B., Sun, X., Anlauf, H., Gerl, S., Nirschl, H., 2010. Mixing agglomeration in a high-shear mixer with a stirred mixing vessel. Chem. Eng. Technol. 33, 321–326.

Dévay, A., Mayer, K., Pál, S., Antal, I., 2006. Investigation on drug dissolution and particle characteristics of pellets related to manufacturing process variables of high-shear granulation. J. Biochem. Biophys. Methods 69, 197–205.

Dhenge, R.M., Washino, K., Cartwright, J.J., Hounslow, M.J., Salman, A.D., 2013. Twin screw granulation using conveying screws: Effects of viscosity of granulation liquids and flow of powders. Powder Technol. 238, 77–90.

Dorvlo, S.K., 2010. Agglomeration of food powders. The University of Sheffield, PhD Thesis.

Dries, D., Vromans, H., 2002. Relationship between inhomogeneity phenomena and granule growth mechanisms in a high-shear mixer. Int. J. Pharm. 247, 167–177.

Durst, F., Melling, A., James, H.W., 1981. Principles and practice of laser-Doppler anemometry. Academic Press, London.

Eirich GmbH & Co KG, n.d. KG, Maschinenfabrick Gustav_Mixing technology [WWW Document]. URL http://www.eirich.com/

Eliasen, H., Kristensen, H.G., Schæfer, T., 1999. Growth mechanisms in melt agglomeration with a low viscosity binder. Int. J. Pharm. 186, 149–159.

Ennis, B.J., 2008. Principles of Size Enlargement, in: Perry, R.H., Green, D.W., Maloney, J.O. (Eds.), Perry's Chemical Engineers' Handbook. McGraw-Hill, New York, p. 2400.

Ennis, B.J., 2005. Theory of Granulation: An Engineering Perspective, in: Parikh, D.M. (Ed.), Handbook of Pharmaceutical Granulation Technology. Taylor & Francis

Group, Boca Raton ; London, p. 532.

Ennis, B.J., Tardos, G., Pfeffer, R., 1991. A microlevel-based characterization of granulation phenomena. Powder Technol. 65, 257–272.

Flore, K., Schoenherr, M., Feise, H., 2009. Aspects of granulation in the chemical industry. Powder Technol. 189, 327–331.

Forrest, S., Bridgwater, J., Mort, P.R., Litster, J., Parker, D.J., 2003. Flow patterns in granulating systems. Powder Technol. 130, 91–96.

Fu, J., Reynolds, G.K., Adams, M.J., Hounslow, M.J., Salman, A.D., 2005. An experimental study of the impact breakage of wet granules. Chem. Eng. Sci. 60, 4005–4018.

Gabbott, I., 2007. Designer Granules: Beating the Trade-off between Granule Strength and Dissolution Time. The University of Sheffield, PhD Thesis.

Gluba, T., 2005. The energy of bed processing during drum granulation. Chem. Eng. Process. 44, 237–243.

Goldsmith, W., 1960. Impact: The Theory and Physical Behaviour of Colliding Solids. Edward Arnold, New York.

Hagemeier, T., Börner, M., Bück, A., Tsotsas, E., 2015. A comparative study on optical techniques for the estimation of granular flow velocities. Chem. Eng. Sci. 131, 63–75.

Hansuld, E.M., Briens, L., 2014. A review of monitoring methods for pharmaceutical wet granulation. Int. J. Pharm. 472, 192–201.

Hapgood, K.P., Litster, J.D., White, E.T., Mort, P.R., Jones, D.G., 2004. Dimensionless spray flux in wet granulation: Monte-Carlo simulations and experimental validation. Powder Technol. 141, 20–30.

Hassanpour, A., Kwan, C.C., Ng, B.H., Rahmanian, N., Ding, Y.L., Antony, S.J., Jia, X.D., Ghadiri, M., 2009. Effect of granulation scale-up on the strength of granules. Powder Technol. 189, 304–312.

Hassanpour, A., Pasha, M., 2015. Discrete Element Method Applications in Process Engineering, in: Martín, M.M. (Ed.), Introduction to Software for Chemical Engineering. Taylor & Francis Group, LLC, Boca Raton ; London, pp. 245–287.

Hassanpour, A., Tan, H., Bayly, A., Gopalkrishnan, P., Ng, B., Ghadiri, M., 2011. Analysis of particle motion in a paddle mixer using Discrete Element Method (DEM). Powder Technol. 206, 189–194.

Holm, P., Schaefer, T., Kristensen, H.G., 1985. Granulation in high-speed mixers Part VI. Effects of process conditions on power consumption and granule growth. Powder Technol. 43, 225–233.

Hoomans, B.P.B., Kuipers, J.A.M., Briels, W.J., van Swaaij, W.P.M., 1996. Discrete particle simulation of bubble and slug formation in a tow-dimensional gas-fluidised bed: a hard sphere approach. Chem. Eng. Sci. 51, 99–118.

Hoornaert, F., Wauters, P. a L., Meesters, G.M.H., Pratsinis, S.E., Scarlett, B., 1998. Agglomeration behaviour of powders in a Lödige mixer granulator. Powder Technol. 96, 116–128.

Ibsen, C.H., Solberg, T., Hjertager, B.H., Johnsson, F., 2002. Laser Doppler anemometry measurements in a circulating fluidized bed of metal particles. Exp. Therm. Fluid Sci. 26, 851–859.

Iveson, S.M., Litster, J.D., 1998a. Growth regime map for liquid-bound granules. AIChE J. 44, 1510–1518.

Iveson, S.M., Litster, J.D., 1998b. Fundamental studies of granule consolidation Part 2 : Quantifying the effects of particle and binder properties. Powder Technol. 99, 243–250.

Iveson, S.M., Litster, J.D., Ennis, B.J., 1996. Fundamental studies of granule consolidation Part 1: Effects of binder content and binder viscosity. Powder Technol. 88, 15–20.

Iveson, S.M., Litster, J.D., Hapgood, K., Ennis, B.J., 2001. Nucleation, growth and breakage phenomena in agitated wet granulation processes: A review. Powder Technol. 117, 3–39.

Iveson, S.M., Wauters, P.A.L., Forrest, S., Litster, J.D., Meesters, G.M.H., Scarlett, B., 2001. Growth regime map for liquid-bound granules: Further development and experimental validation. Powder Technol. 117, 83–97.

Kapur, P.C., 1978. Balling and granulation, in: Drew, T.B., Coketel, G.R., Hoopes, J.W., Vermeulen, T. (Eds.), Advances in Chemical Engineering. Academic Press, INC., New York, London, pp. 55–123.

Kendall, K., 1988. Agglomerate strength. Powder Metall. 31, 28–31.

Knight, P.C., 1993. An investigation of the kinetics of granulation using a high shear mixer. Powder Technol. 77, 159–169.

Knight, P.C., Instone, T., Pearson, J.M.K., Hounslow, M.J., 1998. An investigation into the kinetics of liquid distribution and growth in high shear mixer agglomeration. Powder Technol. 97, 246–257.

Knight, P.C., Johansen, A., Kristensen, H.G., Schæfer, T., Schæfer, T., Seville, J.P.K., 2000. An investigation of the effects on agglomeration of changing the speed of a mechanical mixer. Powder Technol. 110, 204–209.

Knight, P.C.T., lnstone T, Pearson, J.M.K., Hounslow, M.J., 1998. An investigation into the kinetics of liquid distribution and growth in high shear mixer agglomeration. Powder Technol. 97, 246–257.

Koide, T., Nagato, T., Kanou, Y., Matsui, K., Natsuyama, S., Kawanishi, T., Hiyama, Y., 2013. Detection of component segregation in granules manufactured by high shear granulation with over-granulation conditions using near-infrared chemical imaging. Int. J. Pharm. 441, 135–145.

Kuo, H.P., Knight, P.C., Parker, D.J., Tsuji, Y., Adams, M.J., Seville, J.P.K., 2002. The influence of DEM simulation parameters on the particle behaviour in a V-mixer. Chem. Eng. Sci. 57, 3621–3638.

Lacey, P.M.C., 1954. Developments in the theory of particle mixing. J. Appl. Chem. 4, 257–268.

Laurent, B., Bridgwater, J., Parker, D., 2000. Motion in a particle bed agitated by a single

blade. AIChE J. 1734, 1723–1734.

Le, P.K., 2008. The study of high shear granulation across the length scales. The University of Sheffield, PhD Thesis.

Le, P.K., Avontuur, P., Hounslow, M.J., Salman, A.D., 2011. A microscopic study of granulation mechanisms and their effect on granule properties. Powder Technol. 206, 18–24.

Li, Y., Xu, Y., Thornton, C., 2005. A comparison of discrete element simulations and experiments for “sandpiles” composed of spherical particles. Powder Technol. 160, 219–228.

Litster, J., Ennis, B., 2004. The Science and Engineering of Granulation Processes. Kluwer academic publisher, London.

Litster, J.D., Hapgood, K.P., Michaels, J.N., Sims, a., Roberts, M., Kameneni, S.K., 2002. Scale-up of mixer granulators for effective liquid distribution. Powder Technol. 124, 272–280.

Litster, J.D., Hapgood, K.P., Michaels, J.N., Sims, a., Roberts, M., Kameneni, S.K., Hsu, T., 2001. Liquid distribution in wet granulation: Dimensionless spray flux. Powder Technol. 114, 32–39.

Liu, P.Y., Yang, R.Y., Yu, A.B., 2013. DEM study of the transverse mixing of wet particles in rotating drums. Chem. Eng. Sci. 86, 99–107.

Mangwandi, C., Adams, M.J., Hounslow, M.J., Salman, a. D., 2010. Effect of impeller speed on mechanical and dissolution properties of high-shear granules. Chem. Eng. J. 164, 305–315.

McCarthy, J.J., Khakhar, D. V, Ottino, J.M., 2000. Computational studies of granular mixing. Powder Technol. 109, 72–82.

McLeod, A.S., Bordia, S., Gladden, L.F., 1999. Interface roughening during the dissolution of porous media. Europhys. Lett. 46, 571–576.

Merkus, H.G., 2009. Particle Size Measurements: Fundamentals, Practice, Quality. Springer Science+Business Media, Dordrecht.

Michaels, J.N., 2003. Toward rational design of powder processes. Powder Technol. 138, 1–6.

Muguruma, Y., Tanaka, T., Tsuji, Y., 2000. Numerical simulation of particulate flow with liquid bridge between particles (simulation of centrifugal tumbling granulator). Powder Technol. 109, 49–57.

Nakamura, H., Fujii, H., Watano, S., 2013. Scale-up of high shear mixer-granulator based on discrete element analysis. Powder Technol. 236, 149–156.

Ng, B.H., Kwan, C.C., Ding, Y.L., Ghadiri, M., Fan, X.F., 2007. Solids motion of calcium carbonate particles in a high shear mixer granulator: A comparison between dry and wet conditions. Powder Technol. 177, 1–11.

Nilpawar, a. M., Reynolds, G.K., Salman, a. D., Hounslow, M.J., 2006. Surface velocity measurement in a high shear mixer. Chem. Eng. Sci. 61, 4172–4178.

Nold, P., Frey, K., Loebe, R., 2008. Mixing, Granulating, Coating, Plasticizing and Slurrying in the Intensive Mixer. Rferactories Man. 52–56.

Ohno, I., Hasegawa, S., Yada, S., Kusai, A., Moribe, K., Yamamoto, K., 2007. Importance of evaluating the consolidation of granules manufactured by high shear mixer. Int. J. Pharm. 338, 79–86.

Oka, S., Kašpar, O., Tokárová, V., Sowrirajan, K., Wu, H., Khan, M., Muzzio, F., Štěpánek, F., Ramachandran, R., 2015. A quantitative study of the effect of process parameters on key granule characteristics in a high shear wet granulation process involving a two component pharmaceutical blend. Adv. Powder Technol. 26, 315–322.

Oka, S., Smrčka, D., Kataria, A., Emady, H., Muzzio, F., Štěpánek, F., Ramachandran, R., 2017. Analysis of the origins of content non-uniformity in high-shear wet granulation. Int. J. Pharm. 528, 578–585.

Omar, C.S., Dhenge, R.M., Palzer, S., Hounslow, M.J., Salman, A.D., 2016. Roller compaction: Effect of relative humidity of lactose powder. Eur. J. Pharm. Biopharm. 106, 26–37.

Oulahna, D., Cordier, F., Galet, L., Dodds, J. a., 2003. Wet granulation: The effect of shear on granule properties. Powder Technol. 130, 238–246.

Parker, D.J., Forster, R.N., Fowles, P., Takhar, P.S., 2002. Positron emission particle tracking using the new Birmingham positron camera. Nucl. Instruments Methods Phys. Res. Sect. A Accel. Spectrometers, Detect. Assoc. Equip. 477, 540–545.

Pepin, X., Blanchon, S., Couarraze, G., 2001. Power Consumption Profiles in High-Shear Wet Granulation. I: Liquid Distribution in Relation to Powder and Binder Properties. J. Pharamceutical Sci. 90, 322–331.

Pitt, K., Sinka, C., 2007. Tabletting, in: Salman, A.D., Hounslow, M., Seville, J.P.K. (Eds.), Handbook of Powder Technology. Elsevier B.V., Amsterdam.

Plank, R., Diehl, B., Grinstead, H., Zega, J., 2003. Quantifying liquid coverage and powder flux in high-shear granulators. Powder Technol. 134, 223–234.

Polyanin, A.D., Manzhirov, A. V., 2007. Handbook of Mathematics for Engineers and Scientists. Chapman & Hall/CRC, Boca Raton ; London.

Punmia, B.C., Jain, A.K., 2005. Soil Mechanics and Foundations, 16th ed. LAXMI Publictions (P) LTD, Bangalore.

Raffel, M., Willert, C.E., Wereley, S., 2007. Particle Image Velocimetry, 2nd ed. Springer, Berlin Heidelberg.

Rahmanian, N., Ganimi, T. El, Ghadiri, M., 2013. Further investigations on the influence of scale-up of a high shear granulator on the granule properties. Particuology 11, 627–635.

Rahmanian, N., Naji, A., Ghadiri, M., 2011. Effects of process parameters on granules properties produced in a high shear granulator. Chem. Eng. Res. Des. 89, 512–518.

Ramachandran, R., Poon, J.M.-H., Sanders, C.F.W., Glaser, T., Immanuel, C.D., III, F.J.D., Litster, J.D., Stepanek, F., Wang, F.-Y., Cameron, I.T., 2008. Experimental studies on distributions of granule size, binder content and porosity in batch drum granulation: Inferences on process modelling requirements and process sensitivities. Powder Technol. 188, 89–101.

Ramaker, J.S., Jelgersma, M.A., Vonk, P., Kossen, N.W.F., 1998. Scale-down of a high-shear pelletisation process: Flow profile and growth kinetics. Int. J. Pharm. 166, 89–97.

Realpe, A., Velázquez, C., 2008. Growth kinetics and mechanism of wet granulation in a laboratory-scale high shear mixer: Effect of initial polydispersity of particle size. Chem. Eng. Sci. 63, 1602–1611.

Remy, B., Glasser, B.J., Khinast, J.G., 2010. The Effect of Mixer Properties and Fill Level on Granular Flow in a Bladed Mixer. AIChE J. 56, 336–353.

Reynolds, G.K., Fu, J.S., Cheong, Y.S., Hounslow, M.J., Salman, a. D., 2005. Breakage in granulation: A review. Chem. Eng. Sci. 60, 3969–3992.

Reynolds, G.K., Le, P.K., Nilpawar, A.M.., 2007. High Shear Granulation, in: Salman, A.D., Hounslow, M., Seville, J.P.K. (Eds.), Handbook of Powder Technology,. Elsevier, Amsterdam, p. 1402.

Reynolds, G.K., Nilpawar, A.M., Salman, A.D., Hounslow, M.J., 2008. Direct measurement of surface granular temperature in a high shear granulator. Powder Technol. 182, 211–217.

Rix, S.J.L., Glass, D.H., Greated, C. a., 1996. Preliminary studies of elutriation from gas-fluidised beds using particle image velocimetry. Chem. Eng. Sci. 51, 3479–3489.

Saito, Y., Fan, X., Ingram, A., Seville, J.P.K., 2011. A new approach to high-shear mixer granulation using positron emission particle tracking. Chem. Eng. Sci. 66, 563–569.

Saleh, K., Vialatte, L., Guigon, P., 2005. Wet granulation in a batch high shear mixer. Chem. Eng. Sci. 60, 3763–3775.

Saleh, M.F., Dhenge, R.M., Cartwright, J.J., Hounslow, M.J., Salman, A.D., 2015. Twin screw wet granulation: Binder delivery. Int. J. Pharm. 487, 124–134.

Sanders, C.F.W., Willemse, A.W., Salman, A.D., Hounslow, M.J., 2003. Development of a predictive high-shear granulation model. Powder Technol. 138, 18–24.

Sastry, K.V.S., Fuerstenau, D.W., 1973. Mechanisms of agglomerate growth in green pelletization. Powder Technol. 7, 97–105.

Sato, Y., Nakamura, H., Watano, S., 2008. Numerical analysis of agitation torque and particle motion in a high shear mixer. Powder Technol. 186, 130–136.

Schaefer, T., 1996. Melt pelletization in a high shear mixer . X . Agglomeration of binary mixtures. Intemational J. Pharm. 139, 149–159.

Schæfer, T., 2001. Growth mechanisms in melt agglomeration in high shear mixers. Powder Technol. 117, 68–82.

Schaefer, T., Mathiesen, C., 1996. Melt pelletization in a high shear mixer . IX . Effects of binder particle size. Int. J. Pharm. 139, 139 148.

Schæfer, T., Mathiesen, C., 1996. Melt pelletization in a high shear mixer. VIII. Effects of binder viscosity. Int. J. Pharm. 139, 125–138.

Schæfer, T., Taagegaard, B., Thomsen, L.J., Gjelstrup Kristensen, H., 1993. Melt pelletization in a high shear mixer. V. Effects of apparatus variables. Eur. J. Pharm. Sci. 1, 133–141.

Schaffer, T., 1996. Melt pelletization in a high shear mixer VI . Agglomeration of a cohesive powder. Int. J. Pharm. 132, 221–230.

Schubert, H., 1975. Tensile strength of agglomerates. Powder Technol. 11, 107–119.

Seo, A., Schæfer, T., 2001. Melt agglomeration with polyethylene glycol beads at a low impeller speed in a high shear mixer. Eur. J. Pharm. Biopharm. 52 52, 315–325.

Serkowski Habil, M, M., 2004. On the manufacture of dense microporous refractory materials, Part2: Manufacture of microporous and compact refractory materials. Ger. Ceram. Soc. , cfi/Berichte der DKG 81, E19–E24.

Shi, L., Feng, Y., Calvin Sun, C., 2011a. Massing in high shear wet granulation can simultaneously improve powder flow and deteriorate powder compaction : A double-edged sword. Eur. J. Pharm. Sci. 43, 50–56.

Shi, L., Feng, Y., Sun, C.C., 2011b. Origin of profound changes in powder properties during wetting and nucleation stages of high-shear wet granulation of microcrystalline cellulose. Powder Technol. 208, 663–668.

Smirani-Khayati, N., Falk, V., Bardin-Monnier, N., Marchal-Heussler, L., 2009. Binder liquid distribution during granulation process and its relationship to granule size distribution. Powder Technol. 195, 105–112.

Smrčka, D., Dohnal, J., Štěpánek, F., 2015. Effect of process scale-up on the dissolution of granules with a high content of active pharmaceutical ingredient. Powder Technol. 285, 88–95.

Sochon, R.P.J., Dorvlo, S.K., Rudd, A.I., Hayati, I., Hounslow, M.J., Salman, A.D., 2005. Granulation of Zinc Oxide. Chem. Eng. Res. Des. 83, 1325–1330.

Stewart, R.L., Bridgwater, J., Zhou, Y.C., Yu, A.B., 2001. Simulated and measured flow of granules in a bladed mixer- A detailed comparison. Chem. Eng. Sci. 56, 5457–5471.

Tan, B.M.J., Loh, Z.H., Soh, J.L.P., Liew, C.V., Heng, P.W.S., 2014. Distribution of a viscous binder during high shear granulation - Sensitivity to the method of delivery and its impact on product properties. Int. J. Pharm. 460, 255–263.

Tardos, G.I., Khan, M.I., Mort, P.R., 1997. Critical parameters and limiting conditions in binder granulation of fine powders. Powder Technol. 94, 245–258.

Thielicke, W., 2014. The flapping flight of birds. Analysis and Application. University of Groningen, PhD Thesis.

Thielicke, W., Stamhuis, E.J., 2014. PIVlab - Time-Resolved Digital Particle Image Velocimetry Tool for MATLAB [WWW Document]. URL http://dx.doi.org/10.6084/m9.figshare.1092508

Thies, R., Kleinebudde, P., 2000. Melt pelletisation of a hygroscopic drug in a high shear mixer Part 2 . Mutual compensation of influence variables. Eur. J. Pharm. Sci. 10, 103–110.

Thies, R., Kleinebudde, P., 1999. Melt pelletisation of a hygroscopic drug in a high shear mixer Part 1 . Influence of process variables. Int. J. Pharm. 188, 131–143.

Torrecillas, C.M., Halbert, G.W., Lamprou, D.A., 2017. A novel methodology to study polymodal particle size distributions produced during continuous wet granulation.

Int. J. Pharm. 519, 230–239. https://doi.org/10.1016/j.ijpharm.2017.01.023

Tsuji, Y., Tanaka, T., Ishida, T., 1992. Lagrangian numerical simulation of plug flow of cohesionless particles in a horizontal pipe. Powder Technol. 71, 239–250.

Tu, W., Ingram, A., Seville, J., Hsiau, S., 2009. Exploring the regime map for high-shear mixer granulation. Chem. Eng. J. 145, 505–513.

van den Ban, S., Goodwin, D.J., 2016. Development of a two stage batch fluid bed drying process to minimise impact of entrainment on product quality and drying endpoint determination. Powder Technol. 295, 43–46.

Van Den Dries, K., Vromans, H., 2002. Relationship between inhomogeneity phenomena and granule growth mechanisms in a high-shear mixer. Int. J. Pharm. 247, 167–177.

Washino, K., 2011. Multiscale Modelling of Nucleation Processes in Wet Granulation Using Discrete Element Method and Constrained Interpolation Profile. The University of Sheffied, PhD Thesis.

Webb, P.A., 2001. Volume and Density Determinations for Particle Technologists. micromeritics Instrum. Corp 2.16 1–16.

Zhou, Y.C., Wright, B.D., Yang, R.Y., Xu, B.H., Yu, A.B., 1999. Rolling friction in the dynamic simulation of sandpile formation. Physica A 269, 536–553.

Zhou, Y.C., Yu, A.B., Stewart, R.L., Bridgwater, J., 2004. Microdynamic analysis of the particle flow in a cylindrical bladed mixer. Chem. Eng. Sci. 59, 1343–1364.

APPENDICES

APPENDIX A: VALIDATION OF THE MEASUREMENT OF THE SSA

To validate the accuracy of SSA measurement via KEYENCE microscope, a metallic object (small exact sphere) of 3.16 mm actual diameter was viewed under the microscope and the Figure A-1 shows 3D image of that object.

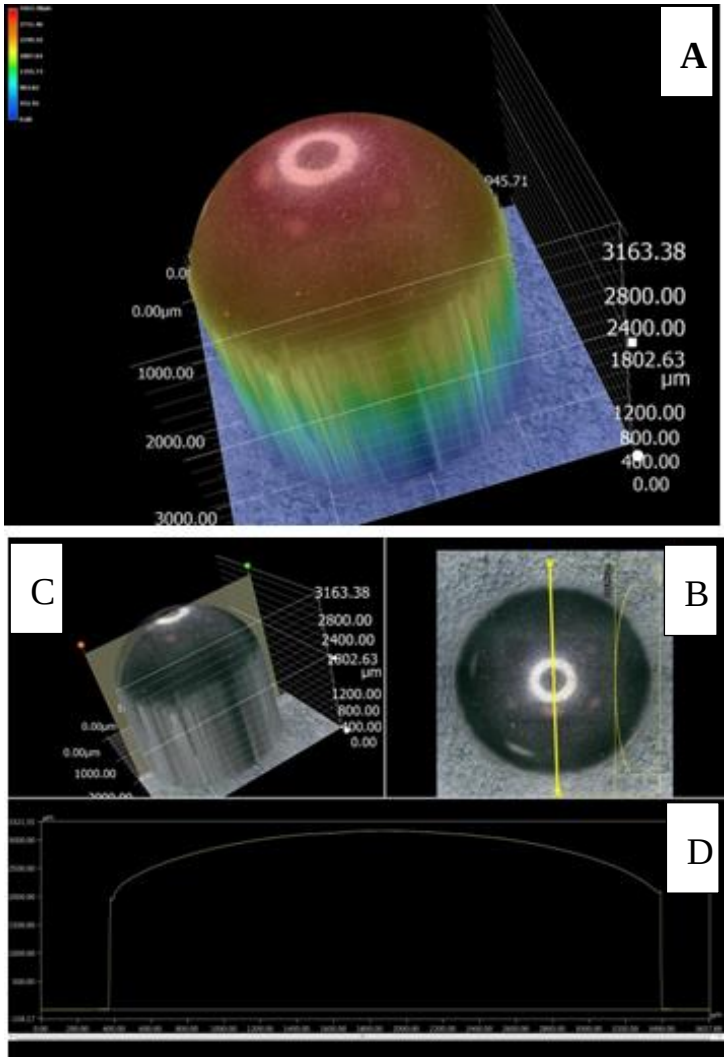

Figure A-1: A 3D image of a metallic sphere (3.16 mm dia), A: is upper part of the sphere (hemisphere) rotated with an angle; B: top-view of the sphere; C: Burr height of the object; D: profile of the section in the C.

From Figure A-1, it's clear that the microscope could see upper part of the object (hemisphere here) which is reachable by the lens of the microscope. The height of the sphere is also can be given in a colour bar scale (see the upper left of the image) the highest point is red and the lowest point (the base) is blue.

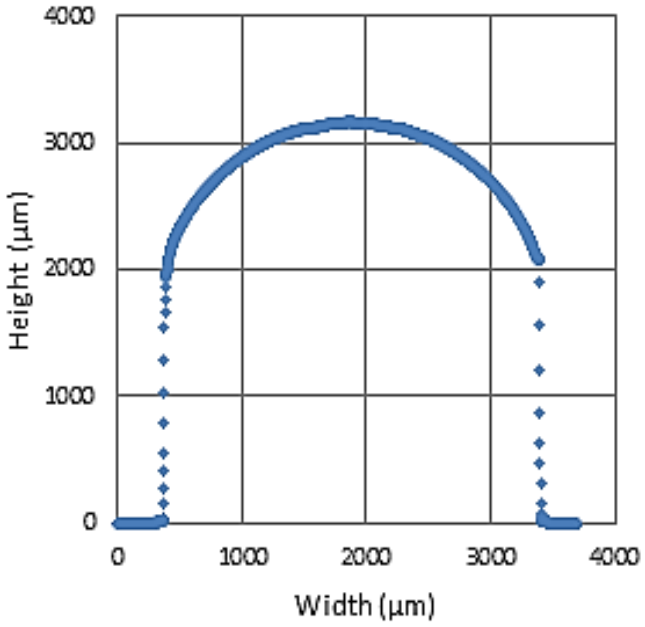

Figure A-2; Profile of a section of the object in the Figure A-1

It is also possible to take a profile of any section through the object as an excel data sheet. Figure 29 shows the profile of a section taken through the object (section in the Figure A-1 B) and profile of Figure A-1 D. The profile shows good sphericity which is very close to the real case. This could be used to study the surface tortuosity of the granules.

The quantitative data of the volume and the surface area of any part of the object within the region of the focus could also be obtained for a certain depth, see Figure A-3.

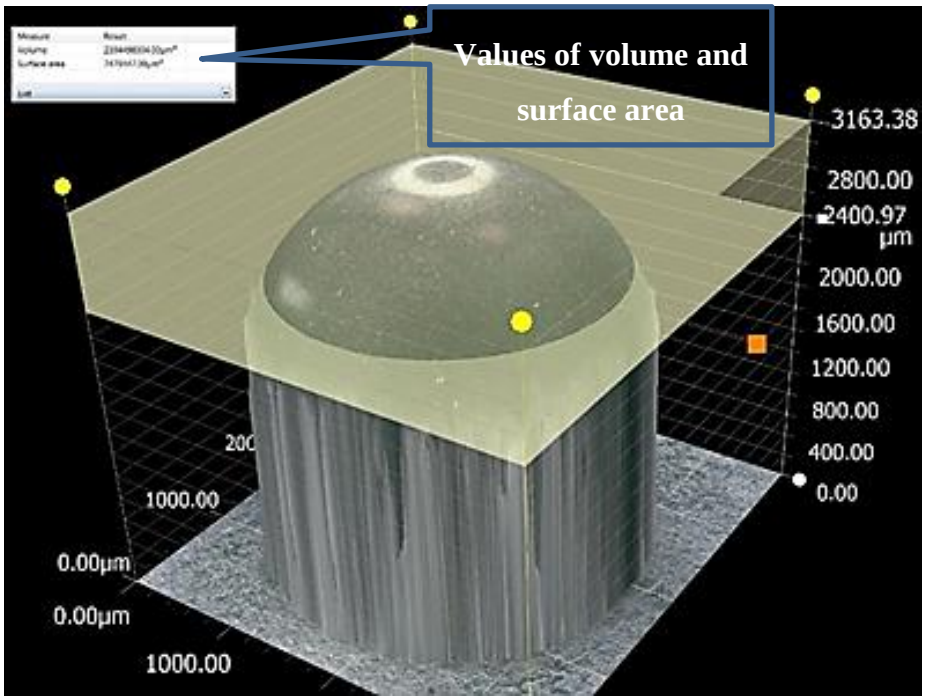

Figure A-3: Measurement of surface to volume ratio for a certain depth (about 762.41 µm) of a spherical object

To check the measurement of the surface area (S) to volume (V) ratio of the section given in the Figure A-3, the surface area to volume ratio of a spherical cap of radius (R=1580 µm) and depth (h=762.41 µm, which equivalent to the depth shown in the Figure A-3, was calculated using the following two equations (Polyanin and Manzhirov, 2007):

$$S = 2\pi\, R\, h$$

$$V = \frac{\pi\, h^2}{3}\,(2\,R - h)$$

The ratio by the microscope is 0.003123 μm^{-1}, and by the calculation is 0.003126 μm^{-1} which they are very close. Samples of the scanned granules are given in Figure A-4 and Figure A-5.

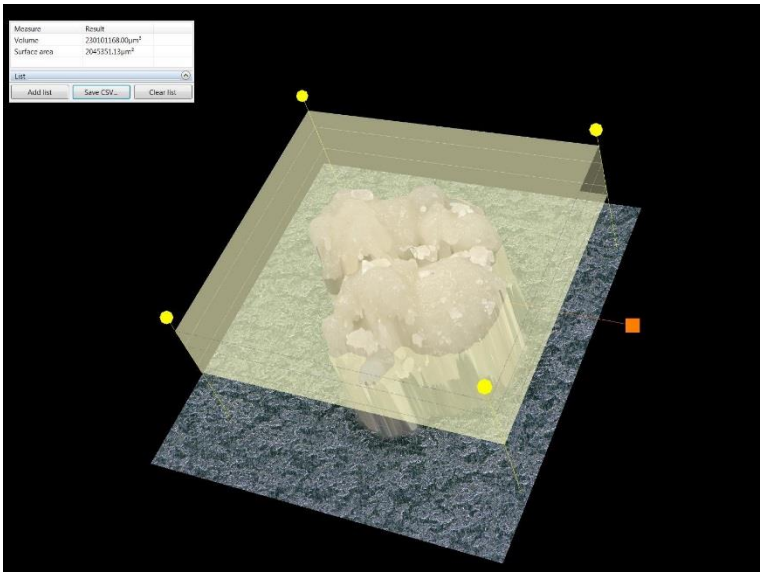

Figure A-4: A granule composed of aggregate of small granules scanned under Keyence microscope

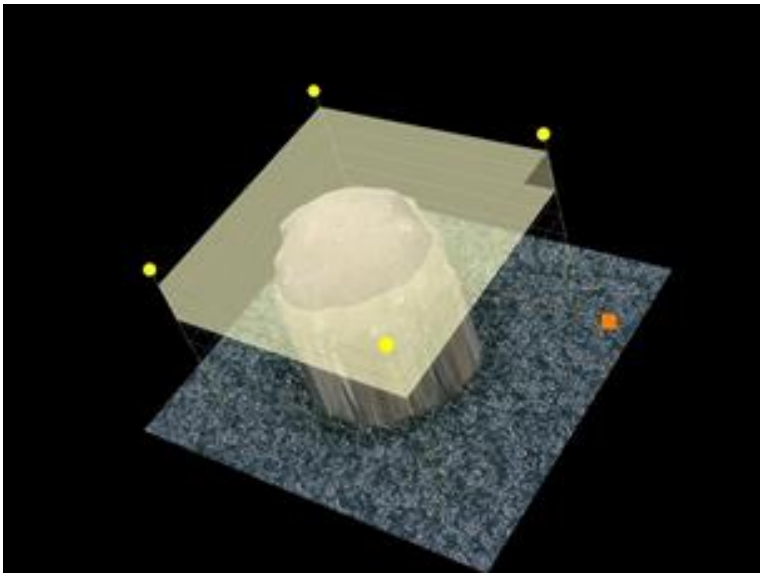

Figure A-5: A single granule scanned under Keyence microscope.

APPENDIX B: GRANULE SHAPE WITH TIME (NG PROCESSES)

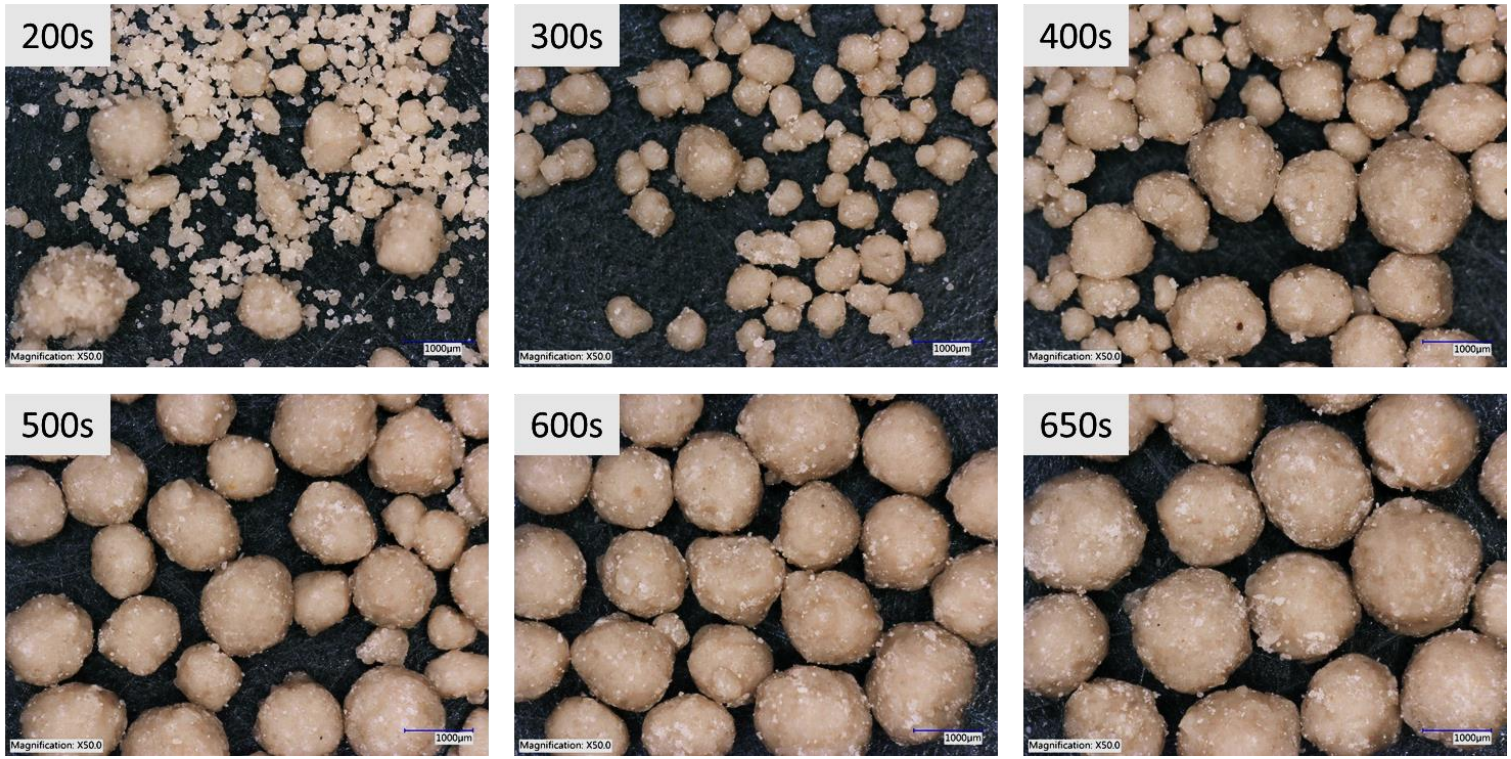

Figure B-1: Shape of granules over the granulation time, NG, L/S = 0.14, Impeller speed = 2000 RPM.

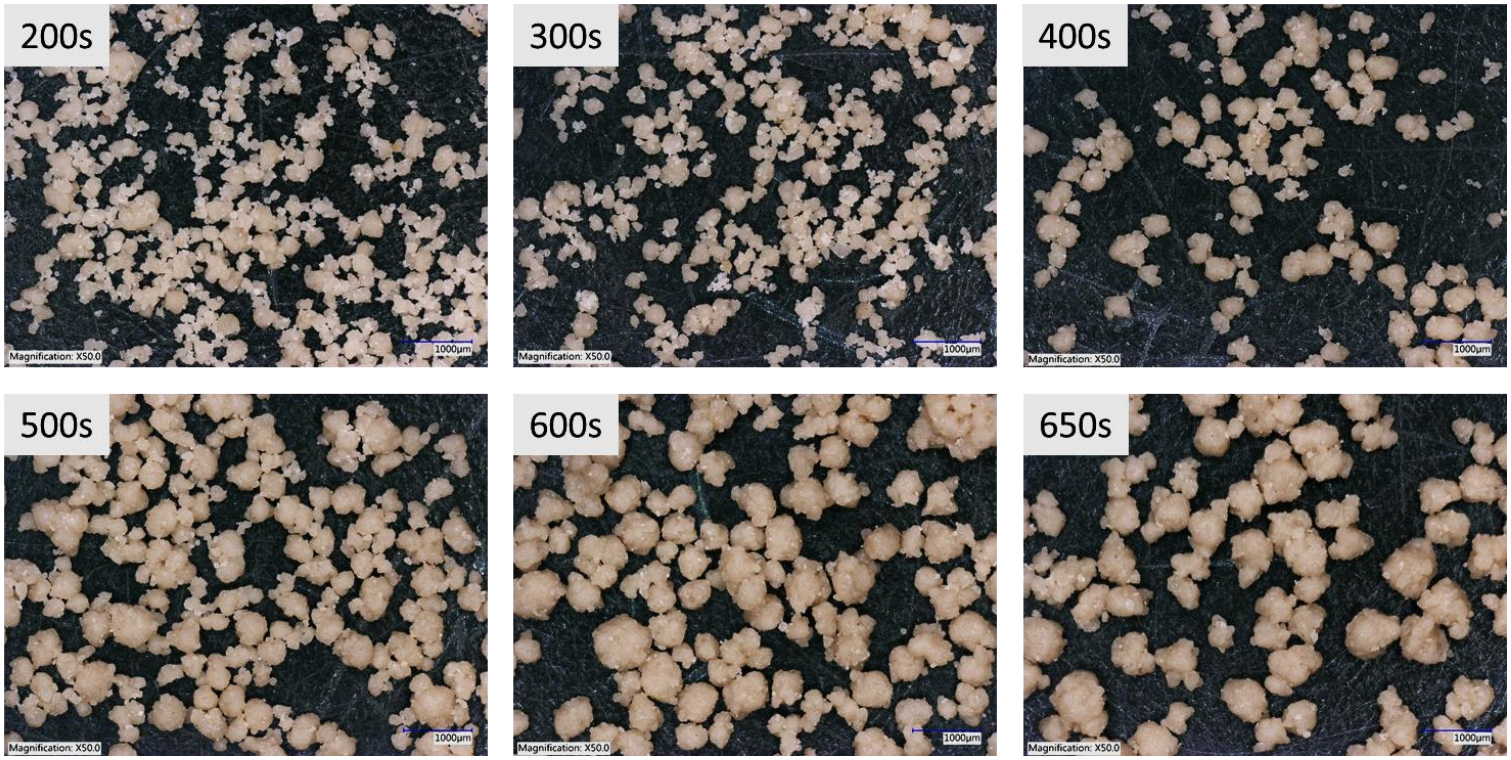

Figure B-2: Shape of granules over the granulation time, NG, L/S = 0.14, Impeller speed = 7000 RPM.

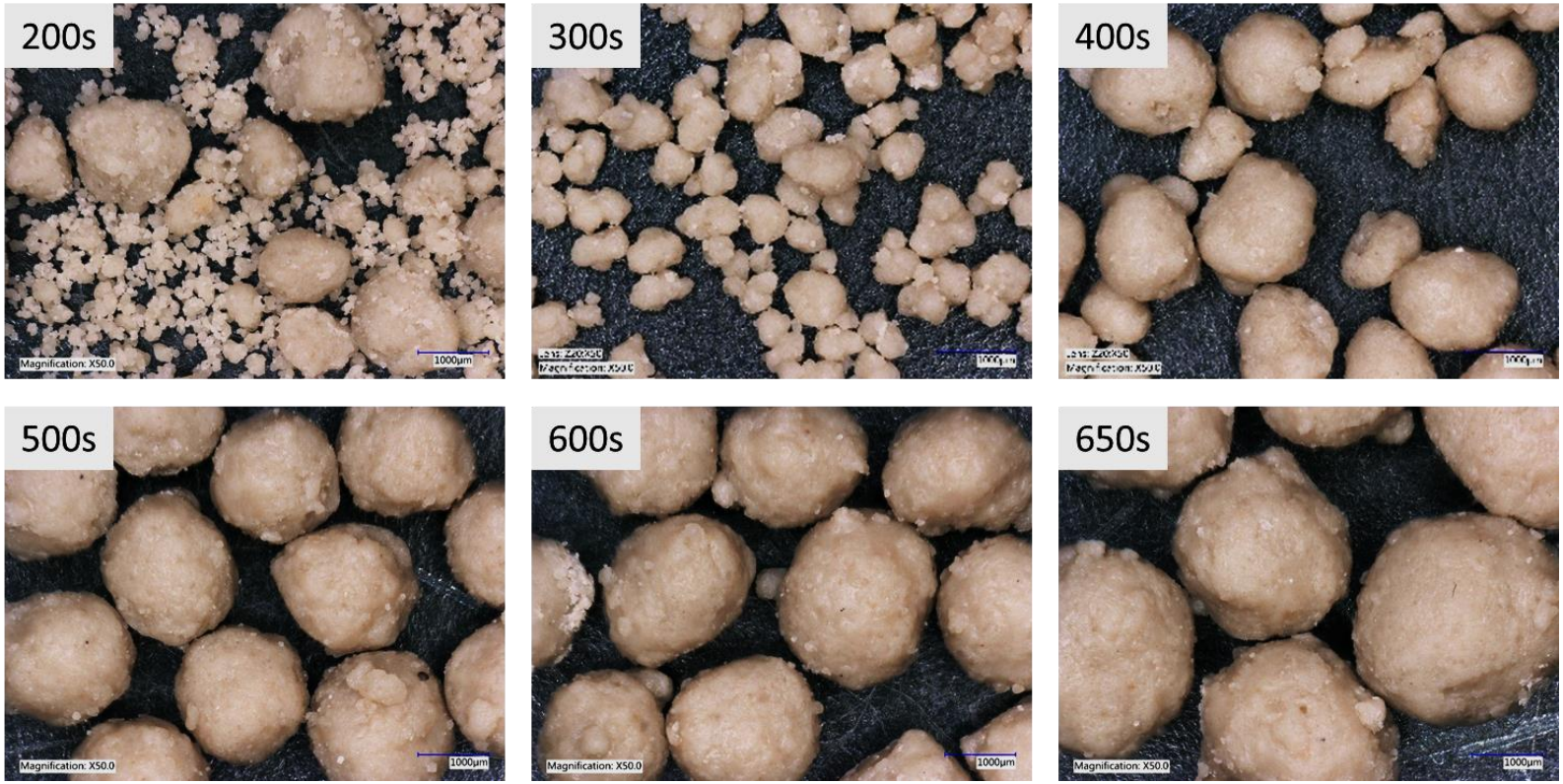

Figure B-3: Shape of granules over the granulation time, NG, L/S = 0.15, Impeller speed = 2000 RPM.

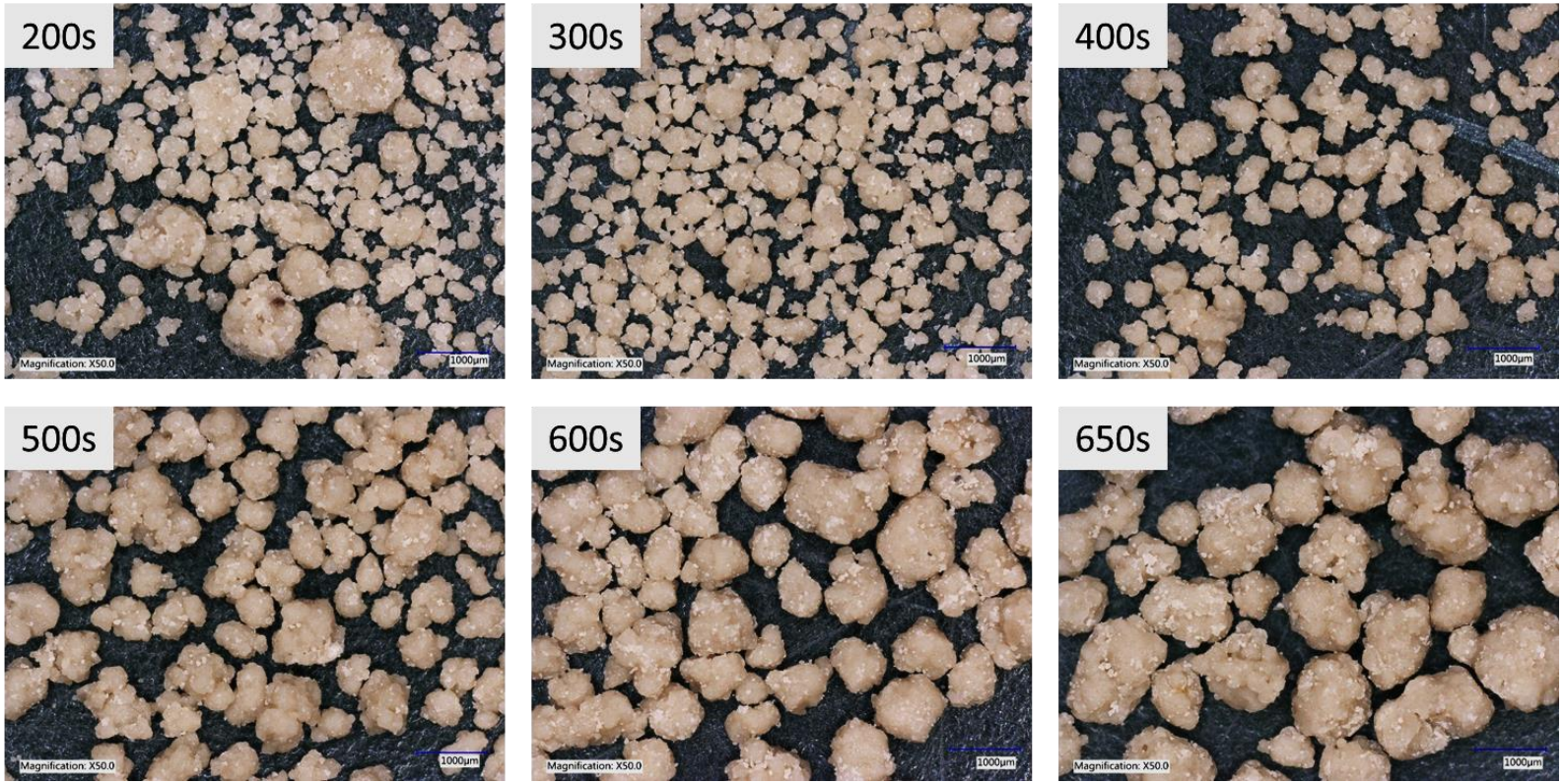

Figure B-4: Shape of granules over the granulation time, NG, L/S = 0.15, Impeller speed = 7000 RPM.

APPENDIX C: X-RAY TOMOGRAPHY FOR THE GRANULES WITH GRANULATION TIME (NG).

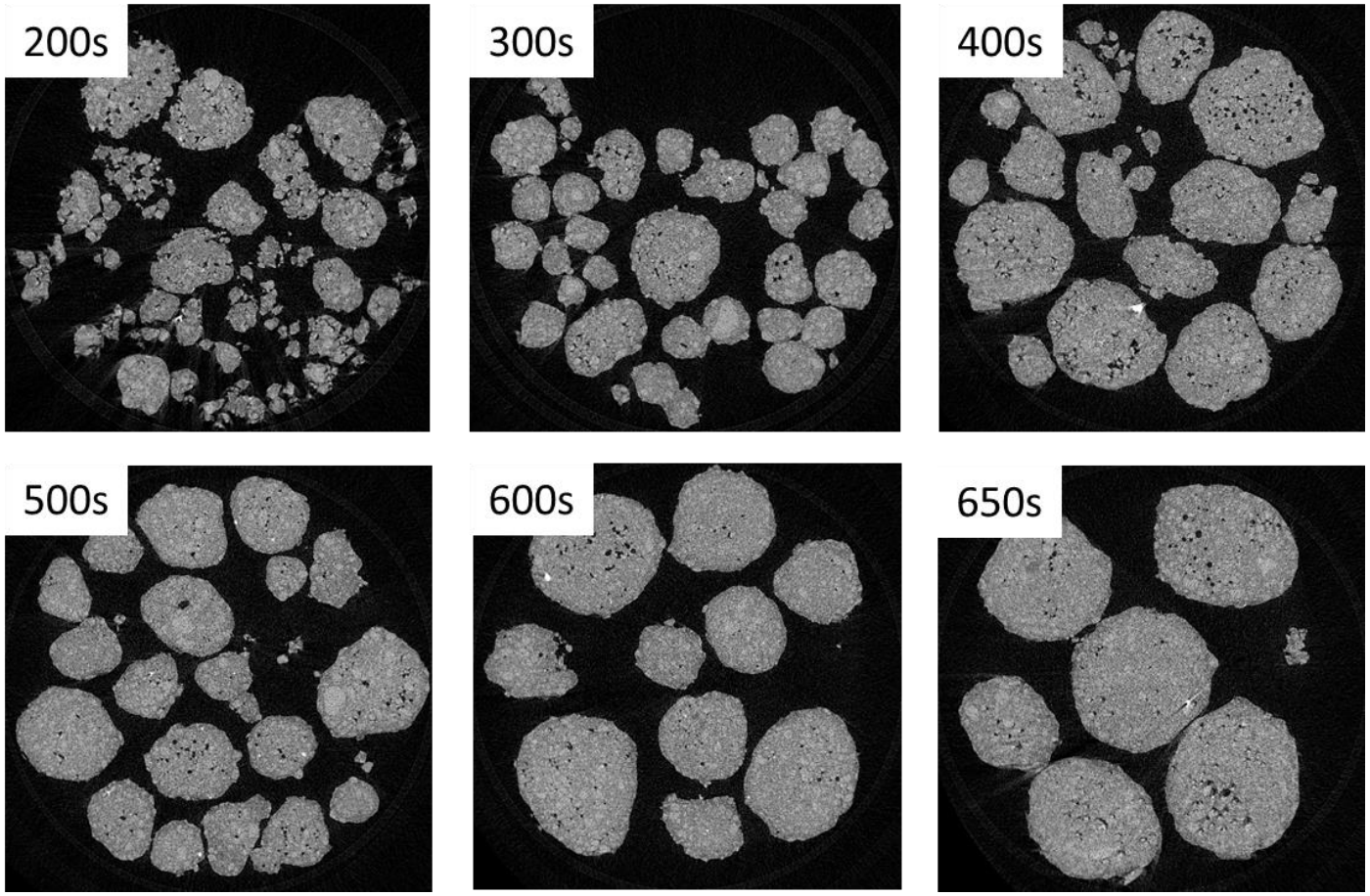

Figure C-1: X-ray tomography for the granule with granulation time, NG, L/S = 0.14, Impeller speed = 2000 RPM.

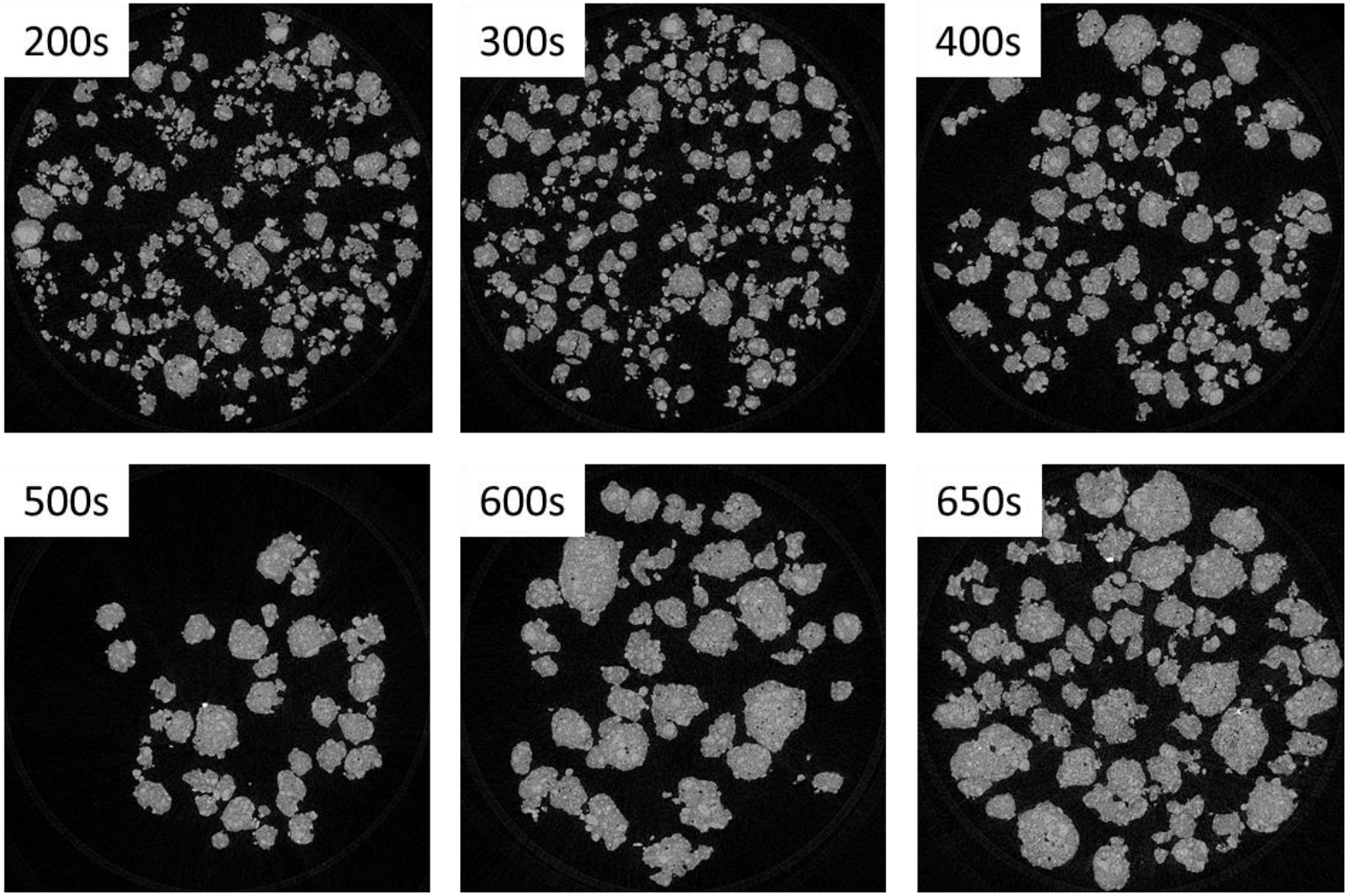

Figure C-2: X-ray tomography for the granule with granulation time, NG, L/S = 0.14, Impeller speed = 7000 RPM.

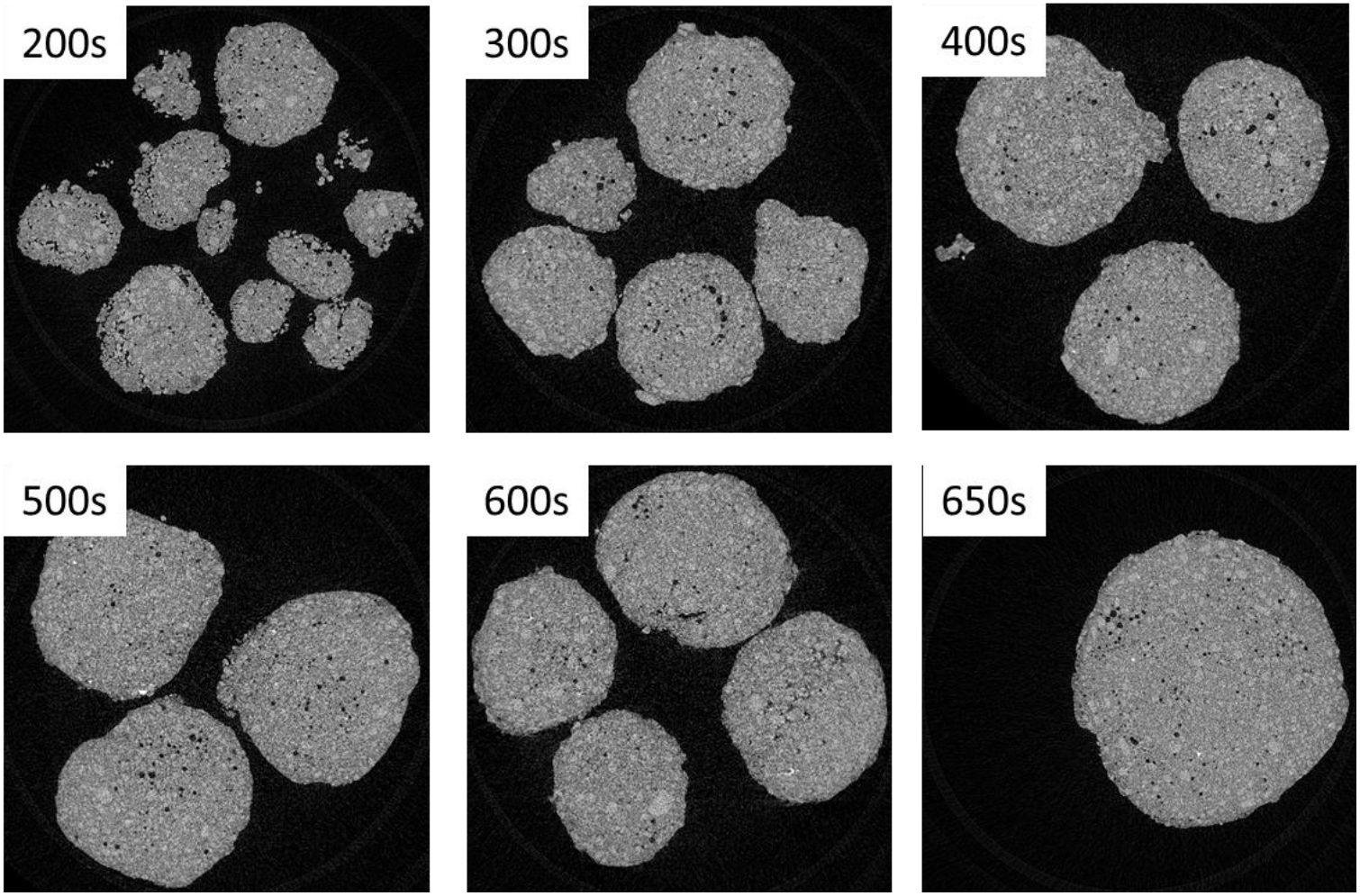

Figure C-3: X-ray tomography for the granule with granulation time, NG, L/S = 0.15, Impeller speed = 2000 RPM.

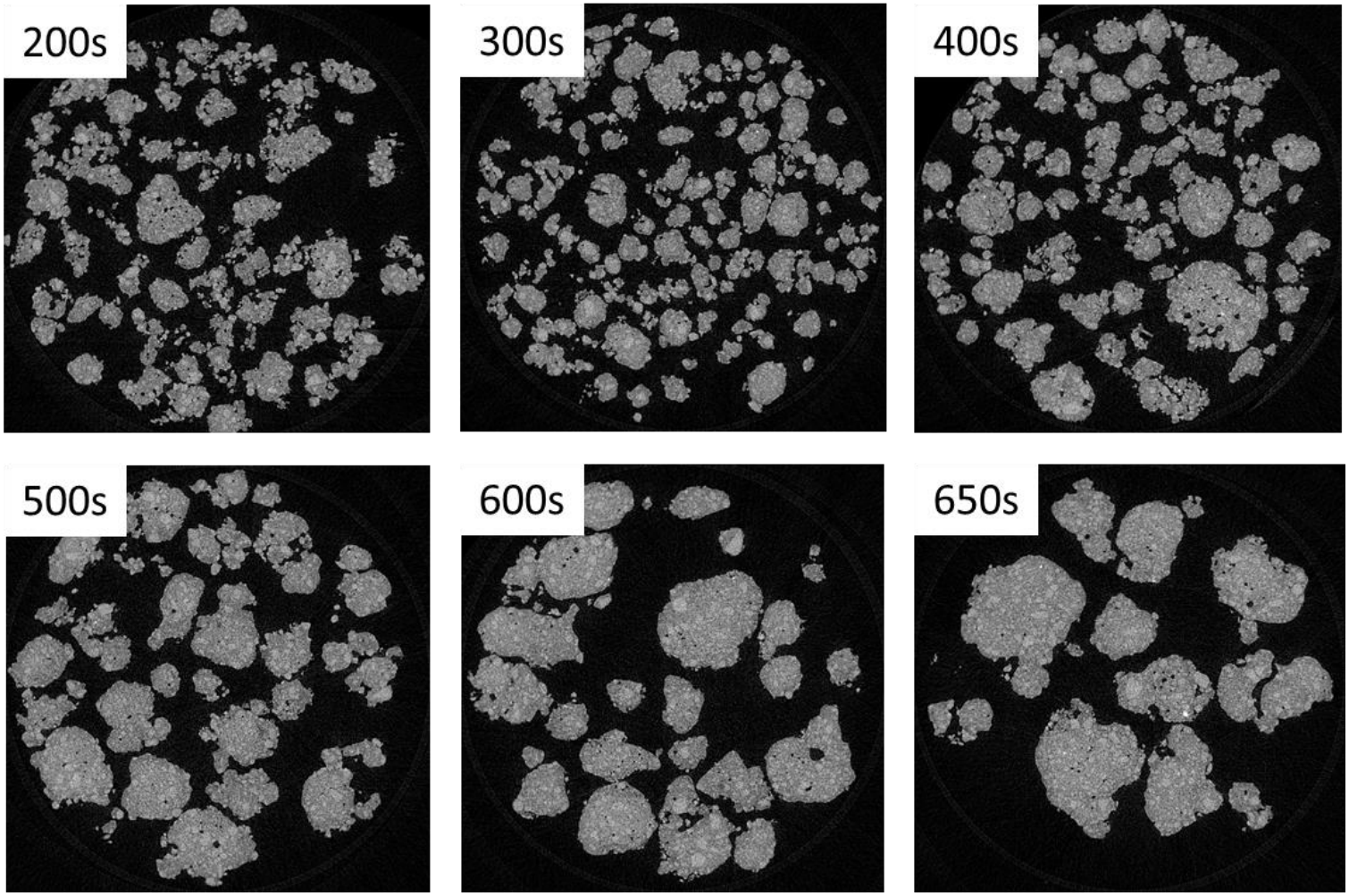

Figure C-4: X-ray tomography for the granule with granulation time, NG, L/S = 0.15, Impeller speed = 7000 RPM.

APPENDIX D: SHAPE OF GRANULES OVER GRANULATION PROCESS (MSG PROCESSES).

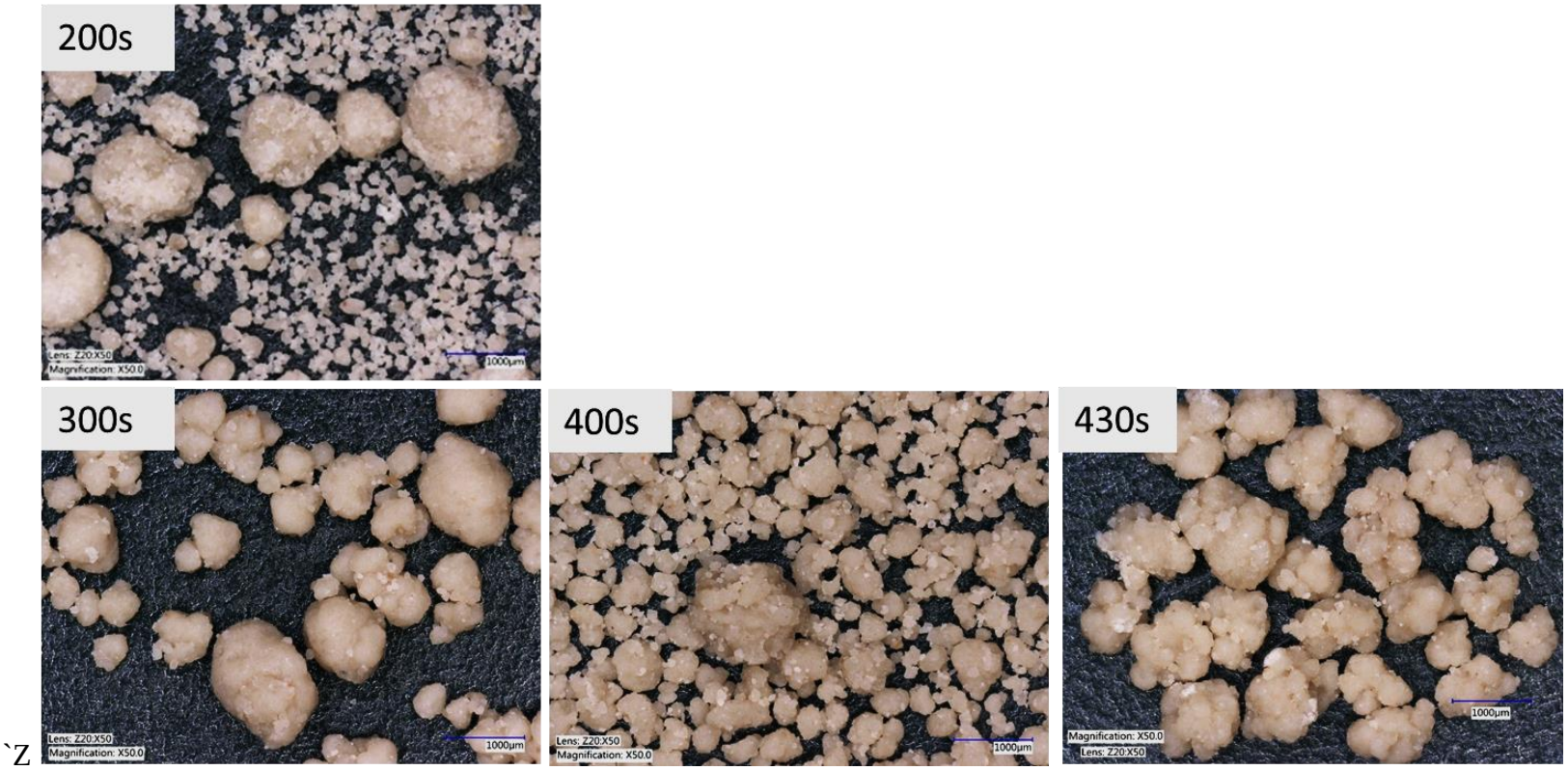

`Z

Figure D-1: Granule shape over the granulation time, MSG/EP, L/S = 0.14.

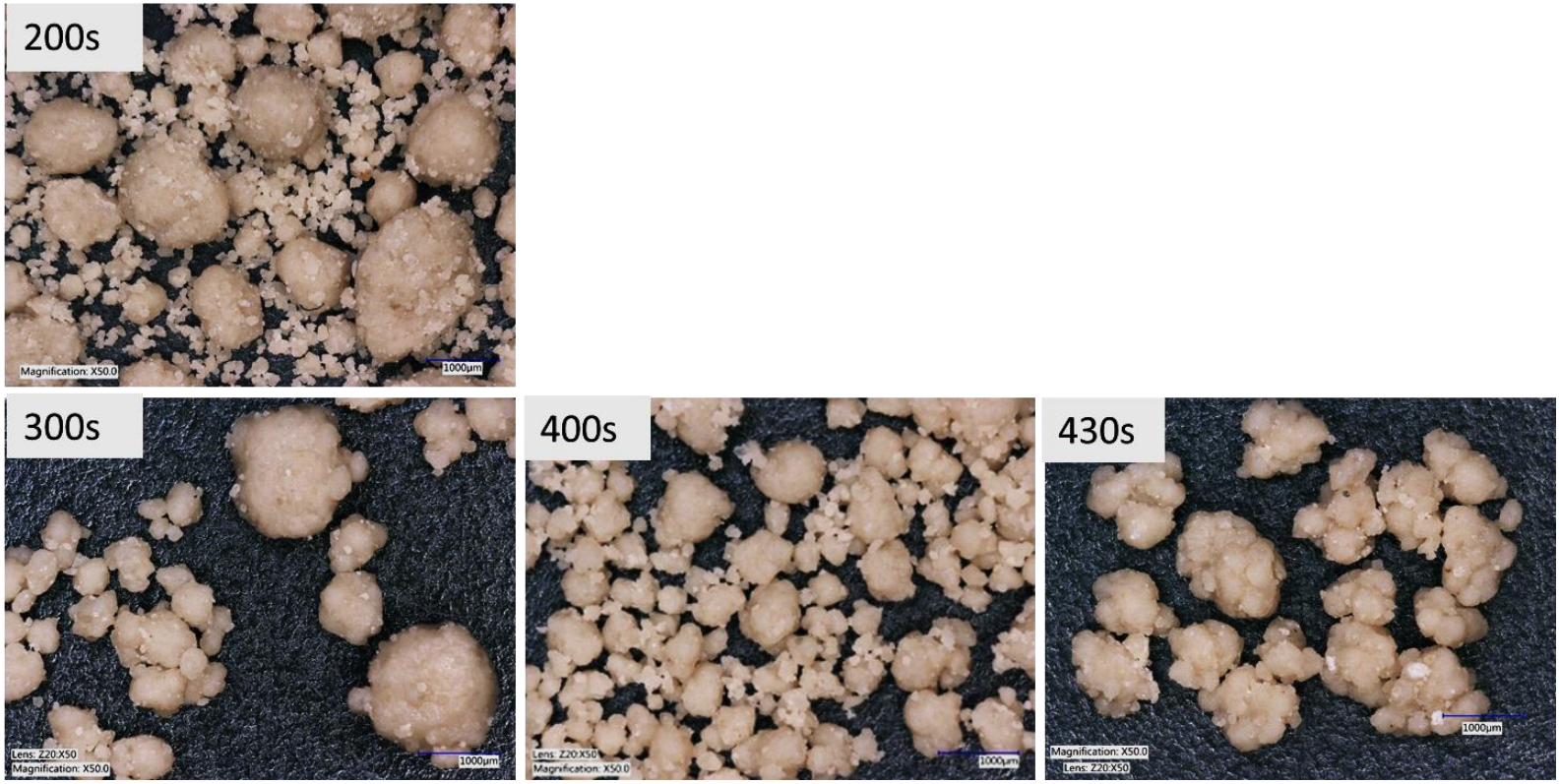

Figure D-2: Shape of granules over the granulation time, MSG/EP, L/S = 0.15.

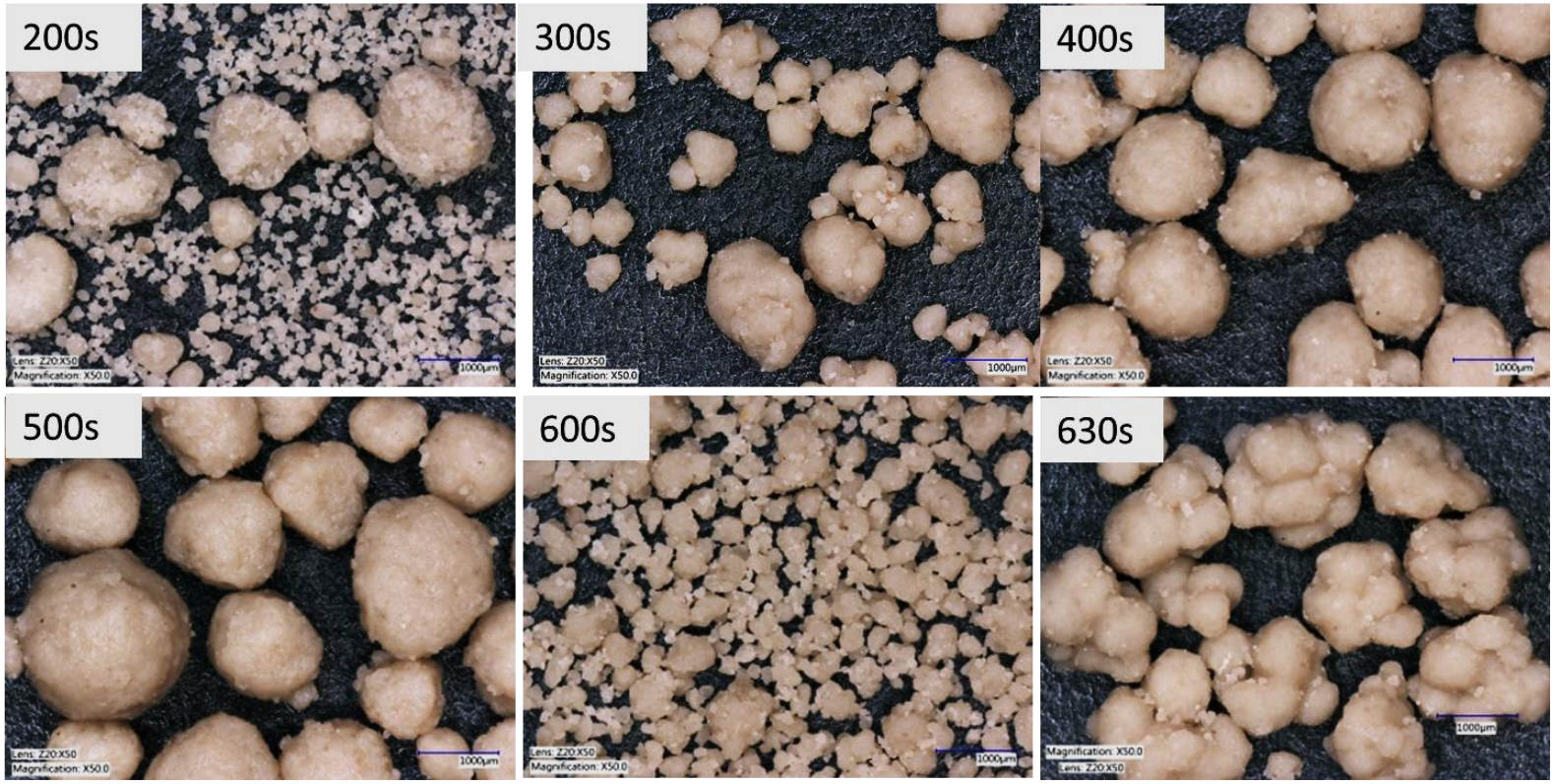

Figure D-3: Shape of granules over the granulation time, MSG/LP, L/S = 0.14.

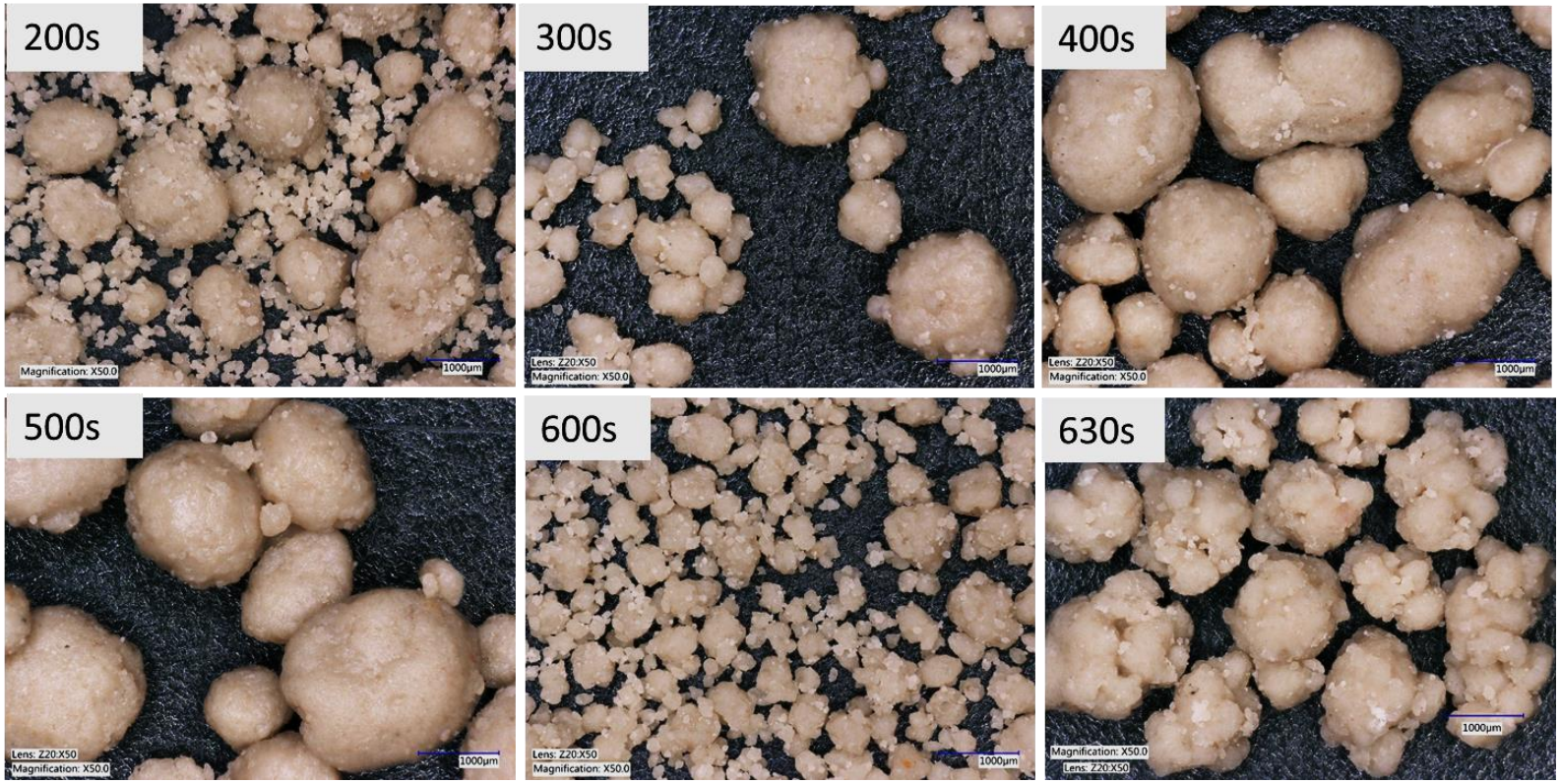

Figure D-4: Shape of granules over the granulation time, MSG/LP, L/S = 0.15.

APPENDIX E: VELOCITY DISTRIBUTION IN MSG

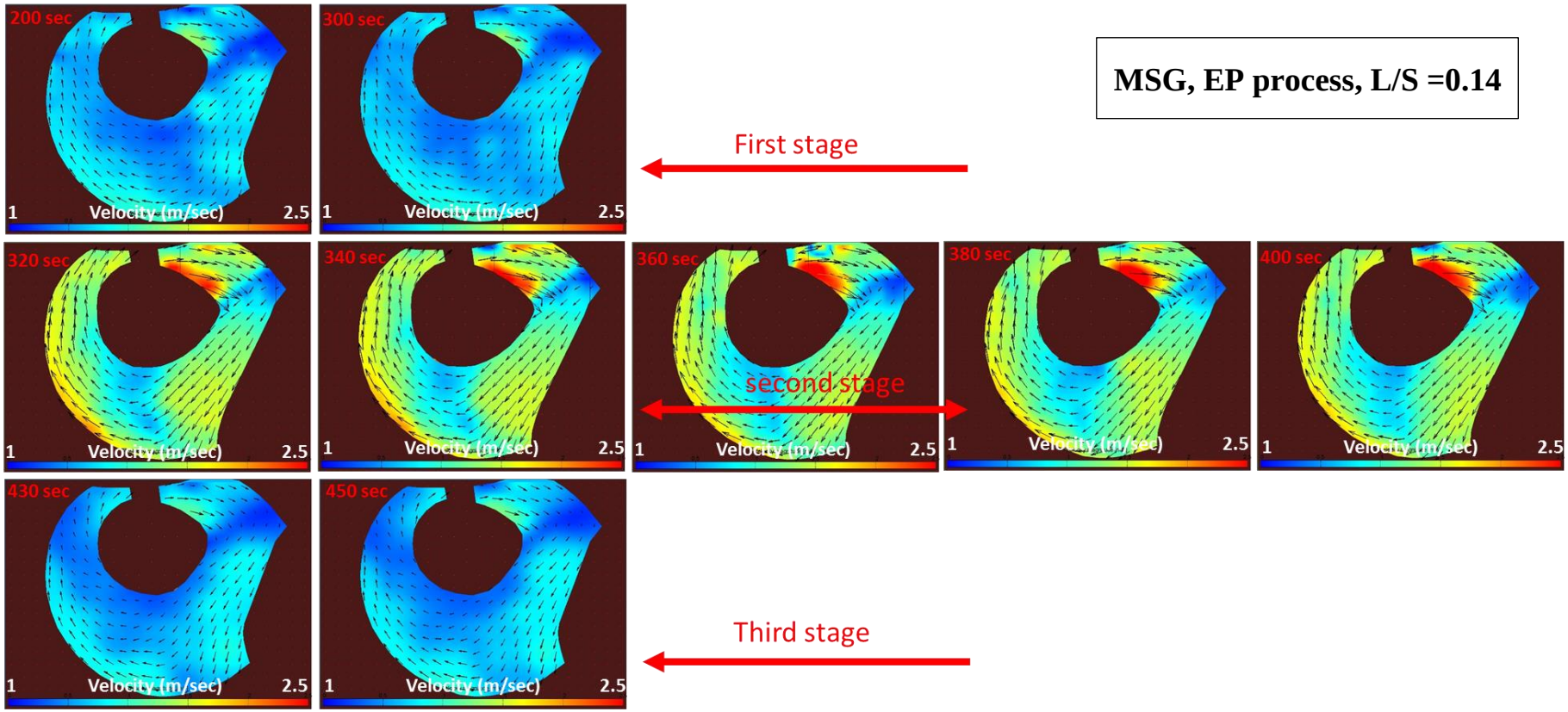

Figure E-1: Surface velocity profile, MSG, EP process, L/S =0.14.

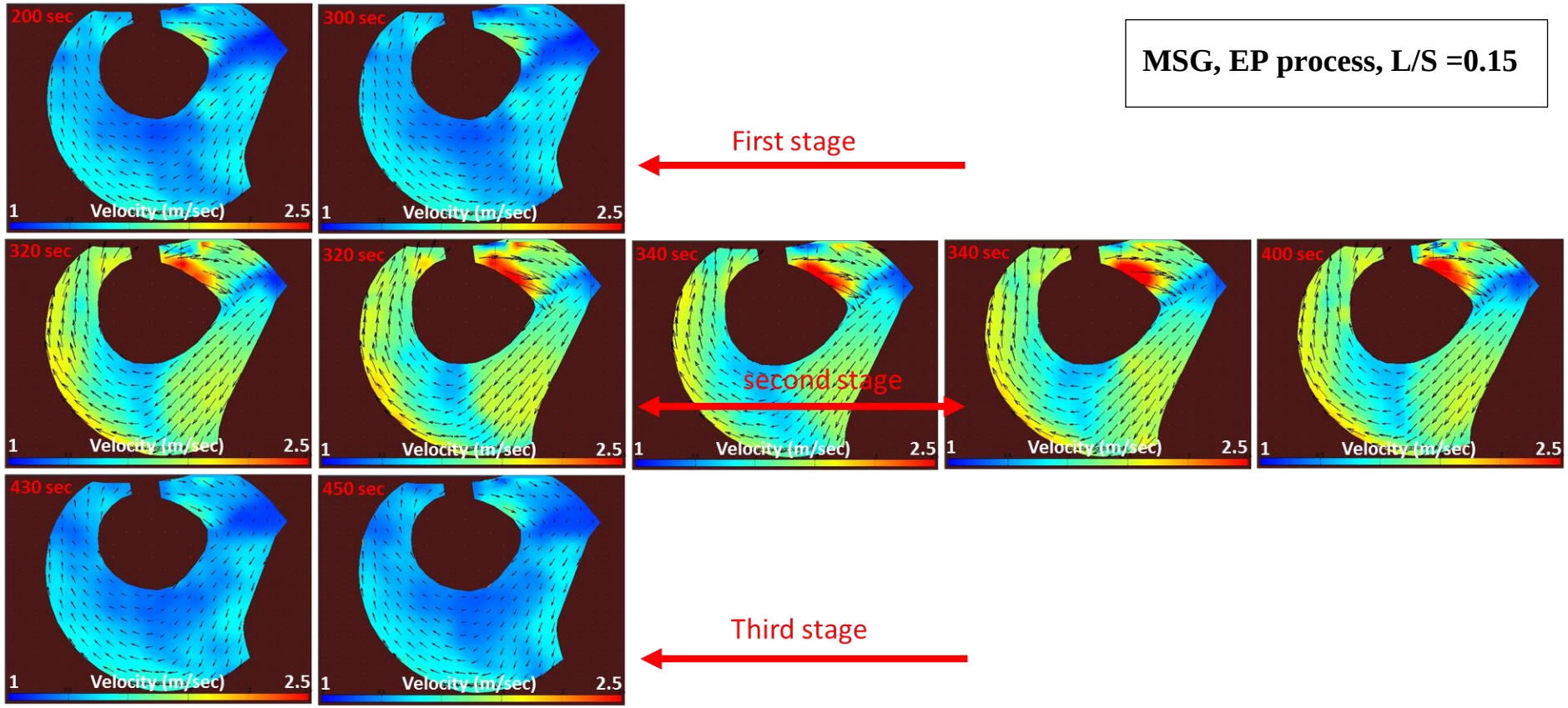

Figure E-2: Surface velocity profile, MSG, EP process, L/S =0.15

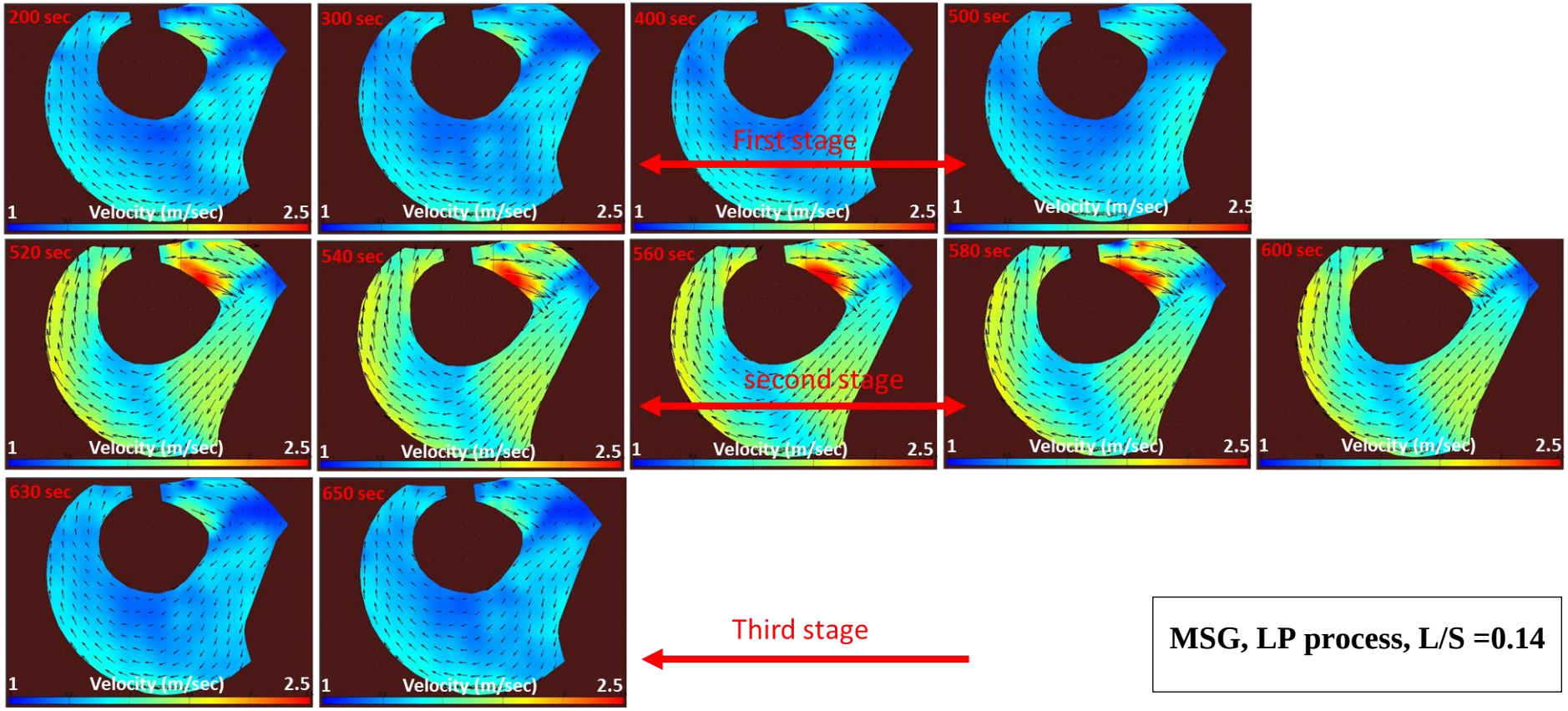

Figure E-3: Surface velocity profile, MSG, LP process, L/S =0.14.

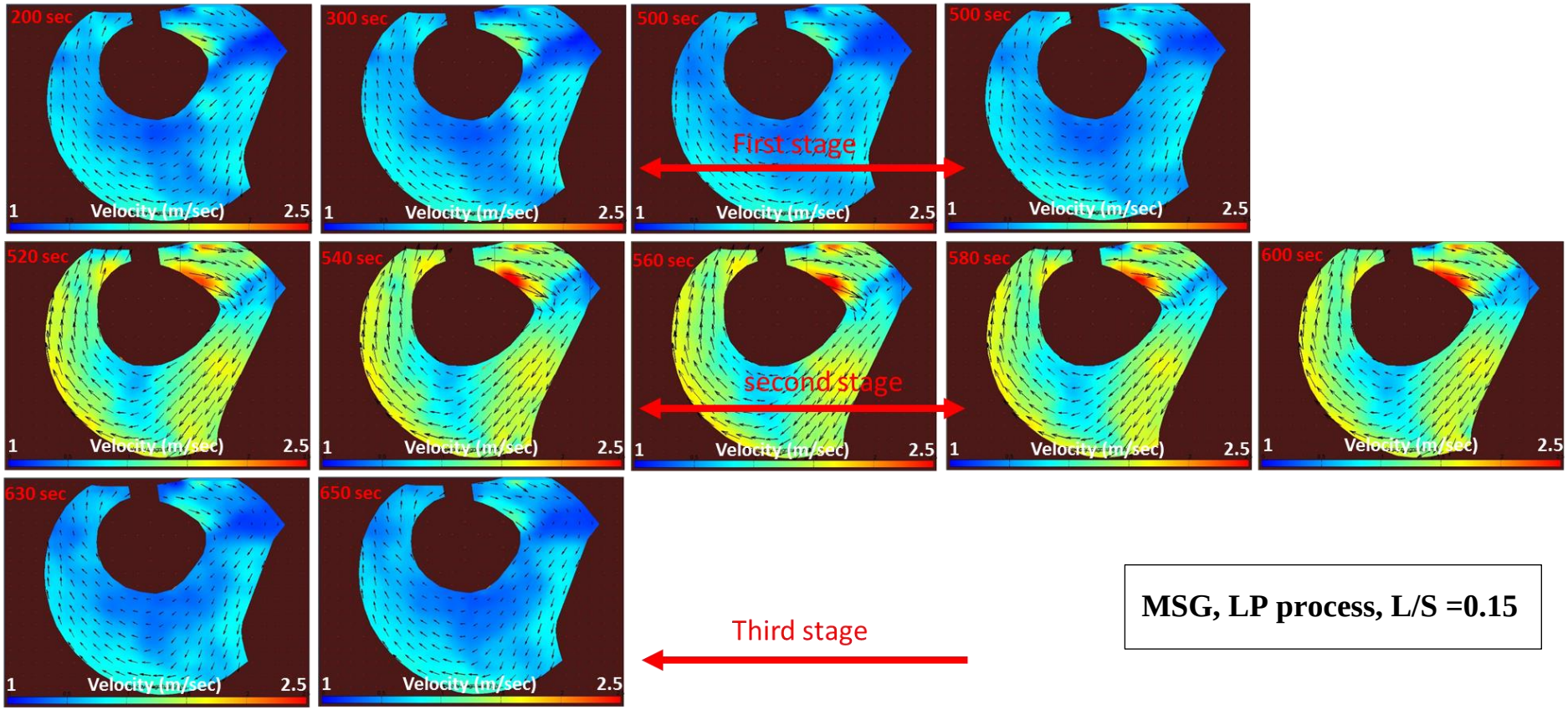

Figure E-4: Surface velocity profile, MSG, LP process, L/S =0.15.